Morphodynamics and driftwood dispersal in braided rivers

Matilde Welber

2013

Front cover: Tagliamento River, Italy, January 2009
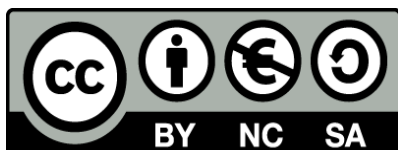
Poi ci siamo travestiti da soldati di ventura
per cercare di scalare questa ripida pianura.

Mercanti di Liquore, *Lombardia*

Abstract

Driftwood is widely recognized as a relevant component of riverine systems due to its complex interactions with flow, sediment transport and vegetation dynamics. In-channel large wood has a relevant geomorphic and ecological role as it enhances morphological diversity and creates a variety of physical habitats that sustain high biodiversity. Its presence can also increase flood risk and therefore wood is often removed from streams especially in densely populated areas. Recent river restoration policies aim to maximise the environmental benefits of driftwood and minimise risks. The study of wood dynamics can provide useful information to define guidelines for sustainable wood management.

Multi-thread systems represent a particularly interesting and challenging context for the investigation of wood dynamics because of their complex geometry, the presence of vegetated islands and the frequent, intense changes in channel pattern observed even for moderate discharge fluctuations. However, comparatively few studies focus on driftwood in large braided rivers and limited quantitative information is available on wood transport, deposition and remobilisation in these systems. The goals of the present work are: a) characterising the spatial organisation of wood deposits and identifying typical retention sites and styles; b) analysing the influence of flow regime, channel morphology, wood supply and log properties (size and shape) on dispersal patterns; c) investigating wood remobilisation induced by discharge fluctuations and bed reworking; and d) analysing long-term wood storage volume and budget.

A combination of field-scale direct observations, remote sensing techniques and physical modelling was used to investigate wood and channel dynamics. Field-scale monitoring carried out on the Tagliamento River (Italy) allowed the observation of complex interactions and feedbacks between channel, vegetation and wood dynamics. Laboratory simulations – carried out in two large flumes at the University of Trento (Italy) and at the University of Hull (UK) – were employed to investigate individual wood dispersal mechanisms under controlled conditions and to explore the role of governing parameters.

In large rivers, floods are the primary driver of wood recruitment through the erosion of vegetated banks and islands; field-scale observations showed that these localised wood inputs control wood storage at sub-reach scale because a large proportion of eroded trees is retained close to the input point in sparse, small jams. Physical modelling highlighted a complex relationships between flow stage and the longitudinal and vertical distribution of

wood; high discharge increases the ability of the system to transfer wood, but at the same time generates complex inundation patterns where a larger number of sites are available for wood retention. No clear link between flow stage and the vertical distribution of wood is observed, probably because water surface elevation exhibits small changes with discharge in flat braided river cross-sections. Driftwood element properties also influence deposition patterns; log diameter controls travel distance as it governs flotation and therefore the likeliness of deposition. High element length and complex piece shape sustain the formation of large jams. The presence of a root bole is also associated to short travel distance and low relative elevation.

At reach-scale, the spatial distribution of wood is the product of local inputs during major floods and reorganisation of deposits induced by minor events. Wood pattern exhibits a threshold behaviour with supply. High input rates determine very high spatial density and the formation of large, stable jams. Two processes govern wood reorganisation over different time scales, namely network inundation – inducing rapid changes in flow field – and bed reworking. In the first case, the persistence of deposits depends on the magnitude of discharge fluctuations as wood dispersed by small floods is easily removed by larger events. High relative elevation and large jam size enhance wood stability, while the presence of a root wad has a dual effect as it determines large accumulations at low elevation. Channel pattern reworking determines intense turnover of driftwood deposits regardless of supply rate, piece properties and jam size, save for very large accumulations. As a consequence, wood deposition occurs mostly on empty braidplain areas as opposed to pre-existing sites.

These results suggests that wood (alone) has little direct effect on reach-scale bed geometry in a large braided river; however, deposited wood significantly influences local hydraulics and morphology, enhancing physical habitat diversity. Moreover, deposited wood favours the accumulation of fine sediment, nutrients and seeds and often exhibits vegetative regeneration. These processes lead to the transformation of instable driftwood pieces into vegetated islands, which in turn can trap more wood. Therefore, wood has a relevant, indirect effect on braided river morphodynamics through the establishment of vegetation, whose presence influences network complexity and evolution.

Contents

List of figures

List of tables

1 Introduction

Driftwood, encompassing large wooden particles found in rivers such as logs, branches, uprooted trees and shrubs, has been recognised as a relevant component of the geomorphic and ecological processes that shape river corridors. Wood deposited in streams interacts with flow and sediment transport, determining complex spatial patterns of variability of the hydraulic conditions at local and reach scale. As a consequence, driftwood favours morphological diversity and creates a variety of physical habitats sustaining high biodiversity. Moreover, uprooted trees, especially if capable of asexual regeneration, support the establishment of in-channel vegetation, further enhancing the morphological and ecological complexity of river floodplains. Therefore, the knowledge of driftwood dynamics, especially in pristine or near-pristine systems, is of major importance for a complete understanding of the geomorphology and ecology of river corridors.

Large wood has long been seen as a natural hazard, especially in low-order mountain streams where it reduces channel conveyance and increases the destructive power of floods and debris flows. Therefore, in densely populated areas driftwood is often actively removed to limit flood risk. Other processes determine a reduction of wood in rivers subject to human intervention, such as channelization and land use change in riparian areas. However, the positive contribution of wood to river functioning is now widely recognised and new management policies and recent river restoration projects often include actions aimed at preserving or re-establishing driftwood in rivers. Therefore, research is needed to define guidelines for sustainable wood management, with the aim of maximising environmental benefits and minimising risks.

Extensive research on driftwood dynamics has been conducted in the last few decades with the aim of a) quantifying wood storage volumes; b) describing typical spatial patterns of wood accumulation; c) characterising wood supply, transport, deposition, retention and remobilisation processes and their contribution to wood budget; d) assessing hydraulic, geomorphic and ecological effects of deposited wood; and e) evaluating the influence of channel morphology, flow regime and riparian vegetation properties on in-channel wood dynamics. Past studies showed that the nature of deposits and the relative relevance of factors governing wood mobility strongly depend on the structure of the riverscape, with distinct downstream trends. In particular, relative wood size (i.e. the log length to channel width ratio) has been identified as a key parameter discriminating between small/medium

systems – where the role of wood size is dominant – and large systems, where dispersal patterns are governed by channel morphology and flow regime.

Wood dynamics have been widely investigated in small/medium streams, while comparatively few studies focus on large rivers. Among the latter, multi-thread systems represent an interesting case because of their complex geometry, the presence of vegetated islands and the frequent, intense changes in channel pattern observed even for moderate discharge fluctuations. In large braided systems, the erosion of vegetated banks and islands during floods is the dominant wood recruitment process and these localised, rapid inputs produce distinctive dispersal patterns. Past research on wood dynamics in braided rivers has been devoted mostly to the evaluation of stored wood volumes and the assessment of its geomorphic and ecologic effects, with special focus on its role in the formation of vegetated islands. On the contrary, limited quantitative information is available on the spatial organisation and time evolution of wood deposits. Moreover, the drivers of wood mobility, retention and remobilisation have been explored in single-thread systems, but little data are available for the specific case of braided networks. An extended literature review is presented in Chapter 2.

The aim of the present work is to improve the existing knowledge of short and long-term wood dynamics in braided systems, with special focus on the following goals:

- providing a detailed, quantitative description of wood deposits generated by localised, flood-induced inputs in terms of typical travel distance, planar and vertical distribution of deposits, typical retention sites and styles;

- analysing the main factors influencing wood deposition patterns, namely flow regime, channel geometry and wood properties (element size and shape);

- investigating wood remobilisation processes – with special focus on the role of inundation and erosion of retention areas due to channel pattern reworking – and evaluating the effect of stabilising factors including log properties, accumulation size and position;

- investigating long-term wood storage volume and budget.

Studying driftwood in a braided river context is a particularly challenging task because of the large spatial scale, high frequency and intensity of disturbances and mutual interactions between ecological and geomorphic processes. The characterisation of these complex dynamics requires the combination of different approaches and methods. In the present work, wood and channel dynamics were investigated using field-scale direct observations, remote sensing techniques and physical modelling. Field-scale monitoring offers the opportunity to observe the full complexity of channel, vegetation and wood dynamics occurring in complex riverine systems; field surveys also provide reference

conditions for the setup of flume-scale models. Laboratory simulations allow the investigation of riverine dynamics under controlled, repeatable conditions and the exploration of an extensive range of governing parameters.

Field surveys were carried out on the gravel-bed braided Tagliamento River (northeast Italy). This riverine system is almost unique in Europe for its low level of management and allows the study of braided river morphodynamics and wood dispersal in near-pristine conditions. Data were acquired through direct measurements and remote sensing techniques. In particular, the latter include automated ground-based imagery providing information during flood events with high temporal resolution. Laboratory simulations were conducted at the Hydraulics Laboratory of the University of Trento (Italy) and at the Total Environmental Simulator of the University of Hull (UK). In the latter case, experimental activities were carried out in the framework of the Hydralab IV project *The morphodynamic impacts of vegetation and large wood in fluvial systems* (HyIV-HULL-01). The physical models do not reproduce specific river reaches, but were used to simulate and analyse wood dispersal in the general context of temperate piedmont braided rivers.

Field-scale experimental activities conducted in the present study are presented in Chapter 3 and can be summarised as follows:

- field-scale investigation of the temporal evolution of braided channel pattern associated with flood events (referred to as *inundation dynamics*);

- field-scale characterisation of wood recruitment and dispersal determined by localised, rapid bank erosion;

- reconstruction of typical size distributions of driftwood elements observed on real-scale braid bars to be used as reference values for the design of physical models.

Laboratory simulations of driftwood dispersal in a multi-thread riverine system represent the core of the present work and are detailed in Chapter 4. The following experimental activities were conducted:

- simulation of flood-induced wood input and characterisation of resulting deposition patterns in terms of spatial organisation, size distribution of accumulations, and association with network geomorphic features. Investigation of the influence of log size and shape and flow stage on wood dispersal;

- analysis of wood pattern reorganisation induced by sequences of flood events and assessment of the role of flow stage, log shape and location of deposits on the persistence of wood accumulations;

- investigation of long-term driftwood dynamics in braided networks subject to various log input rates.

Finally, in Chapter 5 field observations and laboratory scale results are discussed and compared with the findings of previous studies. Special emphasis is placed on the evaluation of the relative relevance of wood dispersal drivers and their mutual interactions. Advantages and limitations of the experimental approaches and techniques employed in the present work are highlighted and implications for future research are briefly discussed.

2   State of the art

2.1   Overview

Driftwood – encompassing large wooden particles such as logs, branches, uprooted trees and shrubs – has been identified as a relevant component of riverine systems since the 1970s, when research addressing the nature and role of wood in streams started in the Pacific Northwest area (US). In this early stage, the nature and distribution of deposited wood were investigated almost exclusively in pristine, low order mountain streams flowing through unmanaged old-growth forests (Keller and Swanson, 1979; Lienkaemper and Swanson, 1987; Bilby and Ward, 1989). Driftwood dynamics in this type of riverine systems are still the object of extensive research in North America (Nakamura and Swanson, 1993; Manners and Doyle, 2008; Warren and Kraft, 2008; Warren et al., 2009) and developed also in the austral hemisphere (Mosley, 1981; Gippel et al., 1996a; Gippel et al., 1996b; Baillie et al., 1999; Brooks and Brierley, 2002; Iroume et al., 2010) and Europe (Piégay and Gurnell, 1997; Gurnell and Sweet, 1998; Díez et al., 2001; Comiti et al., 2006; Millington and Sear, 2007; Rigon et al., 2012).

Many authors showed that in European rivers wood dynamics are strongly influenced by the long history of human intervention on fluvial systems. In particular, channel and forest management and soil protection at catchment scale resulted in a general reduction of disturbances that govern wood recruitment and dispersal. Anthropogenic impacts also influence wood volume, species and physical properties (Gurnell and Sweet, 1998; Hering et al., 2000; Comiti et al., 2006). In recent times, studies focusing specifically on wood in highly modified rivers were conducted, for example by Angradi et al. (2004). Over the last two decades, the study of wood dynamics was extended to a wider range of fluvial systems including high-order, low-gradient, large meandering rivers (Abbe and Montgomery, 1996; Gippel et al., 1996a; Abbe and Montgomery, 2003; Montgomery and Piégay, 2003; Montgomery and Abbe, 2006; Lassettre et al., 2008; Curran, 2010) and very high-gradient streams (Andreoli et al., 2007). At the same time, wood in multi-thread systems – including wandering and braided rivers – has been investigated mainly in Europe (Piégay and Gurnell, 1997; Piégay et al., 1999; Gurnell et al., 2000a; Gurnell et al., 2000b; Gurnell et al., 2001; Gurnell et al., 2002; Wyżga and Zawiejska, 2005; Gurnell and Petts, 2006; Francis, 2007; Bertoldi et al., 2013) but also in other areas (Marcus et al., 2002; Pettit et al., 2005).

Studies focusing on in-channel wood bridge various scientific disciplines including open-channel hydraulics, engineering, geomorphology and ecology. The main objectives of the analysis of driftwood dynamics include:

- characterising driftwood elements in terms of their physical properties, including piece size, shape and density;

- identifying distinctive types of wood accumulation styles and typical retention sites for a wide variety of channel morphologies;

- evaluating wood storage volumes and budget;

- characterising input, dispersal, retention and remobilisation processes and identifying their main driving factors;

- evaluating the hydraulic and geomorphic effects of wood from piece to reach scale;

- analysing the ecological importance of driftwood, its contribution to physical habitat diversity and riparian biocomplexity and its role in vegetation colonisation;

- identifying potential hazard effects of wood in streams and in particular assessing hydraulic risk associated to the presence of wood;

- defining guidelines for in-channel wood management.

It is worth noting that both the scientific approach to in-channel wood management and public perception of wood in streams significantly changed over the past decades. Wood is no longer seen exclusively as threat to human activities and man-made structures; on the contrary, the positive contribution of wood to channel diversity and ecosystem complexity is now widely recognised and driftwood plays a key role in river management and restoration activities (Gippel et al., 1996b; Brooks et al., 2006; Shields et al., 2006; Kail et al., 2007; Millington and Sear, 2007; Le Lay et al., 2008; Coe et al., 2009; Sawyer and Cardenas, 2012)

Field-scale observations obtained by direct surveys and, more recently, remote sensing techniques (MacVicar et al., 2009; MacVicar and Piégay, 2012), represent a major source of information on driftwood dynamics. Moreover, the use of physical models to simulate and analyse wood-related processes at laboratory scale has become increasingly popular. Flume-scale models have been used in particular to investigate local-scale processes and phenomena such as the incipient motion of logs (Braudrick and Grant, 2000; Bocchiola et al., 2006a) and the hydraulic effects of deposited wood (Ranga Raju et al., 1983; Cherry and Beschta, 1989; Young, 1991; Shields and Gippel, 1995; Gippel et al., 1996a; Gippel et al., 1996b; Wallerstein et al., 2001; Wallerstein et al., 2002; Wallerstein, 2003; Mutz et al., 2007). Physical modelling has also been employed to reproduce reach-scale driftwood dispersal,

albeit for a limited range of channel configurations (Braudrick et al., 1997; Braudrick and Grant, 2001; Bocchiola et al., 2006b; Bocchiola et al., 2008; Bocchiola, 2011). Moreover, driftwood dynamics have been investigated through real scale simulations by adding wood to streams (Hygelund and Manga, 2003; Millington and Sear, 2007).

Physically-based analytical models have been proposed, in particular for log entrainment and incipient motion and for the quantification of local-scale hydraulic effects (Abbe and Montgomery, 1996; Gippel et al., 1996a; Braudrick and Grant, 2000; Wallerstein, 2003; Bocchiola et al., 2006a). Statistical approaches based on Monte Carlo simulations have been employed to predict changes in large wood and bedload dynamics as a consequence of the variation of channel, forest and sediment properties (Eaton et al., 2012).

2.2 Wood in riverine systems

2.2.1 Definition and properties

In-channel large wood is usually defined on the basis of size thresholds for element diameter and length. The most widely used criterion identifies large wood as any piece exceeding 1 m in length and 10 cm in diameter, but higher and lower threshold values have been used in past studies. For example, Angradi et al. (2004) chose 5 m and 0.3 m for length and diameter, respectively, for wood in a large meandering river, while Comiti et al. (2006) used 0.3 m for length and 0.05 m for diameter in low-order alpine streams. Different choices of minimum size reflect the need to take into account all elements that are assumed to be relevant within the riverine system of interest (Wohl et al., 2010). The size distribution of in-channel wood is essentially determined by the composition of forests supplying wood to the systems. Piece size depends on plant growth rate, itself a function of tree species and various environmental variables such as moisture, light and nutrient availability. The frequency of disturbances determining wood recruitment – from landslides and storms to bank erosion during floods – and forest management policies set an upper limit to forest age and therefore to element size (Gurnell et al., 2002).

In addition to element length and diameter, Wohl et al. (2010) suggested a comprehensive set of parameters – including piece shape, density, species and decay status – to be used for a detailed characterisation of driftwood accumulations. Large wood exhibits a variety of piece shapes, including logs, branches, root boles and entire uprooted trees and shrubs. Irregularly shaped pieces are most commonly found in rivers draining deciduous forests, as opposed to coniferous woodland where cylindrical logs represent the vast majority of wood supply (Braudrick et al., 1997; Gurnell et al., 2002). Complex shapes have been shown to enhance piece stability as well as local-scale geomorphic and hydraulic

effects, including channel obstruction, bed scour and sediment accumulation. In particular, the presence of a root wad exerts a considerable influence on logs as it tends to determine piece orientation and reduce piece mobility, with most stable elements deposited parallel to flow with the root wad upstream (Abbe and Montgomery, 1996; Kollmann et al., 1999; Piégay et al., 1999; Braudrick and Grant, 2000). Moreover, the development of distinctive scour and deposition patterns around the roots is often observed (Kollmann et al., 1999).

Density exerts a strong control on the fate of recruited elements by determining the minimum flow depth required for piece flotation (Braudrick and Grant, 2000). Density depends on tree species – with conifers usually denser than deciduous riparian species found in temperate systems – and usually ranges between 0.3 and 0.7 kg/dm^3 (Gurnell et al., 2002); a value of 0.5 kg/dm^3 is often used to compute wood mass from volume surveys carried out in European rivers (van der Nat et al., 2003a; Lassettre et al., 2008). Density is also subject to marked variations due to water absorption and wood decay and in particular high moisture content can cause wood to become heavier than water and sink to the riverbed where it tends to be buried by sediments (Curran, 2010). Thévenet et al. (1998) provide a detailed characterisation of the evolution of wood density over time as a consequence of wetting and drying cycles and show that piece mass can double over 24 hours due to water absorption.

Finally, tree species is crucial for driftwood persistence because of the distinctive survival strategies adopted by riparian vegetation. Tree species adapted to fluvial environments – characterised by frequent disturbances – by developing the ability to reproduce asexually from dispersed fragments (see Figure 2.1).

Figure 2.1: Uprooted Populus nigra tree deposited on a bar, showing vegetative regeneration.

Under suitable environmental conditions, large wood fragments can sprout new roots anchoring the piece to the riverbed, while the development of new shoots reduces flow velocities and enhances sediment trapping around the piece (Gurnell et al., 2001; Karrenberg et al., 2003). Asexual regeneration is a distinctive trait of *Salix* and *Populus*, the most common genera in temperate riparian forests. Besides tree species, a number of factors have been shown to control vegetative reproduction potential, including moisture availability, grain size distribution and the frequency and intensity of disturbances. These processes have been investigated in detail especially in multi-thread systems, showing that the spatial distribution of deposits governs tree survival. Optimal conditions for vegetative reproduction require a balance between high soil moisture and low disturbance frequency, which are associated to low and high relative elevations, respectively (Francis et al., 2005; Gurnell and Petts, 2006; Francis et al., 2008; Gurnell et al., 2008; Moggridge and Gurnell, 2009).

2.2.2 Wood supply processes

Wood supply to a riverine system is determined by a variety of processes involving the riverbanks and the catchment (natural tree mortality, forest fires, avalanches, input from tributaries, flood events and mass wasting events such as landslides and debris flows). Wood recruitment is essentially a consequence of individual events and point sources (Gurnell et al., 2002; Manners and Doyle, 2008) and the relative relevance of the various input processes has been shown to change along river corridors (Keller and Swanson, 1979; Nakamura and Swanson, 1993). Catastrophic events (fires, windthrow, debris flows, landslides, avalanches) involving areas located far from the riverbed are most commonly seen in high-gradient, low-order unmanaged streams. On the contrary, wood supply in low-gradient large rivers is governed by bank erosion and channel migration (Nakamura and Swanson, 1993; Gurnell and Sweet, 1998; Comiti et al., 2006).

Among large rivers, meandering piedmont channels show the highest recruitment volume per unit eroded area because the low rate of channel change allows the establishment of mature forest stands in riparian areas. On the contrary, the high turnover observed in braided rivers results in lower overall recruitment volume because of the lack of old stands but also in more uniform distribution of wood input points (Piégay and Gurnell, 1997; Gurnell et al., 2002; Lassettre et al., 2008). Where the hydrologic regime is the main driver of wood recruitment, input volume is determined by flood magnitude, but also by the sequence of high flow events and season (Moulin and Piégay, 2004).

Human pressure can limit wood input to riverine systems not only through management practices specifically designed to eliminate wood from streams but also as a consequence of other forms of human intervention on riparian forests and channels.

Historically, potential wood supply was limited by wood harvesting, especially in European rivers characterised by high human pressure, and more generally by land use change in riparian areas. This process has a disproportionate effect on wood supply to large rivers where recruitment essentially occurs in areas close to the riverbank. The exploitation of forest resources also induces changes in forest succession, usually limiting the number of old trees, further reducing supply volume (Díez et al., 2001; Angradi et al., 2004). The degree of connectivity between channels and their riparian forests also plays an important role in wood supply as channelization, bank protection structures and dams strongly limit wood input by preventing wood from reaching the channel (Gurnell and Sweet, 1998; Angradi et al., 2004). Finally, the alteration of flow regime with the elimination of flood events prevents wood recruitment (Gurnell and Sweet, 1998).

2.2.3 Wood dynamics and river morphology

The comparison of wood dispersal patterns observed in different riverine contexts prompted the definition of conceptual models describing the interaction between channel properties (size, stream order, slope and planform style) and the characteristics of wood deposits, including piece origin, size, mobility, retention mechanism and types of accumulations. Gurnell et al. (2000a) observed that the relative relevance of main wood retention drivers – forest character, hydrological processes, geomorphology and management – changes with stream order, as occurs for sediment storage. In low-order streams, individual roughness elements govern the retention of bed material, but their relative relevance decreases downstream and in large rivers the morphology is determined only by fluvial processes and geological constraints (Church, 1992).

Gurnell et al. (2002) propose the ratio between piece length and channel width as the most relevant scaling factor for wood dynamics and identify three classes of streams:

- *small* rivers: in these systems, channel width is smaller than median piece length. A large number of elements can span the entire channel and are essentially immobile regardless of flow conditions, as observed by Nakamura and Swanson (1993);

- *medium* rivers: channel width is smaller than the upper quartile of log length, implying that a fraction of elements can be remobilised by flood events. Hydrological processes control piece mobility while retention is strongly associated with local-scale features such as pre-existing wood deposits, standing vegetation and boulders;

- *large* rivers: all pieces are shorter than channel width and therefore fully mobile. In these high order streams, dispersal patterns are governed by channel morphology, hydrologic regime and piece density.

In small rivers, the presence of a vast majority of immobile pieces implies that the spatial distribution of wood is almost exclusively determined by input location and often exhibits a near-random spatial pattern associated to local forest characteristics (Figure 2.2). In medium rivers, *debris dams* comprising a large number of tightly interwoven elements represent the most common type of accumulation (Figure 2.3A and 2.3B). Gurnell and Sweet (1998) identified three types of dams: *active* dams completely spanning the channel and causing a step in water surface profile; *complete* dams which do not determine a break in water surface; *partial* dams which are smaller than channel width. The authors note that the composition of riparian forests influences the formation of complete and active dams because deciduous trees provide elements with complex geometry that are more likely to bridge the channel and capture smaller floating pieces.

Braudrick et al. (1997) also underline that small and medium streams are characterised by a distinctive wood transport styles as a consequence of the low discharge and high wood input volumes that can be observed in low-order streams especially after catastrophic events. A high ratio of log input rate to discharge (referred to as *relative log input rate*) results in a huge amount of pieces moving together within the channel in the form of large debris rafts (*congested transport*, Figure 2.4). On the contrary, low relative log input rate is typical of large systems, where channel size and discharge prevent interactions between floating pieces (dominance of *uncongested transport*).

In large rivers, highly distinctive retention sites have been identified and linked with channel planform structures. Unlike logs in small systems, wood in large rivers shows a general tendency to be deposited parallel to flow, thus demonstrating that depth and velocity sustain wood flotation (Marcus et al., 2002). Abbe and Montgomery (1996)
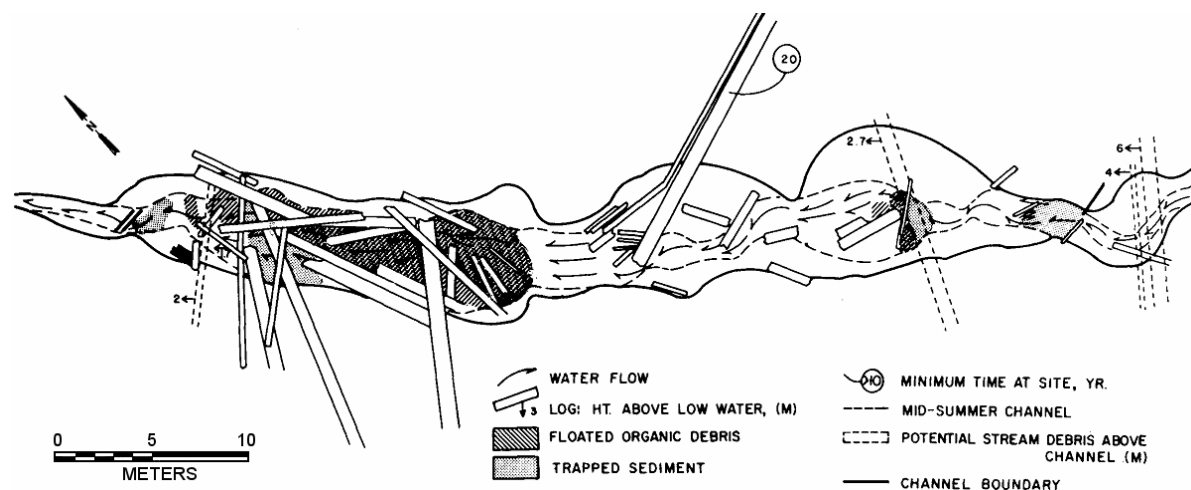
Figure 2.2: Typical 'small river' deposition pattern, with most wood pieces longer than channel width. From Keller and Swanson (1979)

11

observed three main forms of accumulation in a low-gradient meandering river located in the US Pacific Northwest and flowing through old-growth forest stands. In this system, very large uprooted trees tend to deposit at the upstream end of bars, usually aligning themselves parallel to flow and determining the accumulation of more transversal pieces. Resulting *bar apex jams* formed around a *key member* (Figure 2.3C) show great stability over time and are therefore able to exert long-term effects on channel morphology. Large wood also deposits on the concave bank of meander bends, forming stable *meander jams* and reducing bank erosion (Figure 2.3D). Finally, wood can also deposit in loose mats across the upper surface of bars, forming short-lived *bar top jams*. Interestingly, a clear tendency for wood to accumulate at bar head and along the outer margins of meander bends is also observed at laboratory scale (Braudrick and Grant, 2001).

The high morphological complexity of multi-thread systems results in a wide variety of retentive sites and forms of accumulations that are characteristic of other channel planform styles can be found in wandering and braided networks. 'Medium river' conditions can
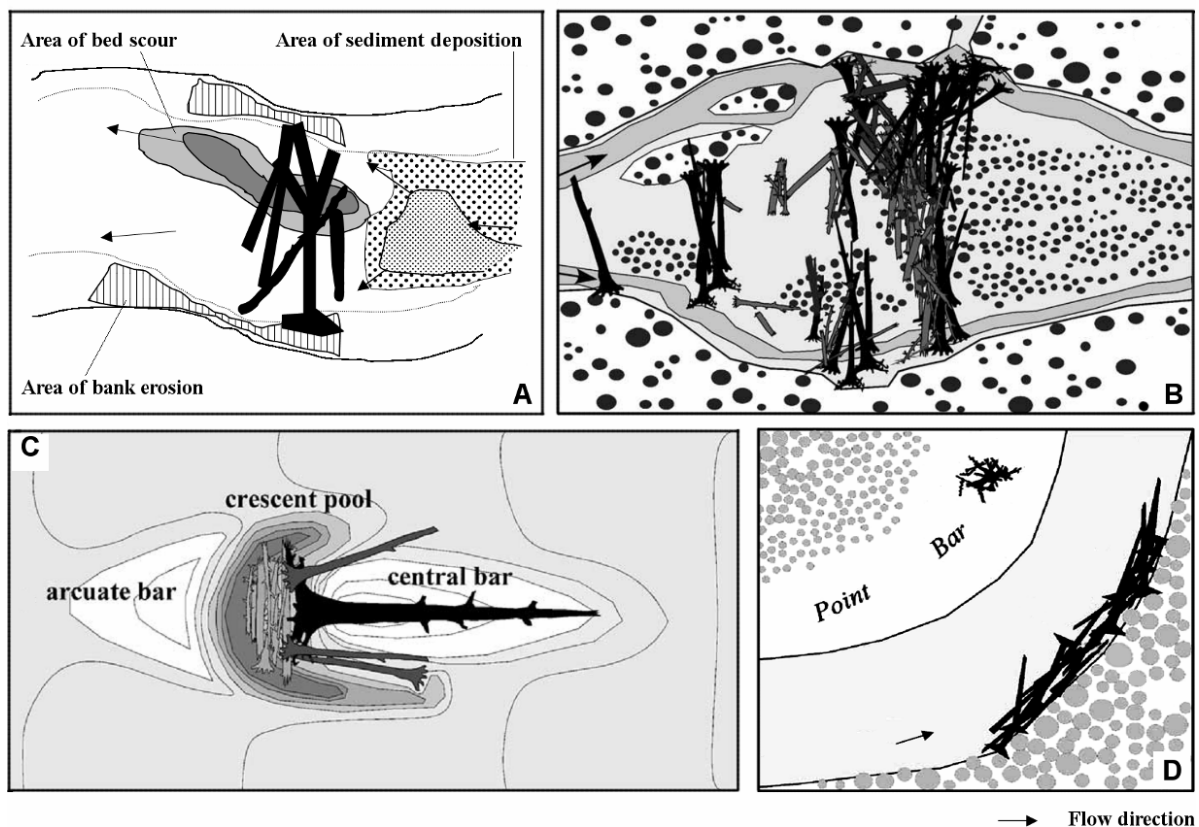
Figure 2.3: Schemes of various types of wood deposits and associated sediment accumulation patterns. (A and B): debris dams, from Wallerstein et al. (2001) and Abbe and Montgomery (1996), respectively; (C) mid-channel jam formed around a key member, from Abbe and Montgomery (2003); (D) meander jam, from Abbe and Montgomery (2003).

occur in side channels determining the formation of debris dams, while bar heads and concave bank areas are associated with high retention and discontinuous wood sheets can be found on the crests of shallow bars (Gurnell et al., 2000b; Wyżga and Zawiejska, 2005). Logs are often deposited parallel to flow with roots upstream, while jams are perpendicular (Piégay et al., 1999; Gurnell et al., 2002). Standing vegetation in the riparian area and islands provides additional accumulation sites and a significant amount of wood is found at the upstream end and along the margins of islands, where it is deposited as a line of debris during floods (Piégay and Gurnell, 1997). The role of islands as preferential wood deposition sites has been extensively investigated in gravel-bed rivers. Van der Nat et al. (2003a) observed that in these systems a large proportion of wood is deposited on bare gravel, but pioneer and established islands – representing a limited share of braidplain area – are associated with very high retention volumes, thus playing a key role in wood dynamics (Gurnell et al., 2000a; Gurnell et al., 2001). Finally, wood in wandering rivers is usually deposited along the floodplain at the edge of the main channel. High channel sinuosity ensures a higher trapping efficiency with respect to braided rivers (Piégay and Gurnell, 1997; Piégay et al., 1999). Figure 2.5 summarises various types of wood accumulations observed in large rivers.

Changes in channel width and geomorphological style along rivers are key factors influencing wood dynamics; however, other processes taking place along the river continuum contribute to determine downstream trends in wood storage volume and style. For example, Gurnell et al. (2001) observed distinct downstream trends in the presence of resprouting wood along the gravel-bed braided Tagliamento River (Italy). The authors linked the spatial distribution of living wood to changes in composition of riparian forest and hydraulic conditions. In this case, tree species exhibiting vegetative reproduction are absent from headwater reaches but become dominant in piedmont areas. At the same time, channel confinement due to the presence of gorges determines upwelling and downwelling processes and local changes in stream power which in turn affect moisture availability and shear stress and ultimately govern the survival of deposited trees.
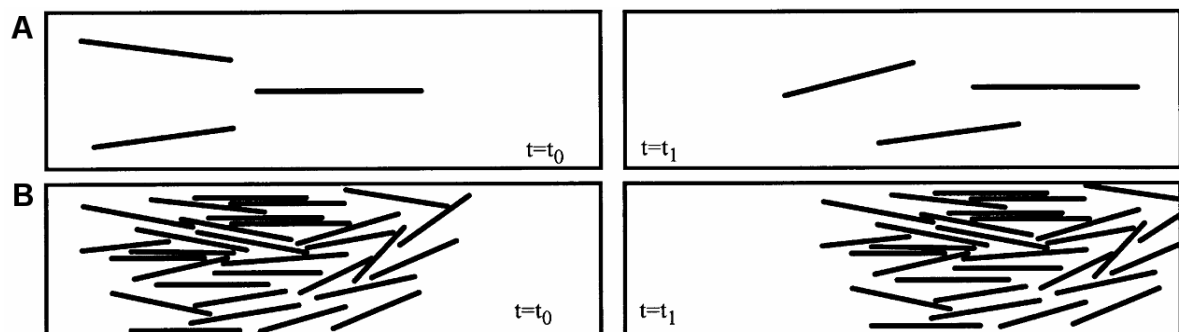
Figure 2.4: Transport styles: uncongested (A) and congested (B). Modified from Braudrick et al. (1997).

It is important to note that even if large rivers allow the mobilisation of all driftwood elements, many studies identified strong links between wood recruitment and deposition areas in both large single-thread and braided systems. Significant accumulations of driftwood are found immediately downstream of eroding banks and this association is particularly evident after major flood events (Wyżga and Zawiejska, 2005; Lassettre et al., 2008; Bertoldi et al., 2013). The large proportion of locally-produced wood – up to 70% of elements in a braided system (van der Nat et al., 2003a) – depends on the availability of retentive sites, but can also be explained by the fact that wood rapidly shatters during transport and is therefore rarely found far downstream of input points. (Gurnell et al., 2002). As a consequence, wood spatial patterns in braided rivers, despite being quite uniform at reach scale, are clearly governed by the distribution of eroding sites at smaller spatial scale (Pettit et al., 2005).

2.2.4 Wood storage and mobility

The amount of wood stored in streams and its governing factors have been the object of intense debate and detailed field investigations, with special focus on the comparison between large / small systems and headwater / lowland reaches. Conceptual models of wood storage and budget have been proposed in analogy with those derived for sediment. In particular, Marcus et al. (2002) noted that, unlike sediment, wood is transport-limited
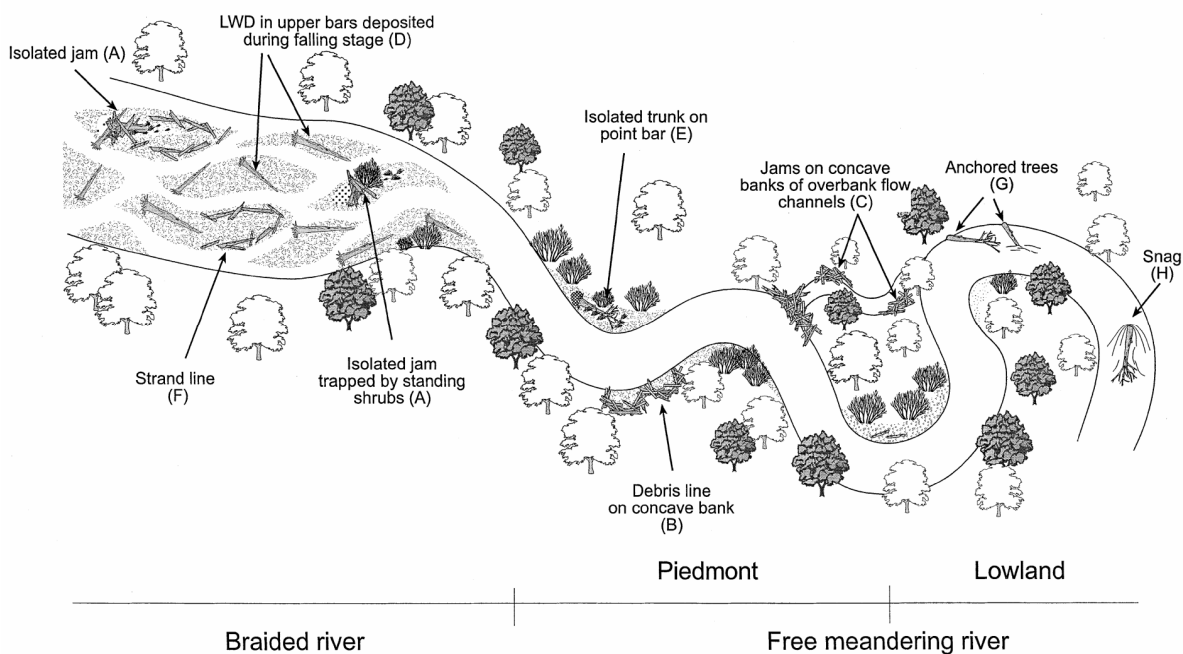
Figure 2.5: Various typologies of driftwood accumulations observed in large braided and meandering rivers. From Gurnell (2002).

in headwater reaches and supply-limited in downstream reaches, as suggested for example by Piégay and Gurnell (1997) for braided rivers.

Numerous studies addressed in-channel wood storage with the following goals: a) defining criteria and techniques for the estimation of driftwood volume; b) quantifying deposited wood in various riverine contexts; and c) analysing the main drivers of wood retention and mobility, including riparian forest composition, recruitment mechanisms, element properties, channel morphology, hydraulic regime and anthropogenic impacts.

Over the past decades, a wide variety of surveying and computing methods have been used to evaluate wood volume. For example, Hering et al. (2000) examined ten studies conducted in Central Europe and highlighted marked differences in the definition of survey area boundaries (including/excluding elements located on banks), metrics used for jam volume estimation (measurement of jam length, width and height instead of survey of individual components) and sampling procedures (by area, by transect). It is worth noting that the variety of piece shapes and the tendency to jam formation imply that simple metrics (such as piece diameter and length) are generally poorly suited to compute wood storage volume. Thévenet et al. (1998) proposed a wood-air box model based on the measurement of piece/jam size along three orthogonal axes and the estimation of wood to air ratios for logs, jams and shrubs. This approach has been applied to various European rivers (Gurnell et al., 2000a; Wyżga and Zawiejska, 2005).

Gurnell (in press) provides a comprehensive analysis of wood storage data collected worldwide at 284 field sites over the last three decades (see Table 2.1). The author classified available data on the basis of geographical region, riparian forest age and composition, channel width and slope and observed that wood volume per unit area shows a strong relationship with forest type. Rivers draining old-growth forests – often associated to redwood species – exhibit the highest wood storage values, five to ten times higher than those observed in streams flanked by young softwood stands.

The characteristics of riparian forests determine piece size distribution, which in turn govern wood retention (Lienkaemper and Swanson, 1987; Andreoli et al., 2007; Warren and Kraft, 2008). Braudrick et al. (1997) defined a *debris roughness* for streams on the basis of two dimensionless ratios, namely *relative log diameter* (log diameter / mean channel depth) and *relative log length* (log diameter / channel width). At flume scale, the authors observed a threshold behaviour of log mobility with diameter, with flotation dropping when relative log diameter is larger than 0.5. A similar behaviour was observed at field scale by Abbe and Montgomery (2003) who found that the relative diameter and length of immobile key members is usually greater than 0.5. Gurnell et al. (2002) observed that each size parameter plays a specific role in wood stability as length governs the likeliness of jam formation, while diameter governs flotation threshold. The association between wood storage and relative element size is confirmed by Gurnell (in press), who found that wood volume

Table 2.1:   *Variations in driftwood volume with riparian vegetation properties. Data from Gurnell (in press).*

Riparian vegetation properties	Median wood volume [m³/ha]
Forest age	
Old growth forests	319
Mature forest	106
Young forest	64
Forest composition	
Redwood	1000
Conifer	227
Mixed	158
Eucalypt	172
Salicaceae	45

shows a weak negative correlation with channel width. However, other factors may play a role in the decrease of storage with increasing stream order, such as lower input from banks per unit riverbed area and higher proportion of dead trees remaining anchored to the banks (Gurnell et al., 2002).

Care has to be taken in predicting element mobility on the basis of size. Braudrick and Grant (2001) emphasized that the relationship between piece and channel size has to be evaluated on the basis of local scale geometry parameters. On the contrary, reach-averaged channel width and depth are poor predictors of piece mobility, as they are unable to capture distinctive cross-section features such as the presence of a deep thalweg. Moreover, the authors observe that element mobility may not be monotonically increasing with decreasing piece diameter and length, as longer, larger pieces are more likely to be trapped by shallow flows but at the same time their greater inertia and momentum can prevent them from stopping (*momentum-maintained transport*).

Local-scale hydraulic effects on piece stability have been investigated through physical and analytical models, with special focus on the characterisation of incipient motion conditions and the quantification of drag force exerted on submerged or semi-submerged logs. Models of incipient motion based on force balance equations for individual logs have been developed in analogy with those used for sediment particles, usually for the simple case of cylindrical logs lying on a sloping riverbed, but also for elements with roots (Braudrick and Grant, 2000; Bocchiola et al., 2006a). Mobilisation mechanisms observed at field and laboratory scale include sliding, rolling and pivoting of logs, with sliding usually identified as the most relevant process. Orientation angle appears to determine the type of motion initiation, with logs perpendicular to the flow first moving by rolling as opposed to sliding (Bocchiola et al., 2006a). Attack angle also influences drag and the highest force was

observed for flow-parallel logs and elements positioned at high angles (Shields and Gippel, 1995). The role of piece orientation and pivoting has been already highlighted in early field-scale studies where a very limited number of elements was found with roots downstream, suggesting that this is the least stable configuration (Bilby and Ward, 1989). Channel obstruction (usually evaluated as *blockage ratio*, that is, the proportion of cross-sectional wetted channel area occupied by wood) was also found to determine a significant increase in drag force (Shields and Gippel, 1995). Several studies highlighted the intrinsic limits of many overly-simplified models used to compute the drag coefficient. In particular, force balance models for incipient motion usually assume uniform flow conditions around the log, therefore neglecting the hydraulic effect of the obstruction as well as bed deformation caused by local scour and deposition patterns. Corrections have been proposed, including the use of local velocity values instead of depth-averaged values (Hygelund and Manga, 2003) and of representative depth instead of uniform flow depth (Bocchiola et al., 2006a).

The importance of fluvial landforms and standing vegetation for wood retention has already been discussed. Various studies conducted in multi-thread systems show that wood volume peaks in wide, island-braided aggrading reaches (Piégay et al., 1999; van der Nat et al., 2003a; Wyżga and Zawiejska, 2005). In particular, Piégay and Gurnell (1997) demonstrated that the number of wood pieces in a reach is positively correlated with network complexity (braiding index) and the number of vegetated islands. Conversely, alterations of channel morphology and/or riparian forest structure can have a negative impact on wood retention. Wood is missing from channelized rivers because of the absence of retentive sites (Angradi et al., 2004) and many rivers in Europe – even those retaining a near-pristine morphology – still show low wood storage as a consequence of a long history of clearance activities (Hering et al., 2000).

In large rivers, the time evolution of wood volume is governed by flow regime over a range of temporal scales because different processes are associated to large (infrequent) and small (frequent) floods. Major events determine wood recruitment from eroding banks and minor events redistribute driftwood within the channel, implying that changes in wood storage occur over a range of discharges. For example, in a system characterised by a near-natural hydrologic regime, van der Nat et al. (2003a) observed that wood input due to large-scale erosion occurs every 2 to 3 years, while the reorganisation of deposits is driven by flood pulses occurring multiple times per year. Therefore, in large systems where wood recruitment from banks is dominant, wood storage peaks immediately after large floods and decreases afterwards (Gurnell et al., 2002). In a field-scale experiment, Millington and Sear (2007) noted that the first flood after element recruitment plays a disproportionately large role in wood dispersal, while subsequent events can be ineffective in removing wood regardless of their magnitude. Figure 2.6, taken from Gurnell et al. (2002), summarises the relative relevance of wood retention drivers in small, medium and large rivers.

2.2.5 The geomorphic role of wood

The influence of deposited wood on channel geometry has been observed over a range of spatial scales. Piégay and Gurnell (1997) identified two main effects, namely a direct control on hydraulics and stream power distribution and a secondary, indirect effect on sediment dynamics leading to geomorphic effects.

Local-scale hydraulic influence of wood is especially relevant in medium to small rivers where wood determines a local reduction in cross-section area associated to energy loss and increase in water level (usually referred to as *afflux*). Simplified models for the quantification of driftwood-induced afflux have been derived in analogy with those used for bridge piers (Ranga Raju et al., 1983), under highly simplified hypothesis for flow conditions. Subsequently, laboratory simulations showed that afflux is positively correlated
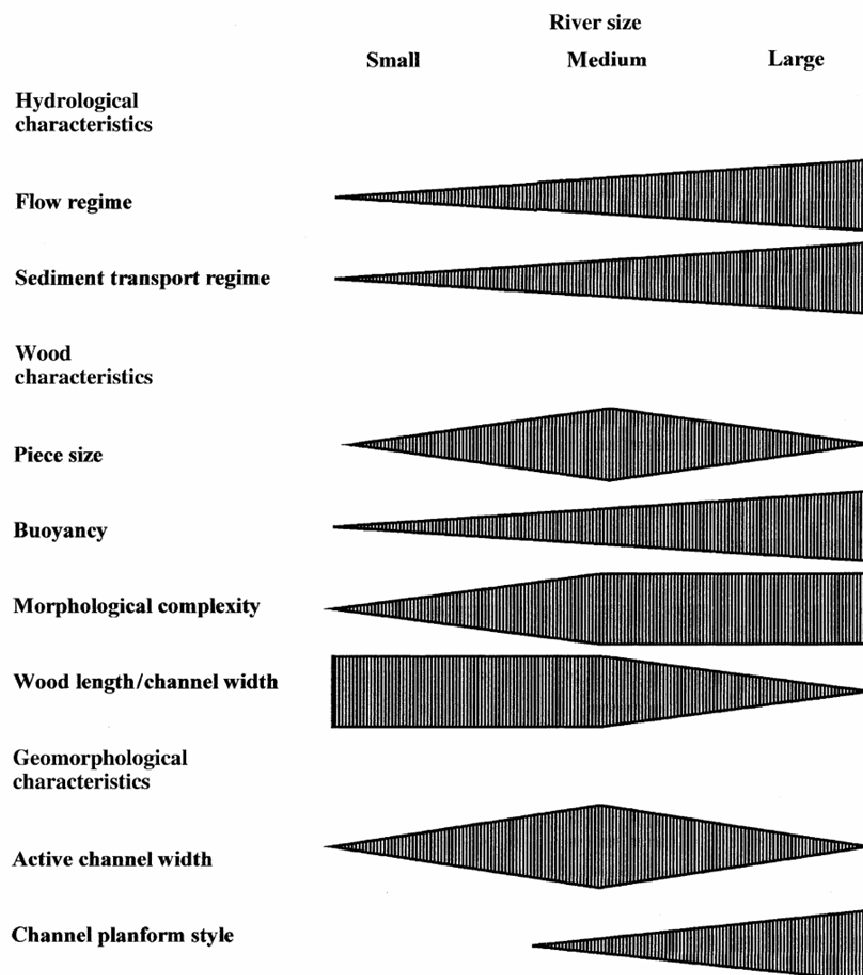
Figure 2.6: The relative relevance of wood, geomorphological and hydrological characteristics in influencing the retention of wood in rivers of different size. From Gurnell et al. (2002).

with blockage ratio and undisturbed water velocity while it is limited in the case of smooth elements (without branches or roots) aligned with flow or streamlined aggregations. (Young, 1991; Gippel et al., 1996b). However, the hydraulic effect of complex aggregations is still debated and some authors suggest that relationships derived for individual driftwood elements can not be extended to complex aggregations and that the hydraulic influence of jams may be significantly larger than that of single elements of comparable size (Richmond and Fausch, 1995; Manners and Doyle, 2008).

The nature and magnitude of the impact of deposited wood on sediment dynamics depends on accumulation type. Dams in small to medium streams are strongly associated with sediment storage and the formation of both downstream plunge pools and upstream dammed pools (Gurnell and Sweet, 1998). In steep channels, wood is responsible for a large proportion of total drop and can facilitate the formation of terraces (Keller and Swanson, 1979; Montgomery and Abbe, 2006; Andreoli et al., 2007). Bar apex jams found in large systems induce flow reversal upstream of the obstruction and lateral flow acceleration which determine the formation of typical crescent-shaped pools at the upstream end. Along the jam, flow separation produces an elliptical deposition area (Abbe and Montgomery, 1996; Kollmann et al., 1999). Local changes in the velocity field determine sediment sorting, as low-velocity areas behind debris are preferential sites for the deposition of fines in gravel bed streams (Gurnell and Sweet, 1998; Gurnell et al., 2001).

Wood can have a major geomorphic effect at a much larger scale especially in association with high sediment input, implying that the knowledge of wood retention dynamics can be crucial for the prediction of landscape change (Nakamura and Swanson, 1993; Abbe and Montgomery, 2003). However, geomorphic effects are often difficult to predict due to the complexity of interactions and feedback mechanisms involving wood, flow and sediment; as a consequence, apparently contrasting processes have been observed. Wood deposits can induce flow diversion towards the margins of the channel, causing bank failure and local channel widening (Keller and Swanson, 1979; Nakamura and Swanson, 1993). At the same time, wood reduces the likeliness of bank failure by promoting energy dissipation and tends to deposit in large jams along channel bends, effectively reducing bank erosion. (Keller and Swanson, 1979).

Moreover, the presence of wood has been shown to both help and hinder the formation of secondary channels, meander cut-offs and anabranches. In meandering systems, driftwood can produce local widening resulting in the development of mid-channel bars and a multi-thread configuration immediately downstream of the accumulation (Keller and Swanson, 1979; Sear et al., 2010). However, Hickin (1984) observed that the formation of very large jams can prevent the formation of chute cut-offs or completely block secondary channels, promoting a simpler planform configuration. Abbe and Montgomery (1996) also observed that, in meandering rivers, vegetated patches developing from wood jams tend to

accumulate sediment and organic material that block chute cut-offs and lead to the attachment of the island area to the floodplain. These different, sometimes contrasting outcomes are the consequence of a different balance between sediment availability, wood supply, jam formation rate and frequency and intensity of disturbances determining wood recruitment and removal. For example, the combination of discharge and relative elevation of log jams within the channel determines the local velocity field and therefore the geomorphic influence of individual jams under given flow conditions. Wood stored on higher bars is more likely to determine favourable conditions for the accumulation of fines, while jams deposited at lower locations are more vulnerable to disturbances, limiting their persistence over time and their ability to induce long-lasting geomorphic changes.

In multi-thread systems, small piece size, low input rate and frequent disturbances prevent wood from exerting a strong, direct effect on channel pattern. However, wood has been shown to sustain the establishment of living vegetation, which in turn is major driver of channel dynamics (Gurnell et al., 2005; Gurnell and Petts, 2006; Corenblit et al., 2007), influencing in particular network complexity and channel change rate (Gran and Paola, 2001; Coulthard, 2005; Tal and Paola, 2007; Tal and Paola, 2010). Overall, river reaches containing resprouting driftwood sustain faster vegetation growth, sedimentation, island development and floodplain accretion and greater resistance to erosion (Francis et al., 2008).

2.2.6 Ecological implications of wood in rivers

The geomorphic effects determined by wood also produce a variety of physical habitats that have major ecological implications for the biocomplexity of riverine systems (Gurnell et al., 2005). The most relevant effects include; a) a marked increase in aquatic habitat diversity especially due to the formation of pools; b) enhanced retention of fine sediments, nutrients and seeds; and c) the formation of stable points sustaining distinctive vegetation succession processes.

Scour and deposition around deposited wood determines the formation of low velocity areas which represent local lentic habitats often surrounded by primarily lotic conditions (Stanford et al., 2005). The effect of wood on fish habitats was evaluated in terms of Weighted usable area (WUA) using hydrodynamic simulations and habitat preference curves for depth and velocity, showing higher WUA in wood-rich streams (He et al., 2009; Bocchiola, 2011). Moreover, driftwood-associated pools are characterised by higher persistence over time and limited water temperature variations, thus acting as refugia for aquatic biota especially during low flow periods (Sawyer and Cardenas, 2012). They also provide optimal conditions in terms of vegetation cover and nutrients (Abbe and Montgomery, 1996) and high rates of exchange with the hyporheic zone as a consequence

of sediment size heterogeneity and hydraulic head (Gurnell and Petts, 2002; Mutz et al., 2007). Large wood plays a major role in trapping coarse particulate organic matter (CPOM) which represents a primary source of nutrients for the biota, with positive effects especially on invertebrate communities (Wallace et al., 1995; Gurnell et al., 2002; Lepori et al., 2005; Millington and Sear, 2007).

The influence of wood on vegetation establishment processes in a riverine context (Figure 2.7) is summarised in the conceptual model of island formation proposed by Gurnell et al. (2001) and further discussed in Gurnell and Petts (2006). The authors identified three island development processes (*trajectories*) characterised by different origin and growth rate of in-channel vegetation. Two distinct effects of driftwood are recognized, both contributing to rapid vegetation establishment. First of all, wood deposits determine a local increase in flow resistance, inducing significant deposition of fine sediment and plant propagules. Surface aggradation, soil moisture availability and reduced shear stress help the germination and growth of new plants; the combination of sheltering and high growth rate determine a higher probability of island survival.
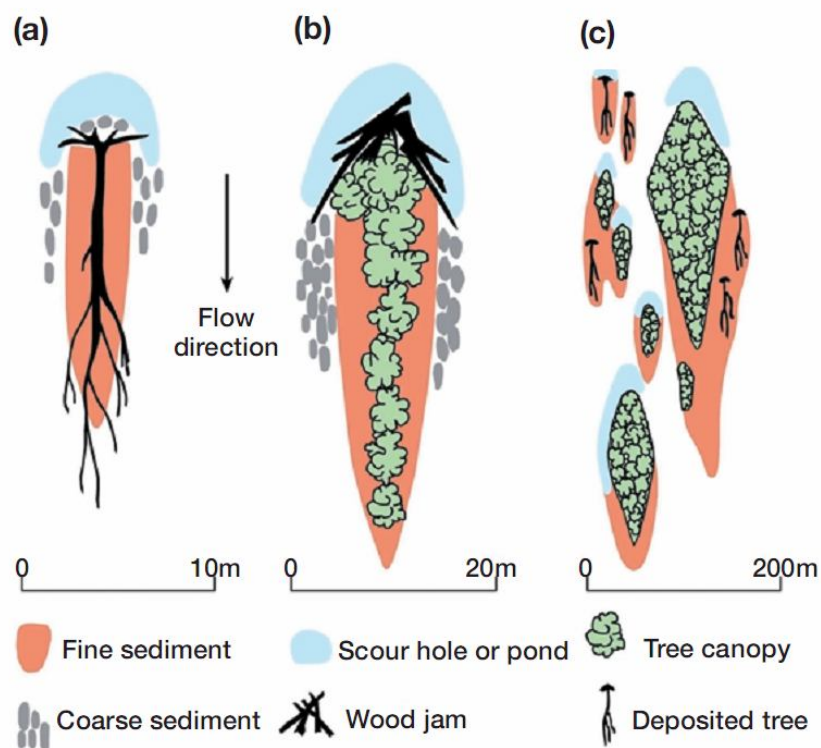
Figure 2.7: Island development from living wood. (a) A deposited tree inducing the development of a suite of linked habitats; (b) a tree sprouting and inducing scour, deposition of fine sediment, and trapping of wood pieces to form a pioneer island; (c) an island complex with deposited trees, pioneer islands, and established islands distributed across an extensive gravel surface. From Gurnell et al. (2005).

A second contribution of driftwood to island establishment is provided by vegetative regeneration of deposited trees and shrubs, which is associated to an even higher plant and island growth rate. This effect is referred to as *living wood benefit* (Gurnell and Petts, 2002). In turn, islands contribute to the biocomplexity of riverine corridors because of the physical proximity of different habitats. Very high plant and seed diversity has been observed, especially in the early phases of establishment of pioneer islands (Kollmann et al., 1999; Gurnell et al., 2005).

In braided rivers, vegetation development and successional processes are limited by the high frequency of disturbances which determine the complete erosion of most islands within a few tens of years from their formation (Zanoni et al., 2008). On the contrary, the lower rate of channel change typical of meandering rivers implies that vegetation originating from wood deposits can develop into mature forest patches sustaining distinctive plant communities. In these systems, stable driftwood accumulations such as bar apex jams help the formation of old stands that provide key members for jams in a positive feedback process (Abbe and Montgomery, 1996; Abbe and Montgomery, 2003; Montgomery and Abbe, 2006).

2.2.7 Management issues

Historically, in-channel wood has been considered as a hazard (due to its association with channel obstruction, flood risk and debris flows), an obstacle to human activities such as navigation and generally an undesirable sight in rivers. Risk perception, combined with the exploitation of driftwood as a readily available source of fuel, resulted in the removal of driftwood from rivers in densely populated areas (Angradi et al., 2004; Piegay et al., 2005; Comiti et al., 2006; Millington and Sear, 2007). Le Lay et al. (2008) investigated the perception of in-channel wood in ten countries and found that its presence in streams is mostly associated with danger and a need for improvement. However, significant cross-cultural variability occurs. Familiarity with forested landscapes and access to education and environmental information result in a more sympathetic approach to wood in rivers.

It is worth noting that driftwood transport does contribute to inundation risk and property damage especially in case of mass wasting events such as debris flows. Its effects are particularly severe at critical cross sections such as narrow bridges, where wood accumulation can damage man-made structures and increase the risk of overflowing (Mazzorana et al., 2011). As a consequence, the presence of wood is taken into account in risk management models as for example in Mazzorana et al. (2012). At the same time, the positive contribution of wood to channel diversity and ecosystem functioning is now widely recognised and many river restoration projects include wood reintroduction in previously cleared rivers.

The need for a balance between river ecosystem preservation / restoration and safety prompted researchers to define guidelines for a sustainable management of in-channel wood. Three key concepts were introduced in early studies (Robison and Beschta, 1990; Gurnell et al., 1995; Gippel et al., 1996b; Gurnell and Sweet, 1998):

- common management practices including channel clearance can actually increase flood risk;

- the magnitude of hydraulic effects of in-channel wood strongly depend on element and channel properties and therefore indiscriminate wood removal is not justified on the basis of safety issues;

- the artificial, localised reintroduction of wood in rivers has a positive but limited effect on ecosystem functioning; a holistic, catchment-scale approach is required to achieve long-lasting effects.

Channelization and removal of standing vegetation and existing wood jams is known to reduce wood retention, implying that floating pieces are more likely to be transported and reach critical cross-sections (Piégay and Gurnell, 1997; Braudrick and Grant, 2000; Angradi et al., 2004). Selective harvesting of large trees from riparian woodland deprives streams of potential key members, strongly limiting jam formation and therefore wood stability (Abbe and Montgomery, 1996). Wood removal can also result in a relevant increase in sediment mobility and bank erosion (Smith et al., 1993; Gurnell and Sweet, 1998). Piégay and Gurnell (1997) pointed out that in large multi-thread systems wood accumulations have an almost negligible impact on reach-scale hydraulics but are very relevant for habitat diversity, implying that wood removal in these systems is likely to have little or no desirable effects.

Gurnell et al. (1995) and Gippel et al. (1996b) observed that even in small and medium streams, only a small proportion of driftwood elements are large enough to significantly increase the risk of overbank flow and therefore proposed selective removal as opposed to indiscriminate channel clearance. The authors also provided guidelines for wood reintroduction and noted that optimal positioning of wood (streamlined pieces, simple shapes) can produce positive feedbacks on river functionality without significantly compromising hydraulic efficiency. Localised, selective interventions also include the reconfiguration of critical cross-sections and man-made structures (Mazzorana et al., 2011).

Wood reintroduction consists in the placement of wood across river channels either as individual logs or as complex structures referred to as *engineered log jams*. This technique has been successfully employed as a restoration measure in systems characterised by channel degradation, excess sediment transport and poor habitat variety (Brooks et al., 2006). Experimental wood placement also shows positive effects in terms of organic matter

retention (Díez et al., 2000; Millington and Sear, 2007), exchanges with groundwater (Sawyer and Cardenas, 2012), and composition of invertebrate and fish communities (Shields et al., 2006; Coe et al., 2009). Kail et al. (2007) analysed the outcomes of a large number of river restoration projects carried out on German and Austrian systems, all including wood reintroduction in streams. The authors observed that *soft-engineering* methods based on the placement of non-fixed elements mimicking natural wood jams are more successful and cost-effective than *hard-engineering* solution based on fixed structures. However, various authors stress that the positive effects of *active* wood restoration practices (that is, wood placement) are spatially and temporally limited and indicate *passive* strategies as the method of choice for long-term, large scale restoration. The goal of passive methods is the restoration of naturally occurring wood recruitment processes through preservation of riparian woodland, improvement of floodplain-channel connectivity and reinstatement of a dynamic flow regime (Díez et al., 2001; Kail et al., 2007; Manners and Doyle, 2008).

2.3 Investigating driftwood in braided rivers

2.3.1 The braided river context

Comparatively few studies specifically address driftwood in multi-thread rivers, yet the geomorphic and ecological processes that shape braided networks produce distinctive conditions for wood recruitment and dispersal, namely a) spatially complex geometry and inundation dynamics; b) intense reworking due to flood events; and c) strong interactions with standing vegetation.

Multi-thread systems show intense fluctuations of hydraulic and geometry parameters – including channel width and slope, flow depth and velocity, shear stress and sediment load – over various temporal and spatial scales (Ashmore, 1991; Hoey and Sutherland, 1991; Ashmore, 2001; Foufoula-Georgiou and Sapozhnikov, 2001; Lane, 2006; Ashmore, 2009; Bertoldi et al., 2009c). Networks are characterised by relatively flat cross-sections which result in distinctive at-a-station relationships between flow stage and wetted width; a small increase in discharge can produce a significant expansion of inundated area (Ashmore and Sauks, 2006; Bertoldi et al., 2009a). Therefore, substantial variations of inundation pattern and major changes in bank line position occur even during moderate flood events. As a consequence, wood is dispersed over a wider area, forming smaller deposits compared with accumulations found in single-thread streams.

Moreover, Mosley (1982) observed that flow depth distribution across a braided network does not change significantly with increasing discharge, as a consequence of the

concurrent deepening of existing channels and formation of new shallow anabranches. Therefore, numerous low-depth, low-velocity areas are available even for moderate to high flow and these sites guarantee wood deposition retention over a wide range of discharges. Finally, water level has been shown to vary between anabranches at the same cross section, thus enhancing the variability of relative elevation of deposited wood within the network, (Zolezzi et al., 2006; Luchi et al., 2007).

Most gravel-bed braided streams exhibit a near-natural flow regime with sequences of flood events determining rapid turnover of channel pattern (Mosley, 1982; Mosley, 1983; van der Nat et al., 2002; van der Nat et al., 2003b; Lorang et al., 2005; Malard et al., 2006; Doering et al., 2007) and the associated recruitment, transport, dispersal and remobilisation of driftwood. Various studies underlined that, in braided networks, morphological evolution is the product of a multiplicity of formative discharges, with local-scale and reach-scale effects determined by small and large floods, respectively (Bertoldi et al., 2009b; Surian et al., 2009; Bertoldi et al., 2010). Therefore, flood event magnitude exerts a strong control on the extent of both channel and wood turnover; at the same time, it governs interactions and feedbacks between sediment and wood transport and standing vegetation including riparian stands and islands.

Islands, a distinctive feature of many braided river reaches, play a key role in both wood supply and retention. Alongside vegetated banks, they act as key wood sources as localised erosion is the dominant wood recruitment mechanisms in large braided rivers (Gurnell et al., 2000b; Gurnell et al., 2001; Zanoni et al., 2008). Moreover, Bertoldi et al. (2011b) show that the presence of islands influences bed morphology at local and reach scale, which in turn affects the retentiveness of the network. Vegetation increases local bed surface roughness, decreasing flow velocity and favouring the local deposition of sediment and wood. Rapid accretion results in high relative elevation of islands, which become preferential deposition sites of driftwood transported by large floods. At the same time, flow in island-braided reaches tend to concentrate in a lower number of deeper, faster channels enhancing mobility of floating driftwood elements. Therefore, complex feedback mechanisms link the presence of islands to wood storage in braided systems; overall, the observations of van der Nat et al. (2003a) suggest that island-braided reaches are net sinks of wood.

Past research on wood dynamics in braided systems has been devoted mostly to a) the evaluation of stored wood volumes (Piégay et al., 1999; Gurnell et al., 2000b; van der Nat et al., 2003a; Wyżga and Zawiejska, 2005); b) the investigation of the drivers of wood accumulation, survival and regeneration (Gurnell et al., 2001; Francis, 2007; Moggridge and Gurnell, 2009); and c) the assessment of the geomorphic and ecologic role of deposited wood (Kollmann et al., 1999; Gurnell and Petts, 2006). On the contrary, limited quantitative information is available in the literature about wood dispersal patterns in multi-thread

systems (in terms of typical travel distance, planar and vertical distribution of deposits and jam size distribution). Moreover, various factors are known to influence driftwood dispersal, including element properties, wood supply, channel geometry and evolution and flow regime. The relative relevance of these factors and their specific contribution to wood mobility and retention have been explored in single-thread systems, but little data are available for the specific case of braided networks. Finally, the understanding of processes governing the persistence of deposits over time and long-term wood budgets in a multi-thread context is still incomplete.

2.3.2 Field observations

The investigation of morphodynamics and wood dispersal in multi-thread rivers is a particularly challenging task due to the large spatial scale of phenomena and the frequent occurrence of morphologically relevant events. Over the last two decades, a wide range of remote-sensing methods have been developed and tested with the aim of obtaining reliable, detailed data covering extensive river reaches. Aerial and satellite imagery are widely employed to reconstruct planform dynamics (Mosley, 1982; Malard et al., 2006; Boruah et al., 2008; Bertoldi et al., 2011a; Hervoue et al., 2011), while three-dimensional information is derived from photogrammetry (Lane et al., 1993; Lane, 2000; Lane et al., 2010) or, more recently, LiDAR surveys (Bertoldi et al., 2011b). However, aerial imagery and LiDAR surveys, while allowing for extended coverage, do not allow for high temporal resolution and are normally used to characterise pre/post event scenarios. On the contrary, ground-based automated imagery provide an economic way of monitoring channel morphodynamics with high temporal and spatial resolution, albeit at a relatively limited scale (Chandler et al., 2002; Ashmore and Sauks, 2006; Bertoldi et al., 2010).

Both direct surveys and remote-sensing methods are used to characterise wood dispersal in braided rivers. Direct surveys are a popular method for the estimation of wood volume and have been applied to several European rivers using transect-based survey protocols (Piégay and Gurnell, 1997; Gurnell et al., 2000b; Wyżga and Zawiejska, 2005; Gurnell and Petts, 2006) as well as random-block design procedures (van der Nat et al., 2003a). However, various authors observe that the highly heterogeneous spatial distribution of large wood in braided rivers can determine significant errors in the estimation of wood volume on the basis of line-intersect sampling strategies (Gippel et al., 1996a; van der Nat et al., 2003a; MacVicar et al., 2009). Early attempts to map wood deposits on aerial images had limited success, most likely due to the low resolution of images (Piégay et al., 1999; Marcus et al., 2002), but recent improvement in instrumentation – including the use of low-altitude, unmanned vehicles – proved that it is possible to reliably map wood as small as 0.1 m in diameter (MacVicar et al., 2009).

MacVicar et al. (2009) provide a detailed comparison of a range of techniques for the quantification of wood budget, including repeated surveys of stored wood – both from direct observation and aerial images – dating of residence time using ^{14}C or dendrochronology and tracking using tags, transponders and video monitoring. The authors observe that traditional direct surveying techniques – including the use of plastic/metal tags to track individual wood pieces (Kollmann et al., 1999; van der Nat et al., 2003a) – are ill-adapted to large rivers because of the low spatial density of wood and higher mobility of individual pieces. In contrast, active and passive radio transmitters, possibly also in combination with high-frequency ground-based and/or video monitoring (Bertoldi et al., 2013) allow for easier long-term piece tracking.

2.3.3 Physical modelling of wood dynamics in rivers

Laboratory-scale modelling offers the opportunity to reproduce and investigate fluvial processes under controlled conditions and to overcome logistic issues typical of field-scale monitoring such as exceeding costs and time and safety constraints. To the author's knowledge, no published study has attempted to investigate driftwood dispersal in braided rivers at flume scale. However, physical modelling has been employed to address a variety of wood-related issues and these studies provide useful information on key model assumptions, experimental protocols and surveying techniques. Laboratory-scale models have been used to investigate:

- local scale hydraulic effects of wood (afflux and scour);

- incipient motion and drag forces acting on logs;

- log transport distance, transport style (congested/uncongested) and typical accumulation style over a range of channel morphologies and in presence of obstacles;

- the role of wood properties (log length, diameter, shape, density, orientation), wood supply (input rate and position) and channel properties (roughness, discharge, morphology).

To evaluate hydraulic effects of wood and incipient motion, wood is placed in the flume at pre-determined locations and elements are assigned a chosen orientation with respect to flow. In most cases, the quantification of afflux has been carried out using driftwood elements fixed to flume bed and/or walls (Ranga Raju et al., 1983; Cherry and Beschta, 1989; Young, 1991; Gippel et al., 1996a; Wallerstein et al., 2001, 2002; Wallerstein, 2003). Incipient motion and drag are usually investigated using individual wooden elements, thus neglecting the interaction between pieces. An exception is represented by

Gippel et al. (1996b) who surveyed the hydraulic influence of debris fields generated by random aggregations of multiple (fixed) elements.

Wood dispersal is simulated by generating an input flux of wooden elements at convenient locations, most frequently at the upstream end of the flume but also along the banks (Bocchiola, 2011). Transport styles (congested/uncongested) are simulated by controlling input volume and frequency (Braudrick et al., 1997; Bocchiola et al., 2008). Driftwood elements are generally simulated using wooden dowels (density ranges between 0.4 and 0.8 kg/dm^3), but other materials such as aluminium (Wallerstein et al., 2001) and plastic (Gippel et al., 1996b) have been employed. In the vast majority of cases, only cylindrical pieces have been used, with the notable exceptions of Braudrick and Grant (2000) – who tested incipient motion of logs with disc-shaped root boles – and Gippel et al. (1996b), who evaluated the hydraulic effects induced by an irregularly-shaped piece simulating an uprooted tree with roots and branches.

A range of diameter and length values have been used, with the majority of dispersal simulations reproducing *medium* river conditions, while afflux, scour and incipient motion are usually tested in *small* river configurations (Wallerstein, 2003; Mutz et al., 2007). Braudrick and Grant (2001) specifically addressed wood transport over a range of channel configurations including flat-bed straight channels, alternate and mid-channel bars and weakly sinuous channels, but little or no data are available for large river conditions and complex, multi-thread networks. The effect of standing vegetation has been simulated by introducing randomly spaced vertical cylinders in a flat bed flume (Bocchiola et al., 2006b; Bocchiola et al., 2008).

A key aspect of the vast majority of studies available in literature is that wood dynamics are simulated under clear water conditions, that is, below the threshold for bed motion or over a fixed bed as in the case of Bocchiola et al. (2006b; 2008; 2011). Sediment motion occurs only as the consequence of local scour determined by the presence of wood, with the exception of the study of Braudrick et al. (1997) where log motion is simulated over a fully mobile bed. In this study, self-organised morphologies are obtained by running the flume in absence of wood. Overall, information about the concurrent effect of wood dispersal and sediment mobilisation is very limited.

Finally, most studies focused on the investigation of wood processes in a general riverine context rather than on the reproduction of a specific river reach at small (flume) scale. Wallerstein et al. (2001) highlighted the need for rigorous scaling procedures to predict real-scale processes from laboratory-scale experiments. Physical modelling of a specific reach requires the definition of geometric, kinematic and dynamic similitudes. Geometric similitude implies the consistency of geometric ratios and produces undistorted models, kinematic similitude requires the conservation of particle path length to travel time ratios and dynamic similitude consists in the preservation of the proportion between forces.

Dynamic similitude is attained with appropriate choices of materials, roughness, density, viscosity and surface tension and can be expressed as the invariance of relevant dimensionless ratios (Froude, Shields and Reynolds numbers) between model and real-scale reach.

It is worth noting that the conditions on Froude and Reynolds numbers can not be respected simultaneously. The condition on Re is usually relaxed once the establishment of turbulent flow is attained. Studies addressing incipient motion and drag force estimation (Braudrick and Grant, 2000; Wallerstein et al., 2001; Wallerstein et al., 2002; Bocchiola et al., 2006a) were carried out under subcritical flow conditions and both the Reynolds numbers of flow and woody elements range between $3 \cdot 10^3$ and $7 \cdot 10^4$, corresponding to turbulent flow, albeit not fully developed. Shields and Gippel (1995) note that these conditions are representative of most piedmont rivers and even if higher values of Reynolds are observed at field scale, the drag coefficient does not change significantly for fully turbulent flow.

3 Field observations

3.1 Objectives

The present chapter is devoted to the investigation of channel morphodynamics and driftwood dispersal in real-scale braided rivers. The main goal of field activities is to provide a deeper knowledge of the distinctive channel and wood patterns observed in multi-thread systems and to investigate their main drivers, with special focus on the role of flood events. A second objective is the collection of detailed data on the physical properties of driftwood to be used as reference values for the design of laboratory-scale models.

Field surveys were carried out over a time span of two years on the gravel-bed braided Tagliamento River (northeast Italy). This riverine system is almost unique in Europe for its low level of management (Ward et al., 1999) and allows the study of braided river morphodynamics and wood dispersal in near-pristine conditions. Data were acquired using a combination of direct measurements and remote sensing techniques; in particular, software-controlled, ground-based cameras provided valuable information during flood events with high temporal resolution. Monitoring activities focused on three main issues, namely: a) assessing the response of braided networks to discharge fluctuations in terms of inundation and channel pattern reworking; b) characterising flood-induced recruiting and dispersal of driftwood; and c) defining typical distributions of driftwood size and shape.

Braided networks exhibit substantial changes in channel configuration even for moderate floods (Mosley, 1982; Mosley, 1983; van der Nat et al., 2002; van der Nat et al., 2003b; Lorang et al., 2005; Malard et al., 2006; Doering et al., 2007). In the present study, ground-based imagery was used to reconstruct the planform configuration of a braided network over a wide range of flow conditions. Changes in the spatial configuration of water bodies (*inundation dynamics*) were analysed with the following objectives:

- defining at-a-station relationships between water level and morphological parameters (wetted area, channel connection, braiding index, shoreline length);

- quantifying the temporal variability of the above at-a-station relationships due to flood-induced morphological changes and the persistence of river features;

- investigating the effect of standing vegetation on planform configuration and turnover rate of channel pattern.

At-a-station relationships between flow and morphological parameters have been proposed for multi-channel systems (Mosley, 1983; Robertson-Rintoul and Richards, 1993; Chew and Ashmore, 2001; van der Nat et al., 2002; Luchi et al., 2007; Bertoldi et al., 2009c), but these relationships are often based on databases covering a limited range of discharge values, because of the difficulty in surveying the network configuration at high flow levels. Previous works recognized vegetation as a crucial parameter controlling fluvial forms and processes and showed that bed stability induced by root reinforcement is able to limit the complexity of braided networks (Tal and Paola, 2007; Braudrick et al., 2009; Gurnell et al., 2009; Eaton et al., 2010; Bertoldi et al., 2011b; Crosato and Saleh, 2011). However, very few field data are available on this topic.

A second objective of field surveys is the investigation of the effects of flood-induced wood input events. Bank erosion has been identified ad the dominant driver of wood supply in large rivers (Gurnell et al., 2000b; Downs and Simon, 2001; Moulin and Piégay, 2004; Lassettre et al., 2008). In the present work, wood recruitment and dispersal were monitored with the following aims:

- deriving mechanistic understanding of wood delivery by bank erosion to a large braided river during single flood events;

- investigating the fate of the delivered wood in terms of local storage on braid bars, linking wood dynamics to the bed elevation of deposition sites.

Over the last three decades, numerous studies have quantified the amount and styles of wood retained in fluvial systems – e.g. see review by Gurnell (in press) – but direct measurements of wood recruitment and transport/retention remain relatively rare across all sizes and styles of river. The correlation between the size of the eroded area and quantity of in-channel deposited trees has so far been explored mainly at a reach rather than a local scale and at relatively coarse timescales, and no data currently exists on the proportion of wood pieces (uprooted trees) that are retained close to erosion sites.

Finally, typical distributions of driftwood diameter and/or length are proposed in literature (Bilby and Ward, 1989; Hering et al., 2000; Moulin and Piégay, 2004; Andreoli et al., 2007; Manners and Doyle, 2008), but in many cases data refer to low-order streams, often flowing through old-growth unmanaged forests. In contrast, riparian vegetation in multi-thread riverine systems is usually made up mainly by young stands, as a consequence of the higher disturbance frequency and/or level of human intervention. Driftwood volume and piece size are therefore expected to be smaller (Piégay and Gurnell, 1997; Beechie et al., 2006; Dufour et al., 2007). Moreover, little information is available on element shape and in particular on root wads, even if roots are known to exert a strong control on element mobility.

3.2   Study site

3.2.1 The Tagliamento River

The Tagliamento River (Figure 3.1) is a large, gravel-bed, braided river in NE Italy that drains from the Alps to the Adriatic Sea. It shows an essentially pristine, highly dynamic braided morphology for most of its 172-km long course (Ward et al., 1999; Tockner et al., 2003). The catchment covers an area of about 2580 km^2 and is characterised by transitional, alpine to Mediterranean climatic conditions. Average annual precipitation can be as high as 3000 mm in the prealpine area of the catchment (Doering et al., 2007). As a result, the river shows a bimodal, flashy pluvio-nival regime. Discharge peaks in spring and in autumn but floods of different magnitude can occur all over the year (Gurnell et al., 2001; Tockner et al., 2003). Although water abstraction for hydropower generation and irrigation occurs in the upper course, this is limited compared to other catchments in the Alps. The river maintains a near-natural, dynamic flow regime (Bertoldi et al., 2009b), where a wide range of discharges is responsible for the river evolution (Surian et al., 2009).

The active floodplain in the braided sections of the river is up to 1.5 km wide and is bordered by nearly-continuous riparian vegetation with *Populus* and *Salix* being the dominant tree genera. Vegetative regeneration, particularly from uprooted trees deposited on gravel bars, is the main process leading to the formation of vegetated islands (Gurnell et al., 2001; Gurnell et al., 2005; Gurnell and Petts, 2006). A relevant portion (approximately 8%) of the braided riverbed is covered by large patches of mature trees that show a relatively fast turnover, on average 20 years (Zanoni et al., 2008). The prealpine section of the river is characterised by specific patterns of surface-ground water interaction, induced by the presence of a natural rocky constraint (the Pinzano gorge). The alternation between downwelling and upwelling reaches controls water availability and hence growth performance of the riparian trees, determining large, local variations in the vegetation abundance (Bertoldi et al., 2011a).

Inundation dynamics and wood dispersal were investigated on two 1-km long reaches – referred to as Cornino and Flagogna – located 9 and 3 km upstream of Pinzano, respectively. The two sites are characterised by a maximum width of 900 m (Cornino) and 650 m (Flagogna) and have similar flow conditions (no major intervening tributaries), longitudinal bed slope (approximately 0.35%), and grain size (D_{50} = 40 mm), but significantly different vegetation abundance. The Cornino reach can be defined as *bar-braided*, with a few vegetated patches formed by sparse, shrubby vegetation. In contrast, in the *island-braided* Flagogna reach dense woody vegetation is found especially on the right part of the braided riverbed. A considerable fraction of fine sediments is trapped by the vegetated patches. Due to the larger number of islands, the Flagogna site shows a larger

main channel (Bertoldi et al., 2011b). Within the two study sites, more than 90% of the basal area of trees in the riparian forest and on established islands belong to one species, *Populus nigra* (Karrenberg et al., 2003).

During the 2008-2010 period, bank erosion during high flows was observed at two locations, within a secondary braid channel on the left of the braid plain at the Cornino study site and within the main braid channel at the Flagogna study site. This main channel carries approximately 60% of the discharge, whereas the secondary anabranch at Cornino carries no more than 20% of the discharge. In late 2010, the main channel in Cornino also caused extensive bank erosion on right side of the braidplain.

3.2.2 Remote sensing facilities

The two study sites are well suited for ground-based remote sensing of riverine features due to their proximity to steep cliffs. Two cameras have been installed in June 2006 on Monte Prat (overlooking the Cornino reach) and in March 2008 on Monte Ragogna (for the Flagogna reach) and are managed by the University of Trento. The cameras (Figure 3.2) are located approximately 350 m above the floodplain, with an horizontal distance between the camera and the floodplain ranging from 0.5 to 1.4 km for both reaches.

1 Venzone gauging station
2 Villuzza gauging station
3 Camera on M. Prat
4 Cornino reach
5 Camera on M. Ragogna
6 Flagogna reach
7 Pinzano gorge
⋯⋯ Area covered by images
● Wood survey locations
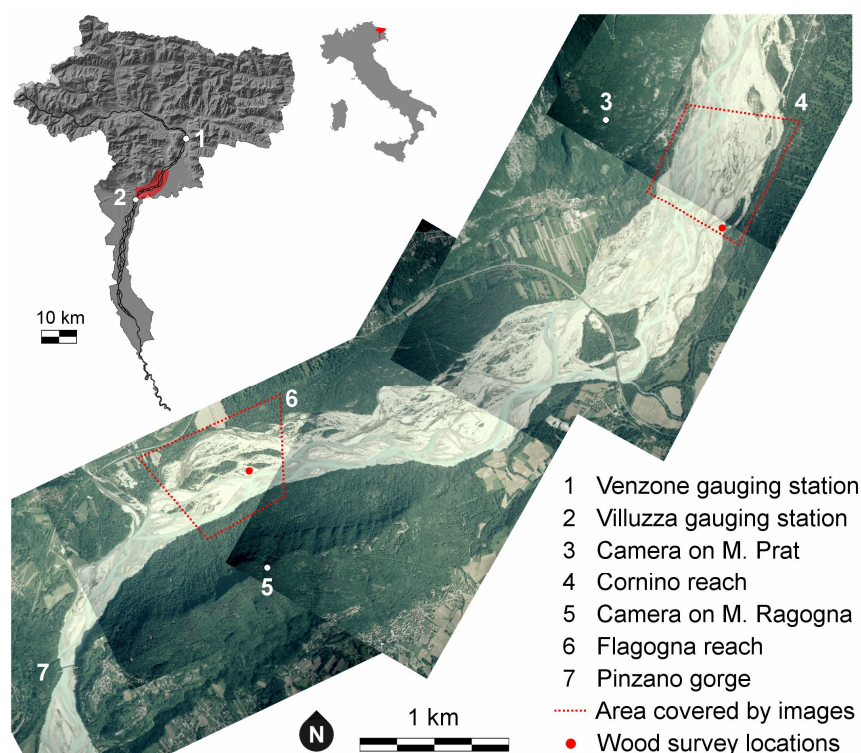
Figure 3.1: Location of the study sites, ground-based cameras and gauging stations within the Tagliamento River catchment. Aerial image acquired in 2009, courtesy of Nicola Surian.

The system consists of solar-powered digital reflex cameras (Nikon D40) with an 18 mm lens and a 6M pixel CCD sensor. The set-up is similar to that used by Chandler et al. (2002) and by Ashmore and Sauks (2006), but in this case picture acquisition and storage is software controlled, with the possibility to set up acquisition time depending on seasonal conditions. A time resolution of 1 hour during daylight was chosen in order to gather a sufficient number of images during rapid floods. Moreover, the extensive database offers the opportunity to reconstruct morphological evolution caused by sequences of high flow events. An example of the use of pictures obtained by this survey system is proposed by Bertoldi et al. (2010) for the analysis of bank erosion and channel shift as a function of flood intensity.

It is worth noting that imagery data do not provide information on bed topography. Recent improvements in remote sensing techniques greatly increased the possibility to map river features and in particular LiDAR and multispectral surveys allow to produce three-dimensional image of the river and to compute bed elevation and/or water depth (Winterbottom and Gilvear, 1997; Antonarakis et al., 2008; Feurer et al., 2008; Legleiter et al., 2009; Marcus and Fonstad, 2010). Nevertheless, these techniques are limited in terms of temporal accuracy, as before/after flood surveys are the best possible scenario. On the contrary, ground-based surveying systems can be automated and their acquisition frequency can be increased without facing prohibitive costs (Chandler et al., 2002; Ashmore and Sauks, 2006).

Figure 3.2: Ground-based camera on Monte Prat overlooking the bar-braided Cornino reach (A) and on Monte Ragogna over the island braided Flagogna (B, white arrow). Flow is from left to right in (A), towards the camera in (B).

3.3   Inundation dynamics

3.3.1 Data acquisition and elaboration

River stage data

Inundation dynamics were investigated over a study period of two years extending from March 2008 to February 2010. During this period, 14 bed-moving flood events occurred, three of which were approximately bankfull (Bertoldi et al., 2009b). Figure 3.3 shows the hydrometric record with 30-min interval data for the Venzone gauging station, located 15 km upstream of the Cornino reach. A water stage equal to 3 m at Venzone roughly corresponds to a 2 years return period. Data were made available by the Servizio Idrografico of the Friuli Venezia Giulia Region[1]. Currently, no official stage-discharge relationship is available for this or any other gauging station on the Tagliamento and therefore water level is used to describe flow conditions. A flow level duration curve was computed for the Venzone station, using a 6-year record covering the 2004-2009 period. Instantaneous flow conditions occurring at Cornino and Flagogna reaches were associated to stage data acquired 1.5 and 2 hours earlier at Venzone, respectively. Flood propagation celerity was estimated for a set of 20 events over the 2002-2009 period by comparing stage data recorded at Venzone with records at the Villuzza gauging station, located 23.5 km downstream. An average travel time of 2.65 hours between the two hydrometric stations was computed, though no clear relationship between peak water level and travel time was found. It is worth noting that a reliable estimation of the water level at the study reaches is particularly relevant during the flashy summer floods, when stage can vary by up to 2 m in a few hours.

Pictures acquisition and selection

Planform configuration of the two study reaches was surveyed using the aforementioned ground-based remote sensing system. A set of 68 images of the two sites was used to characterise the different inundation conditions, with water level at the Venzone hydrometric station spanning a 3 m range. Available pictures cover five different flood events and span a wide range of level duration, from around 330 days/year to few hours/year. Highest points are close to bankfull, though peak flood often occurred at night or under low visibility conditions (fog or heavy rain). A second set of pictures was used to investigate channel reworking induced by floods. For both sites, 12 images corresponding to low flow conditions and 12 for high flow conditions were selected (Figure 3.3).

---

[1] http://www.regione.fvg.it/rafvg/cms/RAFVG/ambiente-territorio/tutela-ambiente-gestione-risorse-naturali

The low flow level (approximately 0.05 m at Venzone) corresponds to a water stage that is exceeded approximately 180 days/year. The high flow level (approximately 0.8 m) represents the condition in which about 50% of the riverbed is submerged and is exceeded 6 days/year. Pictures for the high flow level cover all but two of the 14 bed-moving events that occurred in the study period; the threshold for sediment movement was evaluated following Surian et al. (2009). For the two remaining events, power shortage prevented image acquisition. Overall, 114 pictures of the two reaches were used to completely characterise the inundation dynamics over the two years study period.

Image processing and relevant landform types identification

Oblique pictures were rectified using about 15 GPS-surveyed ground control points, through the Leica Photogrammetric Suite of ERDAS Imagine™. The final image resolution is 1 m for the Flagogna reach and 2 m at Cornino. Planform configuration (gravel bars and water bodies) was manually digitised on each rectified image using the open source GRASS GIS 6.4.2 software[1]. Manual classification was preferred due to the presence of disturbances such as shadows produced by trees, reflections on water surfaces, variability of water and gravel colour that were likely to cause misinterpretations.

In the present study, four classes were used to map the planform configuration and describe the inundation dynamics: gravel bars (class 1), upstream connected water bodies (class 2), partially or totally disconnected water bodies (class 3) and vegetated patches (class 4). In the last case only riparian vegetation (trees and shrubs) was taken into account while aquatic plants and herbs were excluded, as the stream power is too large for these plants to affect the bed morphology on a reach scale. Class 3 comprises ponds and all water
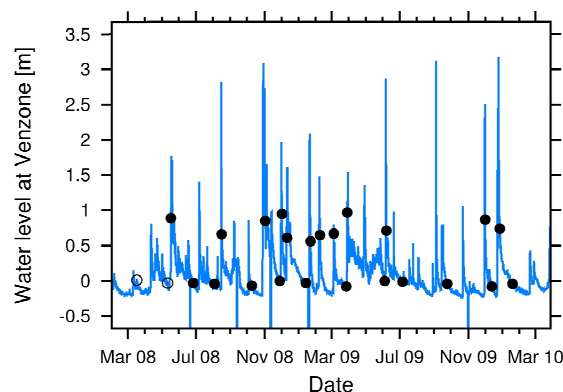
Figure 3.3: Water stage record at Venzone hydrometric station during the study period and timeline of selected pictures for the constant-level analysis. Filled dots represent picture availability for both sites, circles represent images for single sites.

---

[1] http://grass.osgeo.org

bodies whose upstream end was clearly identifiable inside the study reach area, such as backwater channels and groundwater-fed channels. These water bodies differ substantially from full connected channels in terms of water depth, velocity and temperature and their presence significantly enhances aquatic habitat diversity (Arscott et al., 2002; Gray et al., 2006; Sukhodolov et al., 2009). Figure 3.4 presents four examples of digitised maps at each site, showing variations in inundation patterns under increasing water levels (*H* in Figure 3.4 is the water level measured at Venzone hydrometric station, in cm). Vegetated patches are reported only at the lowest flow level, for clarity of the pictures (their area does not change with water level).

A set of four geometrical parameters was automatically computed for each map, in order to characterise the planform configuration, namely: a) the wetted area proportion, evaluated as the ratio between the total wetted area (sum of classes 2 and 3) and the total river corridor area; b) the proportion of disconnected water bodies, computed as the ratio between class 2 and the sum of classes 2 and 3; c) the braiding index (*BI*), evaluated as the reach-averaged value on a set of 16 cross-sections with a spacing interval of about 60 m (Egozi and Ashmore, 2008); d) the shoreline length, computed as km of shoreline per km of river reach. The latter two parameters describe the network complexity, with the shoreline length measuring the extent of aquatic/terrestrial habitat interfaces.

For each cross section, the braiding index was assigned by visually counting all downstream-connected water bodies intersecting the cross-section line, regardless of their condition at the upstream end (in this way excluding all the ponds, but considering the groundwater-fed channels). Gravel bars were taken into account as emerging landforms separating two channels according to their size compared to the width of the adjacent channels. Values of *BI* obtained by visual interpretation were compared with values obtained through an automatic procedure, which takes into account only gravel bars larger than a threshold area. The choice of the threshold does not influence the shape of the braiding index-water stage relationship; a minimum area of 10000 m^2 minimises the difference between the values of *BI* computed by the two procedures.

3.3.2 Results

Planform configuration at variable water level

Morphological parameters extracted from the digitised maps are shown in Figure 3.5 as a function of the water level at Venzone. Inundation dynamics are described through the wetted area extension (Figure 3.5A), as a proportion over the total active corridor area, i.e. excluding floodplain woodland. The 68 images analysed for the two sites cover a range from 10 up to 90 % of wetted area.
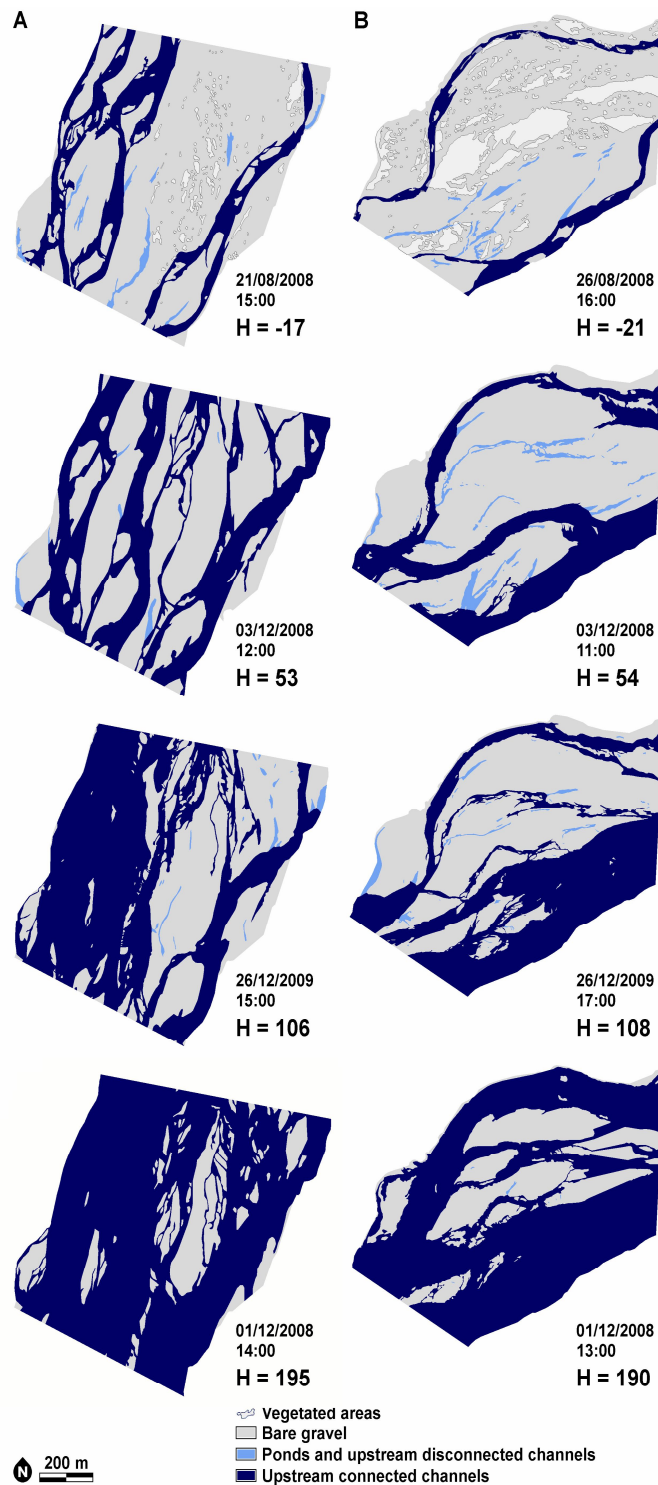
Figure 3.4: Examples of inundation maps for the Cornino (A) and Flagogna (B) reaches showing a range of flow conditions, with the four classes (gravel, upstream connected channels, upstream disconnected channels and vegetation). For figure clarity vegetated areas are reported only at the lowest flow level. H represents water level measured at Venzone hydrometric station (in cm).

Both sites show an almost linear increase of the wetted proportion with water level. The island braided Flagogna site is characterised by a lower wetted area, particularly at medium to high levels.

Figure 5B reports on the ratio between the area of upstream disconnected water bodies (e.g. pools, backwaters and groundwater-fed channels) and total wetted area. At low flow, up to 16% of water bodies area is not connected and therefore characterised by quite different values of flow velocity and water temperature. As water level increases, this ratio decreases rapidly at Cornino, where almost no disconnected water bodies are present at water stage higher than 0.5 m. On the contrary, at Flagogna the ratio keeps higher up to 1 m, with nearly 10% of wetted area still partially or totally disconnected from the network at a water level equal to 0.5 m. At Flagogna, more intense upwelling occurs due to the downstream narrowing in the Pinzano gorge, originating several groundwater-fed branches at low flow. In this case, some scatter of the data may be due to the difficulty in mapping relatively small ponds that are likely to be hidden by vegetation. Nevertheless, the distinct decreasing trend matches those found by Arscott et al. (2002) and van der Nat et al. (2002) for the same study reaches.
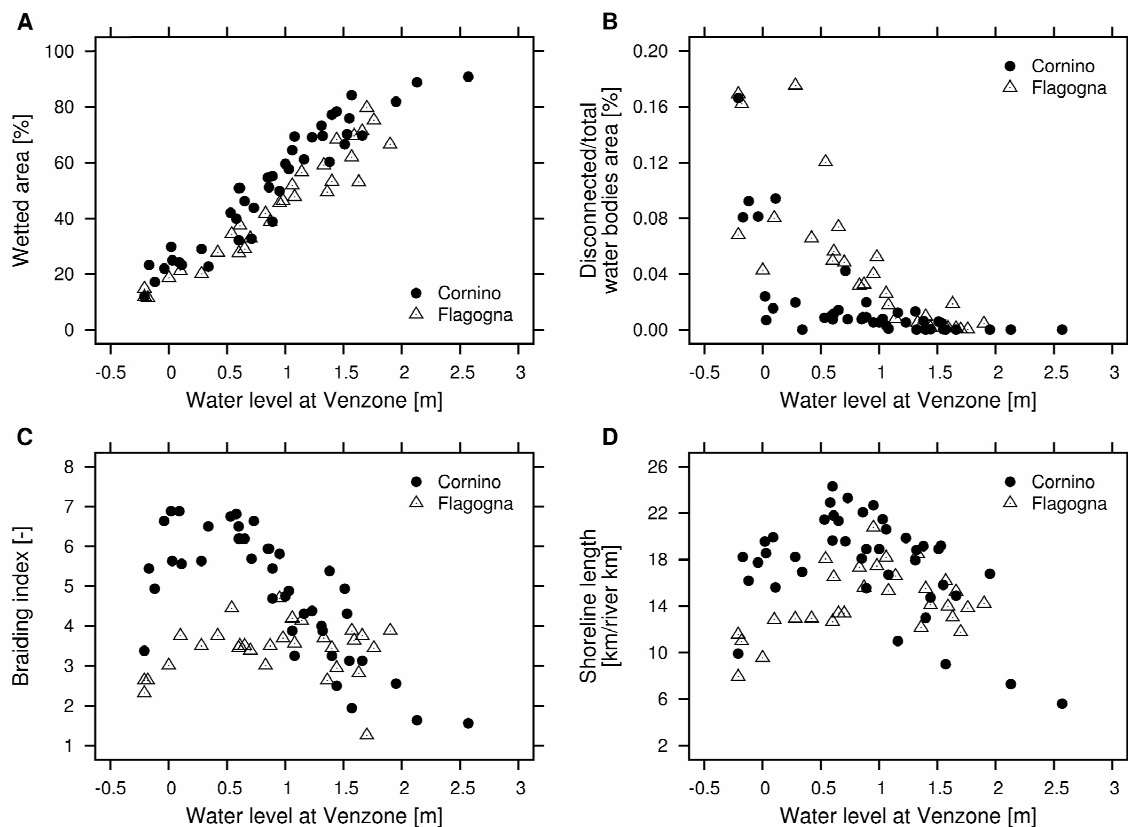
Figure 3.5: At-a-station variability of morphological parameters with water level: wetted area proportion (A); disconnected water bodies ratio (B); braiding index (C); shoreline length (D).

Network configuration is also described by the braiding index (Figure 3.5C). In both reaches the number of branches increases from 2-3 at low flow up to a maximum for water levels of approximately 0.5÷1 m. At higher flows the branches start to coalesce, determining a drop of the *BI* to values close to 1 for a water level higher than 2 m. The two reaches are quite different in terms of maximum braided index: up to 7 branches per cross section (average on the reach) are observed at Cornino, whereas at Flagogna the maximum is about 5, with most of the data falling below 4. Finally, in Figure 3.5D the shoreline length is plotted. On the y-axis, the minimum value of 2 km per river km corresponds to the shoreline length of a straight channel. Both study reaches show values higher than 20 km/river km, with the shoreline length exceeding 6 km/river km even at very low or high flow. This parameter shows a trend similar to that of the braiding index, with a maximum at a water level of approximately 0.5÷1.0 m and generally lower values at Flagogna.

To add a temporal dimension to the inundation analysis the wetted area and the disconnection ratio are plotted in Figure 3.6 as duration curves, i.e. substituting the water level with the number of days per year in which the given level is exceeded. Figure 3.6A shows the wetted area proportion for the two reaches. Water occupies approximately 20% of the active corridor area for most of the year, exceeding 40% for less than 10 days per year. This suggests that the Tagliamento braided corridor is a mainly terrestrial habitat, subject to strong flood disturbances. Figure 6B highlights the role of disconnected water bodies in the island-braided Flagogna reach. These features represent a significant proportion of the total wetted area for most of the year, dropping below 8% for only 10 days per year. In contrast, upstream disconnected water bodies do not exceed 8% of the total for approximately 100 days at the Cornino reach.
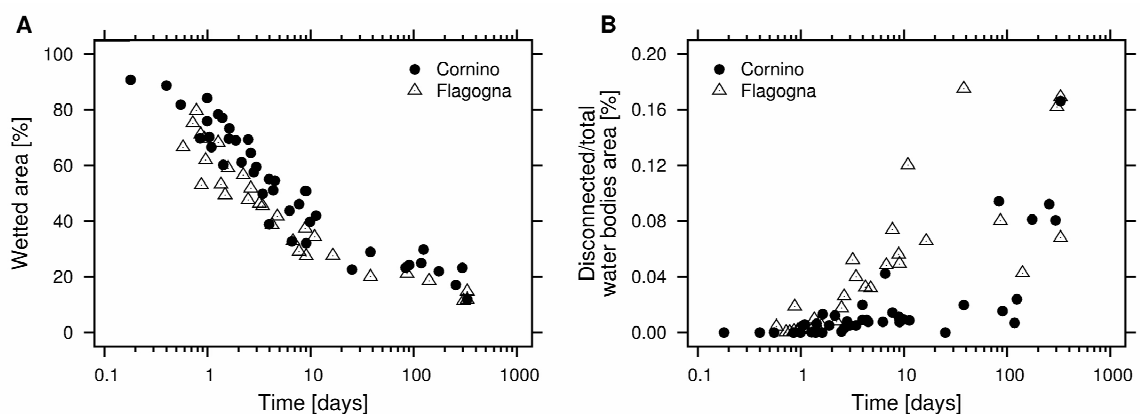
Figure 3.6: At-a-station variability of morphological parameters with water level, shown as a function of water level duration: wetted area proportion (A); disconnected water bodies ratio (B).

The effect of morphological changes

The two sets of images taken at given flow level (roughly corresponding to 0.05 m and 0.80 m at Venzone station) were used to quantify the role of floods in modifying planform morphology and the related parameters (namely wetted area proportion and braiding index). Results are reported in Figure 3.7 for both sites and water level ranges. Figures 3.7A and 3.7B show the changes in the wetted area proportion for the lower and higher water level, respectively. In both cases variations up to 10÷15% are observed. Differences are smaller at Flagogna reach, particularly at low water level, where the wetted proportion fluctuates between 13 and 22%. On average, greater variations occur at the higher water level (at Cornino the wetted area ranges from 39% to 55%).

The braiding index shows large fluctuations at both low and high water level (Figure 7C, D). Changes in the cross section geometry induced by floods can increase (or decrease) the average *BI* by 2÷3 channels for a given flow stage. At the higher water level the variability is slightly lower, with changes limited to 1÷2 channels. At low flow, the *BI* shows a similar fluctuating behaviour at both sites (Figure 7C), with two minima separated by approximately 16 months. The *BI* increases from 2.5 to 4.5 at Flagogna and from 3.5 to 7.0 at Cornino between August 2008 and March 2009; subsequently, a decreasing phase starts and the number of branches reduces close to the minimum observed value. These behaviour can be interpreted in terms of the stochastic variability of bed topography and/or of sediment supply. There is no evidence of major changes in the sediment input in the two reaches, therefore a possible explanation may be related to the aggrading and degrading phases that have been also observed in flume experiments with constant water discharge (Hoey and Sutherland, 1991). Here in particular the simultaneous increase in braiding index and wetted area at low flow that occurred between August 2008 and March 2009 might have been produced by aggradation leading to a larger number of wide, shallow channels. Such a configuration in turn increases the chances of merging of channels as water level rises, which may explain the decrease of the braiding index at intermediate flow over the same period observed in Figure 3.7D.

In principle, one could expect a relationship between flood magnitude and the extent of change in morphological parameter; however, no consistent trend is found in the present dataset. Generally, larger floods induce more substantial changes in the planform configuration, though this is not always the case. Figure 3.7 also reports the water level recorded at the Venzone hydrometric station, to facilitate the comparison between flood magnitude and occurred changes in the planform configuration. For example, the relatively small July 2008 flood (peak level lower than 1.5 m at Venzone) caused the braiding index to drop by approximately 1.5 channels at Cornino at the lower water level; in contrast, after the December 2009 bankfull flood the braiding index decreased by less than one channel.

Moreover, data show that single avulsion/deposition phenomena are able to significantly modify reach-averaged morphological parameters at low flow. For instance, the opening of a bifurcation in the main channel at Flagogna after the November 2008 flood was almost entirely responsible for the increase in braiding index observed in Figure 3.7C between October and December 2008. Hence, single channel/bar-scale phenomena may have a disproportionately large influence on reach-averaged parameters, which may also be a consequence of the limited length of the study reaches.

Morphological changes induced by floods are likely to be the main cause of the scatter of the data in Figure 3.5, which is particularly evident in braiding index (Figure 3.5C). This parameter fluctuates at a given level on a similar range of values as found with the variable stage analysis, thus confirming field observations by Mosley (1983). The wetted area proportion shows greater stability, as the linear increase with the water level (Figure 3.5A) is not undermined by the fluctuations at constant level (Figure 3.7A, B).
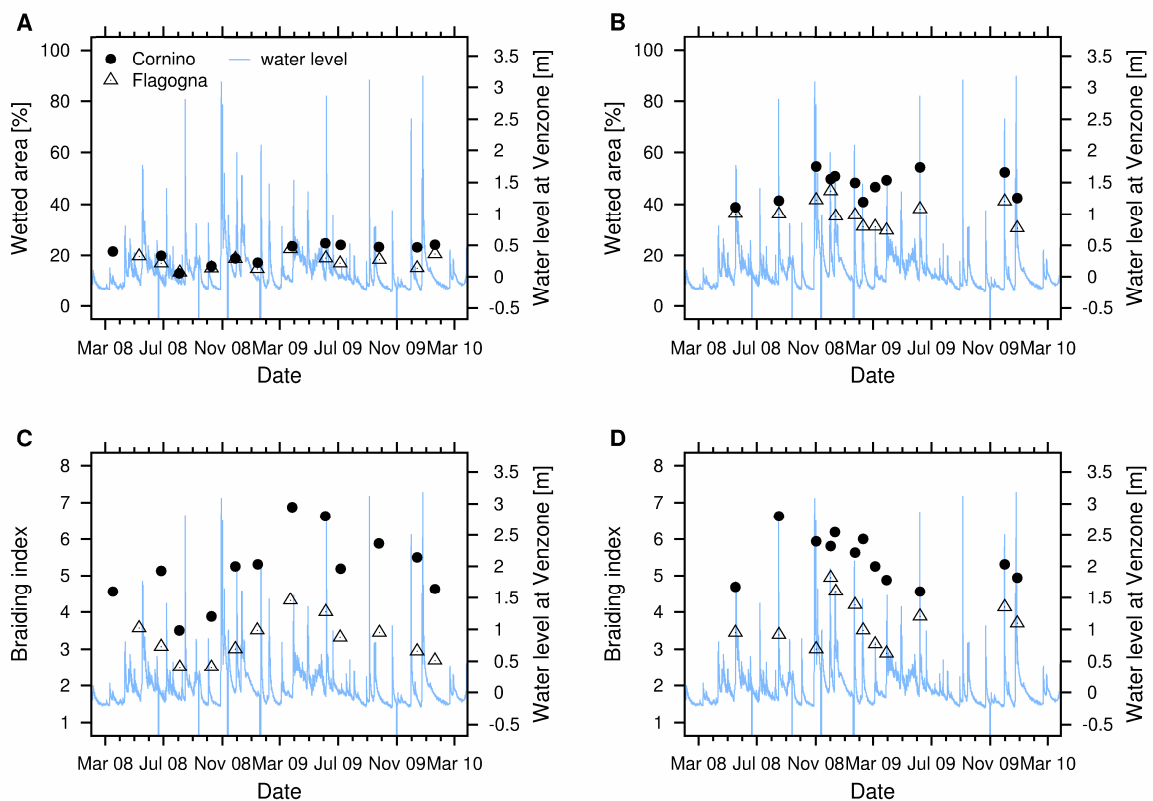
Figure 3.7: Variation of morphological parameters over time at constant water level for the two chosen level ranges. The wetted area proportion and the braiding index for the lower (A, C) and higher water level (B, D) are reported, respectively. Lines represent the water level recorded at the Venzone hydrometric station.

43

Water bodies turnover and their interaction with vegetation

The turnover of water bodies (and hence aquatic habitats) was investigated by comparing the planform pattern of channels before and after bed-moving events. The analysis was performed by combining the 12 maps at low flow level (approximately 0.05 m at Venzone station, see Figure 3.3), reclassified as binary wet/dry maps. For each area unit (pixel) persistence was computed as the maximum number of consecutive maps in which the area was classified as wet. Values in the resulting persistence map range from 0 (areas that were never occupied by water on the 12 maps at low water level) to 12 (areas permanently occupied by water on the 12 maps). Class 1 corresponds to channels that are wet in a single picture, but not in the previous and the following one; these areas were assigned a duration of 2 months (the average time interval between subsequent images).

Persistence maps are shown in Figures 3.8A and 3.8B for Cornino and Flagogna, respectively. Here, persistence is expressed in terms of water bodies' lifespan, assuming an average time interval of 2 months between maps. For clarity, wetted areas lasting for more than 12 months have been aggregated to a single class. The intense reworking of the braidplain occurring in the bar-braided Cornino reach is evident, with 62% of the active riverbed occupied by low flow channels at least for 2 months. In contrast, the island-braided Flagogna reach exhibits a more stable channel pattern, with low flow patterns confined to approximately 46% of the active tract area. Here, the main branch on the left side of the corridor and a secondary channel flowing along the right bank are quite stable and therefore clearly recognizable in Figure 3.8B (darker areas). In particular, the channel on the right experienced only minor variations during the whole study period, due to the confinement of vegetation, especially flourishing in this area.
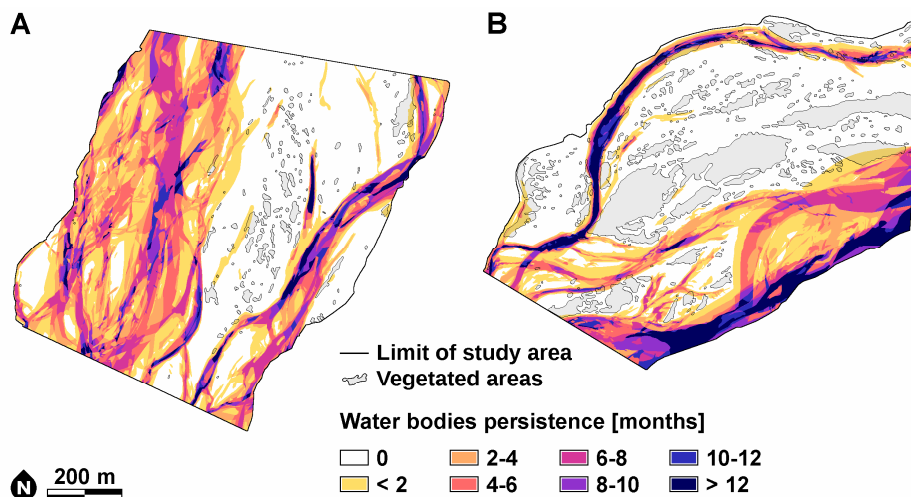
Figure 3.8: Water bodies persistence maps at Cornino (A) and Flagogna (B) reaches. Vegetated areas within the active tract are outlined on the maps.

Table 3.1:   Statistics of vegetation abundance and turnover rate for the two study reaches.

	Cornino reach	Flagogna reach
Total vegetated area / total reach area	4%	21%
Area of persistence class 0 / total reach area	38%	54%
Vegetated area in persistence class 0 / area of persistence class 0	9%	34%
Vegetated area in persistence class 0 / total vegetated area	86%	88%
Bare gravel area in persistence class 0 / total reach area	35%	36%

Conversely, water bodies persisting for more than one year correspond to 3% of the wetted area at Cornino, as opposed to 13 % at Flagogna (Figure 3.9). Short-lived water bodies, i.e. areas classified as wet on at least one picture, but for a period shorter than 2 months, sum up to more than 30% of the wetted area in both reaches.

Since only small changes occurred in the vegetation distribution during the study period, in Figure 3.8 the maximum extension of vegetated patches is reported. It is worth pointing out that typical time scales of vegetation evolution are generally longer than 2 years, though erosion of few patches after the bankfull floods occurred. Statistics on vegetation and channel mobility are summarized in Table 3.1. In the island-braided Flagogna reach vegetation occupies on average 21% of the whole active corridor area, whereas trees and shrubs cover only 4% of the active area in the Cornino reach. On average, at both sites 87% of trees cover falls in persistence class 0 (i.e. areas that were never occupied by water at low flow), showing that riparian vegetation generally lays at a higher elevation and is able to reduce bank erosion. A detailed analysis of the composition of class 0 shows that vegetation covers 9% of this class at Cornino, as opposed to 34% at Flagogna. Moreover, if vegetated areas are excluded from class 0, a similar proportion (approximately 35%) of the two study sites is occupied by bare gravel throughout the two year period.
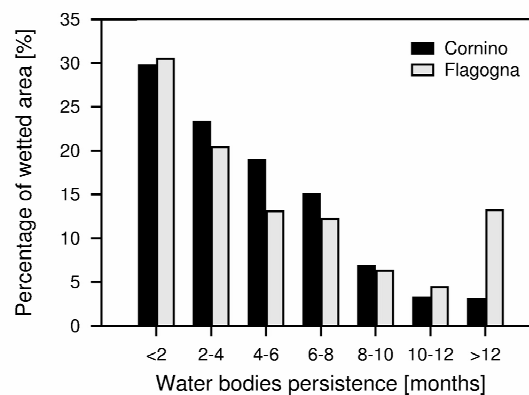
Figure 3.9: Distribution of water bodies over persistence classes.

3.3.3 Discussion

At-a-station relationships

Data on water area extension at increasing flow stage can be expressed as at-a-station relationships between discharge (Q) and reach-averaged free surface width (W). The latter was computed as the wetted area to reach length ratio, consistently with Ashmore and Saucks (2006). Figure 3.10 shows the measured points, with the fitting curves in the form of power law $W \sim Q^n$. A similar trend is found in both reaches, with the exponent n falling in the range 0.52÷0.53. A wide range of values of n has been documented for braided rivers. For example Mosley (1983) and Smith et al. (1996) reported lower values ($n \sim 0.3$) falling in the typical range of single thread channels (Ferguson, 1986). More recently, Ashmore and Saucks (2006) showed that in the proglacial Sunwapta River the width/discharge relationship can be described by a linear function (or by a power law with a coefficient close to 1). Such a large exponent means that cross sectional averaged flow velocity and depth do not increase with discharge as fast as in single thread channels, therefore affecting sediment transport processes. This behaviour has been also confirmed by laboratory and numerical findings of Bertoldi et al. (2009c) who computed an exponent equal to 0.7.

The cause of these discrepancies in the at-a-station width/discharge relationship is not yet known. Different explanations have been proposed that involve the effect of vegetation (Smith et al., 1996) and the flow regime (Ashmore and Sauks, 2006). Data from the Tagliamento River presented in this work give support to the latter, as no significant difference can be observed in the two reaches with contrasting vegetation abundance. On the other hand, the Tagliamento river experiences large discharge fluctuations, with floods of different magnitude being responsible of morphological changes, in contrast to the limited flow variability observed in the Sunwapta river and in the flume experiments of Bertoldi et al. (2009c). An extensive field study by Booker (2010) on 326 gauging stations across New Zealand showed that at-a-station width prediction can be improved by considering the catchment area, therefore underpinning the relevance of the flow regime. More theoretical and empirical research is needed in order to understand how fluvial pattern and flow regime affect the at-a-station relationship.

Different relationships have been proposed in the literature also for the braiding index. For example, Mosley (1983) surveyed four braided rivers in New Zealand and found that the number of channels at a cross-section remains constant over a wide range of discharges, from low flow up to the mean annual flood. For the Tagliamento, the observed unimodal relationship between water level and *BI* apparently does not match the almost linear increase proposed by van der Nat et al. (2002) for the same reaches. However, all but one of the braiding index values reported by van der Nat et al. (2002) correspond to water levels

lower than 2 m at Villuzza, which sets the threshold between a predominantly terrestrial environment and a fully connected surface aquatic system (Bertoldi et al., 2009b). Therefore, the lack of a falling limb in the plot by van der Nat et al. (2002) may be attributed to an under-representation of medium-to-high flow conditions.

The occurrence of a maximum in *BI* is consistent with the obvious observation that at very high flow its value must drop to 1 as the entire active corridor is likely to be submerged. An analogous behaviour was also documented by Egozi and Ashmore (2008) both on the Sunwapta river and in flume experiments. The above observations, along with the results of 1D numerical modelling (Bertoldi et al., 2009c) and the data reported here show that the peak of the *BI* occurs at a level lower than the mean annual flood. This implies that anabranches tend to merge at this stage and therefore most of the previously exposed bars are submerged. Significantly, the present data set shows that the maximum of the braiding index corresponds to a flow level where the proportion of exposed area falls under 50%. Data presented here show that the relationship between braiding index and discharge is complex, difficult to measure, highly variable over time due to network reworking and quite sensitive to the occurrence of vegetated patches.

The role of vegetation

The two study reaches are characterised by largely different vegetation abundance (4% and 21% of the total area, at Cornino and Flagogna, respectively), whereas discharge, longitudinal slope and grain size keep similar. Vegetation colonisation along the Tagliamento is controlled by ground water dynamics and hence moisture availability (Bertoldi et al., 2011a). Annual tree growth rate can be 2 to 3 times faster in the Flagogna reach, due to ground water upwelling forced by the Pinzano narrow gorge (Doering et al, (2007) and Tom Gonser, personal communication).

Recent analysis of the Tagliamento river morphology highlighted the effect of vegetation in modifying the bed elevation distribution (Bertoldi et al., 2011b). Vegetated
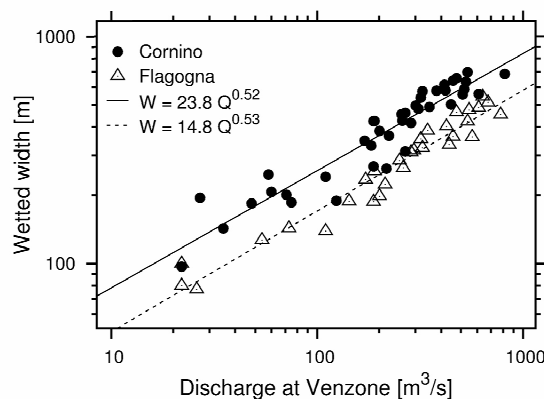
Figure 3.10: Wetted width (W) - discharge (Q) relationships for the two sites and power-law fitting curves.

islands present a much higher bed elevation (due to fine sediment deposition) and are rarely inundated by water, thus reducing the flow area at Flagogna reach. This is clearly visible in Figure 5A, where the island-braided reach shows lower values of wetted area proportion especially at medium to high stages. The occurrence of stable islands determines also the confinement of the flow (particularly at low to medium stages) in smaller and deeper channels. This effect is evident when considering the braiding index (Figure 5C). The average number of branches at Flagogna is roughly half of that at Cornino for a water stage ranging between 0 and 0.7 m at Venzone. On the contrary, *BI* is on average larger at Flagogna at higher flow stage (1.5÷2 m) as the occurrence of vegetated patches (that are not submerged at this stage) are more likely to split the flow in a larger number of branches.

Furthermore, vegetation contributes to the higher proportion of upstream disconnected channels at Flagogna, particularly at flow levels ranging between 0 and 0.5 m. The presence of vegetation enhances the formation and persistence of elongated ponds in large, deep scour holes located along the sides of established islands (Gurnell et al., 2005).

A strong link between vegetation distribution and channel pattern persistence is evident at both sites, with tree cover concentrating in areas that were never occupied by low flow channels during the study period. Turnover data show that the proportion of class 0 to the active tract area is much larger in the island-braided Flagogna reach, where it is 54%, compared to the Cornino reach where it is 38%. Therefore, vegetation colonisation affects the bed morphology mainly by confining and stabilising the channels, whereas the bare gravel area which is never part of a low flow channel is not reduced (approximately 35% in both reaches).

These differences were not recognised in the study by van der Nat et al. (2002), who showed a largely similar behaviour of both reaches in terms of wetted area and braiding index. However, vegetation developed massively in the Flagogna reach in the last 10 years after two large floods in 1996 and 2000 (Bertoldi et al., 2009b). Different sequences of floods (and in particular prolonged absence of intense floods) may cause fluctuations of vegetation diffusion, changing the morphological response of the river as well (Bertoldi et al., 2011a). The persistence maps obtained in the present study demonstrate that the presence of vegetated patches contributes to the higher bed stability of the Flagogna reach, reduces the turnover of bars and islands and hence produces a more favourable environment for vegetation growth. This sequence of processes can establish a positive feedback – described as a 'fluvial biogeomorphic succession' (Corenblit et al., 2007) – and lead to the transition from a fully braided system (like the Cornino reach) to a more stable, vegetated fluvial form.

3.4   Wood dispersal

3.4.1 Remote sensing and field data

Wood recruitment caused by bank erosion of two islands – one at each of the Cornino and Flagogna sites – and in-channel storage of the recruited wood were investigated using a combination of remote sensing and field measurements. Figure 3.11 shows an oblique image of the Cornino site, with marked bank erosion and a clear plume of deposited trees immediately downstream. Four data sources were used, namely: a) airborne LiDAR surveys collected in May 2005 and August 2010; b) oblique photographs captured every hour by ground-based cameras overlooking the two study sites; c) field measurements of standing and deposited trees gathered during June 2010; and d) continuous records of river stage obtained from the Venzone gauging station.

The airborne LiDAR data sets were analysed using the free software FUSION, developed by the U.S. Department of Agriculture, Forest Service, Remote Sensing Applications Center[1]. Analysis of the 2005 data supported the extraction of a digital elevation model (DEM) and the average tree height and vegetation density of the riparian forest on parts of the two islands that were subsequently eroded. The DEM had a resolution of 2 m (the survey had approximately 1.05 points/m²), whereas vegetation parameters were aggregated at a 5 m resolution. Accuracy of the DEM and the vegetation properties was checked through field measurements, showing the errors were limited to a few centimetres for the bed topography and 0.5÷1 m for vegetation height; see Bertoldi et al. (2011b) for further details.

Figure 3.11: Oblique photograph showing bank erosion (left) and tree deposition within the active channel (centre and right) at Cornino, 24 March 2010. Flow is from left to right.

[1] http://www.fs.fed.us/eng/rsac/

Analysis of the 2010 data provided a DEM of the extent of the riparian forest following erosion by several large floods and also the bed morphology of the area where eroded trees were deposited. Because the Cornino bank erosion area was located farther from the camera than that at Flagogna, the photographs for Cornino were of lower resolution, limiting the degree to which they could distinguish between particular erosion or deposition events. Following geocorrection, photographs from the cameras were used to quantify a) changes in bank position; and b) the number and positions of deposited trees before and after two floods (in December 2009 and May 2010) that caused significant bank erosion at Flagogna and two floods (late October to early November 2008 and December 2009) that caused significant bank erosion at Cornino.

Field observations collected during June 2010 provided two sets of information. First, measurements of the species, density, and diameter of standing trees were obtained from eleven 10 m x 10 m plots located adjacent to the two areas of eroding river bank at Cornino (six plots) and Flagogna (five plots) to characterize the riparian forest at the time of field survey. Where the tree top was visible, tree height was also measured using a clinometer so that height could be related to other tree dimensions, and these data were augmented with additional tree height and diameter data obtained from trees that were fully exposed along the top of the eroding banks at the two study sites. Second, measurements of the species, diameter, and height/length of all trees deposited within the active channel close to the eroding banks characterized the dimensions and travel distance of those trees that were retained close to their recruitment site. The geographical locations of all surveyed standing and deposited trees were recorded by hand-held GPS.

Finally, flow stage records from the upstream gauge were used to interpret flow conditions at the time of tree deposition as recorded in the oblique photos. The flow stage record was also used to characterise the recurrence interval of the observed floods. The two events occurred between late October and early November 2008, and during December 2009 (see Figure 3.3). Flow peak stages of 2.72 m and 3 m corresponded to recurrence intervals of approximately 1 and 1.5 years, respectively. The flood in 2008 followed a period of 4 years characterised by low flow and negligible bank erosion. The flood in May 2010 was smaller, with a flow peak stage of 1.65 m and a recurrence interval of 3÷4 months.

3.4.2 Data analysis

Analysis of the data sets provided information on three aspects of wood recruitment and retention. First, the field observations collected in June 2010 were analysed to compare the species and dimensions of trees present in the standing vegetation adjacent to the eroding banks with those deposited nearby within the active channel, and also to describe the spatial distribution of the deposited trees in relation to their source areas.

Second, estimates of the impact of some flood events on the local wood budgets at the two sites were made. The 2010 field measurements of tree dimensions in plots within the standing vegetation were related to properties of the 2005 LiDAR data for the same sites in order to allow tree density and height to be estimated across the riparian forest at the time of the eroding floods. The eroded areas observed from the geocorrected oblique photographs were then overlain on the 2005 LiDAR data to estimate the number of trees that were recruited during the bank erosion events. These estimates were then compared with the number of trees deposited within the active channel immediately after each erosion event as recorded by the oblique photographs. By combining these different estimates, it was possible to estimate the proportion of the recruited trees that were retained close to their source within the active river channel during each flood event.

Thirdly, the process of wood retention was investigated in more detail at Flagogna, because the resolution of the oblique photographs of the bank erosion and tree position was higher than at Cornino. This was achieved by combining the river stage hydrograph for the 2009 and 2010 flood events with the river bed topography data from the 2010 LiDAR surveys and the oblique photograph observations of tree deposition during the events.

3.4.3 Results

Comparison between deposited trees and standing vegetation on the eroding bank

The deposited and standing trees observed in the field in June 2010 showed similar height:diameter ratios at the two sites. When the dimensions of the deposited trees were visually compared with those located along the top of the eroding banks, there was a tendency for deposited trees to have a slightly larger diameter than standing trees of the same height at Flagogna (Fig. 3.12B), whereas the distributions were very similar at Cornino (Fig. 3.12A). The standing and deposited tree data sets at each site were compared using multiple regression analysis incorporating a dummy variable to distinguish
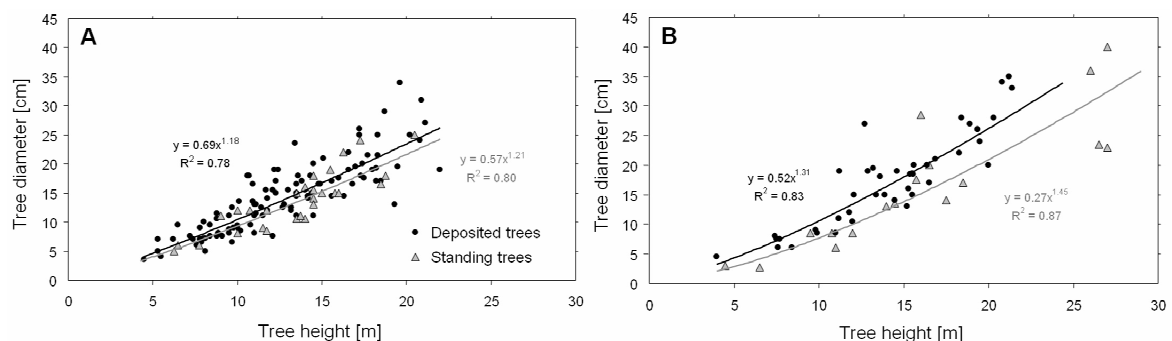
Figure 3.12: Diameter and heights of standing trees in the riparian forest adjacent to the eroding river banks and deposited nearby within the active channel in June 2010 at Cornino (A) and Flagogna (B).

deposited trees (*dummy* = 1) from standing trees (*dummy* = 0). For each site, the tree diameter and height variables were $\log_{10}$ transformed and then $\log_{10}$(*tree diameter*) was regressed on three variables: $\log_{10}$(*tree length*), the dummy variable and the product of the dummy variable and $\log_{10}$(*tree height*). There was no significant difference in the regression slope for deposited or standing trees at either Cornino or Flagogna (i.e. the regression coefficient for the variable *dummy · log10(tree height)* was not significantly different from zero, $p > 0.05$).

However, when the regression models for each site were re-estimated after removing this variable, there was a significant difference ($p < 0.05$) in the regression constant for the deposited and standing data sets at both sites (i.e. the regression coefficient for the dummy variable was significantly greater than zero, $p < 0.05$). Thus, even at Cornino, the deposited trees had a slightly larger diameter than standing trees of the same height ($p = 0.03$) and at Flagogna the difference was highly significant ($p < 0.001$). Cumulative frequency distributions (Figure. 3.13) further illustrate the similarity in the dimensions of standing and deposited trees at Cornino (Figuress. 3.13A and C), and the divergence in dimensions between the standing and deposited trees at Flagogna, particularly in the height of the tallest trees (Figures. 3.13B and D). The large differences at Flagogna and the presence of a few particularly large standing trees(Figure 3.13B) are probably due to the history of the
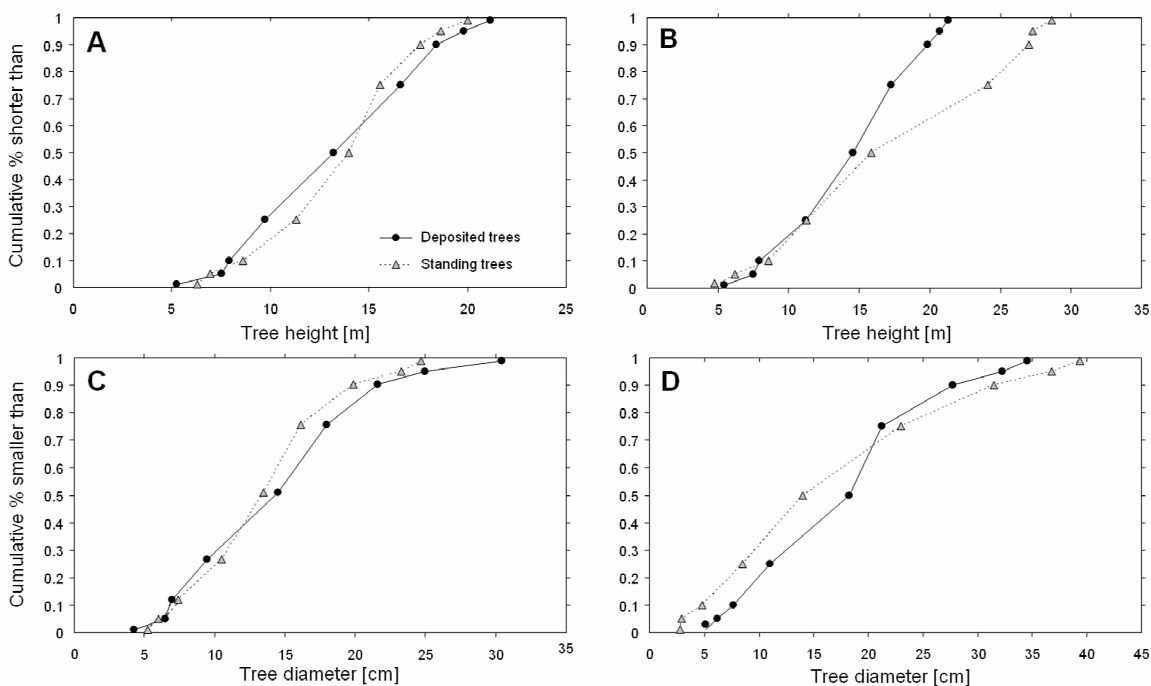
Figure 3.13: Cumulative percentage frequency distributions of tree height (A, B) and tree diameter (C, D) recorded within quadrats in the riparian forest adjacent to the eroding river banks and deposited on the active channel in June 2010 at the Cornino (A, C) and Flagogna (B, D) study sites.

eroded island that was formed by the coalescence of vegetated areas of different age. A second difference between the two sites was the number of trees deposited together to form each jam. Figure 3.14 illustrates a tendency for trees to be deposited individually at Flagogna, with only eight locations showing two trees deposited together and only two locations with more than two trees deposited. In contrast, Cornino showed jams with up to seven trees deposited together and numerous jams of two, three and four trees. Lastly, the spatial distribution of trees and jams of different size was quite random at Flagogna (Figs. 3.15E and F), whereas at Cornino the largest trees (Fig. 3.15B) and the largest jams in terms of tree numbers (Fig. 3.15C) were closest to the bank erosion site.

Local wood budgets

Figure 3.16 shows oblique photographs of the Flagogna site before, during, and after the December 2009 flood. The Figure illustrates not only the potential to identify newly deposited trees but also to track changes in the position of the eroding island bank from the oblique photographs. Information extracted from the photographs provides the first two inputs into the estimation of a local wood budget: the area of woodland eroded and the number of trees deposited locally. The extent of bank erosion identified from the oblique photographs and attributable to the two erosion events observed at Cornino and Flagogna were overlain on air photographs obtained in 2005 at the same time as the LiDAR survey (Figures. 3.15A and D, respectively). This historical LiDAR data allowed estimation of the properties of the woodland that was eroded. LiDAR surveys have been widely used in forestry to monitor tree height, density and growth, e.g., Naesset (2002) and the recent review by Wulder et al. (2012). Here we use the LiDAR data to infer the number of trees that have been uprooted by the flood. We computed the proportion of the points in the LiDAR record that had an elevation at least 5 m higher than the ground surface (hereafter
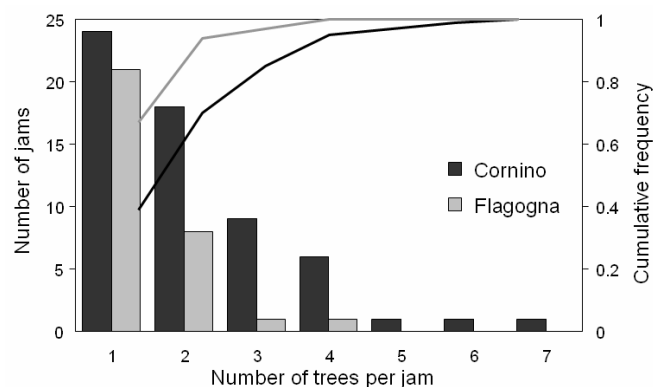
Figure 3.14: Frequency distributions of the number of trees deposited within each wood accumulation in the active channel during June 2010 at the Cornino and Flagogna study sites.

called *proportion of tree points*) in order to estimate the woodland density at that time. Spatial differences in the proportion of tree points in the LiDAR signal in 2005 reflect differences in the forest structure at that time. Because the riparian trees continued to grow at these undisturbed sites from 2005 until the erosion events, it was possible to relate the proportion of tree points information to spatial differences in ground measurements across the forest survey plots in 2010.

Four measures of the forest plot structure in 2010 (total number of trees and number of *P. nigra* trees with a diameter exceeding thresholds of both 5 and 10 cm diameter) were used to examine associations with the proportion of tree points data at the same locations in 2005. It is apparent from Figure 3.17 that the calibrations between ground measurements and LiDAR measurements were most effective at Flagogna (Figure 3.17 C and D), reflecting the wide variety in forest characteristics observed across the five plots at that site. Unfortunately, the six plots at Cornino showed rather similar properties (Figure 3.17 A and B), and so the calibration equation depends heavily upon the assumption that it should pass through the origin of the calibration graph. Because of the generally smaller trees at the Cornino site, Figure 3.17 illustrates calibration relationships with a threshold 5 cm tree
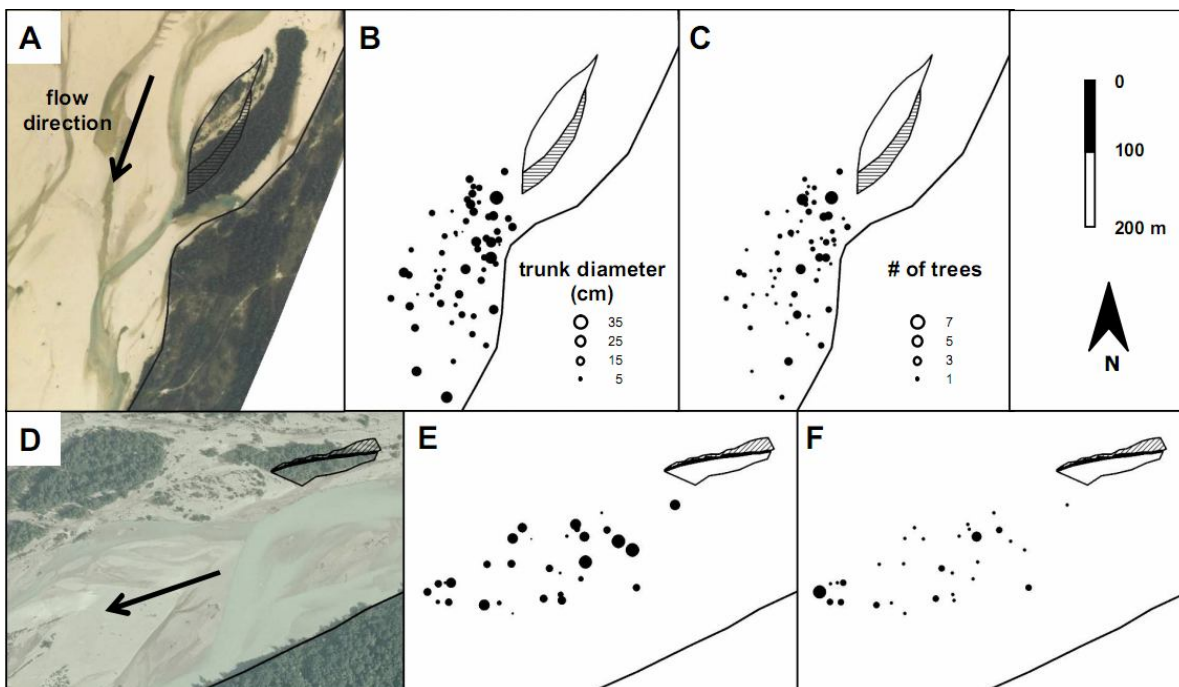
Figure 3.15: Areas of bank erosion in the first (unshaded) and second (cross-hatched) floods superimposed on aerial photographs of the study sites taken in 2005 (A, D), showing the relative sizes of the trunk diameters of deposited trees (B, E) and the relative number of trees in each accumulation (C, F) at the Cornino (A, B, C) and Flagogna (D, E, F) study sites (for Cornino, the two floods were in October-November 2008 and December 2009; for Flagogna, the two floods were in December 2009 and May 2010).

diameter for that site and the larger 10 cm threshold at Flagogna. In practice, calibrations were estimated for both sites using both threshold tree diameters, and these were used to estimate the number of trees of different size eroded in different events from the 2005 LiDAR density data.

Table 3.2 presents estimates of the area of bank eroded in each event at each site (estimated with an accuracy of 25 m² from the geocorrected photographs), the average proportion of tree points in the eroded areas (estimated from the 2005 LiDAR data), and the number of all trees and of *P. nigra* alone with diameters exceeding 5 and 10 cm that were recruited into the channel by this erosion (estimated from the calibration equations). These estimates of the number of recruited trees are compared with the observed deposited trees using the same threshold diameters of 5 and 10 cm. Whilst the dimensions of the deposited trees were measured in the field, the trees that were deposited by particular events were identified from the oblique photographs.
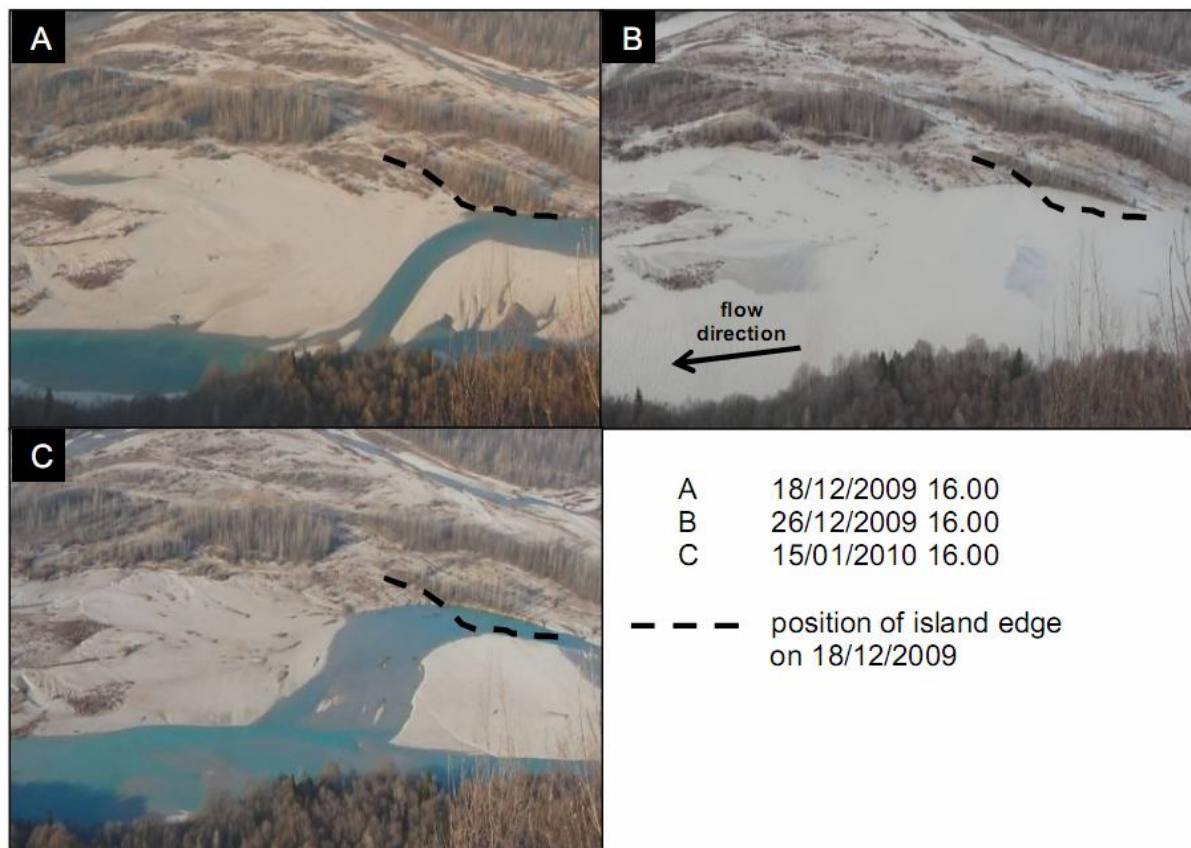
Figure 3.16: Flagogna study site showing (A) the position of the island's bank on 18 December, prior to the December flood; (B) bank erosion and tree deposition within the active channel on 26 December during the flood; and (C) the position of the post-flood island bank and deposited trees (river flows from right to left of the photographs).

Local wood budgets are estimated in Table 3.2 for *P. nigra* based on comparing the number of trees deposited to the estimates of those eroded, accounting separately for trunk diameters exceeding 5 and 10 cm. Because of the lower resolution of the photographs for Cornino, the 2009 flood cannot be easily separated from the 2008 flood; but in both cases, over 30% of trees exceeding 5 cm diameter and over 45% of trees exceeding 10 cm were retained within the nearby channel. Clearly, one cannot be certain that every surveyed deposited tree on the downstream bar came from the nearby eroded bank, but no bank erosion was observed in close proximity upstream of either site and field observation on a 20 km long reach of the Tagliamento showed many examples of this association. Moreover, the high temporal resolution of the photographic survey helps to link the gradual bank retreat (and wood production) to in-channel wood deposition, even if it is not possible to follow the fate of every individual tree. At Flagogna, the higher resolution photographs allowed the calculation of separate retention estimates for both floods and even to split the 2009 flood into the peak (2009a) and recession (2009b) phases. Here, retention was much lower than at Cornino, exceeding 12% for trees > 5 cm diameter and 15% for trees > 10 cm diameter. However, much higher retention ratios (about 40 and 50% for > 5 cm and > 10 cm trees) were observed for bank erosion during the falling limb of the 2009 flood hydrograph.
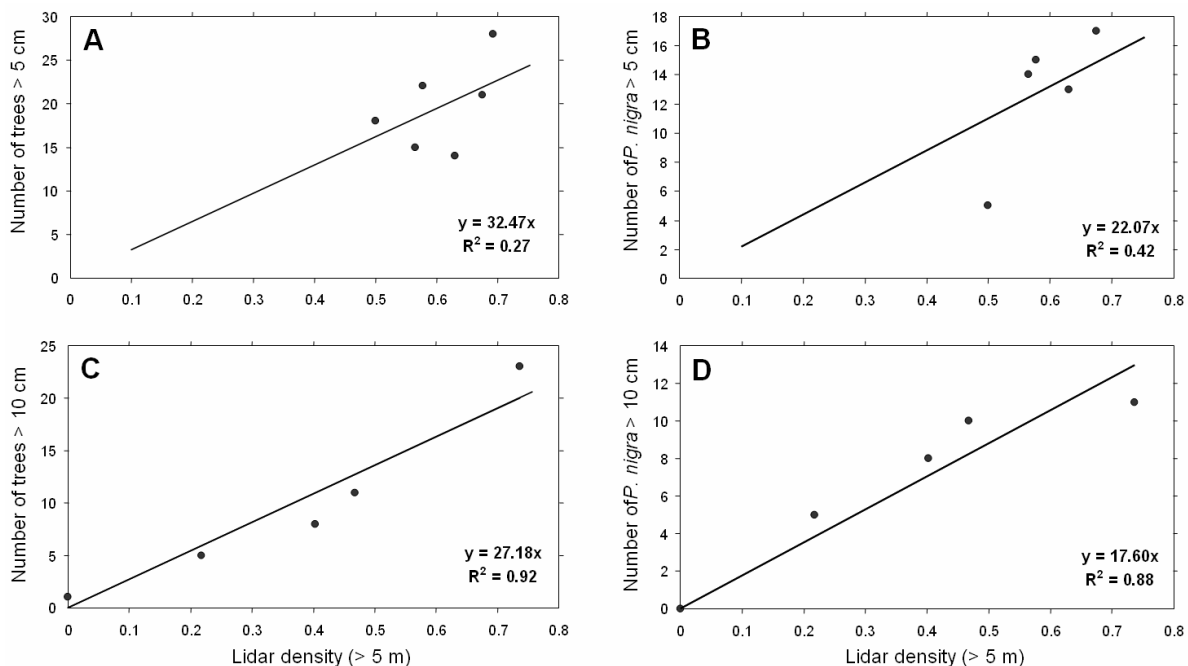
Figure 3.17: Associations between the density of the 2005 LiDAR signal at 5 m above the ground surface and the number of trees (A, C) and Populus nigra (B, D) with trunks wider than 5 cm (A, B) and 10 cm (B, D) at 1 m above the ground surface in 2010 at the Cornino (A, B) and Flagogna (C, D) sites. (Note that a smaller threshold diameter was used for the Cornino site because many of the trees were smaller than at the Flagogna site).

Table 3.2: Estimates of elements of the local wood budget in response to bank erosion associated with two floods at each of the Cornino and Flagogna study sites (the 2009 main channel flood at Flagogna is split into high (a) and receding (b) flood stages to show the higher retention during the latter stages of the flood; whereas at Cornino, the lower spatial resolution of the oblique photographs prevents separation of estimates for the 2009 side channel flood from those of the 2008 side channel flood).

	Cornino		Flagogna		
Flood event(s)	2008	2008 and 2009	2009a	2009b	2010
Area of bank eroded [m²]	3250	9325	3250	570	1370
Proportion of tree points in the eroded area (2005 LiDAR survey)	0.402	0.206	0.255	0.225	0.158
Estimated numbers of trees eroded					
P.nigra (>5cm diameter)	265	389	229	36	60
P.nigra (>10cm diameter)	140	206	152	24	40
All trees (>5cm diameter)	431	634	225	35	59
Number of trees deposited near the erosion site					
P.nigra (>5cm diameter)	87	129	29	14	8
P.nigra (>10cm diameter)	67	98	23	12	7
Estimated proportion of eroded trees retained locally (%)					
P.nigra (>5cm diameter)	32.8	33.2	12.7	38.9	13.3
P.nigra (>10cm diameter)	47.9	47.6	15.1	50.0	17.5

Location and timing of wood retention

Some mechanistic understanding of local wood retention can be gained from the post-flood (2010) detrended DTM (i.e., elevation expressed as a deviation from the mean elevation within the active tract) that was derived from the 2010 LiDAR data (Fig. 3.18). This illustrates that virtually all of the retained wood snagged on the first bar downstream from the erosion site, linking tree deposition to sediment deposition during that event. In particular at Cornino (Fig. 3.18A), the bar where the trees were deposited formed during the same flood, presumably accumulating the sediments eroded from the island immediately upstream as well as the wood. This observation is supported by laboratory experiments performed by Pyrce and Ashmore (2003) who showed that a high proportion of eroded grains are retained on the first bar. Figure 3.19 illustrates the bed elevation frequency distributions of a 500 m long reach downstream of the bank erosion site for both Cornino (A) and Flagogna (B), as well as the elevation frequency distribution of the

deposited trees. The plot shows that trees have been deposited in a very narrow elevation range. At Cornino 80 % of the deposited wood is in the range -0.3 to +0.3 m around the mean bed elevation of the reach, whereas at Flagogna the distribution is slightly wider because by the end of the flood a few trees were deposited in the deep pool left by river bed erosion. Excluding these, the remaining trees were deposited in the range 0 to 0.5 m above the mean reach bed level.

The high resolution of the Flagogna photographs allows comparison of the timing of the first photograph showing the deposition of a tree, with its deposition elevation from the post-flood LiDAR and the gauged river stage at the time of deposition, adjusted to a local datum by relating upstream gauged stage to the position of the water edge in the local oblique photographs (Figure 3.20). It was possible to directly observe the water stage in each reach and in each channel using the photographs from the automatic cameras. In this way, it was possible to relate wood deposition to the actual local water level, which was probably different in the main channel and in the secondary anabranches. The patchy nature of the tree deposition data in Figure 3.20 reflects the fact that tree deposition can only be obtained from photographs taken in daylight hours and that two contiguous photographs are needed to be sure that a particular tree was deposited within a particular hour. The timing of the available pictures is indicated on Figures 3.20A and B. Trees deposited during the night, when there is insufficient illumination on the photographs, have been attributed to the first available picture.
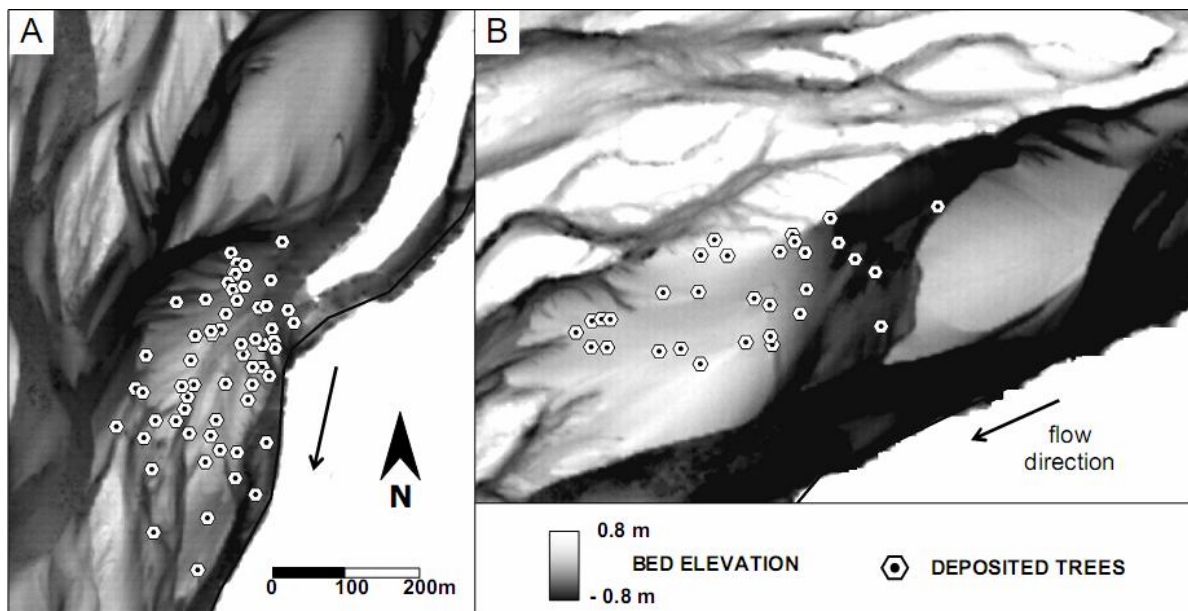
Figure 3.18: Positions of deposited trees at Cornino (A) and Flagogna (B) relative to the bed elevation estimated from the 2010 LiDAR data.

Nevertheless, the large number of trees observed in the 2009 flood illustrates that deposition elevation is constrained by the flood stage. All trees were deposited at elevations between 0.0 m and 0.8 m below the water surface at the time of deposition. Deposition of the small sample of trees identified in association with the more irregular hydrograph in May 2010 shows a less strong association with flood stage; but deposition still occurs when the deposition site is inundated, in this case by up to 1 m of water.

3.4.4 Discussion

Ground-based imagery represent a cost-effective method of observing complex processes with high temporal and spatial resolution despite of their intrinsic limitations (no data during night time and under poor visibility conditions). The integration with LiDAR surveys provides three-dimensional information that crucial to fully understanding the character of wood production and retention environments. Wood tracking on the basis of remotely sensed data would benefit greatly from integration with direct measurements from radio transmitters on both standing and deposited trees (MacVicar et al., 2009).
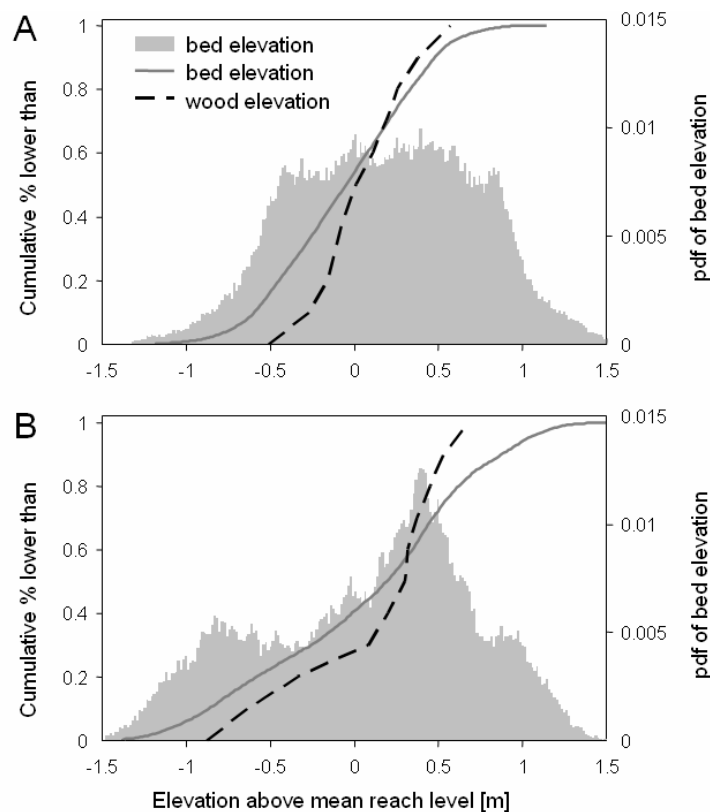
Figure 3.19: Frequency distribution of bed elevation and deposited trees elevation at Cornino (A) and Flagogna (B) as computed from the 2010 LiDAR survey.

59

The present study demonstrated some important contrasts between the Cornino and Flagogna sites that reflect their different wood characteristics and their respective positions adjacent to a relatively shallow secondary channel (Cornino) and a deeper main channel with higher energy to erode and transport wood (Flagogna). Wood retention is higher in the secondary channel than the main channel; and within the main channel, retention is higher on the falling limb of the hydrograph than during the hydrograph peak. This illustrates that flow depth (and possibly velocity) is an important control on wood retention at any particular site. The importance of flow depth in particular is confirmed by the fact that the elevation of deposited trees is strongly linked to the water level at the time of deposition. Furthermore, data from both sites show that larger trees are preferentially retained, with the retention of trees > 10 cm diameter being around 40% higher than retention of trees > 5 cm diameter. In this case, tree diameter is a proxy for tree height, root wad size and size and number of branches. In this case, the presence of one main tree species (*P. nigra*) justifies the use of tree diameter as a proxy, as most of the recently uprooted trees present similar root wad and branching characteristics. All of these properties of tree and channel size/ diameter/depth underpin the observation that trees are deposited once the water is shallow enough and that they are preferentially deposited in shallow areas such as on bar tops. Field observations, as well as the LiDAR survey (Fig. 3.18), show that flow is quite deep close to the eroded bank, thus increasing the probability for the trees to be transported downstream. Only a couple of trees at the Flagogna site were deposited in the pool and this occurred towards the end of the falling limb of the flood. The large sediment load produced by the bank erosion was deposited close by (following the process observed by Pyrce and Ashmore (2003), inducing flow shallowing and deceleration. Such bed forms are preferential locations for tree deposition.
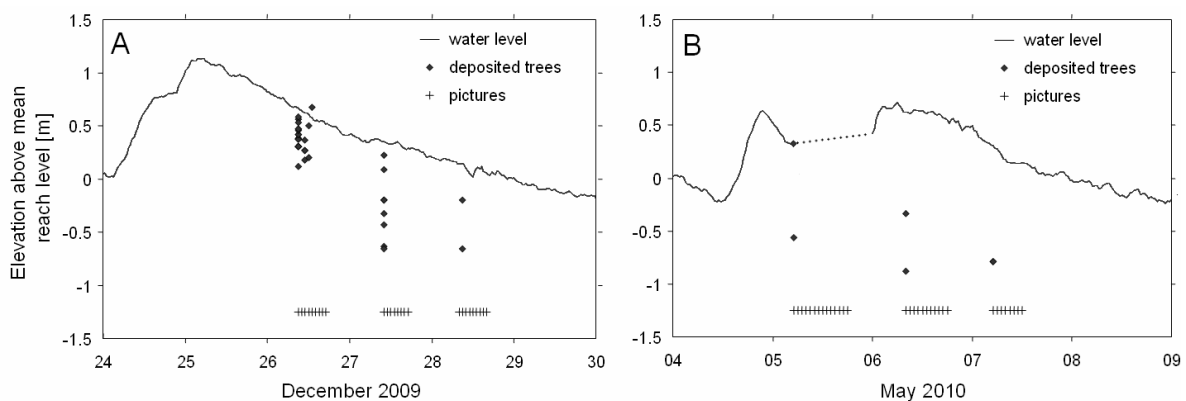
Figure 3.20: Hourly observations of newly deposited trees on the bar downstream of the Flagogna site during the December 2009 (A) and May 2010 (B) floods in relation to the water level and level of the bar top where the deposition occurred. At the bottom of the plots the timing of the available pictures is reported.

These observations shows that wood production accompanying bank erosion is very likely to produce favourable conditions for wood deposition, implying a local control on the wood budget. Furthermore, when deposition occurs in a side channel, the snagging of trees leads to a clear gradient of decreasing tree and jam size with distance from the erosion source. The fact that this pattern is not apparent in the main channel suggests that higher flow depths and velocities cause snagging of trees on bar tops to occur in a less-organized fashion. Similarly, larger (or smaller) floods may determine different deposition patterns, as well as different retention proportions. However, the analysis of the 2010 flood at the Flagogna site shows that, in this case, flood magnitude had a minor impact on wood deposition processes. Both the proportion of deposited trees and the spatial distribution are similar, suggesting that bed morphology played the largest role. These results confirm the recent observations by MacVicar and Piégay (2012), who used video monitoring to track wood passage in the Ain River (France). Their data show that wood transport is larger during the rising limb of the flood, because of a) mobilization of wood stored within the channel; and b) an increasing number of deposition sites during the falling limb. The most relevant wood source during the falling limb is bank erosion that is more likely to occur during the longer receding phase of the flood. This wood availability increases wood transfer only occasionally, as logs are likely to deposit close to source.

3.5   Wood properties

Field surveys of driftwood properties were carried out in spring 2011 at two sites within the Cornino and Flagogna reaches. In both cases, wood mapping was performed on bars located immediately downstream of a vegetated patch that had experienced extensive erosion during the previous winter. The survey site in Flagogna comprises part of the area monitored in 2010, but the two dataset do not overlap completely as several high flow events – including a 1-year flood – occurred in late 2010.

The two sites represent different types of riparian vegetation occurring along the piedmont reaches of the Tagliamento River. In Cornino, the eroding bank hosts a significant proportion of *Salix* and few trees higher than 10 m; in contrast, driftwood surveyed in Flagogna originates from an established island essentially composed by *P. nigra* trees whose height often exceeds 15 m (Figure 3.21). The difference in species composition and tree height is most likely a consequence of the higher growth rate observed for *P. nigra* in Flagogna. In turn, the realisation of optimal conditions for riparian vegetation establishment have been linked to a number of factors, including high moisture availability – due to upwelling fluxes caused by the proximity of the Pinzano gorge – low stream power and high retention of fine sediments (Gurnell and Petts, 2006).

Size threshold values for driftwood survey were set to 5 cm for diameter and 1 m for length. Within the selected survey areas, all wood pieces exceeding minimum size were mapped using a hand-held GPS and their diameter and length were measured with a precision of 0.1 m and 1 cm, respectively. Log diameter was measured 1 m above the root bole – if present – or near the midpoint of broken and heavily degraded pieces for which the root end could not be determined. For a small number of driftwood elements larger than 5 cm in diameter, wood length data are missing because one extremity of the piece was not identifiable (partially buried logs, elements stored in large jams or logs removed by the local population to be used as firewood). For a subset of deposited elements with an exposed, clearly visible root wad, scaled pictures of the root end were acquired in order to evaluate root bole diameter.

Overall, 66 deposition sites were surveyed in Cornino and 56 in Flagogna, comprising 123 and 118 individual driftwood elements, respectively (see Table 3.3). Moreover, two additional elements exceeding diameter threshold were observed in Cornino and 17 in Flagogna, but as their length was not determined, they are excluded from further analyses. Adopting the widely used threshold value of 10 cm for diameter (Abbe and Montgomery, 1996; Gurnell et al., 2002; Abbe and Montgomery, 2003; Andreoli et al., 2007; Curran, 2010),
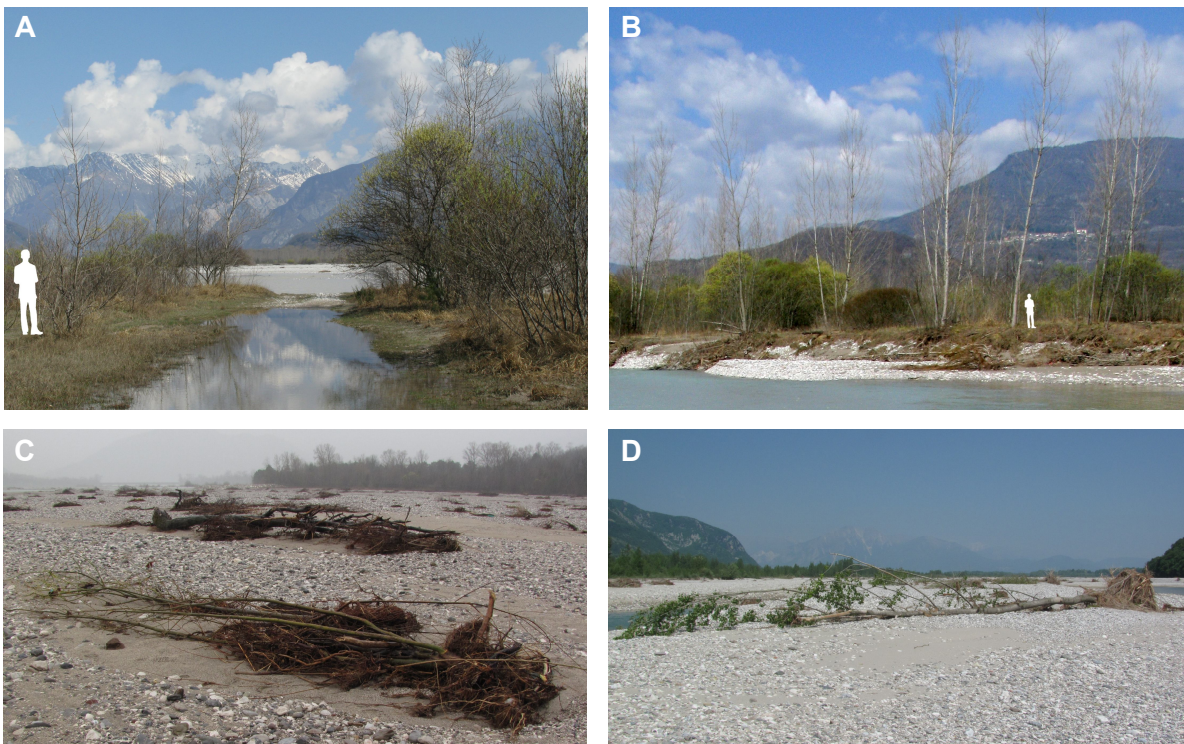
Figure 3.21: Standing vegetation before erosion in Cornino (A) and Flagogna (B) with human silhouette for size comparison. Examples of deposited wood in Cornino (C) and Flagogna (D), the latter showing an example of log with large root wad.

the number of sites and elements drops to 36 and 47, respectively, in Cornino, showing that a large proportion of deposited wood is represented by relatively small pieces. In Flagogna, the relative relevance of driftwood elements larger 10 cm in diameter is greater, with 48 sites and 79 logs. The Flagogna site also shows larger jam size, with up to ten elements stored in a single accumulation.

Frequency distributions of element length and diameter are shown in Figure 3.22 for logs exceeding 10 cm in diameter and selected percentiles are summarised in Table 3.3 for both choices of minimum diameter. The lower tail of piece diameter distributions is fairly similar between sites, while remarkable differences are observed for large values of diameter. In particular, only 20% of elements in Cornino are larger than 20 cm in diameter – five times the median bed particle size – as opposed to more than 40% in Flagogna. More relevant differences occur in terms of length, with 30% of elements longer than 10 m in Cornino as opposed to approximately 65 % in Flagogna. Regardless of diameter threshold value, the 25th, 50th and 75th percentiles of piece length are approximately twice as large in
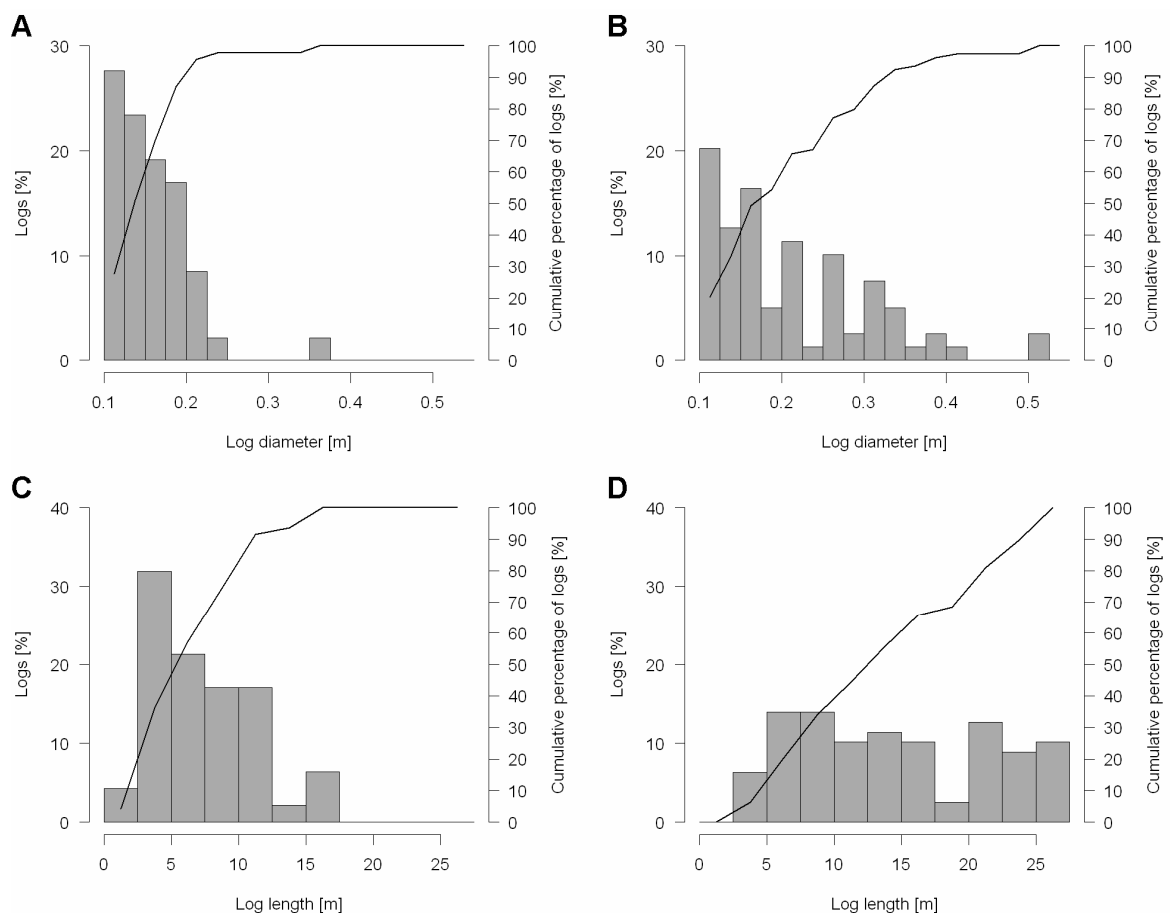
Figure 3.22: Distributions of driftwood diameter and length for the Cornino site (A, C) and for the Flagogna site (B, D). Only elements exceeding 10 cm in diameter and 1 m in length are taken into account.

Table 3.3: Summary of surveyed sites and elements (incomplete records are excluded).

	Cornino		Flagogna	
	D > 5 cm	D > 10 cm	D > 5 cm	D > 10 cm
number of sites	66	36	53	48
number of elements	123	47	118	79
largest jam [elements]	6	3	12	10
element diameter [m]				
25th percentile	0.06	0.12	0.09	0.13
median	0.09	0.14	0.13	0.18
75th percentile	0.13	0.18	0.22	0.27
element length [m]				
25th percentile	4.2	4.1	7.0	8.6
median	5.0	6.4	9.8	14
75th percentile	7.2	10.1	16.9	21.8

Flagogna with respect to Cornino. It is worth noting that for driftwood surveyed in Flagogna, diameter and length appear to increase following a 1:100 ratio up to approximately 25 cm and 25 m, respectively. Larger values of tree diameter were observed (up to 50 cm) but the largest trees do not exceed 27 m in length (Figure 3.23A).

Root wad diameter was derived from images for a subset of 22 trees, 7 of which belong to the Cornino site. The outer edge of the root bole was defined as the limit of the volume of roots and soil that is expected to be able to withstand the weight of the log itself, thus excluding isolated roots protruding from the upper edge that are likely to bend or break when the log is deposited. No relationship between log length and root wad diameter was found, but a fairly consistent ($R^2 = 0.74$) linear relationship between root wad diameter and log diameter can be computed including elements from the two sites (Figure 3.23B).
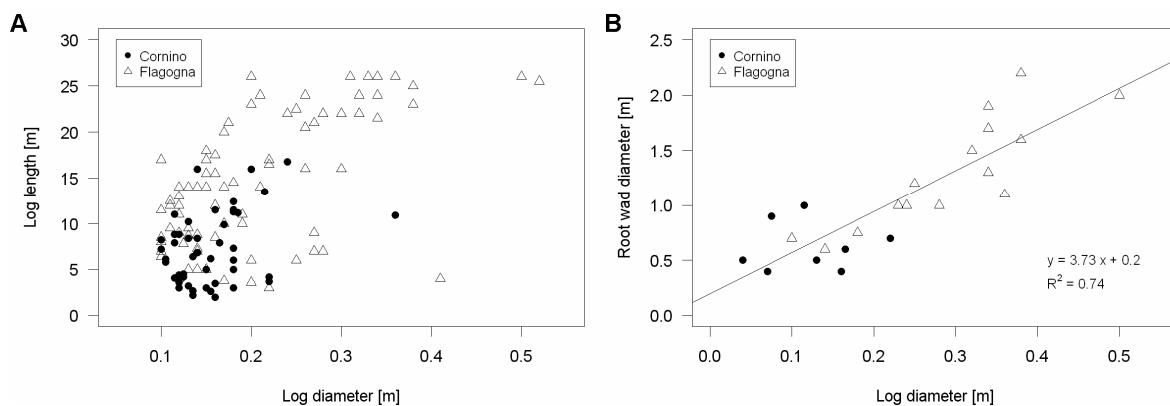
Figure 3.23: Length/diameter relationships (A) and root wad diameter as a function of log diameter (B).

4 Physical modelling

4.1 Objectives

Laboratory simulations of driftwood dispersal in a multi-thread riverine system make up the core of the research activity presented in this thesis. Physical modelling is a widely used technique in river science as it offers the opportunity to investigate a wide range of processes under controlled conditions at convenient temporal and spatial scales. In particular, a proper laboratory setup ensures a) full control on key physical parameters governing the phenomena of interest; b) repeatable, accurate measurements; and c) manageable logistics and safe working conditions.

These issues are of particular importance for the present study because driftwood dynamics are governed by complex interactions between flow conditions, log properties and channel morphodynamics. At laboratory scale, the key drivers of wood dispersal can be separately or jointly tested over a wide range of values to highlight the role of single factors or pre-determined sets of conditions. The remarkable intrinsic variability of dispersal processes also implies a need for repeated simulations to clearly identify typical spatial patterns, temporal trends and causal relationships. Finally, as already pointed out by Braudrick and Grant (2000), physical modelling overcomes a number of safety and logistical constraints of field-scale observations. The strong association between wood transport and high flows limits the use of direct surveying techniques to pre- and post-flood measurements. Remote sensing techniques, albeit free from safety limitations, require a long-term monitoring agenda as the chance to observe relevant phenomena depends on essentially unpredictable flood events. Finally, field-scale investigation of wood dispersal in piedmont braided rivers can be exceedingly time-consuming due to the large spatial and temporal scale of phenomena. Therefore, physical modelling was selected as the primary investigation technique for the present work. However, it is important to stress that any physical model produces a simplified description of natural processes whose complexity can be fully appreciated only at real scale.

The present study focuses on driftwood in piedmont, temperate gravel-bed braided rivers characterised by a low to moderate level of human intervention. Two key concepts define this fluvial context with respect to wood dynamics and serve as the basis for the design of the physical model. Firstly, piedmont braided rivers at high flow conditions fall

into the 'large river' category proposed by Piégay and Gurnell (1997). Relative wood size – usually expressed as log length to channel width ratio and/or as log diameter to channel depth ratio – is small and all wood pieces are potentially mobile. Local recruitment from eroding banks is the primary wood source as pieces are easily broken during transport. Secondly, the low driftwood input rate prevents interaction between pieces during the floating phase, resulting in 'uncongested transport' *sensu* Braudrick et al. (1997). Flume simulations were carefully designed to reproduce these conditions by setting convenient upper thresholds for wood size and input frequency. It must be stressed that in this study the aim of physical modelling is not the reproduction of a specific river reach at laboratory scale, but rather the investigation of driftwood dynamics in the general context of temperate piedmont braided rivers. The specific objectives of physical modelling include:

- reproducing short-term, flood-induced wood dispersal and providing a detailed, quantitative characterisation of resulting accumulation patterns in terms of travel distance and spatial organisation;

- investigating short-and long-term wood storage, remobilisation and persistence with special emphasis on wood mass budget;

- quantifying the effect of wood supply, log properties, flow regime and channel morphology on the spatial distribution, structure and time evolution of deposits.

The main research questions were addressed through an extensive set of simulations conducted at the Hydraulics Laboratory of the University of Trento (Italy) and at the Total Environmental Simulator of the University of Hull (UK). The Trento runs focused on short-term dispersal of driftwood associated to single flood events, while the Hull runs were devoted to the simulation of long-term wood storage evolution. Laboratory activities can be grouped into four main subsets centred on the following topics:

- Trento runs, set 1 (T1): impact of element size and shape on wood mobility and accumulation style;

- Trento runs, set 2 (T2): impact of channel pattern and discharge on wood mobility and accumulation style;

- Trento runs, set 3 (T3): joint effect of element properties, channel pattern and discharge on wood mobility, accumulation style and remobilisation under unsteady flow conditions;

- Hull runs (HU): long-term evolution of wood accumulations under steady flow conditions and different wood input rates.

Preliminary runs were carried out in both facilities for instrument testing, evaluation of accuracy and precision and definition of optimal operative conditions and protocols.

The structure of the present chapter mirrors the organisation of the experimental activities. For each simulation subset, the model setup, monitoring techniques and data elaboration protocols are described in detail. A separate section is devoted to a brief theoretical overview of the main statistical techniques employed for data analysis. Subsequently, experimental results for each subset are presented and discussed.

4.2 Short-term wood dynamics: the Trento runs

4.2.1 Facility

The Pi Flume used for Trento runs is a 3 m wide, 25 m long facility hosted and managed by the Hydraulics Laboratory of the University of Trento (Figure 4.1). The flume is filled with a 0.2 m thick layer of well-sorted sand with a median grain size (D_{50}) of 1.03 mm and a submerged relative density of 1.63. The maximum usable width for braided network simulation is slightly larger than 2.5 m or 2500 times the median particle size. Slope is assigned by levelling the bed material with a carriage (practical range 0÷1.7%). The flume is equipped with a water recirculation system, a helical screw conveyor at the upstream end for sand supply and a filtering crate at the downstream end for bedload collection. Water and sand input can be controlled manually or assigned as a function of time via custom built software. A flow meter at the upstream end of the circuit ensures real-time discharge monitoring while the cumulative weight of output bedload is measured using a set of 4 load cells. Both values are acquired automatically with a time resolution of 1 minute and a precision of 0.01 l/s and 0.01 kg, respectively.

A software-controlled laser profiler mounted on a carriage is used for bed elevation surveys. The carriage moves on high-precision rails and can cover a 2.5 m wide, 22 m long area with a minimum step of 1 mm. Elevation data are acquired with a 0.1 mm precision. A reflex camera (Nikon D3100 with a Nikkor 28 mm/f2.8D AF lens) mounted on a manually operated carriage provides digital imagery for the whole flume. The carriage moves on the high precision rails and the camera is positioned about 3 m above the sand bed. The optical axis is aligned with the flume centreline and is normal to the sand surface. Each image covers an area of 2.8x2.1 m, resulting in an approximate resolution of 1.25 px/mm. Pictures are taken at a series of 15 positions along the longitudinal axis to ensure sufficient overlapping between adjacent images. A set of ground control points for image stitching and rectification was painted on the upper surface of auxiliary rails used for sand levelling. Control points were materialised outside of the sand bed, as levelling implies the rearrangement of the whole sand surface. A scheme of the facility including instrumentation is presented in Figure 4.2.

Figure 4.1: The Pi Flume. Flow is towards the camera.

A	Sand storage tank with screw conveyor	F	Load cells	K	Flowmeter
B	Upstream water tank	G	Recirculating pump	L	Camera carriage
C	Sand bed	H	High-precision rails	M	Reflex camera
D	Underground water tank	I	Laser carriage	N	Auxiliary rails with GCPs
E	Sand filtering crate	J	Laser profiler	O	Levelling carriage
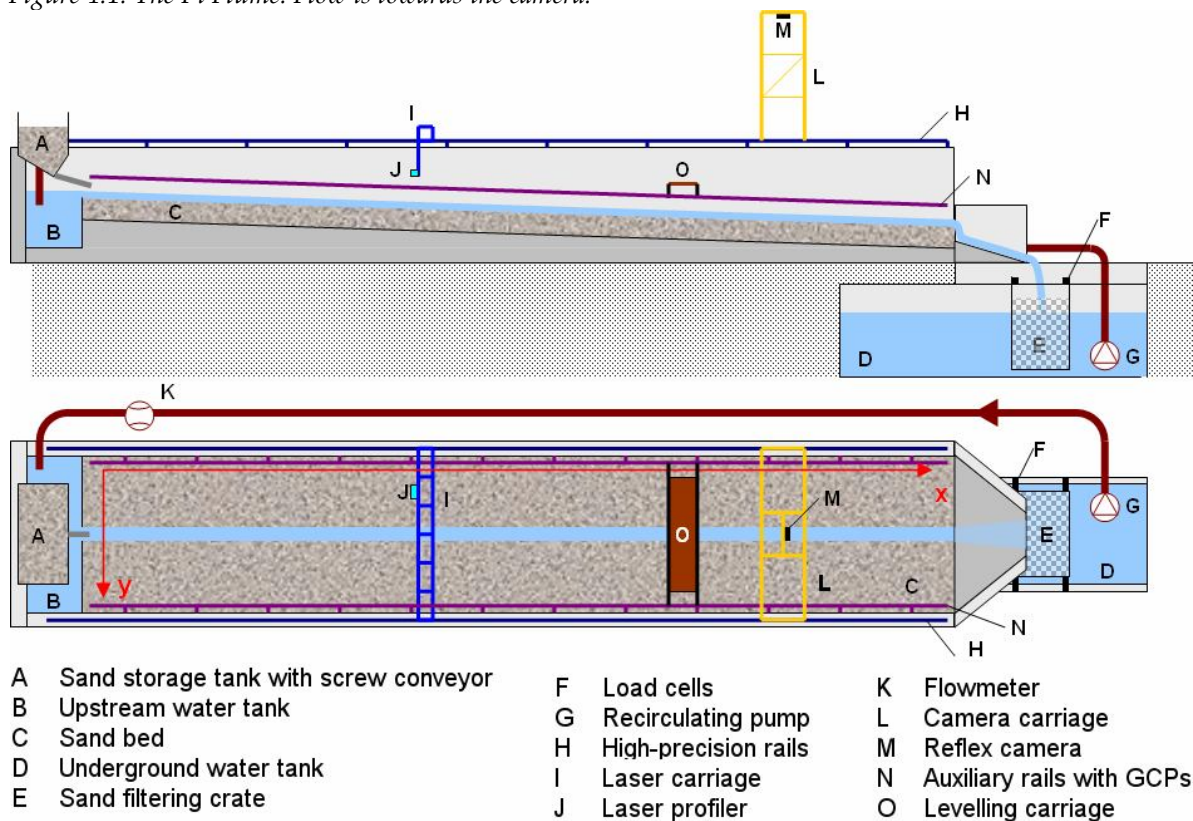
Figure 4.2: Cross-section (top) and upper view (bottom) of the flume in the initial configuration, showing main components and the reference coordinate system used for all spatial data.

4.2.2 Modelling braided river morphology

Physical modelling of braided networks at flume scale was carried out in accordance to procedures that have been developed and applied over the past two decades (Ashmore, 1991; Bertoldi et al., 2009c). A quantitative description of the resulting networks was obtained and analysed using GIS techniques. A detailed characterisation of the spatial structure of the braidplain is required as network morphology is one of the key drivers of wood dispersal. The goal of the analysis is to define a) typical distributions of channel width and length to be used as reference scale values for the design of wood elements; and b) bed elevation distributions, to be compared with relative elevation distribution of wood deposits.

Reproducing braided networks at flume scale

Braided networks in the Pi flume develop freely under steady flow conditions from an initial straight rectangular channel carved along the flume centreline. The width and depth of the initial straight channel are chosen to produce bankfull conditions and a width:depth ratio that is lower than the threshold for alternate bar formation (Colombini et al., 1987). Networks develop through chute cut-off processes and evolve towards a 'steady-state' configuration characterised by the stabilisation of time and space-averaged morphological parameters. Two criteria were used to identify the end of the transient phase: a) the balance between time-averaged sand input and output fluxes; and b) the stabilisation of the reach-averaged braiding index, computed using the channel count procedure suggested by Egozi and Ashmore (2008). The 'steady' braided network configuration was chosen as the reference condition for wood transport simulations as it allows easier comparison of model outputs across runs. As a consequence, wood dispersal simulations were conducted only over 'steady' networks and dowels used to simulate driftwood were designed on the basis of cumulative distributions of channel width and depth computed at this stage.

In this study, discharge and slope for network formation were set to 1.8 l/s and 0.01, respectively, for all model runs. This combination of parameters was defined through a set of preliminary simulations and produces networks with desirable properties: a) the channel pattern is fully braided; b) the values of Shields stress and Froude parameter are typical of natural gravel-bed braided rivers (Bertoldi et al., 2009c); and c) the time scale of network evolution is compatible with operative times. Preliminary runs also provided information on evolution time scales and bed load. For the selected values of discharge and slope, the bed load output flux decreases steadily for the first 6 hours and fluctuates around a constant value afterwards. The sand output rate averaged over a 24 hour-long period excluding the initial transient phase corresponds to 1.5 g/s. This value was assigned as sand

input rate for all model runs. However, the stabilisation of braiding index is attained after 20 to 24 hours and thus the end of the transient phase was set to 24 hours after run start.

Overall, eight realisations of the braided network were used for this study because the channel pattern tends to degenerate when the braidplain width is too close to the flume width. As a consequence, networks were discarded whenever the influence of the lateral constrains (concrete walls) on the channel configuration was deemed non-negligible. The use of multiple networks also reduces the influence of any peculiarity in network geometry on wood dispersal simulations. Table 4.1 summarises the key properties of the model.

Post-processing of laser and imagery data

The present chapter details procedures and techniques used for the post-processing of laser and imagery data and their integration and management in a GIS context. The protocols defined here were also applied to spatial data acquired during wood dispersal simulations. Bed elevation surveys and imagery data were organised in a Geographical Information System (GIS) using GRASS GIS 6.4.2[1]. A common reference coordinate system was defined, with x, y and z corresponding to the longitudinal, transversal and vertical coordinate, respectively (Figure 4.2). Bed elevation was sampled on a regular grid with a resolution of 5 mm along the y axis and 25 mm along the x axis, corresponding to 500 cells along the transversal direction. Laser surveys use an intrinsic 2D reference system formed by the left high-precision rail and the laser carriage and elevation data are acquired as vertical distance from a reference horizontal plane.

The laser carriage was found to be tilted upstream by 1° with respect to the left rail and the error was taken into account for the computation of the coordinates of laser sampling points in the reference coordinate system. Laser points were corrected for channel slope by subtracting a local mean elevation value computed on a moving window. For each cross section, the averaging area extends for 1.25 m (0.5 maximum braidplain widths) along the x axis in either direction and is limited by the outer banks of the outermost channels of the network. A Digital Elevation Model (DEM) was interpolated from vector point cloud data over a 5x25 mm grid using the Inverse Distance Squared Weighting routine available in GRASS GIS (*v.surf.idw*). As this procedure tends to smooth feature edges, differences between vector points and corresponding DEM cells were computed. The interpolation routine yields acceptable results as deviations exceeding ± 1 mm were found for less than 3% of map cells. The output map contains relative elevation values that were rounded to the nearest millimetre as information at the sub-grain scale is not relevant for subsequent analyses.

---

[1] GRASS Development Team, 2012. Geographic Resources Analysis Support System (GRASS) Software. V. 6.4.2. Open Source Geospatial Foundation. http://grass.osgeo.org

Table 4.1: Overview of the Pi Flume and the formative conditions for braided networks.

Parameter	Value
Total flume length and width [m]	25 x 3
Usable flume length and width [m]	22 x 2.5
Grain size [mm]	1.03
Slope [-]	0.01
Formative discharge [l/s]	1.8

A protocol for the post-processing of imagery data was defined in analogy with ortho-rectification procedures commonly used for field-scale aerial surveys. 32 control points were painted on the auxiliary rails and surveyed twice with a Leica TPS 700 total station, attaining a precision of 1 mm. A second set of 30 check points scattered on the sand surface was used to assess the quality of the rectification procedure. Image processing requires a three-step procedure:

- correction of lens distortion: barrel distortion was corrected using PTLens 8.7.8[1]. The software includes a set of warping parameters (calibrated on test images) for the specific lens model used in this study. The highest values of residual distortion observed in corrected images are located close to the flume margins (i.e. the image margins) and are smaller than 4 mm;

- georeferencing: images are georeferenced on the basis of GCPs using the available GRASS routine (*i.rectify*). A linear transformation is applied as the flume configuration allows for a maximum of four ground control points per image. At this stage, image pixels corresponding to the upper surface of the rails are correctly positioned with respect to the reference coordinate system, while the sand bed is downsized as it lies on a parallel plane located 190 mm below the GCPs. Control points are approximately equidistant from the image centre and the camera is normal to the sand surface, therefore the position of the image centre are also correct;

- scaling: the scaling factor for each georeferenced image is computed for each picture on the basis of the distance between the GCP plane, the sand surface and the camera.

The maximum rectification error of output images evaluated using the check point set is 5 mm, corresponding to the minimum DEM cell size. The results of the procedure were deemed satisfactory, as output images allow for accurate network characterisation.

---

[1] http://www.epaperpress.com/ptlens/index.html

Computation of inundation maps

The computational domain for the analysis of network morphology is the *total braidplain area* (A_b), defined as the portion of the flume that has been active at any point during the simulation. The cumulative distribution of relative elevation was computed on this domain. To evaluate channel depth and width distributions, water depth maps were reconstructed from DEMs and imagery. As laser surveys can be carried out only over a dry bed, a procedure was defined to reconstruct channel margin position and free surface elevation from the combination of spatial data.

Channel shoreline was mapped on rectified images for the whole network and stretches of gently sloping bank with a clearly identifiable channel margin were selected. Local free surface elevation was evaluated for each stretch as the median value of all DEM cells intersected by channel margin. Care was taken in having at least one estimation of water stage for each individual anabranch as free surface elevation in a braided network has been show to vary between channels (Zolezzi et al., 2006). However, for a small number of anabranches no information was available and the free surface elevation was set to the average over all sample stretches.

Vector shoreline maps were converted into binary wet/dry raster maps. For all DEM cells belonging to the wetted area (*gross wetted area*, A_{wg}), water depth was computed as the difference between bed and free surface elevation. Only areas characterised by depth values greater than 2 mm – i.e. twice the median particle diameter – were taken into account for further analyses (*net wetted area*, A_{wn}). Moreover, a distinction was made between upstream connected channels (*connected wetted area*, A_{wc}) and other water bodies including backwaters, pools and channels fed by subsurface flow.

Figure 4.3 illustrates an example of the procedure: a relative bed elevation map is shown alongside the corresponding ortho-image series (taken in this case for a discharge value of 1.5 l/s). Free surface elevation is shown for individual anabranches only within net wetted area. The resulting water depth map is presented for four values of discharge.

Results: spatial structure of braided networks

28 laser surveys were used to evaluate the cumulative distribution of relative elevation within the braidplain. Data were acquired during the steady phase of three different network realisations and cover a 18.5 m long portion of the flume. The upper 4 m and lower 2.5 m of the flume were excluded from computations to avoid the influence of inlet and outlet areas. A second data set comprises four series of images taken over a range of flow conditions (0.9, 1.2, 1.5 and 1.8 l/s) within 15 minutes. A laser survey was carried out at the end and used as a reference datum for all image series. Changes in network morphology between the first and the last set of images are deemed negligible.
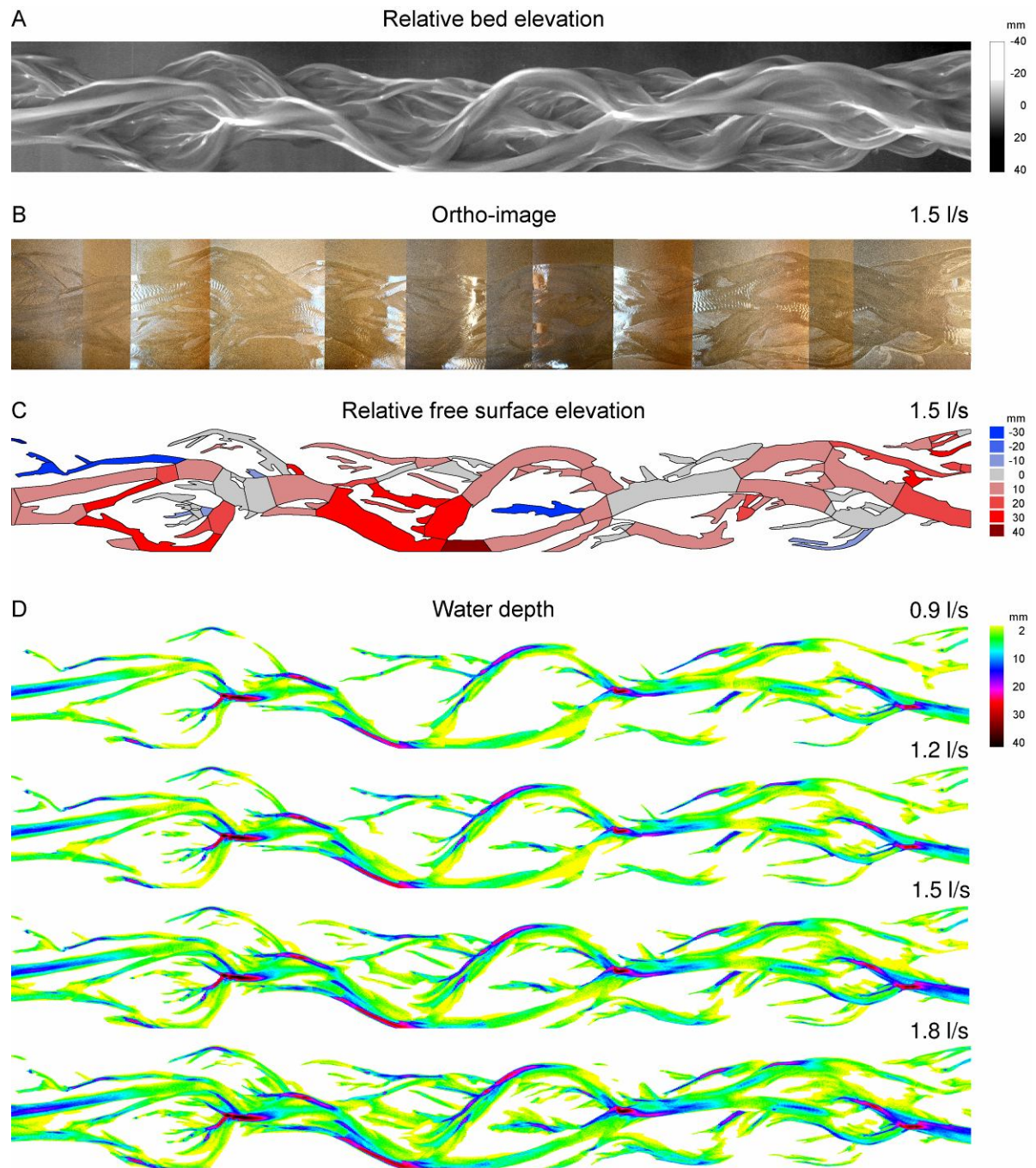
Figure 4.3: An example of channel pattern reconstruction from laser survey and imagery: (A) relative bed elevation map; (B) corresponding ortho-image series taken at Q = 1.5 l/s; (C) map of net wetted area with free surface elevation for individual anabranches; (D) water depth maps for four discharge values. Flow is from left to right.

Frequency distributions of bed elevation (Figure 4.4) are negatively skewed, implying that the incised thalwegs represent a limited proportion of the whole braidplain area. Skewness ranges between -1.39 and -0.89 with a median value of -1.1, corresponding to the highest values reported by Bertoldi et al. (2011b) for 19 sub-reaches of the Tagliamento River. Interestingly, sub-reaches characterised by low or zero vegetation cover provide the best agreement with physical model outputs. Distributions are also similar across network realisations.

Channel patterns observed at four flow stages were characterised in terms of proportion of inundated braidplain area and braiding index (Table 4.2). The latter was evaluated on a set of 18 cross-sections with a spacing interval of 1 m using the channel count procedure employed for Tagliamento River data (Egozi and Ashmore, 2008). The analysis was first conducted over net wetted area (taking into account all channels) and then for upstream connected anabranches only (connected wetted area). From the point of view of wood dispersal, connected wetted area provides an upper limit to the portion of braidplain area where wood transport can occur, while the actual proportion depends on the relationship between log size and channel size.

In formative conditions, 52% of the braidplain area is inundated with water depth values exceeding 2 mm and A_{wn}/A_b decreases with discharge to just above 25% for the lowest flow stage. Braiding index computed over all channels (BI) peaks for intermediate flow conditions. If upstream-disconnected anabranches are excluded, a difference is observed between higher (1.5 and 1.8 l/s) and lower (0.9 and 1.2 l/s) values of discharges; A_{wc}/A_b decreases from approximately 40% to 25% and braiding index (BI_c) from 2.5 to less than 2.

Channel pattern properties are summarised in Figure 4.5. The cumulative frequency distribution of channel width for upstream connected anabranches was defined by computing the average width of each channel and evaluating the associated frequency as the ratio between the length of the anabranch centreline and the total length of all channels. Median channel width is slightly larger than 20 cm at the lowest flow and increases to approximately 27 cm in formative conditions. It is important to remember that these values also exclude all portions of the network where water depth is lower than 2 mm. Small channels (narrower than the 40th percentile) show quite similar distributions for the four discharges, while values in the upper quartile differ substantially between low flow and formative conditions.

Channel depth distribution over upstream connected anabranches is essentially identical regardless of discharge with a median value slightly larger than 5 mm (five times the median grain size). Therefore, discharge controls the proportion of inundated braidplain area but plays no role in determining the percentage of wetted area exceeding a given depth threshold. This is in agreement with observations from field scale studies; in

Table 4.2: Proportion of inundated braidplain area and braiding index computed for all channels (A_{wn} / A_b and BI, respectively) and upstream-connected anabranches only (A_{wc} / A_b and BI_c).

Discharge [l/s]	All channels		Upstream-connected channels	
	A_{wn} / A_b [%]	BI [-]	A_{wc} / A_b [%]	BI_c [-]
0.9	29.8	3.2	25.3	1.8
1.2	35.6	3.5	25.9	1.9
1.5	45.4	4.1	37.3	2.5
1.8	52.3	3.9	43.2	2.4

particular, Mosley (1982) showed that in a braided network, an increase in discharge is associated with an increase in depth of existing channels but also to the generation of new, shallow anabranches.

Finally, differences in free surface elevation for pairs of discharge values were computed by subtracting the corresponding water surface elevation maps. Cumulative distributions are shown in Figure 4.6. Increasing the discharge from 0.9 to 1.2 l/s produces minimal changes over most wetted area, while moving from the lowest flow stage to formative conditions determines a median increase of less than 3 mm. These distributions strongly depend on the procedure used to build free surface maps and ultimately on the correct identification of channel margins (see Chapter 4.2.2); however, they provide an approximate estimation of the magnitude of at-a-station change in water depth. As expected for a braided system, an increase in discharge generates a rapid change in wetted width and a considerably slower increase in channel depth (Bertoldi et al., 2009a).
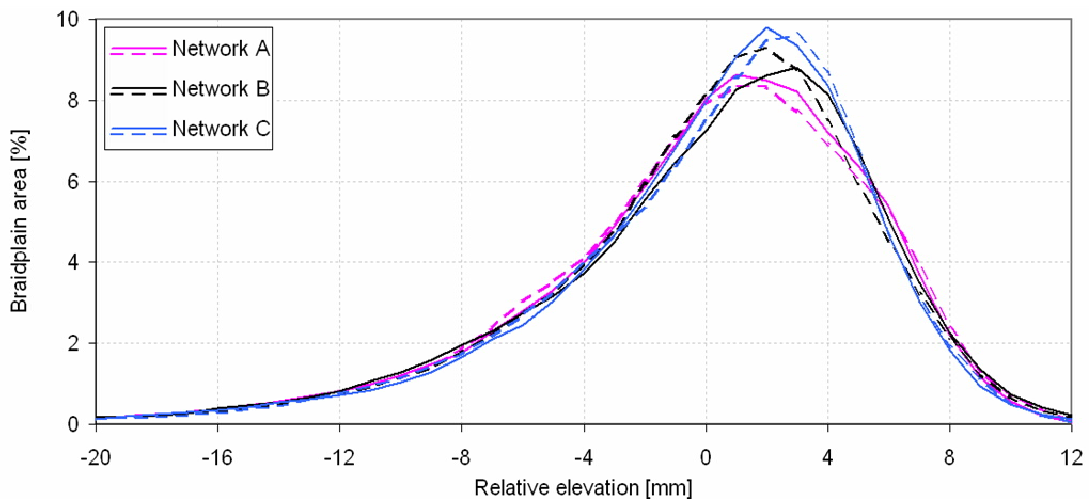
Figure 4.4: Frequency distributions of bed elevation computed over total braidplain area for a sample of six laser surveys belonging to three network realisations.
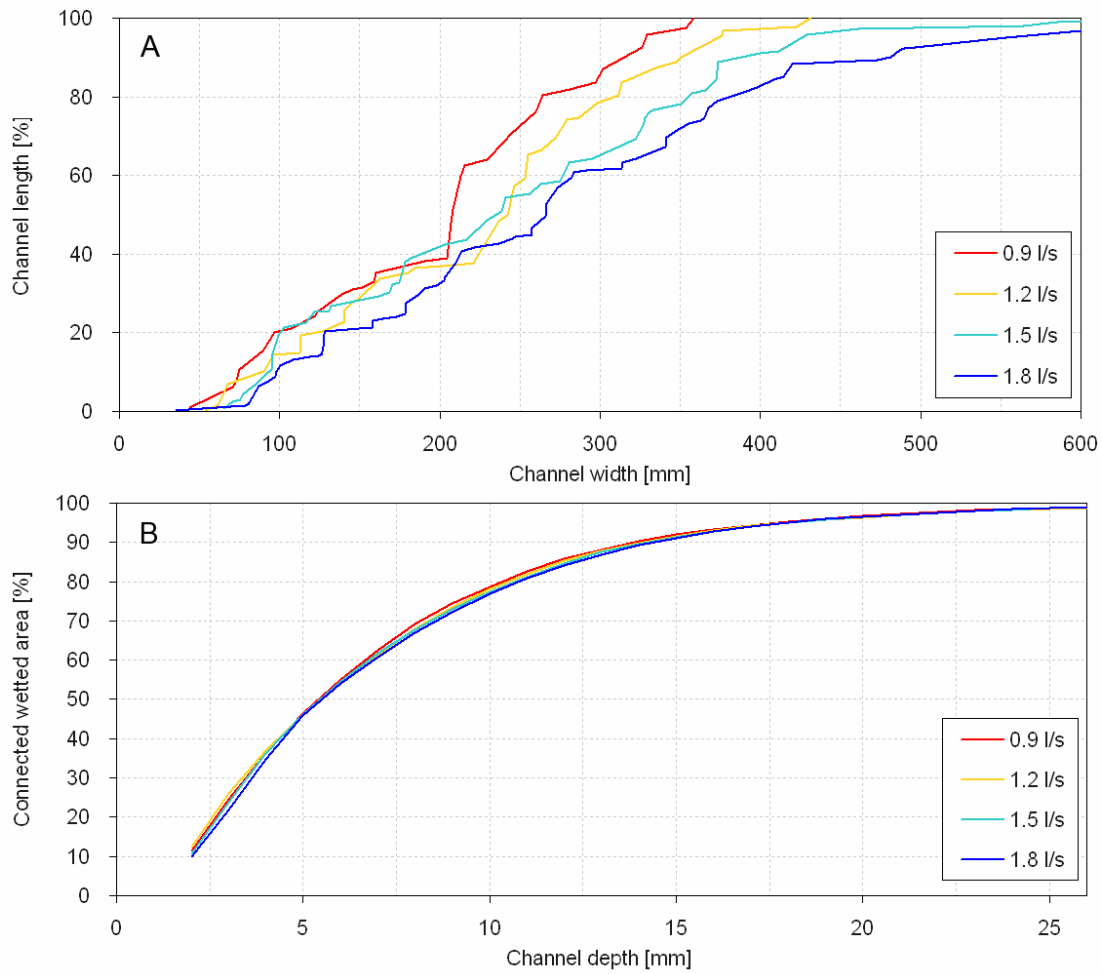
Figure 4.5: Cumulative frequency distribution of channel width (A) and depth (B) for four values of discharge, computed over connected wetted area.
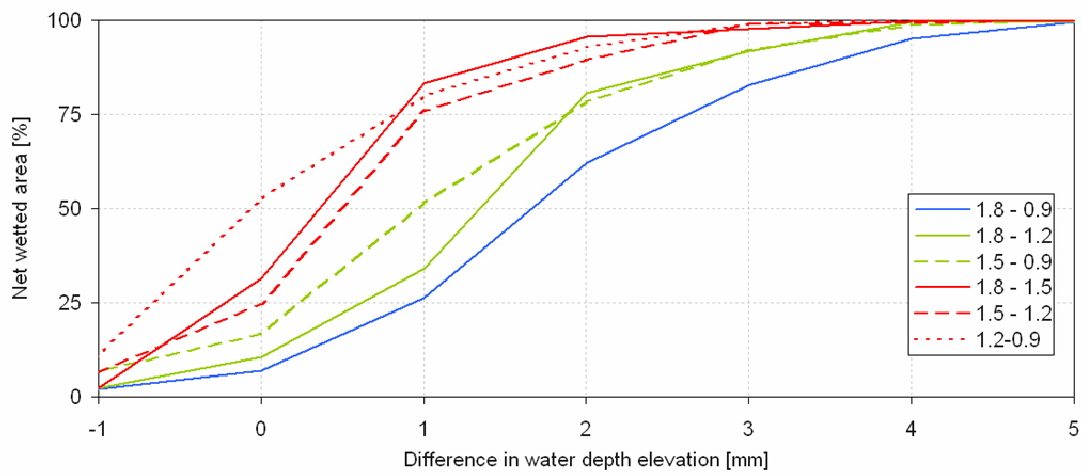
Figure 4.6: Cumulative frequency distribution of at-a-station variations of free surface elevation.

4.2.3 Modelling wood dispersal

Driftwood elements

Driftwood elements are reproduced at flume scale using wooden dowels of various size and shape in order to evaluate the effect of log properties on dispersal processes. Dowel design was based on field-scale data collected on the Tagliamento River (see Chapter 3) and on a review of flume-based studies carried out in the past few years. The parameters of interest include overall shape, element length and diameter and wood density. Large woody debris is usually defined on the basis of size thresholds (Wohl et al., 2010) and includes single branches, shrubs, logs and whole uprooted trees. However, the present study focuses exclusively on logs and trees, as their morphological and ecological influence on the riverine system is by far the most relevant (Gurnell and Petts, 2006).

Cylindrical logs are used in the vast majority of theoretical and experimental models of wood entrainment; two exceptions are represented by the works of Gippel et al. (1996b) (logs with roots and branches) and Braudrick and Grant (2000) (disc-shaped root wad). The presence of a rootwad is known to exert a strong control on element mobility, while the effect of branches is probably limited as they tend to snap during transport (Abbe and Montgomery, 1996; Piégay et al., 1999; Millington and Sear, 2007). Therefore, cylindrical elements with and without cross-shaped rootwads were used for this study.

Four values of length and diameter were used to reproduce the variability of driftwood size (see Table 4.3 and Figure 4.7). Three scaling criteria were used for dowel size:

- diameter values were chosen on the basis of grain size to reproduce typical field values of the diameter to bed roughness ratio (See Figure 3.22);

- length values were selected according to the distribution of channel width observed in the flume networks to ensure 'large river' conditions (see Figure 4.5). The procedure used to reconstruct channel geometry from laser surveys and imagery is detailed in Chapter 4.2.2;

- rootwad size was set to four times the log diameter on the basis of the linear relationship derived from Tagliamento River data (see Figure 3.23B).

It is worth noting that resulting diameter to length ratios are larger than those found in the field, but this choice of parameters satisfies 'large river' conditions. Overall, three parameters of interest were identified for this study, namely log length (L), log diameter (D), and log shape, taken into account either as the proportion of input wood with roots (X) or, for the individual dowel, the presence/absence of roots (R, a binary variable). The present study does not cover the investigation of wood density as a driver of element

mobility and therefore the same type of wood was used for all model runs. Thévenet (1998) provides reference wood density values measured on the Ain and Drôme Rivers (France). The most common tree species observed at these field sites (*Salix sp.*, *Alnus glutinosa*, *Populus nigra*) are typical of European piedmont rivers (Dufour et al., 2007; Francis, 2007). Observed dry and wet density values range from 0.15 to 0.45 kg/dm³ and from 0.45 to 0.8 kg/dm³, respectively. Dowels used in most laboratory studies fall within the range for wet wood. For the present study, a set of wetting/drying tests was performed on various types of commercially available wood products to assess both density and durability. Chestnut wood was chosen as it shows the best results in terms of wet density (0.65÷0.77 kg/dm³) and good resistance to wetting and drying cycles. Root wads were made out of heavier, more durable walnut wood (0.79÷0.84 kg/dm³). Dowels used to investigate wood remobilisation (set T3) were colour-coded to ensure a quick and reliable identification of individual elements.

Structure of model runs

Run subsets T1 and T2 focused on wood transport and deposition under steady flow conditions for different values of log properties and discharge, respectively. They were carried out according to a common protocol and were structured as follows:

- wood input to a wood-free network at a convenient upstream cross-section;

- wood dispersal under constant flow until the last element stops;

- lowering of discharge under the threshold for bed motion;

- image acquisition (run subset T2 only) and manual mapping of wood deposits.

Figure 4.7: Size range of the dowels and an example of colour-coding.

Table 4.3: Properties of dowels.

Parameter	Value
Wet density [kg/dm^3]	0.65 ÷ 0.77
Log length [cm]	4, 6, 8, 12
Log diameter [mm]	2, 3, 4, 6
Root wad diameter [mm]	12

Only channels with observable bed transport were used as wood input locations because bank erosion is expected to occur only along active channels. Input frequency was set to one element every four seconds to ensure uncongested transport conditions and rapid input. In this way, the effects of concurring processes such as wood remobilisation and bed evolution can be neglected. A short input phase also allows for the approximation of constant discharge during the whole process. Cohorts of 48 identical dowels were used for the two run sets. For T1 runs (focusing on log properties), four values of log length, log diameter and percentage of elements with roots were used. For T2 runs (focusing on discharge), dowels were added to the network under four different steady flow conditions. In this case two cohorts were used, with a different percentage of logs with roots. The combinations of parameters tested in sets T1 and T2 are summarised in Table 4.4; runs were repeated ten times for each combination using different input sections, for a total of 180 simulations carried out on five network realisations. The 100 runs in set T1 were conducted in random order to filter out any influence of local geometry or network evolution stage.

Model runs in set T3 consist of a first phase of wood flotation and deposition analogous to T1 and T2 runs and a second phase of wood remobilisation associated to the simulation of a subsequent flood. The same set of discharges used for T2 runs (0.9, 1.2, 1.5 and 1.8 l/s) was used for wood input, while the following flood was simulated as a stepped hydrograph with a peak discharge of 1.8 l/s for all model runs. The simulation protocol and structure were defined in analogy with those used for run sets 1 and 2:

- wood input to a wood-free network and dispersal under constant flow until the last element stops;

- lowering of discharge under the threshold for bed motion, image acquisition and manual mapping of wood deposits;

- simulation of a hydrograph of given magnitude, shape and duration;

- lowering of discharge under the threshold for bed motion, image acquisition and manual mapping of the new configuration of wood deposits;

- laser survey of network geometry.

Table 4.4: Combinations of wood properties (length, diameter, percentage of logs with roots) and flow conditions used for T1 and T2 runs

Target parameter	Wood and flow properties				N° of runs
	D [mm]	L [cm]	X [%]	Q [l/s]	
Log diameter (D)	2, 3, 4, 6	8	0	1.8	40
Log length (L)	3	4, 6, 12	0	1.8	30
% of logs with roots (X)	3	8	25, 50, 100	1.8	30
Discharge (Q)	3	8	0	0.9, 1.2, 1.5, 1.8	40
	3	8	50	0.9, 1.2, 1.5, 1.8	40

Table 4.5: Combinations of wood properties (length, diameter, percentage of logs with roots) and flow conditions used for T3 runs.

Target parameter	Wood properties			Discharge [l/s]		N° of runs
	D [mm]	L [cm]	X [%]	input	remobilisation	
Discharge (Q)	3	8	50	0.9, 1.2, 1.5, 1.8	1.8	40

As for run sets T1 and T2, wood was added to active channels with an input frequency of one element every four seconds. The input phase lasts for approximately five minutes while the flood hydrograph comprises an initial 5-minutes step at 0.5 l/s, three 3 minutes steps at 0.9, 1.2 and 1.5 l/s and a 10-minute plateau at 1.8 l/s, for a total run time of slightly less than 30 minutes. Wood cohorts comprised 72 colour-coded dowels (50% of which with roots) and experiments were repeated ten times for each value of input discharge, for a total of 40 runs. Model configuration for run set T3 is summarised in Table 4.5;

Wood mapping techniques and protocols

Direct mapping of wood deposits by visual inspection was identified as a fast and effective technique to reconstruct 2D wood deposition patterns at flume scale. Wood was mapped on a 5x5 cm grid and dowels touching each other were considered as a log jam, thus setting the minimum size of a jam to two logs in analogy with Comiti et al. (2006). For log jams (Figure 4.8), the position of the approximate centre of the accumulation was recorded. Direct mapping was used as the primary monitoring technique for wood surveys in run sets T1 and T2. Output data for each run are represented by a list of deposition sites identified by a unique combination of x and y and include the following attributes:

- the number of logs present at each site (size, S);

- travel distance (T) computed for each site as the difference between the x coordinate of site and that of input cross section, i.e. neglecting channel curvature.

Logs exiting the flume (less than 2% of overall wood input) were assigned a x coordinate corresponding to the flume outlet but were excluded from all subsequent analyses of jam size distribution. For run set T3, accurate positioning of logs with respect to channel pattern is needed to evaluate the interaction between network topography and wood dispersal. Moreover, information on individual dowels is required to obtain a detailed description of wood remobilisation processes. Consequently, wood mapping for run set 3 was based on the identification of individual elements – each of which is characterised by a unique colour code – on rectified images.

Preliminary tests showed that image-based mapping is prone to errors, especially for large jams where dowels are stacked on top of one another and thus direct mapping was used as a support technique to ensure the correct identification of logs. For each element, the coordinates of either end were recorded and relative elevation was sampled from the DEM along each dowel with a 5 mm step, resulting in 17 values of z per log. Remobilisation was evaluated by comparing pre- and post-flood imagery. Logs were assigned to three categories on the basis of the displacement of log midpoint: *stable* logs (no displacement); *reorganised* logs (travel distance is shorter than 2 log lengths); *remobilised* logs (travel distance is larger than 2 log lengths). Output data for each run are represented by a list of records identified by a unique dowel colour code and include the following attributes:

- dowel centre coordinates (x_g, y_g);

- travel distance (T);

- average, median, minimum and maximum relative elevation along the dowel (z_{ave}, z_{med}, z_{min}, z_{max}, respectively);

- presence or absence of the root wad (R);

- size of the accumulation that includes the dowel (size, S);

- remobilisation category, referred to as *fate* (F).

Figure 4.8: Accumulation styles: an isolated log and a log jam comprising 11 elements.

4.2.4 Overview of statistical techniques

The present chapter provides an overview of the statistical methods used to evaluate the association between wood dispersal processes – transport, deposition, remobilisation – and key governing factors, including log properties, channel morphology and flow regime. Evaluating the role of these drivers implies testing the hypothesis that different levels of the factor produce *significant* effects on the variables used to describe dispersal processes, that is, that the difference between samples associated to each level of the factor exceed the intrinsic (random) variability of the observed phenomenon.

Methods for inferential statistics used in the present work include:

- *t*-test;

- analysis of variance family methods, including ANOVA and MANOVA;

- discriminant analysis;

- logistic regression.

The theoretical background provided here is derived from Lowry's online textbook (2012) for univariate statistics and from Tabachnick and Fidell (2012) for multivariate analyses.

t-test

The *t*-test determines the statistical significance of the difference between the means of two samples. The null hypothesis of the test H_0 states that the samples are drawn from the same population and thus their means are identical and equal to the mean of the source population. If the null hypothesis is rejected, the two sample means are significantly different, implying that the two samples are taken from different populations. The *t*-test can be one-tailed (directional), when the sign of the difference between the means is known in advance, or two-tailed (non directional) when no *a priori* information is available. The assumptions of the *t*-test are:

- independent random sampling;

- continuous interval scale or ratio scale observed variable;

- normally distributed source population.

The *t*-test is applied to two samples *A* and *B* comprising n_A and n_B observations of a generic variable *x*, respectively. Under the null hypothesis, both samples belong to the same normally distributed source population. The distribution of sample means is also normal and its mean μ_d corresponds to the mean of the source population μ_P. The test is

based on the computation of the sum of squared deviates (also called *sum of squares*) SS_j, which, for the *j*-th sample reads

$$SS_j = \sum_{i=1}^{n_j} \left(x_{ij} - \mu_j \right)^2$$

where x_i is the *i*-th observation of the *j*-th group and μ_j is the mean of the group. Sums of squares are used to estimate the variance of the source population σ^2_p

$$\sigma^2_p = \frac{SS_A + SS_B}{(n_A - 1) + (n_B - 1)}$$

and the standard deviation of the distribution of sample means σ_d as

$$\sigma_d = \sqrt{\frac{\sigma^2_p}{n_A} + \frac{\sigma^2_p}{n_B}} \ .$$

The test statistic *t* is computed as

$$t = \frac{\mu_A - \mu_B}{\sigma_d} \ .$$

The resulting value of *t* is compared to a critical value t_{crit} computed from Student's *t*-distribution with a number of degrees of freedom equal to $n_A + n_B$ - 2 for a given level of significance α. If $t > t_{crit}$ the null hypothesis is rejected, implying that the means of the two samples are different at a level of significance equal to α; the probability that the difference between means is due to a genuine effect and not to mere chance is 1 - α.

A wide range of methods is available to to test sample normality. If the assumption is violated, the equivalent non-parametric Mann-Whitney Test is used. In this case, the values of *x* are substituted with their rank, evaluated over the combination of the two samples.

One-way Analysis of Variance (ANOVA)

One-way ANOVA can be seen as the generalisation of the *t*-test for experimental designs with more than two samples. In this case, running multiple *t*-tests would result in an uncontrolled inflation of Type I error (incorrect rejection of a true null hypothesis). Samples, usually referred to as *groups*, can correspond to different levels of an external factor (the *independent* variable, *IV*). In analogy with the *t*-test, the null hypothesis of ANOVA is the identity of group sample means:

$$H_0: \ \mu_1 = \mu_2 = ... = \mu_k \ .$$

The null hypothesis is tested by partitioning the variance of the observed variable (also called *dependent variable, DV*) into a component associated to within-group variability (often

referred to as *error*) and a component due to between-group differences (*treatment*) and comparing the two quantities. The assumptions of ANOVA are:

- independent random sampling;

- continuous interval scale or ratio scale observed variable;

- normally distributed source population;

- homogeneity of variance across groups *(homoscedasticity).*

One-way ANOVA is applied to g groups of observations of the dependent variable *x*. The mean of the *j*-th group μ_j is

$$\mu_j = \frac{1}{n_j} \sum_{i=1}^{n_j} x_{ij} \ ,$$

where n_j is the number of observations in the *j*-th group and x_{ij} denotes the *i*-th observation of the group. A grand mean μ is computed for the whole dataset as

$$\mu = \frac{1}{N} \sum_{j=1}^{g} \sum_{i=1}^{n_j} x_{ij} \ ,$$

where N is the total number of observations over all groups. The total sum of squares SS_t, a measure of the total observed variance of the dataset, is defined as

$$SS_t = \sum_{j=1}^{g} \sum_{i=1}^{n_j} (x_{ij} - \mu)^2 \ .$$

It is easily shown that SS_t can be partitioned into two components, the within-group or 'error' component SS_e and the between-group or 'treatment' component SS_h:

$$SS_e = \sum_{j=1}^{g} \sum_{i=1}^{n_j} (x_{ij} - \mu_j)^2 \qquad SS_h = \sum_{j=1}^{g} n_j (\mu_j - \mu)^2 \qquad SS_t = SS_h + SS_e \ .$$

The two components are divided by the appropriate number of degrees of freedom (corresponding to g-1 for treatment and N-1 for error) and the test statistic F is computed as

$$F = \frac{SS_h / (g-1)}{SS_e / N - 1} \ .$$

F is compared with a critical value F_{crit} deduced from a F distribution with [g-1, N-1] degrees of freedom for a significance level α. If $F > F_{crit}$ the null hypothesis is rejected, implying that at least one of the group means is different from the others. It is important to underline that ANOVA yields no information about the statistical significance of the difference between specific pairs of group means. If ANOVA highlights a significant

overall effect of treatment, a post-hoc test is needed to identify which levels of the independent variable actually induce a significant variation of group mean. A widely used technique is Tukey's HSD (Honestly Significant Difference) test, which requires the computation of the Studentized range statistic Q. For a pairs of groups with means $\mu_1 > \mu_2$ and equal number of observations n, Q is computed as

$$Q = \frac{\mu_1 - \mu_2}{\sqrt{\dfrac{SS_e}{n(N-1)}}} \, .$$

Critical values of Q are computed on the basis of g, N-1 and α; differences between means are statistically significant if $Q > Q_{crit}$.

In addition to normality, homoscedasticity has to be verified, for example using Levene's test. If the assumption of normality and/or homogeneity of variance are violated, the equivalent Kruskal-Wallis test can be used. As for the Mann-Whitney test for two samples, this is a non-parametric technique where the values of x are substituted with their rank. However, ANOVA has been shown to be robust to violations of normality and/or homogeneity of variance (including the presence of outliers) if the number of observations is the same for all groups (balanced design).

Factorial MANOVA

One-way univariate ANOVA applies to sets of observations of one dependent variable as a function of one independent variable. More complex experimental designs can be constructed if more than one factor is used to define groups (n-way or *factorial* analysis of variance) and if multiple DVs are monitored (multivariate analysis of variance, MANOVA). Methods for inferential statistics have been developed for all four combinations of number of *IVs* (one-way *versus* multi-way analysis) and number of DVs (univariate *versus* multivariate analysis); however, the present chapter focuses on the ones used in the study, and in particular, only factorial MANOVA in its simplest, two-way form is described.

The goal of factorial multivariate analysis of variance is to evaluate the joint effect of two or more factors (treatments) on two or more dependent variables. The key reason for conducting a factorial MANOVA instead of multiple factorial ANOVAs for individual DVs is the ability to take into account relationships between dependent variables. Moreover, MANOVA protects from excess Type I errors, but this can be achieved also by employing correction techniques such as the Bonferroni correction. However, only a truly multivariate approach can provide information on the interaction between multiple DVs (Bray and Maxwell, 1982; Haase and Ellis, 1987). Two-way MANOVA is applied to experimental designs with two independent variables (factors) A and B with a and b levels, respectively. Each of the resulting $g = a \cdot b$ groups comprises n elements and p dependent variables are

measured for each element. $\boldsymbol{x}_{ijk}$ represents a vector of p measurements for the k-th element of the group identified by the i-th level of A and the j-th level of B. The two-way MANOVA model for a generic observation x_{ijk} can be written as

$$x_{ijk} = \mu + \alpha_i + \beta_j + \gamma_{ij} + \epsilon_{ijk} \; ,$$

meaning that the individual element (here, a vector of DVs) differs from population mean μ because of the effect of factor A at its i-th level (α_i), factor B at its j-th level (β_j), their interaction (γ_{ij}) and the intrinsic variability ε_{ijk}. The null hypothesis H_0 is written separately for each effect; for example, for factor A it reads

$$H_{0A}: \; \alpha_1 = \alpha_2 = ... = \alpha_a \; .$$

The assumptions and requirements of MANOVA are

- independent random sampling;

- continuous interval scale or ratio scale observed variable;

- absence of multicollinearity and singularity, meaning that none of the DVs can be written as a linear combination of the others;

- cell size (number of observations in each group) larger than the number of DVs;

- multivariate normality, implying that the sample distributions means of the various DVs in each group and their linear combinations are normally distributed;

- homogeneity of variance-covariance matrices.

It is worth noting that multivariate techniques including MANOVA imply some degree of correlation between DVs and thus should not be applied to sets of completely uncorrelated variables. Testing the null hypothesis in a multivariate context implies taking into account the interactions between dependent variables. Therefore, the sum of square deviates used in ANOVA (a scalar quantity akin to variance) is substituted by a sum of square and cross product matrix ($SSCP$, analogous to a variance-covariance matrix). In ANOVA, sums of squared are partitioned between treatment and error. In two-way MANOVA, the total sum of square and cross product matrix T is partitioned into components associated to factor A, factor B, their interaction and the error component:

$$T = H_A + H_B + H_{AB} + E \; .$$

T is a p x p matrix; its generic l,m-th element for the l-th and m-th dependent variables is written as

$$t_{l,m} = \sum_{j=1}^{g} \sum_{i=1}^{n} (x_{ijk,m} - \mu_m)(x_{ijk,l} - \mu_l) \; .$$

$x_{ijk,m}$ is the value of the m-th variable for element x_{ijk} and μ_m is the grand mean of the m-th variable. Diagonal terms with $l = m$ are analogous to variance and off-diagonal terms to covariances. The computation of *SSCP* matrices requires the definition of the grand mean vector μ, the g group mean vectors μ_{ij} and the means over individual factors μ_i (a set of a vectors) and μ_j (a set of b vectors). These vectors are computed as

$$\mu = \frac{1}{nab}\sum_{ijk} x_{ijk} \qquad \mu_i = \frac{1}{nb}\sum_{jk} x_{ijk} \qquad \mu_j = \frac{1}{na}\sum_{ik} x_{ijk} \qquad \mu_{ij} = \frac{1}{n}\sum_k x_{ijk} \ .$$

SSCP matrices for and the corresponding degrees of freedom are defined as follows:

$$
\begin{aligned}
\boldsymbol{T} \quad &= \quad \sum_{ijk}(\boldsymbol{x}_{ijk}-\boldsymbol{\mu})(\boldsymbol{x}_{ijk}-\boldsymbol{\mu})' & d_{fT}&=abn-1 \\
\boldsymbol{H}_A \quad &= \quad nb\sum_i (\boldsymbol{\mu}_i-\boldsymbol{\mu})(\boldsymbol{\mu}_i-\boldsymbol{\mu})' & d_{fA}&=a-1 \\
\boldsymbol{H}_B \quad &= \quad na\sum_j (\boldsymbol{\mu}_j-\boldsymbol{\mu})(\boldsymbol{\mu}_j-\boldsymbol{\mu})' & d_{fB}&=b-1 \\
\boldsymbol{H}_{AB} \quad &= \quad na\sum_{ij}(\boldsymbol{\mu}_{ij}-\boldsymbol{\mu}_i-\boldsymbol{\mu}_j+\boldsymbol{\mu})(\boldsymbol{\mu}_{ij}-\boldsymbol{\mu}_i-\boldsymbol{\mu}_j+\boldsymbol{\mu})' & d_{fAB}&=(a-1)(b-1) \\
\boldsymbol{E} \quad &= \quad \sum_{ijk}(\boldsymbol{x}_{ijk}-\boldsymbol{\mu}_{ij})(\boldsymbol{x}_{ijk}-\boldsymbol{\mu}_{ij})' & d_{fE}&=ab(n-1)
\end{aligned}
$$

Multivariate statistics used for hypothesis testing are based on the computation of the eigenvectors of the matrix product

$$A = HE^{-1} \ ,$$

where H is a *SSCP* matrix for a generic treatment (in the two-way case, either H_A, H_B or H_{AB}). Let λr denote the r-th eigenvector of A; the four most common statistics, namely Wilks' lambda (Λ), Pillai's trace (V), Hotelling-Lawley's trace (T) and Roy's greatest characteristic root criterion (Θ) are defined as follows:

$$
\begin{aligned}
\Lambda \quad &= \quad \prod_{r=1}^q \frac{1}{1+\lambda_r} \quad &= \quad \frac{|\boldsymbol{E}|}{|\boldsymbol{E}+\boldsymbol{H}|} \\
V \quad &= \quad \sum_{r=1}^q \frac{\lambda_r}{1+\lambda_r} \quad &= \quad trace[\boldsymbol{H}(\boldsymbol{H}+\boldsymbol{E})^{-1}] \\
T \quad &= \quad \sum_{r=1}^q \lambda_r \quad &= \quad trace[\boldsymbol{H}\boldsymbol{E}^{-1}] \\
\Theta \quad &= \quad max(\lambda_r)
\end{aligned}
$$

The overall number of eigenvalues q is equal to the smaller of either the number of DVs (p) or the minimum number of degrees of freedom for the hypotheses:

$$q = min(p, d_{fA}, d_{fB}, d_{fAB}) \ .$$

This implies that if there are only two DVs or one of the factors has only two levels, only one eigenvalue is extracted and the four statistics yield the same result. The critical

values of the four statistics are exact or approximate values of a F distribution with the appropriate number of degrees of freedom. The null hypothesis is rejected for small values of Λ and large values of the other statistics.

Testing of MANOVA assumptions includes the evaluation of correlation between DVs, usually computed as Pearson's coefficient r. MANOVA is sensitive to violations of normality, especially if caused by outliers; consequently, it is recommended to identify and remove multivariate outliers from each group. Homogeneity of variance and covariance matrices is often tested using Box's M test, but the test has been shown to be very sensitive to violations of normality. Removal of outliers and variable transformation is often used to overcome these problems. Violation of assumptions is a particularly serious issue for unbalanced designs. In this case, Tabachnick and Fidell (2012) suggest using only Pillai's criterion for hypothesis testing.

MANOVA does not provide information on individual group differences. Multiple ANOVA comparisons have been used as follow-up tests, but as a univariate approach, this technique ignores intercorrelation between dependent variables and thus fails to grasp the multivariate nature of the problem. Various truly multivariate follow-up procedures have been suggested (Bray and Maxwell, 1982; Enders, 2003); in the present work, discriminant analysis was used to assess group differences.

Discriminant analysis

Discriminant analysis is a multivariate technique often used to identify differences between groups of observations on the basis of multiple correlated variables and also to assign new observations to groups on the basis of combinations of measured quantities. However, discriminant analysis has also been suggested as a follow-up technique for MANOVA (Haase and Ellis, 1987; Enders, 2003). The objective of the method is to derive one or more new variables (*composite variables*) as linear combinations of observed quantities (*predictors*). The new set of variables maximises the between-group differences and is identified through an optimisation process based on the partitioning of variance between treatment and error effect. This procedure is computationally equivalent to a one-way MANOVA. Therefore, the assumptions of discriminant analysis are essentially the same of multivariate analysis of variance.

Discriminant analysis applies to experimental designs with g group of n_g elements for which p predictors are observed. The functions defining linear combinations of predictors are *canonical discriminant functions*

$$Z_i = a_1 x_1 + a_2 x_2 + \ldots + a_p x_p$$

where Z_i is the composite variable and x_i are the predictors; the a_i weights are obtained through optimisation. Predictors are usually standardised so that the mean of discriminant

function scores over all observations is also zero. A maximum of n_d orthogonal discriminant functions are defined with

$$n_d = max(g - 1, p)$$.

The set of functions is organised so that the first one maximally separates groups, i.e. accounts for the greatest proportion of between-group variance. Each successive function corresponds to the largest share of remaining variance. Variance partitioning requires the computation of two *SSCP* matrices, a within-group matrix **W** and a between-group matrix **B**. For one composite variable *z*, matrices are defined as

$$\mathbf{W} = \sum_{j=1}^{g} \sum_{i=1}^{n_j} (z_{ij} - \mu_j)(z_{ij} - \mu_j)' \qquad \mathbf{B} = \sum_{j=1}^{g} n_j (\mu_j - \mu)(\mu_j - \mu)'$$

where z_{ij} is the *i*-th element of the *j*-th group, μ_j is the mean of the *j*-th group and μ is the grand mean. It can be shown that the trace of **B** represents the separation between groups. Significance is usually tested using Wilks' lambda:

$$\Lambda = \frac{|\mathbf{W}|}{|\mathbf{W} + \mathbf{B}|}$$.

Each computed discriminant function describes the dataset in a new space where the number of variables is reduced from *p* to one. Group means of Z_i are usually called *centroids* and their distance represents the degree of group separation that is associated to Z_i. The proportion of total variance explained by each discriminant function is commonly called *proportion of trace*.

Logistic regression

Logistic regression belongs to a category of statistical models called *generalized linear models* (also including ordinary regression and the analysis of variance family of models) The aim of logistic regression is to predict the outcome of a process from a set of observed parameters. In binomial logistic regression, the outcome or *response* variable *y* is a dichotomous variable taking two values (usually coded as *y* = 0 and *y* = 1*)*. Multinomial logistic regression is the extension of the method to experimental designs with *N* possible outcomes. In this case, the statistical technique is applied to *N*-1 pairs of outcomes. Observed parameters, usually referred to as *predictors*, can be expressed as continuous, discrete or dichotomous variables. A key feature of logistic regression is that this method makes no assumption about the distribution of predictors (normality, homogeneity of variance), unlike analysis of variance and discriminant analysis. However, all the aforementioned multivariate methods require independent random sampling and absence of multicollinearity between predictors.

Logistic regression defines the relationship between the response variable and a set of n independent variables as a logistic regression function:

$$logit\,(P) = \log\frac{P}{1-P} = \beta_0 + \sum_{i=1}^{n} \beta_n x_n \ .$$

P is a probability value in the range (0,1) and x_i are a set of independent variables – comprising predictors and/or combinations thereof – while β_i are the corresponding coefficients. β_0 (*intercept*) represents the value of logit (P) computed by excluding any effect of the independent variables. For each observation in the sample, the value of P is computed as

$$P = \frac{e^{\beta_0 + \sum_{i=1}^{n} \beta_n x_n}}{1 - e^{\beta_0 + \sum_{i=1}^{n} \beta_n x_n}} \ .$$

Coefficients are determined for the whole sample on the basis of the observed outcomes of the response variable using maximum-likelihood estimation.

Logistic regression modelling is used to evaluate the influence of individual predictors and/or combinations of predictors (interactions) on the outcome of the process of interest. A number of techniques are used, including:

- log-likelihood tests to evaluate the significance of a set of predictors;

- Wald χ^2 tests to evaluate the significance of individual coefficients;

- interpretation of effect magnitude using odds;

- classification accuracy.

A logistic model – defined as a given set of n independent variables – yields statistically significant results if the prediction of the response variable obtained with the model is more accurate than that of a null model containing only the intercept. The G^2 statistic for the likelihood ratio test is

$$G^2 = 2\,(\log L - \log L_0) \ ,$$

where L is the likelihood of the tested model and L_0 is the likelihood of the null model containing only the intercept. The term $2 \cdot \log(L)$ is usually referred to as *deviance*. G^2 is approximately χ^2-distributed with n degrees of freedom. A significant model has $G^2 > \chi^2$ for the desired significance level α. The likelihood test is also employed to evaluate the role of individual predictors by comparing pairs of *nested* models where the simplest of the two uses a subset of the predictors of the more complete one. In this case, the number of degrees of freedom for the test is equal to the difference between the number of predictors in the

two models. For $G^2 < \chi^2$, the difference between the two models is not statistically significant and redundant predictors can be discarded. In particular, backward stepwise regression analysis starts from a full model – including all predictors and all combinations of two or more predictors – and proceeds with the elimination of non-relevant parameters in an iterative process.

Moreover, the statistical significance of a coefficient β_i can be assessed via a Wald test; the test statistic Z_i is χ^2-distributed and is computed as

$$Z_i = \frac{\beta_i^2}{S(\beta_i^2)} \ ,$$

where $S(\beta_i^2)$ is the squared standard error of the coefficient. However, the test has been found to be too conservative for large values of β_i and less robust for small sample sizes.

The contribution of the i-th independent variable to the estimation of P can be evaluated in terms of the *odds ratio* (o)

$$o = \frac{P}{1-P} \qquad o_i = e^{\beta_i} \ .$$

The i-th variable increases (or decreases) the likeliness of the response $y = 1$ by a factor equal to o_i. In particular, dichotomous predictors are coded as $x = [0,1]$ and the outcome coded as $x = 0$ is taken as a reference condition. The corresponding β_i coefficient represents the change in $\log(o)$ associated to the other outcome. A categorical predictor with m levels is converted to a series of m-1 dummy dichotomous indicators and the m-th level is assumed as a reference condition. In this case, the coefficient β_k for the k-th dummy variable represents the effect of the k-th level of the original predictor compared with reference conditions. Finally, for a continuous predictor, β_i represents the change in $\log(o)$ for a unit change of the predictor.

Finally, continuous probability values computed for individual elements in the sample can be converted into a dichotomous variable on the basis of a threshold or *cut-off* value of P and compared with the observed outcome y. The number of false positives (*FP*), false negatives (*FN*), true positives (*TP*), and true negatives (*TN*) are summarised in a *table of confusion* or *confusion matrix*. In health sciences, *specificity* and *sensitivity* are defined as follows:

$$specificity = \frac{TN}{TN+FP} \qquad sensitivity = \frac{TP}{TP+FN} \ .$$

It is worth noting that, for a given model, the optimal cut-off value as well as the relevance of sensitivity and specificity ultimately depend on the underlying research question.

4.2.5 Effects of log properties on wood dispersal

The present chapter details the outputs of model runs belonging to subset T1. These simulations focus on the role of log diameter (D), length (L) and percentage of wood with roots (X) on wood transport and deposition. As shown in Table 4.4, four different values of each property were tested while keeping the other two factors constant, in order to isolate the effect of each property. In the present chapter, the resulting ten combinations of D, L and X are referred to as *wood types*, while the series of ten repetitions conducted for each wood type are called *groups*.

Figure 4.9 shows an example of wood deposition patterns obtained at flume scale for three different wood types. Distinctive deposition styles can be identified by visual inspection, as longer logs tend to form large accumulations while smaller elements are found scattered across bar surfaces. However, relevant differences in the spatial organisation of wood deposits were observed across sets of runs carried out with identical dowels. Consequently, the average behaviour for each wood type was investigated initially by aggregating outputs over the ten simulation repetitions.

Subsequently, the within-group variability was investigated by running a one-way analysis of variance (ANOVA) and Tukey post-hoc tests. The equivalent non-parametric technique (Kruskal-Wallis test) was also used when the requirements of normality and homoscedasticity were not met. However, the results of the Kruskal-Wallis test are always identical to those of ANOVA, indicating that the parametric test is robust to violation of assumptions (as expected for a balanced design) and therefore only ANOVA results are shown. To improve readability, outputs are presented in the compact form ($F(a,b) = c$, $p = d$) where c is the test statistic, a and b represent the hypothesis and error degrees of freedom, respectively, and d is the computed significance level of the test). Statistical analysis was conducted using R 2.15.2[1].

Travel distance

As a first step, the frequency distribution of travel distance was defined for each wood type by aggregating the output over groups of 10 runs (for a total of 480 logs per group). For all wood types, a large proportion of dowels is deposited just downstream of the input section, resulting in positively skewed distributions (Figure 4.10). Higher wood mobility determines higher values of median transport distance, larger standard deviation and lower skewness. Log diameter exerts the strongest effect on distributions, with both the median and the standard deviation of transport distance increasing for thinner elements.

---

[1] R Development Core Team, 2008. R: A language and environment for statistical computing. V. R Foundation for Statistical Computing. http://www.R-project.org.
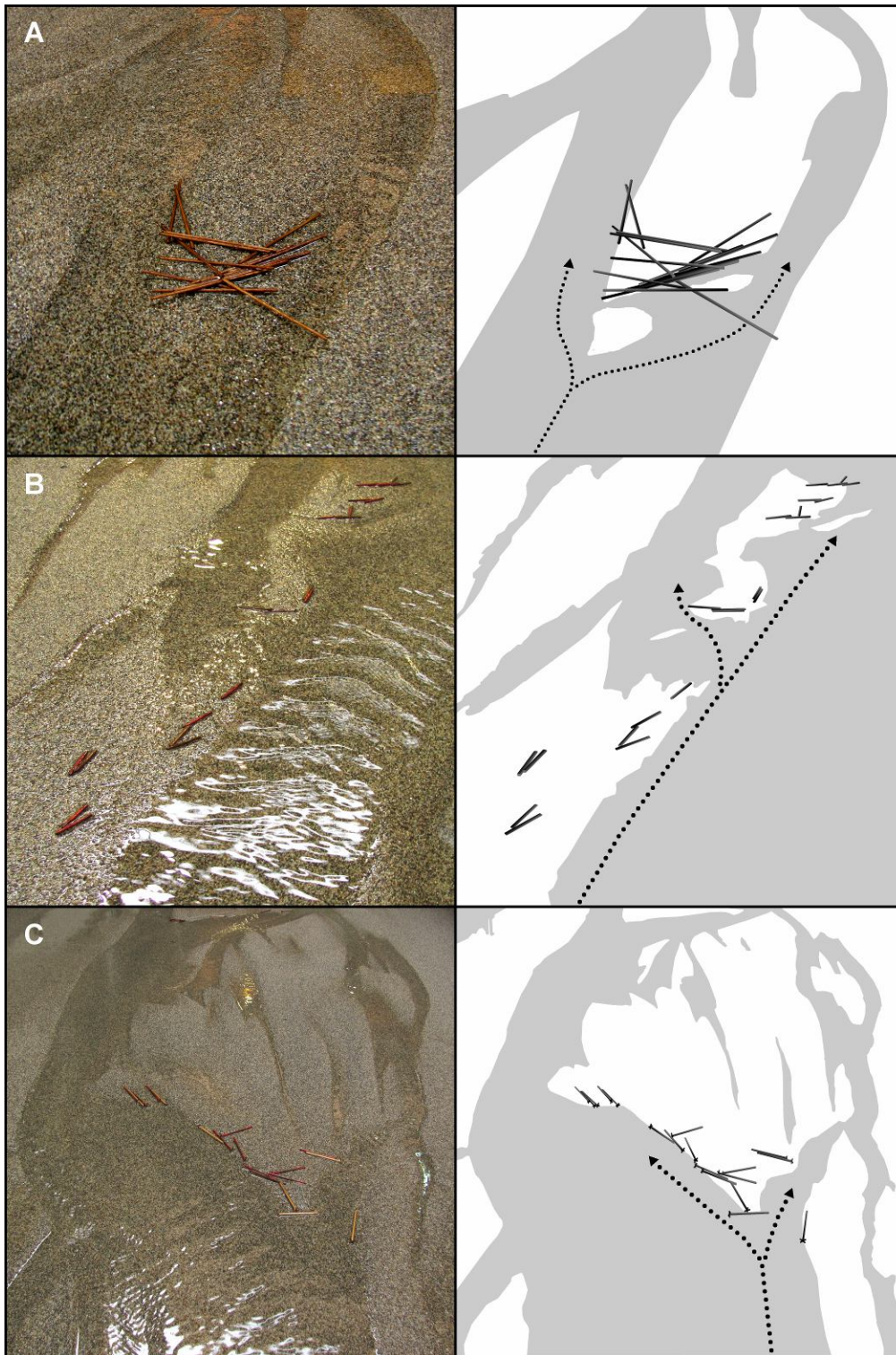
Figure 4.9: Examples of wood deposition patterns from run set T1: (A) jam on a mid-channel bar (L = 12 cm, D = 3 mm, R = 0); (B) logs scattered across bars (L = 4 cm, D = 3 mm, R = 0); (C) log accumulation at bar head (L = 8 cm, D = 3 mm, R = 50%). Dotted lines represent flow direction.

Median travel distance values computed for individual runs (for a total of 48 logs) are presented as boxplots in Figure 4.11 following the guidelines suggested by McGill et al. (1978). Here, for a generic variable b, outliers are defined as data lying outside the interval

$$b_{25} - 1.5 \cdot (b_{75} - b_{25}) < b < b_{75} + 1.5 \cdot (b_{75} - b_{25})$$

where b_{25} and b_{75} are the 25th and 75th percentile of b, respectively. Whiskers extend to the minimum and maximum value excluding outliers. ANOVA highlighted a significant effect of diameter ($F(3,36) = 5.63$, $p = 0.003$) and percentage of logs with roots ($F(3,36) = 2.99$, $p = 0.043$) and Tukey tests were performed to identify significant between-group differences (Table 4.6). As already observed for aggregated data, diameter is the main factor governing travel distance. A statistically significant difference was found between small ($2 \div 3$ mm) and large diameters ($4 \div 6$ mm).

No significant effect of length was found, while only one pair of values of X showed a significant shift. It is worth noting that large within-group variability is observed especially for extreme values of L and intermediate values of X. In the latter case, direct observations suggest that, when mixed dowel cohorts are used ($X = 25\%$ or $X = 50\%$ of logs with roots), log input order might have a role in determining deposition patterns. Dowels with and without roots were added to the flume in random order; however, when many logs with roots were among the first to enter the flume, their influence appeared to be comparatively larger. Results for other percentiles closely mirror those found for the median.

Jam formation and size distribution

The percentage of isolated logs (*PSI*) can be interpreted as a measure of the (un)likeliness of jam formation. This parameter was computed for individual runs (Figure 4.12). No differences associated to log diameter were found, while a significant decrease in the percentage of isolated logs occurs for the largest values of both length and percentage of wood with roots (ANOVA for *L*: $F(3,36) = 9.51$, $p = <0.001$; ANOVA for *X*: $F(3,36) = 6.77$, $p = <0.001$) see Table 4.7 for Tukey test outputs).

Furthermore, the relationship between wood type and jam size distribution was investigated in terms of relative relevance of accumulations of a given size. Jams were classified into four classes (2, 3 , $4 \div 9$ and more than 9 logs) and frequency values were computed for type-aggregated data in terms of a) number of jams per size class (Figure 4.13); and b) total amount of wood per size class (Figure 4.14). Small aggregations of logs are by far the most frequent, with 40 to 60% of all jams formed by 2 logs regardless of wood properties. If jams composed by 3 logs are also included, figures increase to $60 \div 80\%$. The relative relevance of small jams appears to decrease with log length, while no trend can be identified for log diameter and percentage of logs with roots. Large jams (10 logs or more) represent almost 20% of all aggregations for high dowel length and percentage of roots,
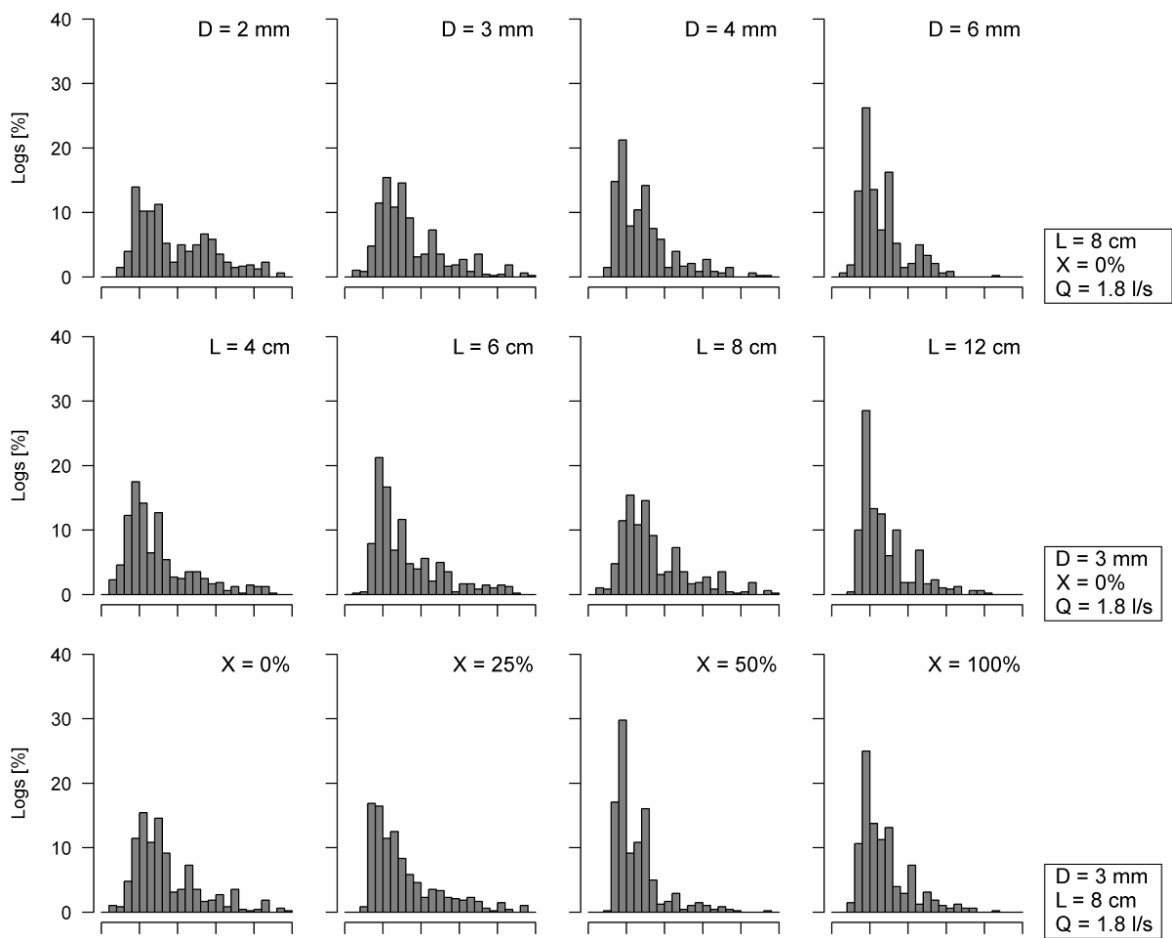
Figure 4.10: Histograms of travel distance. D is log diameter, L is length, X is the percentage of logs with roots and Q is discharge.
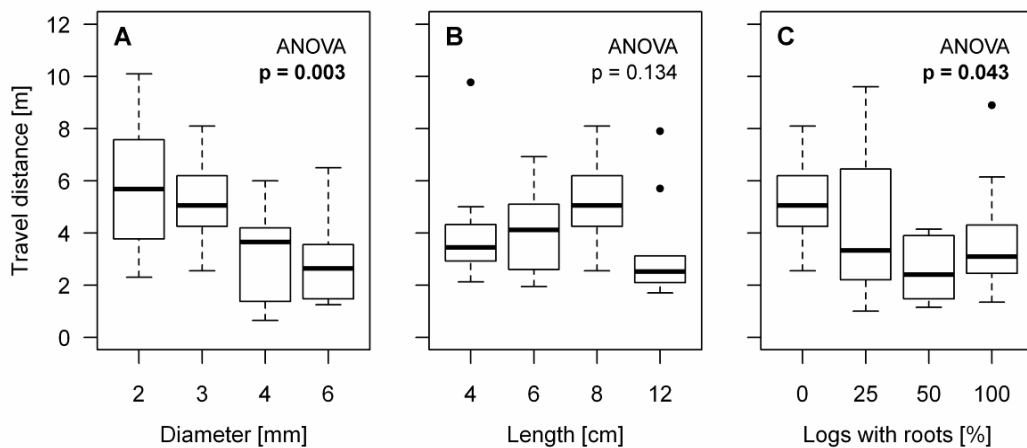
Figure 4.11: Median travel distance of log cohorts with different values of log diameter (A); log length (B); percentage of logs with roots (C). Data for sets of 10 runs are presented as boxplots with dots indicating outliers. Significant ANOVA p values are shown in bold.

Table 4.6: Tukey test for median transport distance. Significant p values are shown in bold.

D [mm]	3	4	6		X [%]	25	50	100
2	0.915	**0.026**	**0.009**		0	0.706	**0.028**	0.367
3		**0.113**	**0.045**		25		0.262	0.940
4			0.974		50			0.574

Table 4.7: Tukey test for the percentage of isolated logs. Significant p values are shown in bold.

L [cm]	6	8	12		X [%]	25	50	100
4	0.558	**0.049**	**<0.001**		0	0.885	0.937	**0.004**
6		0.515	**0.002**		25		0.562	**<0.001**
8			0.078		50			**0.018**

Table 4.8: Tukey test for the average size of the 3 largest jams. Significant p values are shown in bold.

L [cm]	6	8	12		X [%]	25	50	100
4	0.731	0.446	**<0.001**		0	0.993	0.403	**<0.001**
6		0.965	**<0.001**		25		0.267	**<0.001**
8			**0.001**		50			**0.013**

while they are virtually absent for low values of *L*. These trends are more clearly observed in terms of percentage of logs per jam size class. 30÷40% of wood stored as jams belongs to small jams (2÷3 logs) regardless of dowel diameter, but this value drops from 70 to 30% for increasing values of log length. Large values of *L* and *X* are strongly associated with large accumulations that can store more than 40% of all wood in jams.
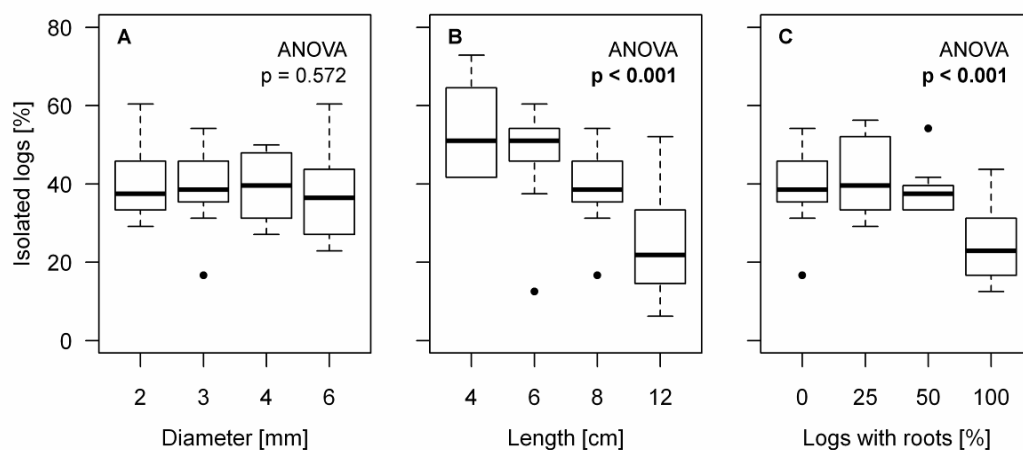
Figure 4.12: Percentage of isolated logs for different values of log diameter (A); log length (B); percentage of logs with roots (C). Data for sets of 10 runs are presented as boxplots with dots indicating outliers. Significant ANOVA p values are shown in bold.
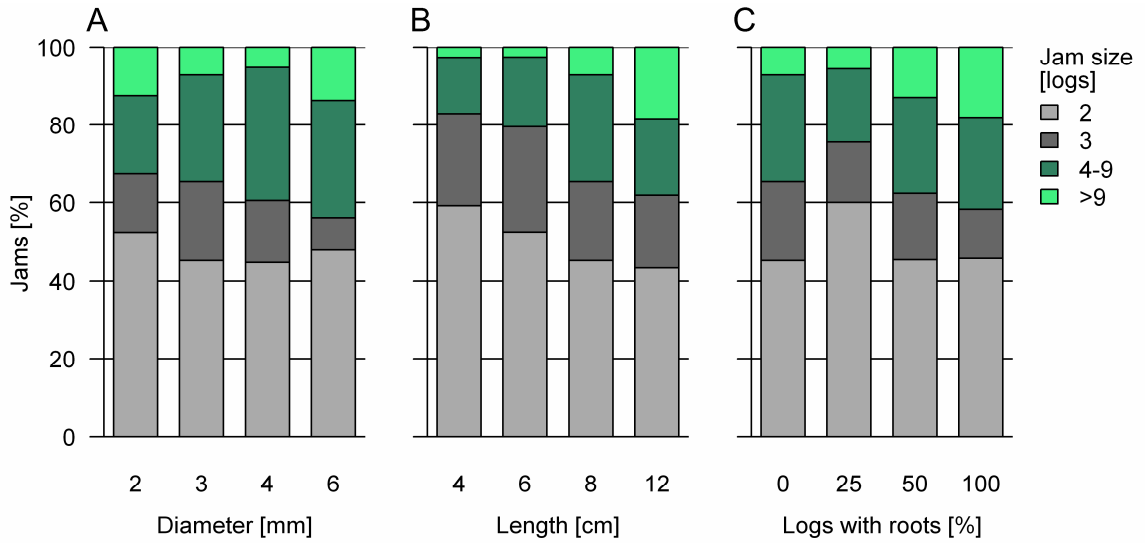
Figure 4.13: Distribution of jam size for different values of log diameter (A); log length (B); percentage of logs with roots (C).
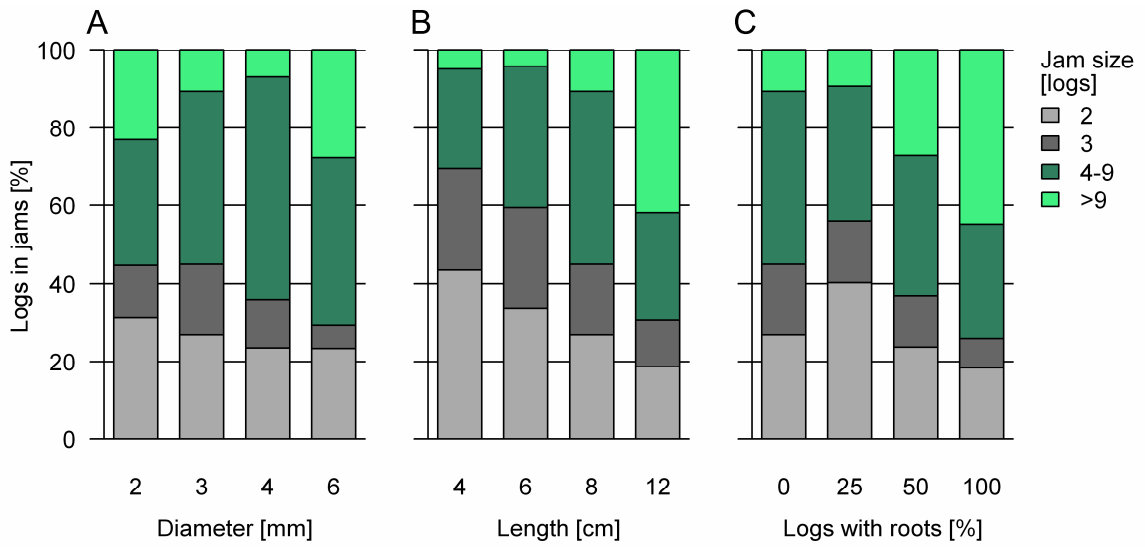
Figure 4.14: Wood distribution over jam size classes for different values of log diameter (A); log length (B); percentage of logs with roots (C).

4.2.6 Effects of flow stage on wood dispersal

The present chapter details the outputs of model runs belonging to subset T2. In these simulations, the effect of discharge (Q) on wood dispersal was investigated by adding wood to the network under different steady flow conditions. The concurrent role of log shape was evaluated by using two cohorts of dowels, one if which included elements with roots. Data analysis was carried out in analogy with run set T1. In addition, sets of runs performed under the same flow conditions but with different values of X were compared using a *t*-test or (whenever needed) the equivalent non-parametric Mann-Whitney test. A series of ten runs (*group*) was performed for each of the eight combinations of Q and X.

Travel distance

A frequency distribution of travel distance was computed for each run group (480 logs). Distributions are positively skewed and median travel distance tends to increase with discharge. Skewness increases and standard deviation decreases if roots are present. The variability of distribution moments associated with flow stage is comparable to the effect of the introduction of roots (Figures 4.15 and Figure 4.16).

The median value and 90th percentile of travel distance were computed for individual runs (48 logs) and are presented as boxplots in Figure 4.17. No significant differences were found for median travel distance, whereas the 90th percentile significantly increases with discharge if roots are absent (ANOVA: $F(3,36) = 5.71$, $p = 0.003$). Tukey test p values are summarised in Table 4.9. The effect of the presence of roots on travel distance over a range of different flow conditions was evaluated by applying the *t*-test to selected percentiles of the distribution (10th, 25th, 50th, 75th, 90th) As shown in Table 4.10, the relevance of roots changes with discharge. For wood input occurring at lower flows, the presence of roots induces a significant reduction of all percentiles, while at higher flows the presence of roots influences only the tail of the distribution (higher percentiles).

Jam formation and size distribution

The percentage of isolated logs for an individual run does not appear to be influenced by discharge, with only one pair of discharge values yielding significant differences. The comparison among runs performed under identical flow conditions but with different values of X also shows no statistically significant effects. The distribution of wood over jam size classes is shown in Figure 4.18. The combination of low discharges and presence of roots produces a relevant increase in wood stored as large jams (up to 40%). However, ANOVA and *t*-tests did not highlight any significant effect of discharge and/or proportion of roots on the size of the largest jams.
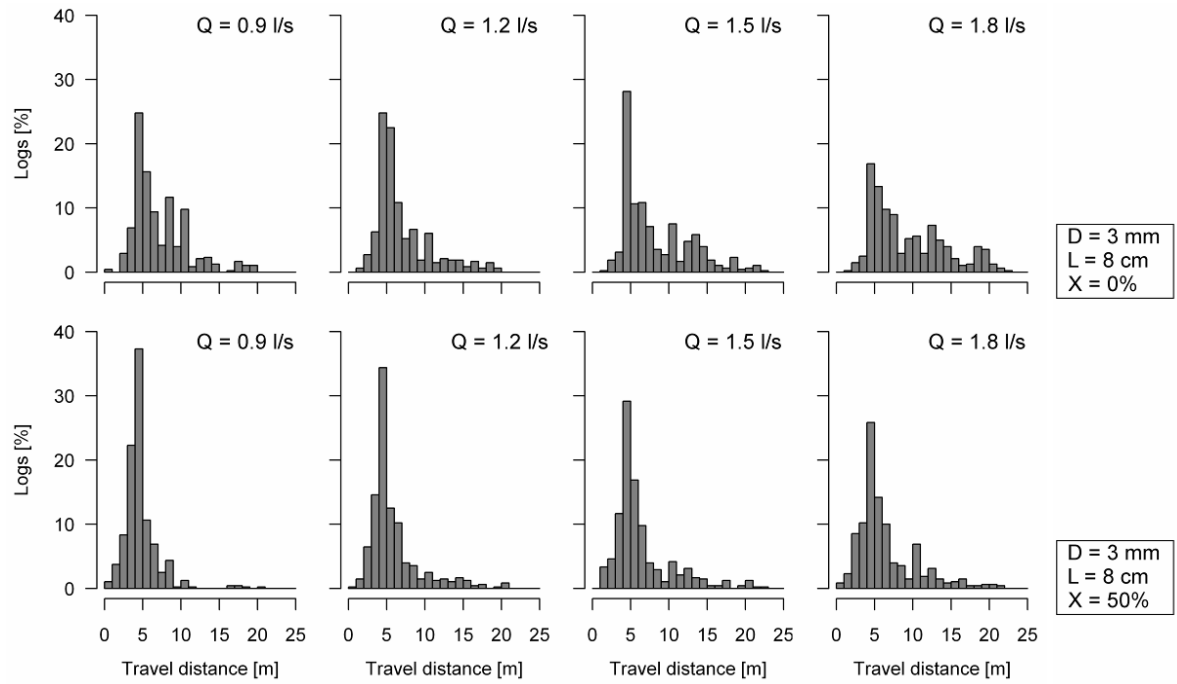
Figure 4.15: Histograms of travel distance. D is log diameter, L is length, X is the percentage of logs with roots and Q is discharge.
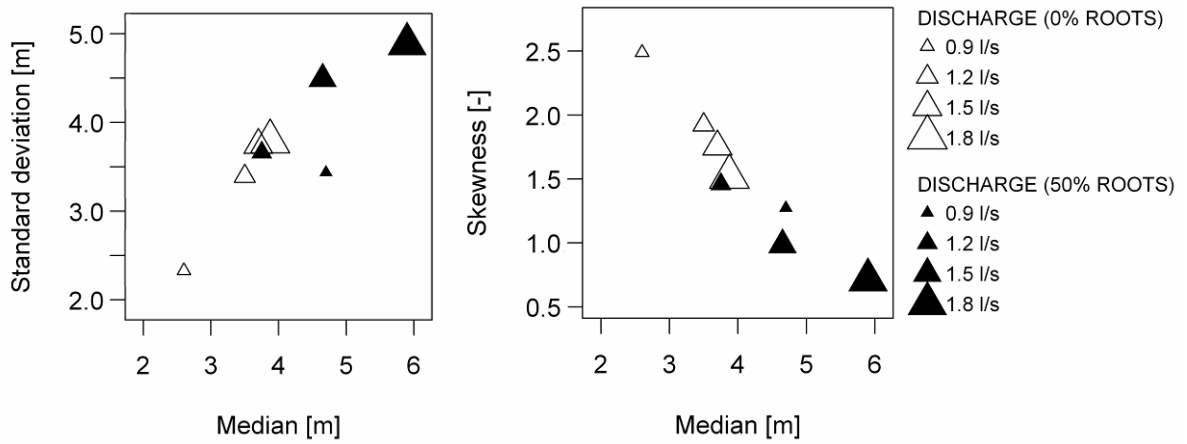
Figure 4.16: Median, standard deviation and skewness of travel distance distributions for the eight combinations of discharge and prevalence of dowels with roots.

Table 4.9: Tukey test for the 90th percentile of travel distance. Significant p values are shown in bold.

Q [l/s]	1.2	1.5	1.8
0.9	0.867	**0.034**	**0.007**
1.2		0.177	**0.047**
1.5			0.921

Table 4.10: t-test for a set of percentiles of transport distance. Significant p values are shown in bold.

Percentiles	t-test p value			
	0.9 l/s	1.2 l/s	1.5 l/s	1.8 l/s
10th	**0.023**	0.996	0.055	0.007
25th	**0.036**	0.414	0.185	**0.112**
50th	**0.014**	0.361	0.703	0.095
75th	**0.049**	0.409	0.062	**0.004**
90th	0.056	0.541	**0.047**	**0.008**
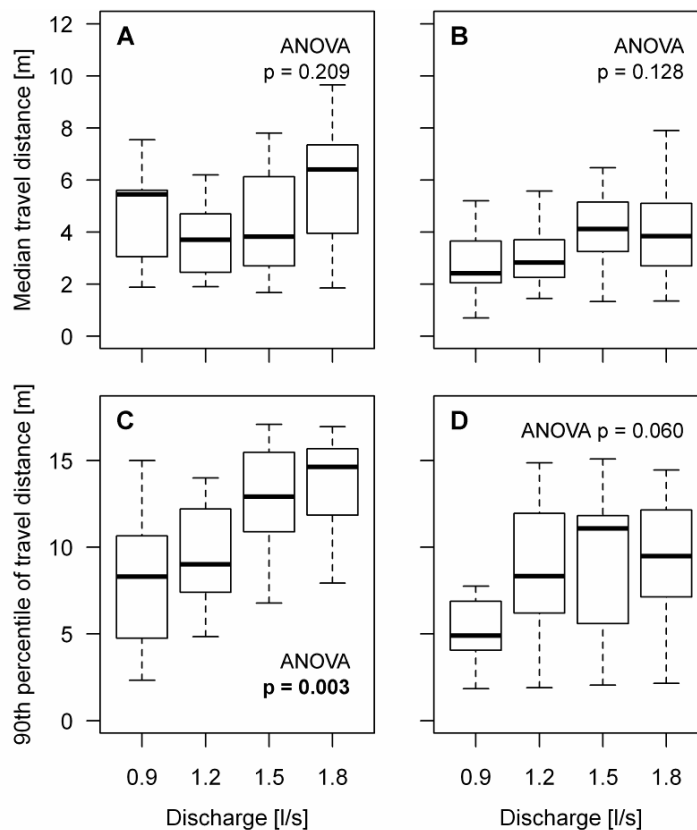
Figure 4.17: Travel distance of log cohorts for different values of discharge and percentage of log with roots: median, for X = 0% (A) and X = 50% (B); 90th percentile for X = 0% (C) and X = 50% (D). Data for sets of 10 runs are presented as boxplots with dots indicating outliers. Significant ANOVA p values are shown in bold
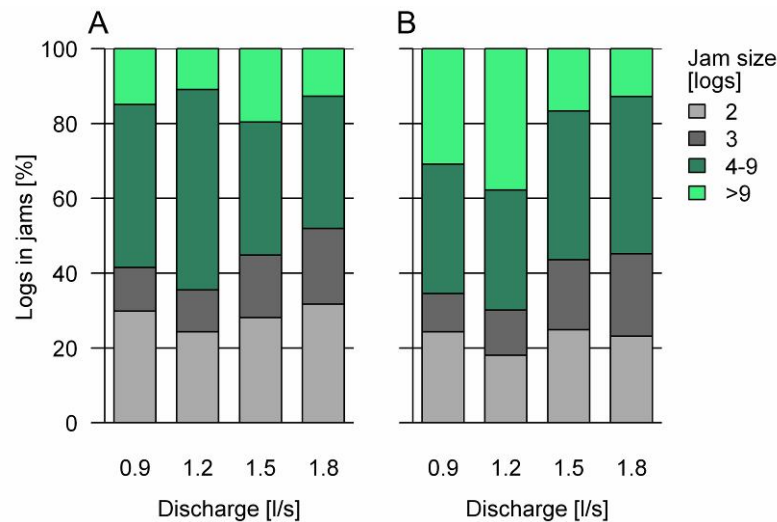
Figure 4.18: Wood distribution over jam size classes for cohorts of wood without roots (A) and with 50% of elements with roots (B).

4.2.7 Braid bar pattern and wood dispersal pattern

Wood dispersal patterns observed in the physical model clearly show wood storage mostly occurring at bar apex (Abbe and Montgomery, 1996) and along concave channel banks. Preferential deposition sites correspond to those identified at field scale (Abbe and Montgomery, 1996; Piégay et al., 1999). Figure 4.19 illustrates an example of the similarity between the spatial organisation of deposits at flume and field scale. In both cases, a log jam has developed at bar apex, and more wood lines the banks of the two anabranches.

The relationship between the spatial distribution of wood accumulations and channel planform was investigated with special focus on the role of bar apex sites. As a first step, the analysis was carried out on wood dispersal data from run set T2. Deposition sites located at bar apex were identified on images and the number of sites and dowels was recorded. Bar apex sites make up 30 to 40% of all deposition sites and logs deposited in these areas correspond to 40 to 60% of all wood. ANOVA and *t*-test analyses show no statistically significant effect of discharge and presence of roots on these figures. Therefore, the contribution of bar apex sites to overall wood storage is large regardless of flow conditions and log properties. This implies that the spatial organisation of braid bars is likely to be reflected by the planar distribution of wood deposits. In particular, fluctuations of wood density along the longitudinal direction are expected to be linked with bar wavelength.

To test this hypothesis, a second set of ten runs from subset T1 was used, comprising one simulation for each combination of *D*, *L* and *X* (see Figure 4.20). Runs were carried out
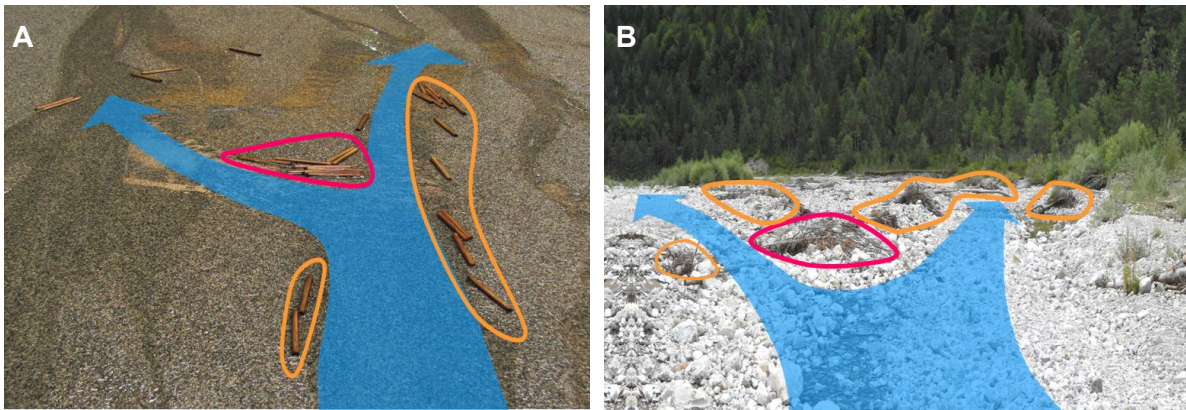
Figure 4.19: Preferential sites for wood deposition observed in the Pi flume (A) and on the Tagliamento River (B). Anabranches are highlighted in blue, bar apex jams in purple, channel margin jams in orange
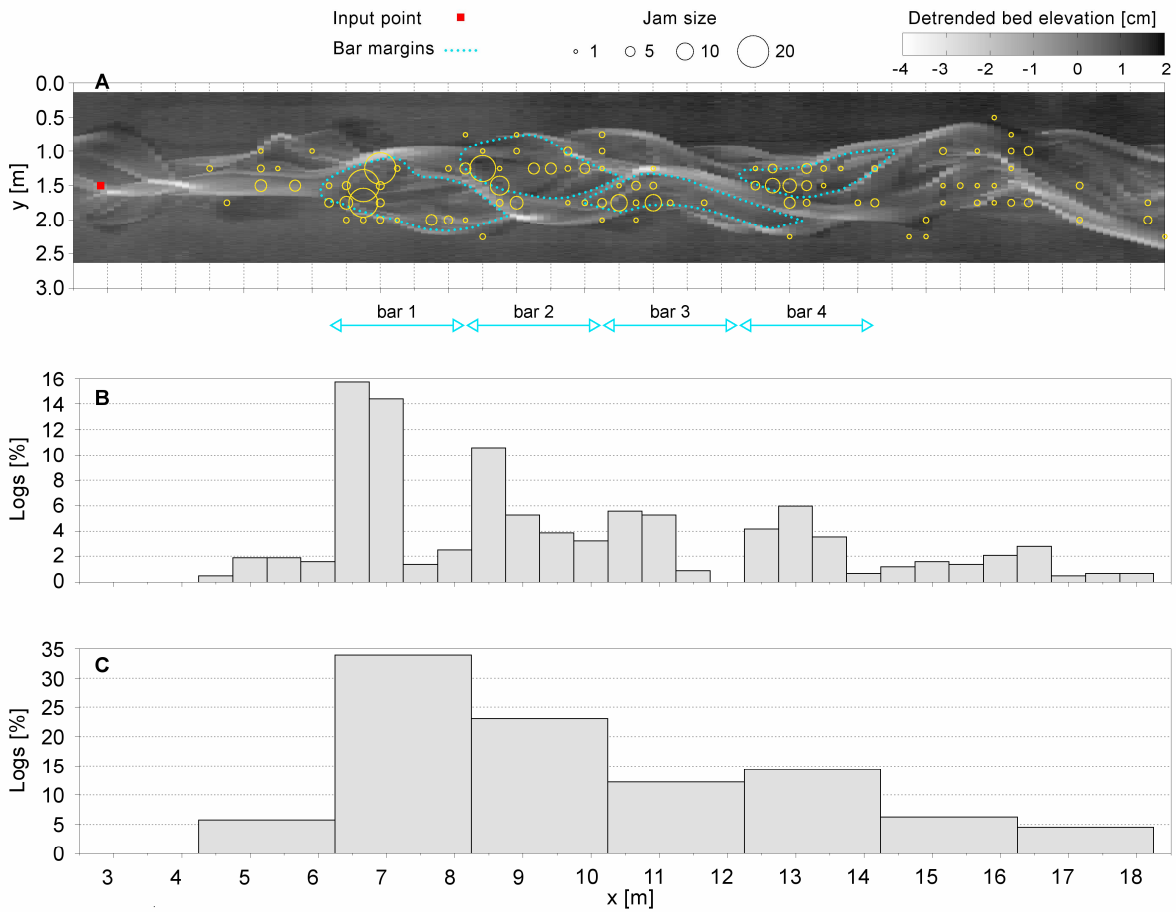
Figure 4.20: Map of wood deposition across the network (A); downstream distribution of wood aggregated over ¼ of bar wavelength (B); downstream distribution of wood aggregated over one bar wavelength (C).

back to back and a laser survey was carried out at the end (the overall network evolution time is slightly over 30 minutes, therefore channel change between the first and the last run can be assumed to be minimal).

The characteristic length of a braid bar was evaluated from imagery and bed elevation data and corresponds to approximately 2 m. Wood deposition maps were summed over the ten runs and resampled over a 20 x 20 cm grid. The frequency distribution of wood along the x coordinate was built at two different spatial scales by aggregating accumulations over 1/4 of bar wavelength and over single wavelengths, respectively. The relationship between bar pattern and wood dispersal is evident in histograms presented in Figure 4.20. At the smaller scale, wood retention peaks at the apex of the four main braid bars identified in the network. Furthermore, at reach scale the first bar downstream of the input point hosts more than 30% of wood and this proportion steadily decreases with distance from input. These results match real-scale observations on the Tagliamento River especially in terms of retentiveness of the first bar (see Chapter 3).

4.2.8 Concurrent effect of morphology, water depth and log shape

The present chapter is devoted to the investigation of wood dispersal as the result of the interactions of three key factors, namely wood properties, flow conditions and network geometry. The analyses follows a multivariate approach described by the conceptual model shown in Figure 4.21. Inundation pattern – resulting from the combination of network morphology and discharge – and log properties are assumed as external drivers of wood transport and deposition. Jam size, travel distance and relative elevation of deposits are the parameters used to describe dispersal patterns.
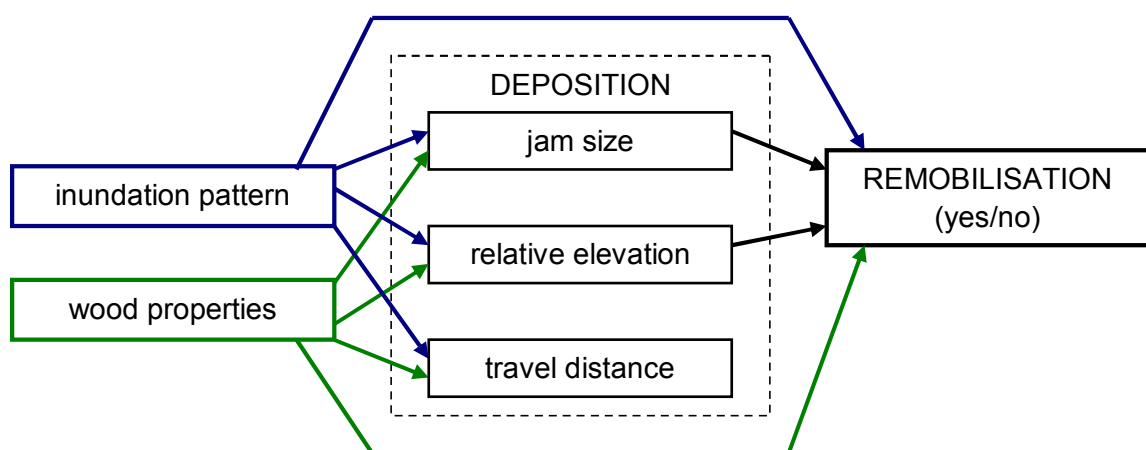
Figure 4.21: Conceptual model of wood transport, deposition and remobilisation including the key governing factors.

The analysis was carried out on wood dispersal maps built for run set T3, comprising ten repetitions of model runs for four values of discharge carried out using cohorts of 72 logs half of which with roots. Available information obtained by direct mapping and image processing is detailed in Chapter 4.2.3. For the present analysis, data from all runs were organised in a database with one entry per log. Records are identified by the combination of run code and log code and are assigned the following attributes:

- discharge (Q, treated as a categorical variable with four levels);

- presence / absence of a root wad (R, categorical binary variable);

- travel distance (T, ratio scale continuous variable);

- jam size, i.e. the size of the accumulation that includes the dowel (S, ratio scale variable);

- relative elevation (Z, ratio scale continuous variable).

Relative elevation (average, median, minimum and maximum) was derived from the DEMs. Preliminary univariate analyses showed that the four parameters have a very similar behaviour and therefore only the average elevation is used. An example of database entries is shown in Table 4.11. The table also includes the binary categorical variable *fate* (F) used in subsequent analyses. Total wood input for the 40 runs comprises 2880 dowels; information on relative elevation is missing for a small fraction (1%) of input wood because they were deposited outside the area covered by the laser surveys. Subsequent analyses were carried out only on complete observations, corresponding to a total of 2842 records.

Descriptive statistics

Frequency distributions of the three dispersal parameters used to describe patterns – relative elevation, jam size and travel distance – are shown for the entire database in Figure 4.22. The distributions of S and T are strongly positively skewed while Z is fairly symmetric with a peak corresponding to a relative elevation of 3 mm above the mean. Wood dispersal patterns have been already characterised in terms of jam size and travel distance using data from run sets T1 and T2 and therefore for run set T3 the role of these two parameters will be investigated only in multivariate analyses.

Cumulative frequency distributions of Z were computed for different values of discharge and compared with the frequency distribution of the DEM (Figure 4.23). Relevant percentiles for DEM and wood elevation distributions are summarised in Table 4.12. As previously shown in Figure 4.4, bed elevation distributions are similar over all runs and therefore one of the 28 elevation maps was randomly selected to represent the typical spatial structure of the braided networks. Wood deposited at the lowest tested discharge

Table 4.11: An example of the database used for multivariate analysis of wood dispersal.

Run code	Log code	Q [l/s]	R [-]	S [logs]	Z [mm]	T [m]	F
1215-1	AAO	1.2	no	27	1	1.22	moved
1215-1	AAX	1.2	yes	1	-3	0	stable
...	...	...	...	...	...	...	...

Table 4.12: Median and inter-quartile ranges of the relative elevation of the riverbed and of relative distributions of wood for four values of discharge.

Percentile	Bed relative elevation [mm]	Wood relative elevation [mm]			
		Q = 0.9 l/s	Q = 1.2 l/s	Q = 1.5 l/s	Q = 1.8 l/s
10th	-8.0	-3.0	-2.0	-2.0	-2.0
25th	-3.5	0.0	0.0	0.0	-1.0
50th	0.5	3.0	1.0	2.0	2.0
75th	3.5	5.0	3.0	5.0	4.0
90th	6.0	6.0	4.0	7.0	5.0

(Q = 0.9 l/s) is scattered over a wider range of Z and can be found at very low elevations (Z < -5 mm). In contrast, a minimal proportion of wood dispersed by higher flows is found below this threshold, which corresponds to approximately 20% of the braidplain width. However, no clear relationship between discharge and relative elevation can be identified, possibly due to the large between-run variability observed in flume simulations.
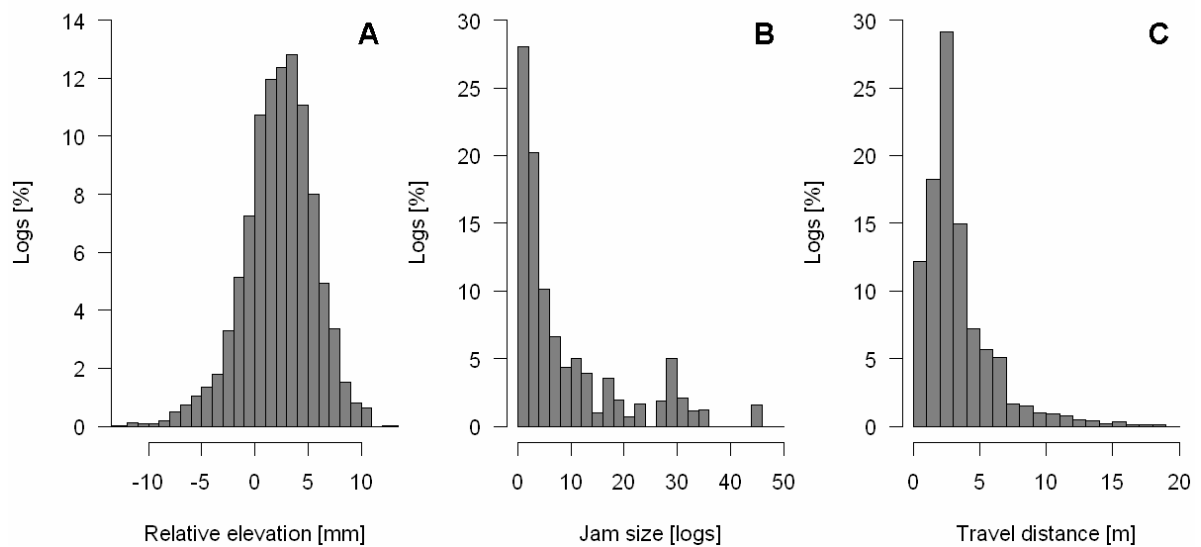
Figure 4.22: Histograms of relative elevation (A), jam size (B) and travel distance (C) for the complete database

A qualitative analysis of the interaction between flow stage, log shape and jam size is proposed in Figure 4.24. CDFs of relative elevation for each value of discharge are split on the basis of the presence of roots (yes/no) and of accumulation style, i.e. dividing isolated elements from elements in jams. Isolated elements appear to be deposited at a lower elevation for low discharge while no clear difference with logs in jams can be detected at higher flow. Logs with roots are found at lower values of Z for all flow conditions, but the difference tends to diminish for increasing discharge.

Multivariate analysis: testing of hypotheses

Multivariate analysis was carried out using MANOVA and discriminant analysis was employed as follow-up test. The theoretical background of the methods is outlined in Chapter 4.2.4. Experimental design can be summarised as follows:

- the combination of input discharge (Q) and presence of roots (R) defines individual groups of observations (Q and R are independent variables for MANOVA);

- relative elevation (Z), jam size (S), travel distance (T) are the observed quantities corresponding to dependent variables for MANOVA and predictors for discriminant analysis.

The assumptions and requirements of the two methods are essentially the same and include a) independent random sampling; b) moderately correlated dependent variables (predictors); c) group size larger than the number of DVs; d) multivariate normality; and e) homogeneity of variance-covariance matrices.
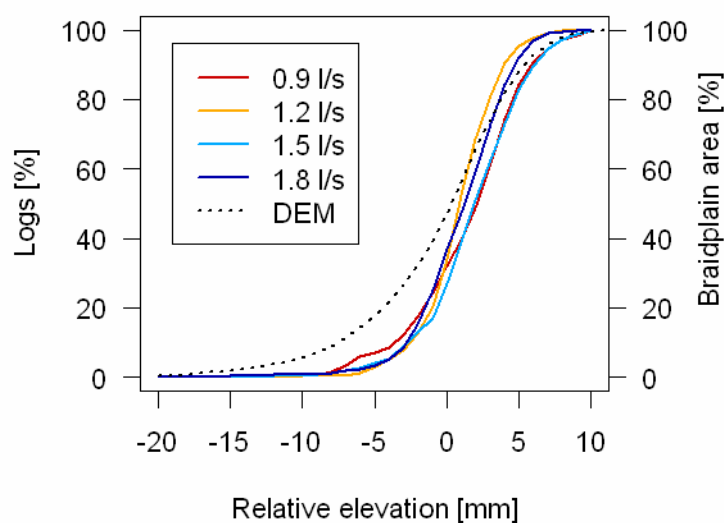
Figure 4.23: Cumulative frequency distribution of relative elevation of wood for four values of discharge.
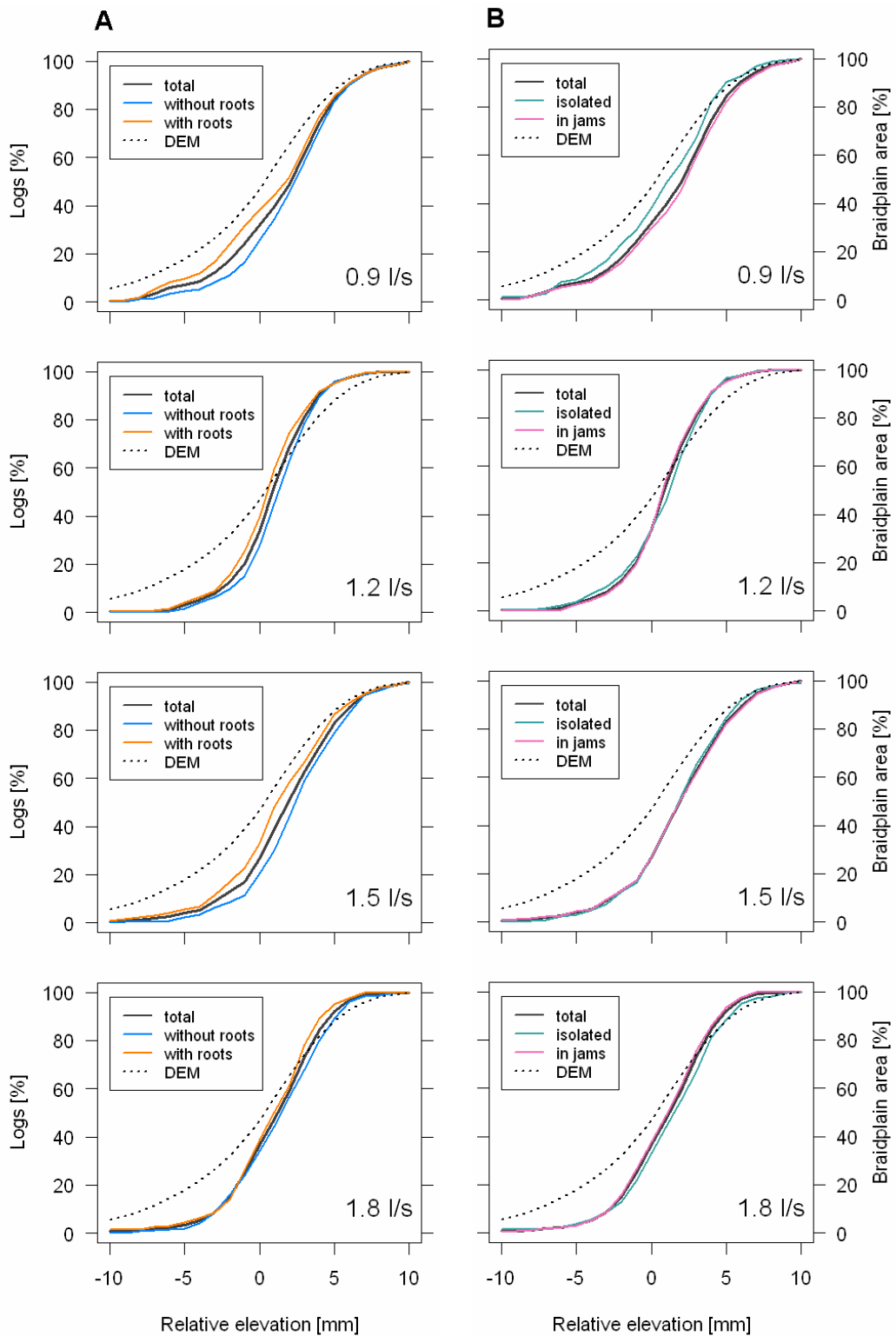
Figure 4.24: Cumulative frequency distribution of relative elevation of wood for four values of discharge: comparison between isolated logs and elements in jams (A) and between logs without roots and with roots (B).

Protocols and techniques used for physical modelling ensure that conditions a and c are met, while the other hypotheses need verification. Data pre-processing steps include

- transformation of variables for skewed distributions;

- evaluation of correlation;

- identification and removal of multivariate outliers;

- balancing of group size and discussion of normality and homogeneity of variance-covariance matrices;

- evaluation of correlation on the remaining data.

Log transformation was applied to S and T to reduce skewness and limit the influence of outliers and correlation between Z, $\log(S)$ and $\log(T)$ was evaluated in terms of Pearson's coefficient r (Table 4.13). The coefficient varies in magnitude from −1 (perfect negative linear relation) to 1 (perfect positive linear relation) with 0 indicating uncorrelated variables. Thresholds for effect magnitude (i.e. strength of correlation) were identified in accordance with Cohen (1988), where three classes are identified: *small* ($0.1 \leq r \leq 0.23$), *medium* ($0.24 \leq r \leq 0.36$) and *large* ($r \geq 0.37$). In the present case, r does not fall into the third class and this result was taken as an indication that multivariate techniques can be safely applied to this set of variables.

A common procedure to identify multivariate outliers is the Mahalanobis distance criterion (Tabachnick and Fidell, 2012). In the present study, however, the *PCOut* method (Filzmoser et al., 2008) was employed, as it is robust to violations of normality and computationally efficient for a number of observations ranging in the thousands. The procedure is based on principal components analysis and is implemented in the *mvoutliers* R package[1]. The method requires four parameters, two for location estimate (the multivariate equivalent of sample mean) and two for scatter (dispersion). Optimal values are provided by the authors, but in this case they were fitted visually on scatterplots. Outlier removal was conducted for each of the eight groups identified by the combination of Q and X, resulting in the overall rejection of 112 records (out of 2842). The resulting experimental design is unbalanced with group size ranging from 314 to 355 elements.

As suggested in Nimon (2012), group size was equalised by removal of random records from groups with more than 314 elements; the database in its final form comprises 2512 elements in 8 groups, corresponding to 88% of the original set of complete observations. Distributions of the transformed variables are shown in Figure 4.25 and their moments are summarised in Table 4.14.

---

[1] Filzmoser, P., Gschwandtner, M., 2012. Mvoutlier: Multivariate outlier detection based on robust methods. V. 1.9.8. http://CRAN.R-project.org/package=mvoutlier.
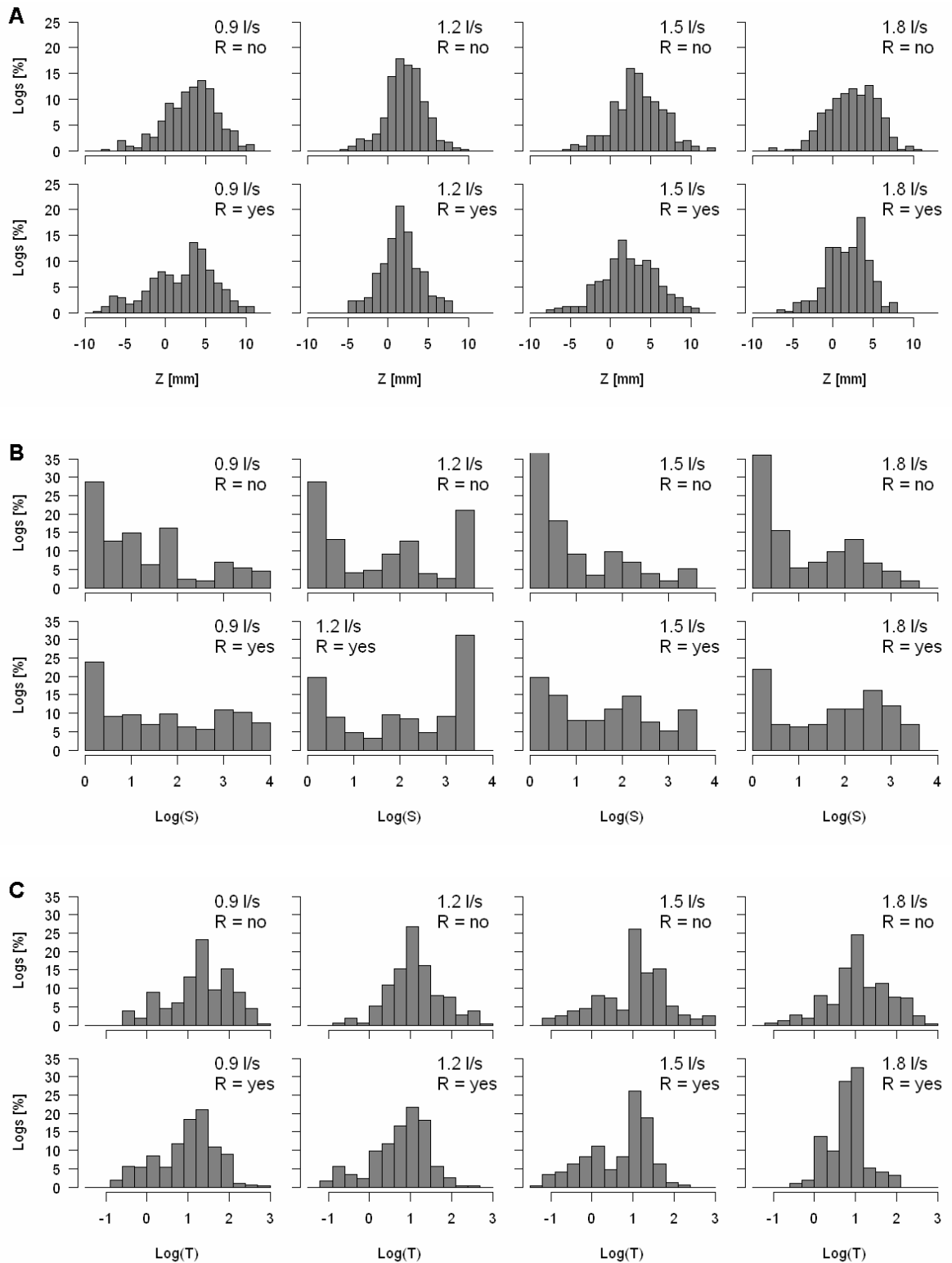
Figure 4.25: Distributions of dependent variables after data pre-processing for each group comprising 314 observations; relative elevation (A); log-transformed jam size (B) and log-transformed travel distance (C)

Table 4.13: Correlation between dependent variables for the original dataset of complete observations (left) and for the final dataset after outlier removal and equalisation (right). Significant p values are shown in bold.

		log(S)	log(T)
Z	r	-0.03	0.21
	p	0.178	<0.001
log(S)	r		-0.24
	p		<0.001

		log(S)	log(T)
Z	r	-0.04	0.24
	p	0.067	<0.001
log(S)	r		-0.26
	p		<0.001

Table 4.14: Main statistics of groups.

Q	R	n	Z		log(S)		log(T)	
			mean	std. dev.	mean	std. dev.	mean	std. dev.
0.9	no	314	2.72	3.18	1.32	1.16	1.27	0.74
	yes	314	1.51	4.10	1.69	1.32	0.95	0.72
1.2	no	314	1.68	2.46	1.54	1.3	1.10	0.63
	yes	314	1.04	2.53	1.97	1.32	0.76	0.68
1.5	no	314	2.94	3.14	0.99	1.04	1.02	0.85
	yes	314	1.86	3.37	1.49	1.09	0.66	0.79
1.8	no	314	1.77	3.07	1.11	1.03	1.09	0.71
	yes	314	1.31	2.63	1.66	1.13	0.81	0.44

Normality of $\log(S)$ can not be assumed but MANOVA and discriminant analysis have been shown to be robust to violations of normality and homogeneity of variance-covariance matrices if a) non-normality is caused by skewness and not by outliers; and b) the design is balanced. This is especially true for large data samples (Tabachnick and Fidell, 2012). Correlation for the data set in its final form is slightly stronger (Table 4.13). In the end, the final database meets all requirements for statistical methods of interest. It is worth noting that all subsequent analyses were repeated several times, each time with a different randomly drawn subset of 2512 observations with negligible differences in outputs.

MANOVA

A 2 x 4 MANOVA was performed using the software R. Dependent variables are Z, $\log(S)$ and $\log(T)$ and independent variables are Q and R. Therefore, variance is partitioned between the effect of discharge, presence of roots and the interaction of the two factors, plus the within-group variability (error). As R is a dichotomous variable, all multivariate tests (Wilks' lambda, Pillai's trace, Hotelling-Lawley's trace and Roy's root) yield the same result (see Chapter 4.2.4). The outcomes of the analysis are summarised in Table 4.15.

Table 4.15: Pillai's multivariate test of significance for 2 x 4 MANOVA.

Source of variation	Pillai's V	Approx. F	Hypothesis df	Error df	Significance level
Roots	0.076	68.866	3	2502	**<0.001**
Discharge	0.073	20.869	9	7512	**<0.001**
Roots + Discharge	0.004	1.063	9	7512	0.3868

For each source of variation, Pillai's *V* statistic is converted into an approximate F value; F is compared with its critical value F_{crit} ($df_{hypotheiis}$, df_{error}) computed on the basis of the number of degrees of freedom (*df*) associated to hypothesis and error. The multivariate test identifies a strong significant effect of the two independent variables but no interaction effect.

Discriminant analysis

Discriminant analysis was used as a follow-up test using *Z*, log(*S*) and log(*T*) as predictors of membership into the eight groups defined by the combination of four values of discharge and two levels of presence of roots. The goal of discriminant analysis is to identify the dimension(s) along which groups exhibit the greatest difference. The experimental design has three degrees of freedom (the minimum between the number of groups minus one and the number of predictor variables) resulting in 3 orthogonal discriminant functions (dimensions) in the form

$$LD = \alpha_Z \cdot Z + \alpha_S \cdot \log(S) + \alpha_T \cdot \log(T)$$.

As a first step, individual predictor values were standardised and significance was verified using Wilks' lambda. The test statistic is equal to 0.85 and the associated approximate F (21,7185) is 18.922 ($p < 0.001$), implying that the separation between groups based on the three predictors is highly statistically significant.

Discriminant analysis coefficients for the three predictors and proportions of explained variance for the three discriminant functions *LD1*, *LD2* and *LD3* are summarised in Table 4.16. The first two functions represent 95% of variance; further analyses are therefore limited to composite variables *LD1* and *LD2*. Discriminant analysis determines group separation in the space of composite variables; however, as the object of investigation is the differentiation of driftwood patterns in terms of measured properties (i.e. predictors), it is useful to quantify the sign and strength of the correlation between predictors and composite variables. This is achieved by computing *LD1* and *LD2* for each observation using discriminant analysis coefficients. Scatter plots and correlation coefficients are shown in Figure 4.26.
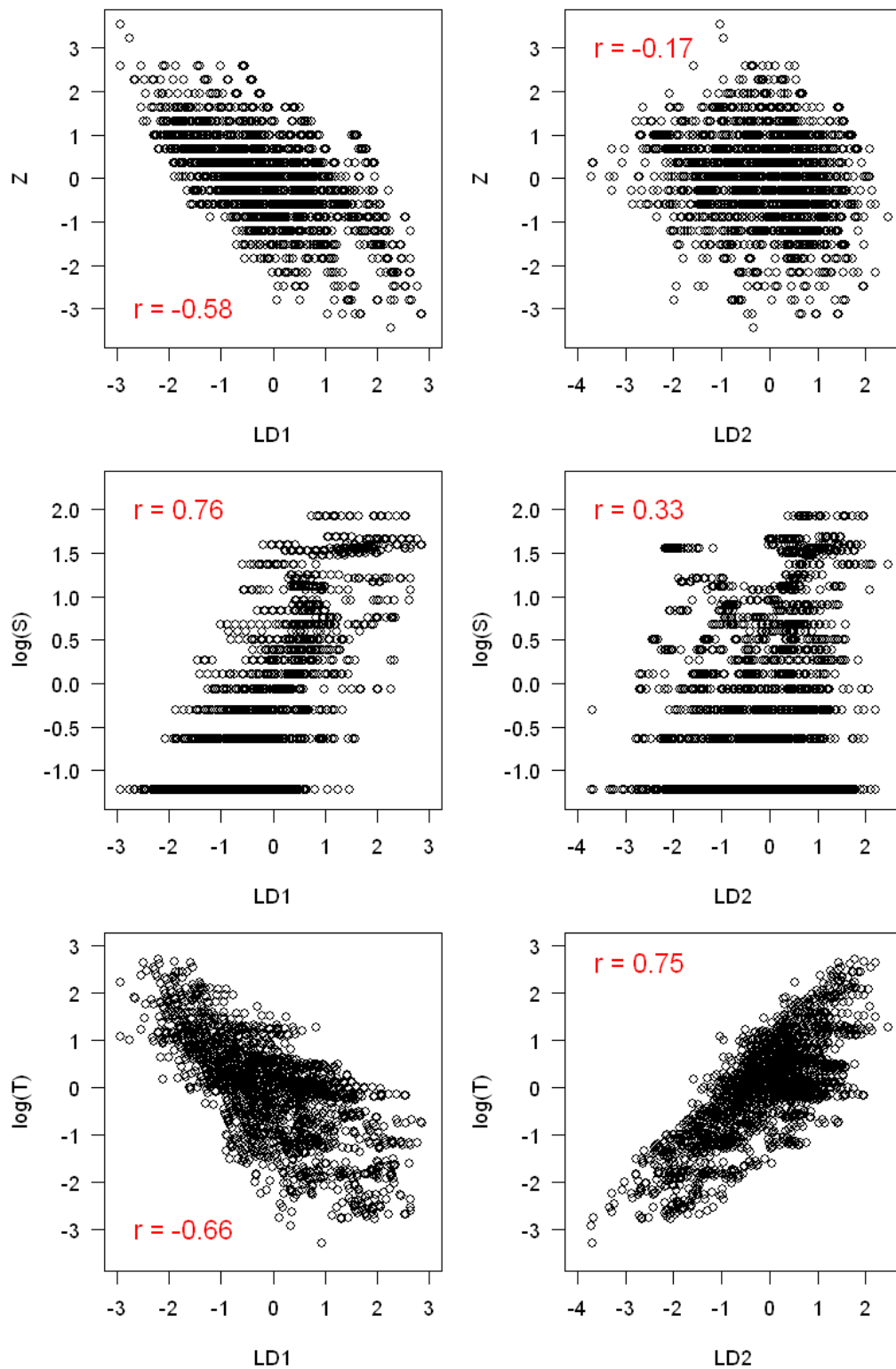
Figure 4.26: Correlation between predictors and composite variables (discriminant function scores). Pearson's correlation coefficients are shown in red.

Table 4.16: Discriminant functions: coefficients and proportions of explained variance.

Predictor	Discriminant function coefficients α		
	LD1	LD2	LD3
Z	-0.481	-0.398	0.843
log (S)	0.665	0.590	0.588
log(T)	-0.399	1.022	-0.071
Proportion of variance	0.63	0.32	0.05

LD1 is positively correlated with log(*S*) and negatively correlated with *Z* and log(*T*), while *LD2* shows a positive correlation with log(*T*). Correlation coefficients smaller than 0.45 are considered non significant in accordance with Tabachnick and Fidell (2012).

Group separation on the basis of composite variables is easily interpreted if presented in graphical form as a scatter plot of centroids (group means) as in Figure 4.27. The first discriminant function – explaining 63% of variance – clearly separates groups with roots from those without roots (low scores), in particular if pairs of groups characterised by the same discharge are compared. The different behaviour of logs with and without roots in terms of *LD1* can be re-interpreted in terms of measured properties o the dispersal pattern by looking at the sign of the correlation between *LD1* and the predictors. Wood with roots shows high scores of *LD1* corresponding to low relative elevation and short travel distance (negative correlation coefficient) and to large jam size (positive *r*). Analogously, wood without roots is found further downstream at higher elevations and forms smaller jams.

The second discriminant function – explaining 32% of variance – separates groups on the basis of discharge but does not contribute to the differentiation on the basis of roots presence/absence. Wood deposited at 0.9 and 1.2 l/s shows the same behaviour in terms of *LD2*, while wood deposited at 1.5 l/s shows the most pronounced difference. Interpretation in terms of predictors is not straightforward, as *LD2* is correlated only with travel distance, which in turn is also significantly related to *LD1*. For a given value of discharge, wood with roots tends to be associated to slightly smaller values of *LD2* – and therefore of travel distance – in comparison with wood without roots. However, no clear overall effect of discharge can be assessed. Finally, it is worth noting that the distribution of *Z* and log(*T*) is reasonably close to normality for all groups, while log(*S*) shows high values at the extremes (especially at low flow), suggesting that the assumption of normality is more likely to be violated for jam size.
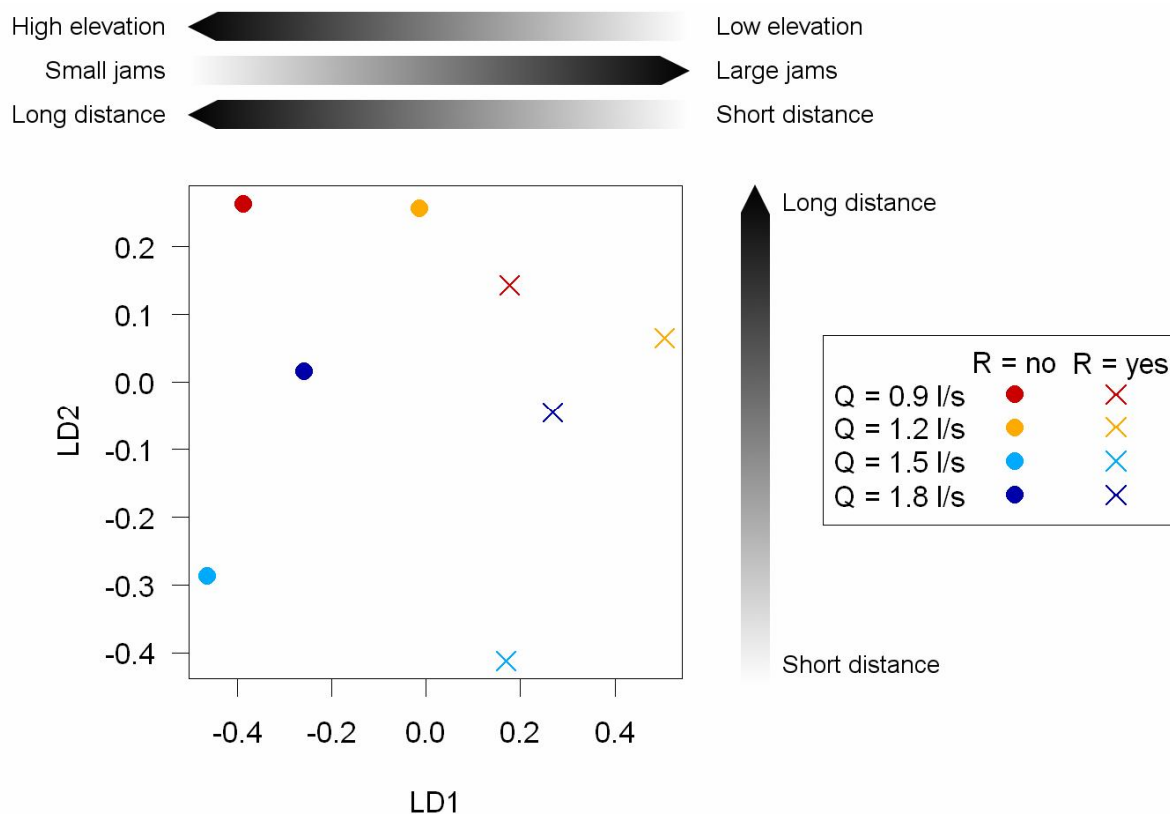
Figure 4.27: Centroids in the LD1, LD2 space and association with predictors.

4.2.9 Driftwood remobilisation

Preliminary data analysis

Wood remobilisation caused by discharge fluctuations was investigated with the aim of highlighting the most relevant mechanisms governing wood persistence over time. The key factors taken into account for the analysis are summarised in the conceptual model shown in Figure 4.21. Wood deposition pattern prior to the flow pulse – described in terms of jam size, relative elevation and transport distance distribution – is expected to exert a strong influence on remobilisation. In turn, the spatial organisation of deposits was shown to be governed by wood shape while flow conditions occurring during driftwood dispersal (referred to as *input discharge*) play a secondary role. Wood shape and input discharge are also expected to exert a direct control on wood remobilisation.

Multivariate observations from run set T3 were analysed using logistic regression with *fate* (*F*) as the predicted response. *F* is a categorical variable with three levels for stable logs (*F_S*, no motion), reorganised logs (*F_R*, displacement by less than two log lengths) and remobilised logs (*F_M*, downstream transport for more than two log lengths). Available data

comprise 2842 complete observations of individual dowels; however, reorganised logs were excluded from the present analysis to reduce uncertainty. Consequently, the database used for logistic regression includes 1317 dowels in class F_S and 880 dowels in class F_M for a total of $N = 2197$ observations.

The five predictors taken into account for the analysis – input discharge (Q), presence of roots (R), relative elevation (Z), jam size (S) and travel distance (T) – predictors are entered in the model as continuous variables, with the exception of the dichotomous variable R. As logistic regression makes no assumptions about the distribution of predictors, no transformation was applied to predictors. Multicollinearity between predictors was tested using squared multiple correlation (SMC) as suggested by Tabachnick and Fidell (2012). SMC is a scalar parameter akin to Pearson's r and is represents the strength of correlation between a predictor and the combination of the others. Small values of SMC indicate absence of multicollinearity (Table 4.17).

Preliminary inspection of frequency distributions of the five predictors for stable and remobilised logs (shown as histograms in Figure 4.28) indicates that input discharge and jam size are likely to play a major role in wood remobilisation. A large proportion of wood dispersed at low flow and stored as isolated dowels is removed by flow pulses, as opposed to logs deposited at high flow and in jams.

Procedures for logistic regression modelling

A series of logistic regression models was built using various sets of predictors and interaction terms representing the joint effect of two ore more predictors. Model testing and optimisation requires the following steps:

- evaluation of model significance;

- assessment of classification accuracy;

- testing of significance of individual predictors;

- quantification of the effect of individual predictors.

Model significance is defined as the predictive power of the set of variables as a whole and as tested using log-likelihood tests. Classification accuracy was assessed by comparing probability values computed for individual dowels with the corresponding observed outcome of the response variable (stable/remobilised). As model outputs are continuous probability values, they were converted into a dichotomous variable by selecting a threshold value (P_c) and classification accuracy was computed as the proportion of correctly classified observations. Overall accuracy is defined as N_{corr}/N where N is sample size and N_{corr} is the number of correctly predicted observations. Moreover, accuracy can be separately evaluated for stable logs ($N_{corr,stable}/N_{stable}$) and analogously for remobilised logs.
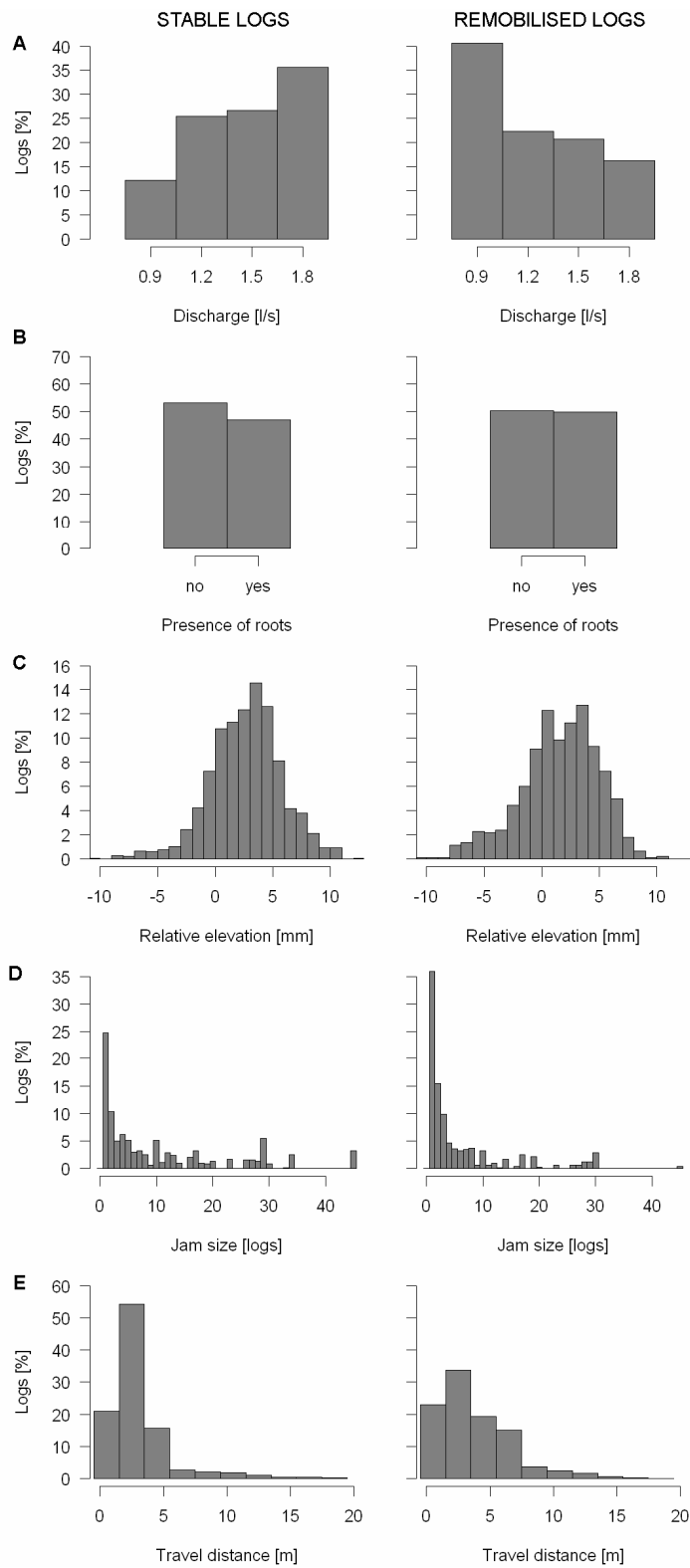
Figure 4.28: Frequency distributions of the five predictors for stable and remobilised logs: input discharge (A); presence of roots (B); relative elevation (C); jam size (D); travel distance (E).

Table 4.17: Squared multiple correlation for predictors.

Predictor	SMC
presence of roots	0.07
discharge	0.04
relative elevation	0.05
jam size	0.09
travel distance	0.13

The relevance of individual predictors was assessed by comparing the classification accuracy of models including and excluding each variable (a more rigorous evaluation of the significance of predictors would require a very large number of log-likelihood comparisons). The significance of model coefficients was tested using Wald's χ^2 test. Finally, the influence of predictors was quantified in terms of odds ratio. Wood stability was assumed as the reference condition for the response variable F, implying that the observed probability value for a stable dowel is $y = 1$. As a consequence, the odds ratio for a generic predictor x_i is written as

$$o_i = \frac{P(stable)}{P(remobilised)} \ .$$

If o_i is larger than one, logs are more likely to remain stable for larger values of the associate predictor x_i. The reference condition for the dichotomous predictor R corresponds to logs without roots, implying that any observed effect of R has to be interpreted as the contribution of the presence of roots ($R = yes$) to log stability.

Logistic regression: the full model

As a first step, a full model with all predictors and their multivariate interactions (ten two-way, ten three-way, five four way terms and one five-way term) was built to assess the best fit that can be attained with the available set of measured quantities. The outputs of significance tests and accuracy analysis for the present model (M0) are summarised in Table 4.18. The log-likeliness test statistic G^2 exceeds the critical value of χ^2 ($df = 31$), implying that the chosen set of variables significantly contributes to the prediction of model response. Model accuracy was assessed by assigning $P_c = 0.5$ as probability threshold, obtaining acceptable results with 72% of all cases correctly classified. However, model performance is noticeably poorer for remobilised logs (57%) in comparison with stable logs (82%). Probability values computed with model M0 (Figure 4.29, first panel) exhibit a much flatter distribution for remobilised logs, thus explaining the different performance; for $P_c = 0.6$, classification accuracy is 71% for all wood categories. Out of 31 terms, only 14 (plus

Table 4.18: Logistic regression model M0 (full model). Significant p values are shown in bold.

Log-likeliness test of significance		Accuracy	Pc = 0.5	Pc = 0.6
G^2	644.8	All wood	72.1%	70.8%
df	31	Remobilised wood	57.2%	70.7%
χ^2_{crit}	19.3	Stable wood	82.1%	70.9%
Significance level	**<0.001**			

Predictor	Model coefficient β			Wald's test	
	Estimate	Standard error	Odds ratio	Z	Significance level
Intercept	-4.665	0.775	0.009	-6.016	**<0.001**
Q	3.476	0.548	32.339	6.348	**<0.001**
S	0.375	0.113	1.455	3.322	**0.001**
Z	0.413	0.213	1.511	1.936	0.053
T	0.304	0.161	1.355	1.884	0.060
Q + S	-0.233	0.088	0.792	-2.662	**0.008**
R + T	-0.621	0.345	0.538	-1.797	0.072
Q + T	-0.281	0.121	0.755	-2.320	**0.020**
S + T	-0.108	0.045	0.898	-2.405	**0.016**
R + Q + T	0.419	0.238	1.521	1.761	0.078
Q + S + T	0.080	0.035	1.084	2.307	**0.021**
R + Z + T	0.242	0.097	1.273	2.500	**0.012**
R + Q + S + Z	-0.055	0.032	0.947	-1.698	0.090
R + Q + Z + T	-0.167	0.067	0.846	-2.514	**0.012**
R + S + Z + T	-0.036	0.018	0.964	-2.061	**0.039**

intercept) are significant at $p = 0.1$ and only 9 (plus intercept) are significant at $p = 0.05$. Among individual predictors, discharge and jam size are strongly significant while travel distance and relative elevation are barely above $p = 0.05$ and the effect of roots appears to be non-significant.

Odds ratios highlight a very strong effect of flow conditions on wood stability, as a unit (1 l/s) increase in input discharge multiplies the probability of log persistence by 32. In the present study, discharge values for initial wood dispersal cover a range of 0.9 l/s (from 0.9 to 1.8 l/s). Consequently, wood deposited at maximum flow is expected to be more than an order of magnitude more likely to remain stable than wood deposited at minimum flow. Odds ratios for S, Z and T are also larger than one, meaning that wood stored in larger jams, at higher relative elevations or at greater distance from the input point is more stable.

Logistic regression: reduced models

The quantification of the role of individual predictors is hampered by the presence of high-order terms; moreover, Tabachnick and Fidell (2012) indicate model comparison as a more reliable way to assess significance, as opposed to Wald's test for individual coefficients. For these reasons, simplified models were built by a) removing high-order terms; and b) excluding individual predictors. The complete set of 24 models includes:

- the 5th order full model with 5 predictors (M0);

- five 4th order models (M1$_j$, excluding the *j*-th predictor);

- a 2nd order model with 5 predictors (M2);

- five 2nd order models (M3$_j$, excluding the *j*-th predictor);

- a 1st order model with 5 predictors (M4);

- five 1st order models (M5$_j$, excluding the *j*-th predictor);

- three models including only *Q*, *S* and *Z* of 3rd, 2nd and 1st order (M6$_3$, M6$_2$, M6$_1$);

- three 2nd order models (M5$_j$, excluding the *j*-th predictor between *Q*, *S* and *Z*).

Log-likeliness tests between pairs of nested models always yield significant results, implying that the exclusion of high-order terms and/or individual predictors produces a non-negligible difference in model outputs. However, changes in model performance are more easily evaluated in terms of classification accuracy (Figure 4.30).

Variations associated to the removal of high-order terms are minimal (within 5%) regardless of the number of predictors used in the model (compare M0 with M2 and M4 with five predictors and M6$_3$, M6$_2$ and M6$_1$ for three predictors). Discharge clearly appears as the key variable, as its removal produces a large drop in model performance, especially for remobilised logs. It is worth noting that for $P_c = 0.5$ models without *Q* appear to perform better for stable logs, but this is a spurious effect caused by the shape of probability distributions and disappears for $P_c = 0.6$. A noticeable decrease in model performance also occurs when jam size is excluded, while relative elevation and especially travel distance and roots essentially have no influence on model accuracy.

Moreover, the relative relevance of individual predictors can be evaluated using Wald's test for model coefficients and computing the corresponding odds ratios (summarised in Table 4.19 for significant first and second-order terms). As expected, *Q* is always significant and the associated odds ratio fluctuates between 10 and 15 in most cases, with the notable exception of the full model. *S* and *Z* are significant for the majority of models and the positive values of odds ratio confirm that wood stability is favoured by large jam size and high relative elevation. As expected, roots and travel distance play no role in most models.
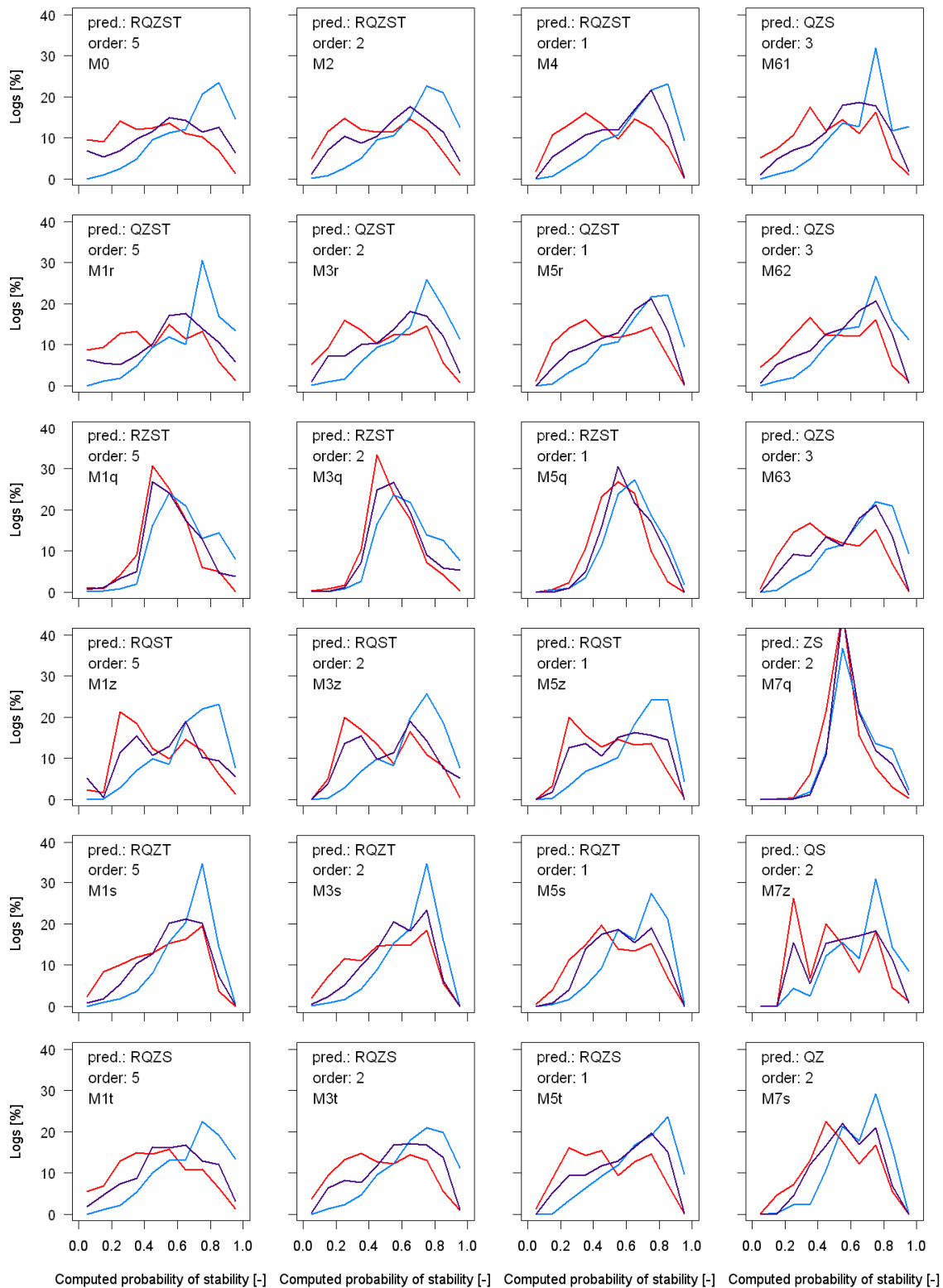
Figure 4.29: Distributions of computed probability of wood stability for remobilised (red), stable (blue) and reorganised logs (purple) for the complete set of 24 logistic regression models.

Table 4.19: Odds ratios for significant first-order and second order terms (Wald's test p < 0.05). Empty cells correspond to non-significant coefficients and shaded cells indicate that the term was not included in the model. Models missing Q or S are not shown due to their poor performance.

Model	INT.	R	Q	S	Z	T	QS	RZ	QZ	SZ	QT	ST
M0	0.01		32.34	1.46			0.79				0.75	0.90
$M1_R$	0.01		28.03	1.46	1.61		0.81		0.72			0.89
$M1_Z$	0.05		10.81	1.28								0.93
$M1_T$	0.02		14.78		1.36			1.52				
M2	0.04		10.53	1.12	1.44			0.93	0.84	1.00		0.97
$M3_R$	0.03		10.92	1.13	1.41				0.84			0.97
$M3_Z$	0.11		5.89									0.99
$M3_T$	0.02		14.59		1.43			0.92	0.86			
M4	0.04	0.69	12.01	1.07	1.13	0.93						
$M5_R$	0.03		11.91	1.06	1.14	0.94						
$M5_Z$	0.05	0.64	10.83	1.06		0.95						
$M5_T$	0.03	0.74	12.68	1.07	1.12							
$M6_3$	0.02		16.91	1.06	1.63				0.75	0.98		
$M6_2$	0.02		13.71		1.40				0.86			
$M6_1$	0.02		12.49	1.07	1.13							
$M7_Z$	0.05		8.78				1.04					

It is crucial to underline that absolute values of odds ratio depend on the unit of measurement of the corresponding variable and therefore on the typical range of variation of predictors (for the present simulations: 0.9÷1.8 l/s for discharge, 1÷45 logs for jam size and approximately -3÷6 mm for relative elevation).

Frequency distributions of probability values computed for remobilised and stable logs are shown in Figure 4.29; as already pointed out, frequency distributions tend to degenerate – approaching a normal distribution centred in $P = 0.5$ – if Q is excluded from the set of predictors. All other models produce comparable distributions, especially for stable logs (computed probability of persistence peaks at $P = 0.8$). The rather flat curve observed for remobilised logs in the full model changes in shape especially if S is missing from the model, but does not exhibit a clearly unimodal shape. Overall, the two series of distributions show that models predict remobilisation – corresponding to low values of P – essentially only for dowels that actually moved (true negatives), while logs that are predicted as stable – with high values of P – also comprise a non-negligible portion of actually remobilised elements (false positives). This suggests that wood dispersed in the flume can be divided into two main categories representing a) logs that are clearly prone to

remobilisation; and b) logs that are more likely to be stable, but have a non-negligible probability of remobilisation.

Finally, logistic regression models calibrated on the available database of stable and remobilised logs were applied to reorganised logs with the aim of evaluating the distributions of probability values for this class (Figure 4.29). The distribution computed with the full model shows an intermediate shape as expected; however it tends to approximate the distribution of stable logs if reduced models are used.
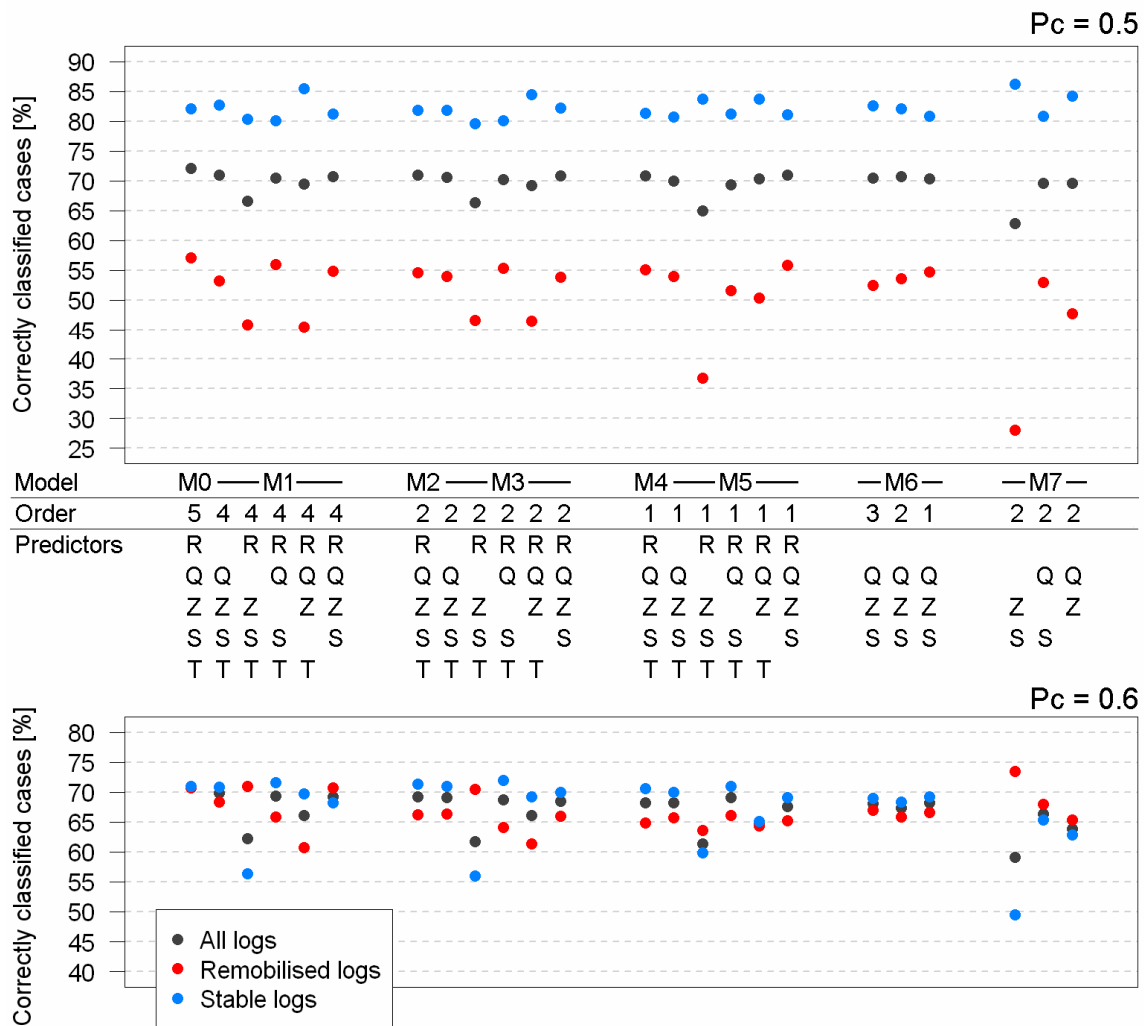
Figure 4.30: Classification accuracy for the complete set of 24 logistic regression models computed using P_c = 0.5 (top) and P_c = 0.6 (bottom).

4.3   Long-term wood dynamics: the Hull runs

4.3.1   Modelling procedures

Flume setup and driftwood elements

Long-term driftwood dispersal simulations were carried out in the framework of the Hydralab IV[1] project *The morphodynamic impacts of vegetation and large wood in fluvial systems*. (Group Leader: L. Mao; Project code HyIV-HULL-01). A physical model was built in the Total Environmental Simulator[2] (TES) managed by the University of Hull (UK) and hosted by The DEEP Aquarium. The TES is a 11 m long, 6 m wide, 1.6 m deep tank designed for fluid and sediment dynamics modelling. For the present work, three 1.7 m wide parallel flumes were built in the facility (Figure 4.31) and filled with a 0.2 m thick layer of well-sorted sand (median grain size, D_{50} = 0.73 mm; submerged relative density, Δ = 1.6). Each channel was equipped with a submerged pump for water recirculation, a sand feeder for sediment supply and a filtering crate for output bedload collection. Both water and sand input were controlled manually and pumps and feeders were calibrated by volumetric measurements; output bedload volume was measured with a precision of 1 l.

A reflex camera (Nikon D3100 with a Nikkor 18-55 mm AF lens) mounted on a manually operated overhead gantry was used to acquire digital images of the three flumes. The camera was positioned horizontally 1.5 m above the sand bed; images cover an area of approximately 2.1x1.9 m with a resolution of about 2 px/mm. Pictures were taken at a series of 7 positions along the longitudinal axis to ensure sufficient overlapping between adjacent images. A set of ground control points for image positioning and stitching was painted on the flume walls. Red dye was used to enhance contrast between wet and dry areas.

Physical modelling of braided networks at flume scale was carried using the same procedures defined for the Trento runs (see Chapter 4.2.2). In this case, slope was set to 0.013 and discharge to 1.26 l/s and kept constant throughout the experiment. Sand feeding rate was determined during a preliminary testing phase and set to 1.9 g/s. Once the network was fully formed, the physical model ran for a total of 23 hours to monitor the evolution of the braided network over time. In analogy with the Trento model, the reference condition for wood dispersal simulations is a 'steady' network where space-averaged morphological parameters are constant over time. For each flume, a single realisation of the braided pattern was used throughout the experiment, as opposed to Trento runs where networks were discarded when braidplain width reached flume width.

---

[1] http://www.hydralab.eu/index.asp

[2] http://www2.hull.ac.uk/science/geography/research/deep.aspx

However, to limit the influence exerted by non-erodible banks, 10 cm long groynes made of corrugated plastic were placed at approximately regular intervals along the walls. Table 4.20 summarises the key properties of the model.

Wooden dowels used to reproduce driftwood at flume scale were built in analogy with those employed for the Trento runs (Table 4.21) and in particular the selected combination of diameter and length is identical to that of run set T3. For the Hull experiment, birch wood was used and colour-coding patterns were applied to help the identification of dowels with roots and facilitate dowel count (Figure 4.32).

Figure 4.31: The TES Flume showing the configuration used for the present work. Flow is towards the camera.

Figure 4.32: Dowels with roots (striped) and without roots (solid colour) used for the simulations.

Table 4.20: Overview of the TES flume and flow properties assigned for model runs.

Parameter	Value
Total tank length and width [m]	11 x 6
Flume length and width [m]	10 x 1.7
Grain size [mm]	0.73
Slope [-]	0.013
Discharge [l/s]	1.26

Table 4.21: Properties of dowels.

Parameter	Value
Wet density [kg/dm^3]	0.67
Log length [cm]	8
Log diameter [mm]	3
Root wad diameter [mm]	12

Structure of model runs and data acquisition

Long-term driftwood dispersal processes were simulated by adding cohorts of dowels to the network at regular time intervals and monitoring wood output and storage. Run set HU consists of three 18 hour simulations conducted simultaneously in the three flumes (referred to as C1, C2 and C3) under identical steady flow conditions but different wood input rates, with a 1:2:3 ratio between rates for C1, C2 and C3. During the first six hours,, cohorts were added every 10 minutes and comprised 10, 20 and 30 logs respectively, 60% of which with roots; afterwards, input frequency was lowered to one cohort every 15 minutes and the proportion of logs with roots was reduced to 40% (see Table 4.22). Wood was added to the flume immediately downstream of the inlet section and within the same input, dowels were spaced by approximately 3 seconds to ensure uncongested transport conditions. Care was taken in adding dowels with and without roots in random order.

Wood dispersal and bed evolution were monitored through direct measurements of wood and sand output fluxes and high-resolution imagery. Data acquisition was carried out according to the following protocol:

- dowels exiting the flume were collected and counted immediately after each input (every 10 minutes during the first 6 hours and every 15 minutes afterwards). Separate totals for elements with and without roots were computed;

- sand output volume was measured every hour;

- images were acquired every hour immediately after wood input.

Table 4.22: Wood input rate for the three flumes.

	C1		C2		C3	
	H 0 ÷ 6	H 7 ÷ 18	H 0 ÷ 6	H 7 ÷ 18	H 0 ÷ 6	H 7 ÷ 18
Wood input rate [logs/hour]	60	40	120	80	180	120
Input frequency [cohorts/hour]	6	4	6	4	6	4
Cohort size [logs]	10	10	20	20	30	30
Logs with roots [%]	60%	40%	60%	40%	60%	40%

Simulations were subdivided into three 6-hour long sessions conducted over three days. Discharge was set to zero between sessions and raised to approximately 0.2 l/s to saturate the sand bed before restarting the experiment. Low flow condition prevented both bedload and wood remobilisation during the saturation phase.

Wood mapping techniques and protocols

The 2D planar spatial pattern of wood deposits was reconstructed from high-resolution imagery with a time resolution of 1 hour and the formation, growth and erosion of individual deposition sites was determined by comparing subsequent pictures. As spatial data analysis is site-based, accuracy requirements for image rectification are less stringent than those for Trento data. Image pre-processing requires a three-step procedure:

- correction of barrel distortion using PTLens 8.7.8 (see Chapter 4.2.2);

- image stitching on the basis of easily recognizable features present in overlapping areas. The resolution of output pictures was lowered to 1 px/mm to obtain more easily manageable data;

- image georeferencing using control points painted on walls. A common reference coordinate system was defined, with x and y corresponding to the longitudinal and transversal coordinate, respectively. Rectification error of output images is approximately 1 cm.

Spatial data were organised in a Geographical Information System (GIS) using GRASS GIS 6.4.2. Two 1 m long section of the flumes at either end were excluded from the analysis to avoid any influence determined by inlet and outlet, resulting in a 7.65 m long, 1.5 m wide survey area. Wood deposition sites were manually mapped on images and each site was assigned a unique code number c to facilitate the reconstruction of the site history throughout time. Dowels displaced by more than one log length (8 cm) were assumed as remobilised and assigned a new code number. The accuracy of image georeferencing was deemed sufficient to assess log motion.

Site attributes evaluated at time step $t = t_i$ include information on wood *storage* – group size, $n(t_i)$ – and wood *fluxes w*, representing the amount of wood that joins or leaves the site between t_{i-1} and t_i. It is worth noting that sites – and especially large jams – can experience both log deposition and log remobilisation within the same time interval and therefore wood turnover is not correctly quantified if fluxes are computed simply as differences in group size between pictures. In particular, jam size can be preserved also in the case of equal, non-zero incoming and outgoing fluxes. In the present study, colour-coding allowed the identification of individual dowels moving between two pictures. For the generic time step t_i, the following attributes were recorded for each site:

- group size;

- wood deposition fluxes for wood without roots and with roots;

- wood remobilisation fluxes for wood without roots and with roots.

For a site forming at $t = t_i$, the sum of the two deposition fluxes corresponds to group size $n(t_i)$, while remobilisation fluxes are zero by definition for $t = 1$. Special care was taken in characterising very large jams that can store tens of dowels often stacked one on top of the other. The complete database comprises three series of 18 wood deposition maps for a total of 5759 sites observed throughout the experiment. Examples of wood deposition pattern at bar and flume scale shown in Figures 4.33 and 4.34, respectively.

Figure 4.33: Detail of wood deposited on a bar, including jams of various size and isolated log; solid colour dowels have no root wad. Flow is from left to right.
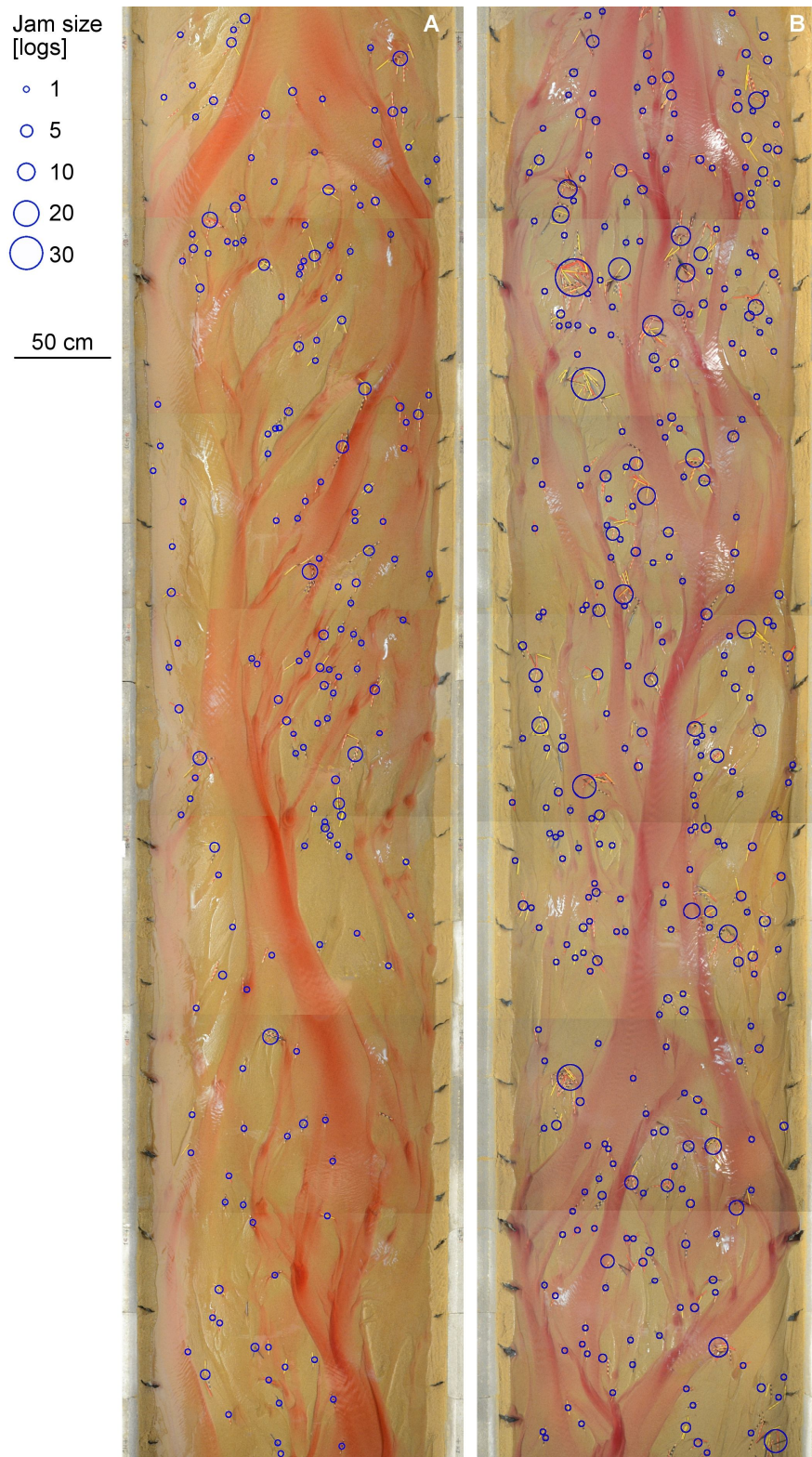
Figure 4.34: Two examples of wood dispersal pattern: low wood density in channel C1 after 7 hours of simulation (A); high wood density in channel C3 after 18 hours of simulation (B). Flow is from top to bottom.

Data analysis overview

The analysis of long-term dynamics focuses on the quantification of wood storage volumes and log deposition and remobilisation processes. The temporal evolution and spatial trends observed for wood retention and turnover are linked with wood input rate, log shape and accumulation size distributions. In the present chapter, the three flumes are referred to as C1, C2 and C3 while subscripts o and x indicate elements without and with roots, respectively; isolated dowels and elements in jams are marked as I and J.

Storage at flume scale was computed on the basis of wood input assigned at the upstream end of the flume and wood output measured at the downstream end. For the generic time step t_i, the number of logs stored in the network $S_T(t_i)$ is

$$S_T(t_i) = \sum_{k=1}^{i} F_{in}(t_k) - F_{out}(t_k) \, ,$$

where $F_{in}(t_k)$ and $F_{out}(t_k)$ are the input and output fluxes at $t = t_k$. Both fluxes can be divided into two components for logs without and with roots ($F_{in,O}$, $F_{in,X}$, $F_{out,O}$, $F_{out,X}$). Storage can be computed separately for the two types of logs (elements without roots, S_O; elements with roots, S_X) and partitioned on the basis of accumulation size (isolated dowels, S_I; elements in jams, S_J).

For an individual site, the mass balance equation at $t = t_i$ can be written as

$$n(t_i) = n(t_{i-1}) + w_{in,O}(t_i) + w_{in,X}(t_i) - w_{out,O}(t_i) - w_{out,X}(t_i) \, .$$

Local fluxes w_{in} and w_{out} are evaluated from image data and represent logs joining and leaving the site between t_{i-1} and t_i. In analogy with total input and output fluxes, they were recorded separately for elements without and with roots. Total wood storage can be defined also as the sum of local deposition and remobilisation fluxes over the whole flume:

$$S_T(t_i) = W_S(t_i) + W_D(t_i) \qquad W_S(t_i) = S_T(t_{i-1}) - W_M(t_i) \, ,$$

where deposited wood W_D and remobilised wood W_M are computed as

$$W_D(t_i) = \sum_{s=1}^{N_s} w_{in,O}(t_i,s) + w_{in,X}(t_i,s) \qquad W_M(t_i) = \sum_{s=1}^{N_s} w_{out,O}(t_i,s) + w_{out,X}(t_i,s) \, .$$

Stable wood W_S comprises all dowels maintaining their position between t_{i-1} and t_i; Figure 4.35 summarises naming conventions. Remobilisation and persistence can be also expressed as a function of stored wood observed at t_{i-1}:

$$R_S(t_i) = \frac{W_S(t_i)}{S_T(t_{i-1})} \qquad R_M(t_i) = \frac{W_M(t_i)}{S_T(t_{i-1})} \, .$$

R_S is called *persistence rate* and R_M is *remobilisation rate*. Wood stability can be analysed also on longer time scales by considering elements displaced over an arbitrarily long time interval. In this case, $W_M(t_{i-k})$ represents the total number of logs removed over k hours and remobilisation rate $R_{M,k}(t_i)$ is computed with reference to wood stored at $t = t_{i-k}$:

$$R_{M,k}(t_i) = \frac{W_M(t_i)}{S_T(t_{i-k})}$$

Finally, downstream trends in wood storage and pattern reorganisation were reconstructed by dividing each flume into a set of five 1.53 m long sub-reaches, numbered from L1 to L5 with L1 being located at the upstream end. Braidplain width is often used as a scale length for the analysis of longitudinal variation of morphological parameters. In the present study, the length of sub-reaches closely approximates one braidplain width.

4.3.2 Wood storage

Accumulation and input / output fluxes

The time evolution of wood storage was reconstructed on the basis of input and output fluxes at flume extremities (F_{in} and F_{out}). During the first six hours of simulation log input rate was set to 60, 120 and 180 logs/hour for channel C1, C2 and C3, respectively; rapid accumulation of wood was observed in all flumes, with higher rates for larger input. The remarkable retention capacity of (empty) braided networks is evident as wood output to input ratio (F_{in}/F_{out}) is lower than 25% during the first three hours and does not exceed 50% for another three (Figure 4.36A). The flumes show different responses to the reduction in wood input rates that occurred after 6 hours; C1 continues to accumulate wood, albeit at a slower rate; the output flux is almost always smaller than the input flux. Channel C2 shows a strong output flux between $t = 7$ h and $t = 9$ h and then stabilises around a total storage of about 400÷450 logs (Figure 4.36B), corresponding to a spatial density of approximately 37÷42 logs/m². Notably, towards the end of the simulation channel C1 reaches a very similar density value (36÷39 logs/m² after $t = 14$ h). Wood volume in C3 is fairly constant during the interval $t = 7÷14$ h – with a total of approximately 800 logs and a spatial density of 72÷75 logs/m² – and increases again afterwards up to more than 900 logs (87 logs/m²).
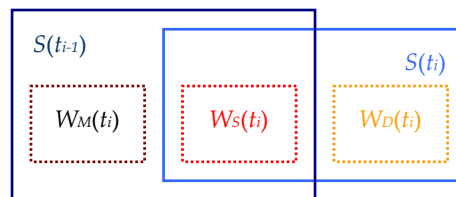
Figure 4.35: Naming convention for wood fluxes.

The different response of the systems to the reduction of input fluxes becomes more evident if ratios between stored wood volumes in the three flumes are computed. As shown in Table 4.22, wood supply was reduced after the first six hours but the ratio between input fluxes in the three flumes was maintained ($F_{in,2}/F_{in,1}$ = 2; $F_{in,3}/F_{in,1}$ = 3; $F_{in,3}/F_{in,2}$ = 1.5). During the first phase, storage rates are close to input rates, but differences between C3 and the other two flumes in terms of storage are smaller (S_{T3}/S_{T1} is about 2.75 and S_{T3}/S_{T2} is 1.35; see Figure 4.36C). In the second phase, higher retention rates in C1 determine a marked decrease in both S_{T3}/S_{T1} and S_{T2}/S_{T1}; interestingly, S_{T3}/S_{T2} quickly stabilises around 1.9, showing that in terms of retention channel C2 is closer to C3 during the first six hours ($F_{in,2}$ = 120 and $F_{in,3}$ = 180 logs/hour) but it is closer to C1 afterwards ($F_{in,1}$ = 40 and $F_{in,2}$ = 80 logs/hour). This result suggests that the response of the network to wood supply may have a threshold with a cut-off value between 80 and 120 logs/hour.

The percentage of elements with roots ($F_{in,X}/F_{in}$) in input cohorts was lowered from 60% to 40% after 6 hours. The proportion of logs with roots within stored wood (S_X) ranges between 65% and 70% during the first phase, indicating higher retention of elements with a root wad. The response of the system to the change in cohort composition is quite slow, with S_X/S_T experiencing a relevant decrease only from t = 9 h onwards. However, in all flumes the proportion of stored wood with roots remains higher than the percentage in input cohorts throughout the simulation (S_X/S_T > 60%, see Figure 4.36D), suggesting that the presence of roots helps long-term wood retention.

Jam size distribution

Wood accumulation patterns in the three flumes were characterised in terms of jam size distributions on the basis of storage maps (from here onwards, all analyses are conducted on data derived from image processing). Deposits show marked differences between flumes and distinct trends over time (Figure 4.37). As expected, the proportion of isolated logs (S_I/S_T) decreases in time, with a clearer trend in C1 and C3 and a weaker effect in C2. As already observed for total stored wood, S_I/S_T in C2 and C3 is essentially the same during the first phase of the experiment, dropping from 50% to 30% during the first 4 hours; at the same time, S_I/S_T in C1 decreases from 67% to 55%. However, the proportion of isolated logs in C3 further decreases to 25% towards the end of the experiment, while values for C2 approach those of C1, fluctuating between 40% and 45% after t = 9 h.

Large accumulations (n > 10 dowels) form in channel C1 only from t = 11 h onwards and represent less than 10% of wood in both C1 and C2; in contrast, rapid formation of large jams is observed in C3, where up to 30% of logs are stored at sites comprising more than 10 elements from t = 6 h onwards. Moreover, a distinctive trait of channel C3 is the formation of very complex jams with more than 20 elements (up to 51 in one case), appearing as early as t = 6 h. These accumulations are responsible for the storage of 10÷20% of total wood.
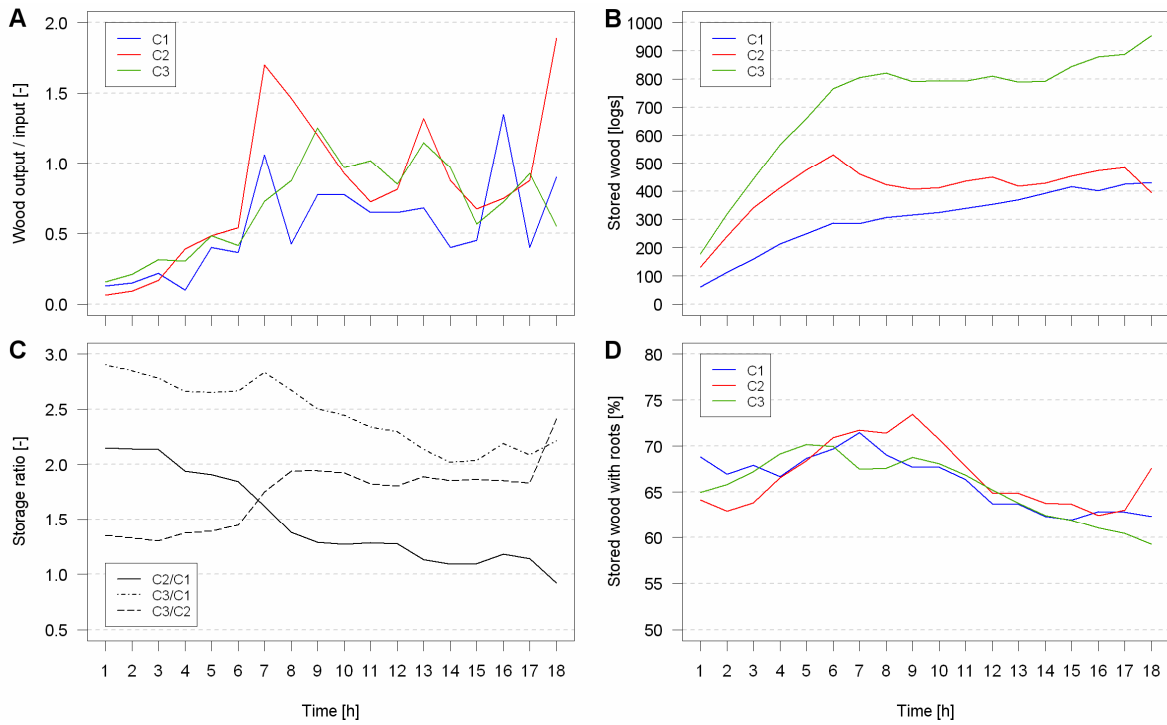
Figure 4.36: Accumulation and input/output fluxes: wood output: input rate F_{out} / F_{in} (A); total wood storage S_T (B); stored wood rate (C); proportion of stored wood with roots S_X (D).
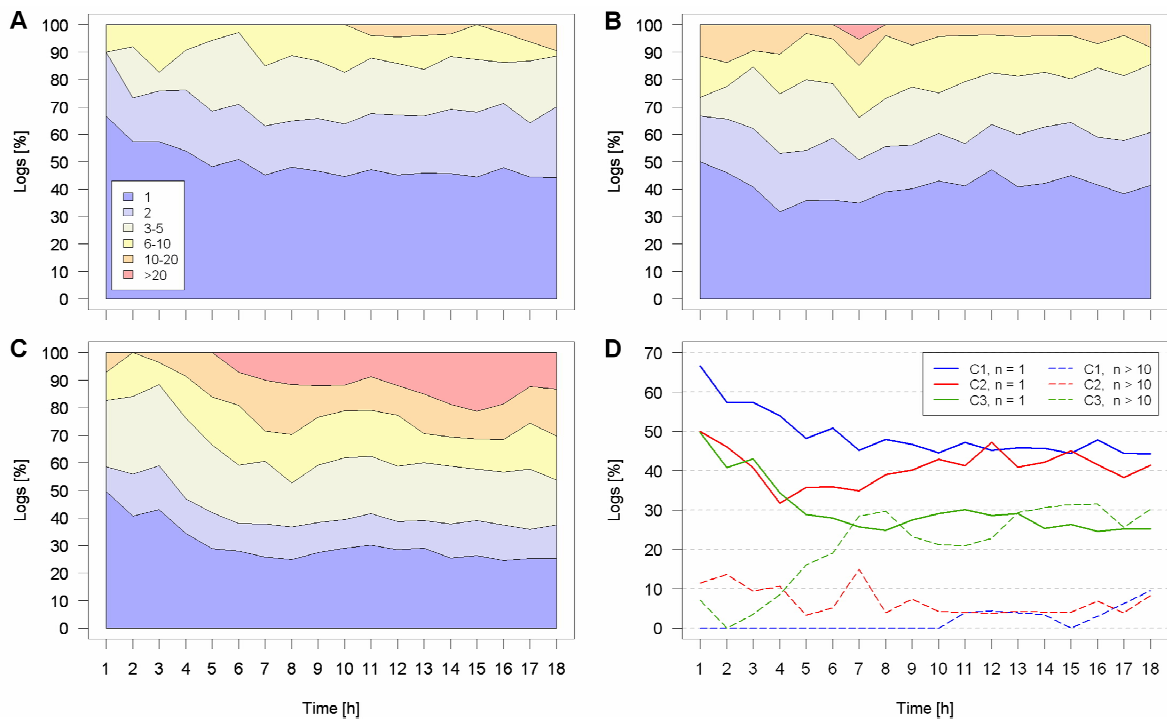
Figure 4.37: Distribution of wood over jam size classes for channels C1 (A), C2 (B) and C3 (C); proportion of wood stored as isolated logs and in jams with more than 10 elements for the three flumes (D).

Spatial trends

Log density and the proportion of isolated elements S_I/S_T and of logs with roots S_X/S_T were computed for the five sub-reaches L1÷L5 and compared within the same flume and between flumes (Figure 4.38). In terms of wood density, marked differences can be observed both in space and time, as the number of logs and sites per unit area can vary by a factor of two between sub-reaches of the same flume. Channel C1 shows a very high accumulation rate in L1, where log density reaches a value of almost 40 logs/m² in 3 hours and remains fairly constant afterwards; this value corresponds to storage per unit area computed over the whole flume area during the last few hours of the simulation. Similar, lower accumulation rates are observed for L2 and L3 – where density approaches 30 logs/m² in 6 hours – and even lower rates occur for L4 and L5 (approximately 13 hours are needed for density to reach the same value). The number of sites per unit area show analogous trends, but differences tend to disappear earlier, implying that downstream dispersal of wood occurs on a shorter timescale while jam growth is a slower process.

Sub-reach L1 of channel C2 exhibits a strong increase in density during the first four hours and a marked drop for the following four, while L2 experiences high deposition rates for t = 4÷6 h and intense remobilisation immediately afterwards, but maintains a significantly higher log density for the rest of the simulation. No major peaks are observed further downstream in the following hours, suggesting that remobilised wood either disperses evenly in the rest of the network or exits the flume (and indeed the output flux peaks for t = 7 h). With the exception of L2, the flume reaches a relatively uniform density after about 7 hours.

Finally, no clear dominance of L1 is observed in C3, where the first three sub-reaches exhibit the same value of density in the first picture (20÷25 logs /m²) and similar accumulation rates over the first six hours. In contrast, log density in L4 and L5 is close to zero at t = 1 but increases at a similar pace and reaches the same values observed in L1÷3 after 7 hours in terms of both sites and logs.

Therefore, a 'quasi-steady' condition is attained after 3 hours in the upstream section of C1, while 6 hours are needed for reaches L2 and L3 of C1 and for the entire length of C2 and C3, while the downstream portion of C1 is still accumulating wood towards the end of the simulation. For each flume, the downstream trend in log storage can be evaluated also in terms of the contribution of each sub-reach to total storage (Figure 4.39). The different behaviour of the three flumes is evident, with L1 hosting a much larger share of S_T in C1 in comparison with C2 and C3. The proportion of isolated logs is generally higher in the downstream part of all flumes, but values tend to equalise after approximately 10 hours in C1 and 7 hours in C2 and C3 (Figure 4.40). On the contrary, no distinct downstream trend is observed for the percentage of logs with roots.
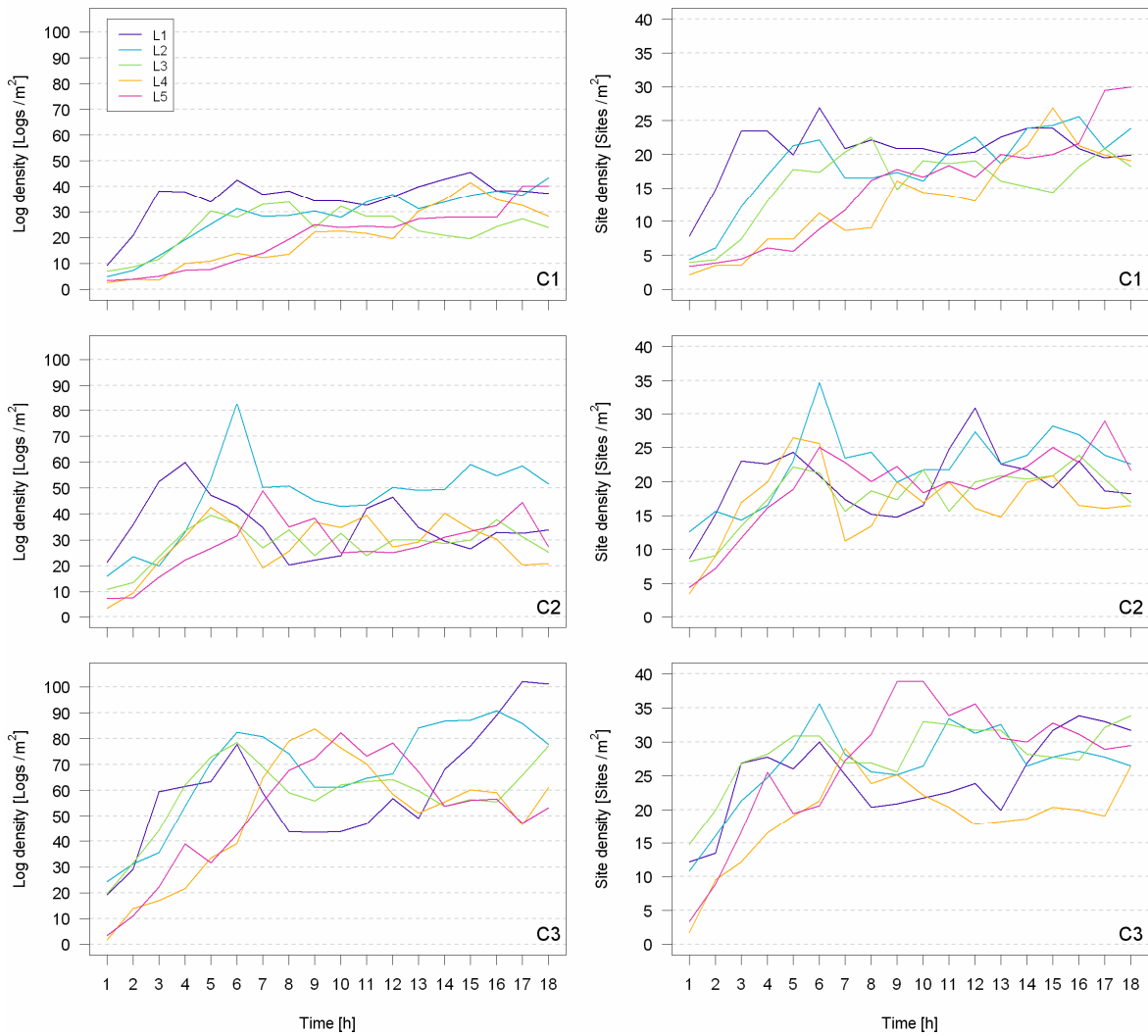
Figure 4.38: Downstream trends in log density (left) and site density (right) for C1, C2 and C3.
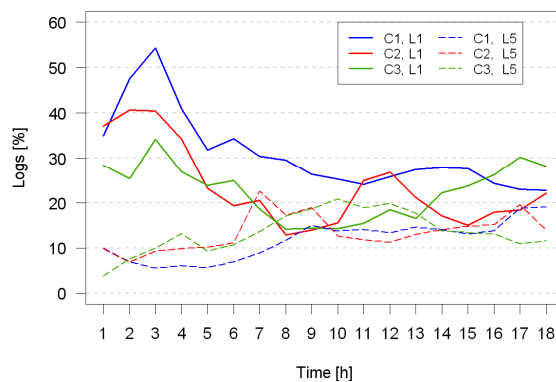
Figure 4.39: Proportion of stored wood in sub-reaches L1 and L5 for the three flumes.

4.3.3 Wood deposition, remobilisation and persistence

Deposition

Wood depositing in the network at each time step can be divided into two components, corresponding to elements joining pre-existing sites (W_{DE}) and logs that are responsible for the formation of new sites. Retention on pre-existing sites increases from 5% to slightly more than 15% in C1 throughout the simulation and fluctuates around similar values in C2 (Figure 4.41). 'Old' sites play a larger role in C3 especially during the last part of the experiment; this effect can be at least partially explained by the presence of large jams ($n >$ 10 elements) in C3, as retention associated to smaller accumulations is closer to that observed for all sites in C1 and C2 (Figure 4.41A). Overall, 85÷90% of deposited wood in C1 and C2 and 70÷80% of deposited wood in C3 forms new sites, implying that wood deposition occurs mostly on empty network areas.

The influence of piece shape on retention was investigated by evaluating the number of newly deposited elements without roots ($W_{D,O}$) retained on 'old sites' ($W_{DE,O}/W_{D,O}$). The relative relevance of deposition on pre-existing sites is higher if computed only for wood without roots, and this effect is particularly evident in C3 (Figure 4.41B).
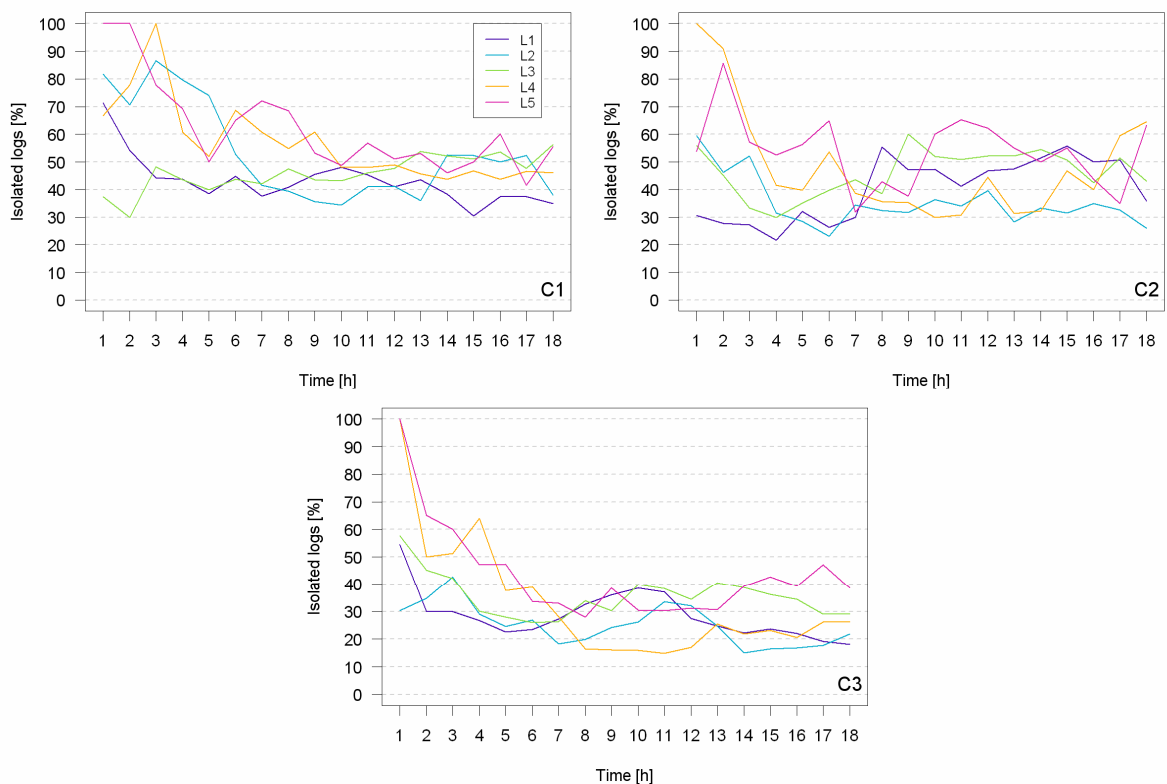
Figure 4.40: Proportion of isolated logs in the five sub-reaches of C1, C2 and C3.

135

Newly deposited sites can be characterised also on the basis of size distribution. In particular, the proportion of wood deposited as isolated dowels (W_{DI}/W_D, Figure 4.42) is significantly higher in C1 (45÷60%) than in C3 (30÷45%) and in both cases is generally greater than the corresponding value for stored wood (equal to 45% and 25% respectively, see Figure 4.37). No temporal trend is observed in C1 and C3, while values of W_{DI}/W_D for C2 approximate those computed for C3 during the first 9 hours but increase sharply afterwards, reaching values typical of channel C1. It is worth remembering that C2 shows a similar tendency also in the case of S_I/S_T (see Figure 4.37), with a clear transition from a C3-like behaviour to a C1-like one.

Finally, all flumes show significant variations in deposition parameters between sub-reaches but no obvious downstream trends, suggesting that distance from input section does not control deposition style nor its association with existing accumulations.
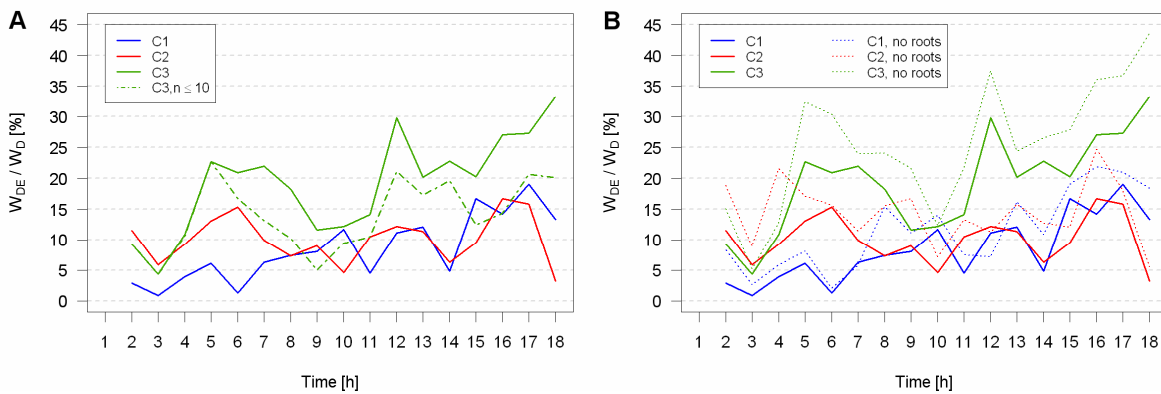
Figure 4.41: Proportion of wood deposited on existing sites; in (A), the dashed line represents deposition on sites comprising up to 10 elements; in (B), dotted lines indicate the proportion of elements without roots deposited on pre-existing sites ($W_{DE,O}/W_{D,O}$).
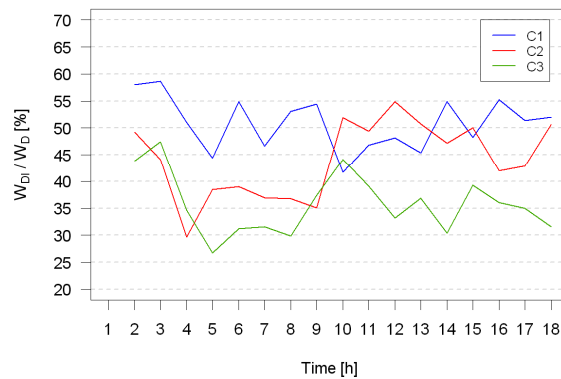
Figure 4.42: Proportion of wood deposited as isolated logs.

Remobilisation

The number of logs displaced between subsequent images (W_M) increases sharply during the first hours of simulation and shows a fluctuating behaviour afterwards, with relevant differences between flumes and over time (Figure 4.43A). Remobilisation rate R_M ranges between 30% and 60% with a weak decreasing trend in time for C1 and C3. Interestingly, no clear differences between flumes are observed, suggesting that intense log turnover occurs over a 1 hour interval in all flumes regardless of wood input rate (Figure 4.43B).

Remobilised wood W_M originates from sites disappearing between t_{i-1} and t_i but also from accumulations preserved between images (W_{ME}). Generally, the latter component accounts for 5% to 20% of all remobilised wood, showing that the complete erosion of accumulations is the dominant phenomenon (Figure 4.44). Wood removal is also expected to be influenced by log shape and jam size and therefore remobilisation rates were also evaluated separately for wood without and with roots ($W_{M,O}/S_O$ and $W_{M,X}/S_X$, respectively) and for isolated logs *versus* logs in jams ($W_{M,I}/S_I$ and $W_{M,J}/S_J$).

The presence of a root wad appears to enhance log stability, but differences in remobilisation rate between the two types of dowels are small if compared with the range of fluctuation of R_M (Figure 4.45A). Similarly, remobilisation rate does not change significantly between isolated elements and logs in jams in channels C1 and C2 (Figure 4.45B). On the contrary, R_M computed for channel C3 from $t = 6$ h onwards ranges between 40% and 60% for isolated logs ($W_{M,I}/S_I$) but falls to 20÷40% for logs in groups ($W_{M,J}/S_J$). A much larger difference is observed if only jams with more than ten components (*large* jams) are taken into account. Less than 20% of logs stored in large jams are removed and in only one case a group of more than 10 elements disappeared completely within one hour. This result suggests that accumulation size governs wood stability, but only in the case of large jams.

Finally, as already observed for deposition, remobilisation rates can vary significantly between sub-reaches, but the spatial analysis did not highlight any trends in the longitudinal direction.

Long-term wood persistence

The stability of wood accumulations on a longer time scale was evaluated by computing remobilisation rates over time intervals ranging from two to five hours. Results are summarised in Figure 4.46. Here, in accordance with definitions introduced in Chapter 4.3.1, the proportion of wood displaced between t_{i-k} and t_i is shown as $R_{M,k}(t_i)$. Remobilisation rate significantly increases for longer intervals, with approximately 90% of wood removed over the first five hours in all flumes. Wood removal declines over time and

fluctuates around 70% towards the end of the simulation in C1 and C3. C2 also shows a weak increase of long-term log persistence over time. Interestingly, the stabilisation of $R_{M,k}(t_i)$ computed over 5 hour and 4 hour intervals occurs from $t_i = 12$ h and $t_i = 11$ h onwards, respectively (that is, as soon as the first six hours of simulation are excluded from
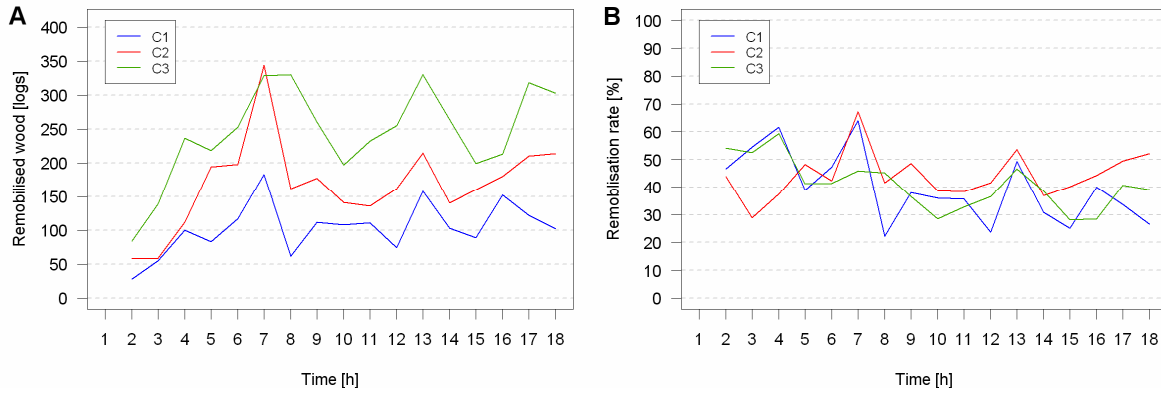
Figure 4.43: Remobilised wood W_M (A) and remobilisation rate R_M (B).
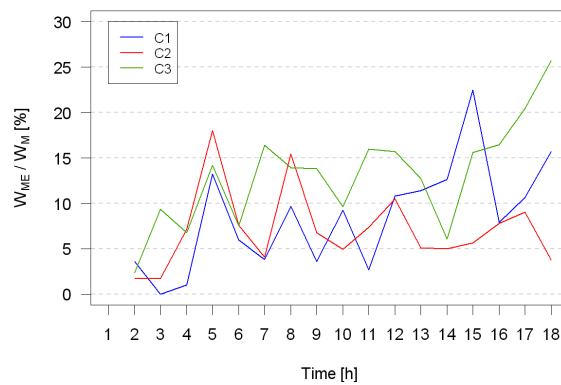
Figure 4.44: Wood remobilised from preserved sites: W_{ME} as a proportion of all remobilised wood W_M.
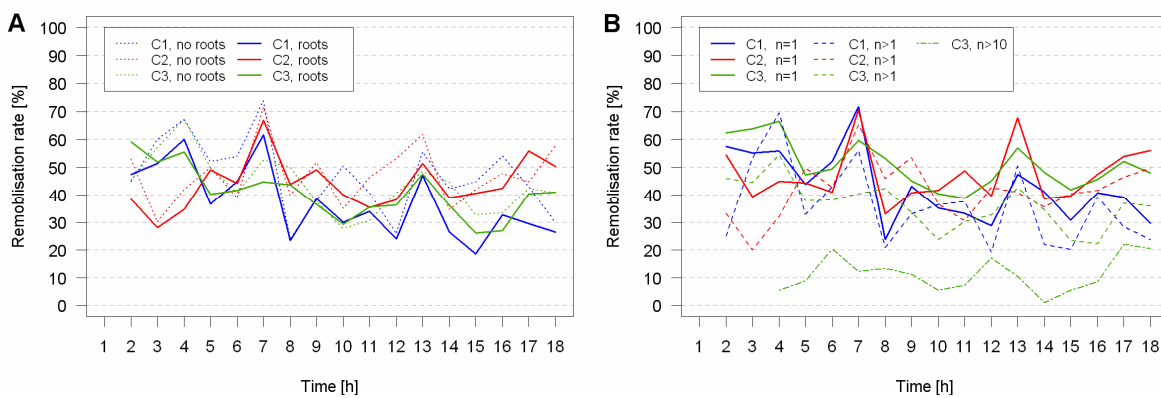
Figure 4.45: Remobilisation rate: for logs without/with roots (A); for various classes of accumulation size n (B)

computations). This result suggests a non-negligible reduction of wood remobilisation after six hours, even if R_M computed over 1 hour intervals shows only a weakly decreasing trend in time. The choice of a longer time interval may filter out short-term fluctuations and therefore provide a better understanding of overall trends.

Short and long-term wood retention can be also evaluated in terms of site persistence, computed as the number of maps in which individual accumulations are present. It is important to underline that the number of observations provides upper and lower limits for site age but no information about its real value. For example, the persistence of a site appearing in two subsequent images but not in the previous and following ones is greater than one hour but smaller than three hours. For the present analysis, sites are assigned the maximum value of age so that cumulative frequency distributions of site age can be expressed in the form of probability of non-exceedance curves. All sites that were present in the last image were excluded from the analysis, as their age is 'artificially' determined as a consequence of the end of simulation time; the database comprises 1175 sites in C1, 1674 sites in C2 and 2105 sites in C3, corresponding to 83%, 89% and 87% of total sites, respectively.

Cumulative frequency distributions of site age were computed for all sites and then separately for isolated logs and jams; the latter group includes all accumulations that hosted more than one element in at least one picture. It is worth noting that this assumption has a negligible effect on frequency distributions, as only 6% of sites changed in size from 1 to more than one during the experiment. Moreover, log jams in channel C3 were further divided into *small* accumulations of up to 10 logs and *large* accumulations, characterised more than 10 elements in at least one picture.

Frequency distributions are essentially identical between flumes if all sites are taken into account (Figure 4.47A), but they are also remarkably similar if only isolated logs or only logs in jams are considered (Figure 4.47B). Overall, 60% of sites are observed in a single picture – implying that their age does not exceed 2 hours – while only about 10% of sites last for more than five hours and a negligible proportion of them persists for more than 10 hours. In all flumes, jams are slightly less prone to erosion if compared to isolated logs, with 50% of jams and 70% of isolated logs lasting for less than two hours. On the contrary, a dramatically different behaviour is observed for large jams. In this case, approximately 40% of sites lasts for more than 5 hours, while a rapid erosion of jams with more than 10 elements is a rather rare event.
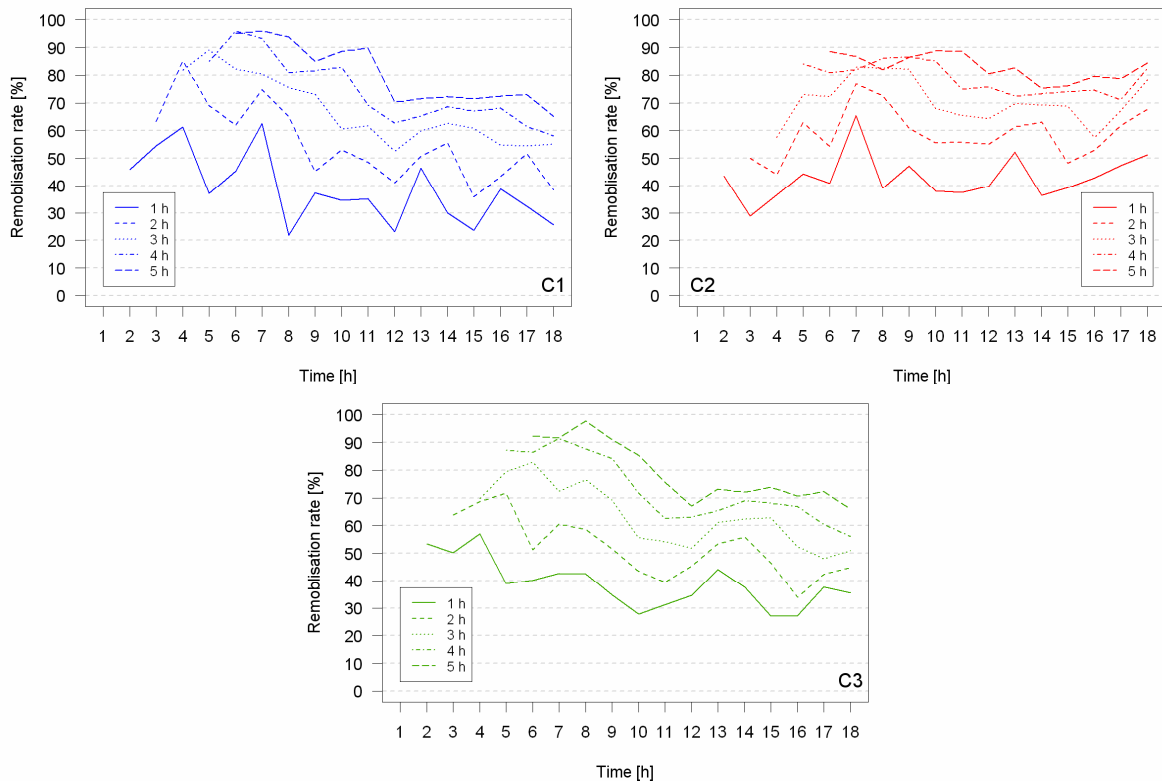
Figure 4.46: Remobilisation rate observed over time intervals of 1 to 5 hours in the three flumes.
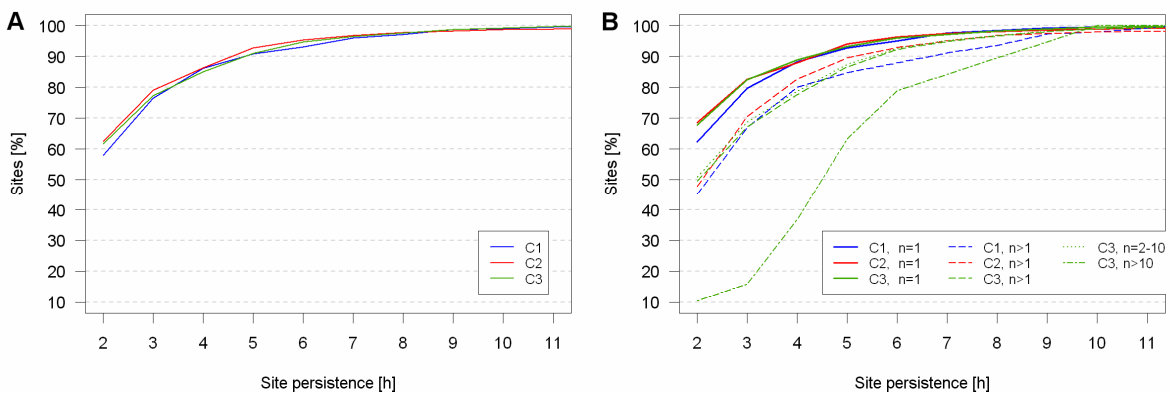
Figure 4.47: Probability of non-exceedance of site persistence for all sites (A) and for different classes of accumulation size n (B).

5 Discussion

5.1 Inundation and wood dispersal in braided systems

5.1.1 Planform distribution of wood

Wood dispersal patterns and processes in braided rivers can be linked to two key properties of multi-thread systems, namely a) network morphology, determining distinctive inundation patterns and therefore the ability of the system to transport and capture wood at various flow stages; and b) channel pattern reworking, governing wood supply as well as the persistence of deposits over time. Moreover, flow regime and channel dynamics in braided systems govern wood supply, because the erosion of vegetated banks and islands is the primary wood recruitment mechanism in large rivers. The frequency and intensity of disturbances also influences the nature and composition of riparian vegetation which in turn govern the physical properties of recruited driftwood elements. Therefore, inundation dynamics, channel change, log properties and wood supply mechanisms and rates represent distinguishing features of large braided rivers.

Past research highlighted that discharge fluctuations in braided networks determine changes in inundation pattern and characteristic sequences of network configurations (Mosley, 1982; Mosley, 1983; van der Nat et al., 2002; van der Nat et al., 2003b; Lorang et al., 2005; Malard et al., 2006; Doering et al., 2007; Bertoldi et al., 2009b). These configurations correspond to different wood dispersal mechanisms and patterns. At low to moderate flow, most water concentrates in a sinuous main channel with few bifurcations and wood entering the system is found along the main anabranch. As discharge increases, water forms numerous channels divided by bars and these emerging or submerged features become preferential deposition locations for floating wood pieces. At higher flow stages channels tend to coalescence and stored wood is found at progressively higher elevations within the network, which are often occupied by standing vegetation (Gurnell et al., 2000b; Bertoldi et al., 2009b).

These simple qualitative considerations show that the abundance, distribution and nature of deposition sites change with discharge, as does the ability of the network to transfer floating organic material downstream. Flow stage fluctuations in single-thread systems also generate wood accumulations at different relative elevations. However,

systems characterised by a simpler cross-section shape exhibit limited changes in wetted area and therefore less disperse and diverse wood deposition sites.

In the present study, a quantitative characterisation of inundation dynamics was obtained at real scale on the Tagliamento River (Chapter 3.3) and also for laboratory-scale networks (Chapter 4.2.2). Field observations show that wetted area proportion increases with discharge, while network complexity – represented by braiding index and shoreline length – peaks for intermediate flow levels. Wetted area is related to the ability of the network to disperse buoyant particles, while braiding index and shoreline length can be interpreted as measure of network retentiveness, because bar heads and channel margins are major wood deposition sites. However, care must be taken in estimating network transfer and storage capacity as only some channels – upstream connected anabranches with sufficient flow depth – are effectively accessible to wood. Unfortunately, field-scale monitoring based on automated ground-based cameras provides valuable high resolution data for a wide range of flow stages but no information on water depth distribution.

On the contrary, a fully three-dimensional characterisation of inundation patterns was derived for network configurations observed in the Trento flume, albeit for a smaller range of flow conditions. In laboratory-scale networks, the portion of braidplain area where wood transport can occur (*connected wetted area*, as defined in Chapter 4.2.2) is about 25% for low to medium values of discharge (50% and 66% of formative discharge) and increases to approximately 40% for flow conditions approaching formative conditions. Braiding index follows a similar trend, increasing from less than 2 for the two lowest values of discharge to approximately 2.5 for the highest two. These results show that an increase in discharge from 50% to 100% of the bankfull value determines a significant extension of the area that can sustain the downstream transfer of wood, but also a larger number of retention sites.

These trends provide an explanation for wood dispersal patterns observed at flume scale under different flow conditions. Experimental findings (run set T2) show no clear relationship between travel distance and discharge, most likely as a consequence of the two aforementioned, opposite effects. Under moderate flow conditions, discharge is concentrated in a single channel with a limited number of potential deposition sites, while at high flow, the increase in local water depth and velocity is counterbalanced by the higher retentiveness of the network. Therefore, wood mobilised during a small flood is not necessarily found close to the input point and conversely large events may not be associated to greater dispersal distances. However, a qualitative comparison of driftwood patterns shows that under moderate flow conditions (that is, in simpler networks), a higher concentration of elements occurs immediately downstream of the input point. This suggests that local retention may be more relevant in the case of small floods.

It is important to observe that the dispersal of wood originating from a localised source such as an eroding bank is also influenced by bed geometry close to the input point. In

braided rivers, longitudinal variations in network complexity are associated to sequences of aggrading /degrading reaches (Hoey and Sutherland, 1991) and the presence of vegetation. (as suggested in Chapter 3.4) Wood recruitment and deposition patterns observed on the Tagliamento River (Chapter 3.3) represent an example of this. The island-braided Flagogna reach – characterised by a simpler channel configuration and a higher proportion of flow concentrated in the main channel – exhibits lower close-range retention if compared to the Cornino reach, which shows a higher braiding intensity.

Changes in the number of available retention sites also influence wood accumulation style and in particular jam size distribution. Various authors have noted that log jams in braided rivers are generally small in comparison with those found in single-thread systems, and accumulations of hundreds of pieces have been reported for meandering streams. In the present work, wood deposited under moderate flow conditions shows a marked tendency to form large accumulations, unlike wood dispersed at high flow. Interestingly, the drop in the proportion of wood stored in large jams (from 35÷40% to less than 20%) corresponds to the increase in braiding index. The cumulative frequency distribution of jam size (see Figure 5.1) confirms that wood deposited by a discharge of 1.2 l/s (the second-lowest value) forms the largest jams.

5.1.2 Relative elevation of wood accumulation

Past studies have shown that the relative elevation of wood deposits is of primary importance for the persistence and evolution of accumulations. In particular, elevation determines disturbance frequency and intensity and moisture availability, which in turn represent the most relevant limiting factors for the vegetative regeneration of deposited trees (Francis, 2007). Therefore, the investigation of vertical distributions of wood is crucial for the understanding of the geomorphic and ecologic role of driftwood.

Frequency distributions of relative elevation were computed for wood deposits at field and flume scale (run set T3). In both cases, wood concentrates within a relatively narrow
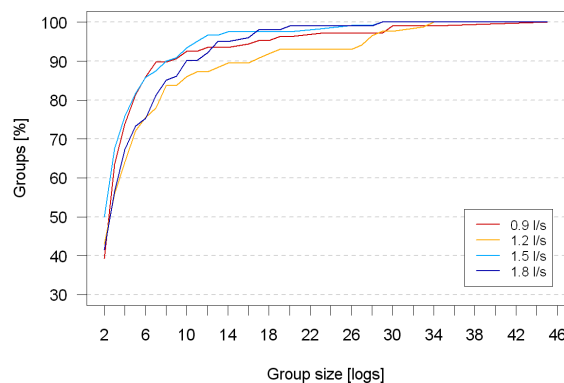
Figure 5.1: Cumulative frequency distribution of jam size for four values of discharge. Data from run set T3.

143

band of elevation values. In particular, wood on the Tagliamento River was found within an approximately 1-m wide elevation band, while the range of bed relief was two to three times larger. A similar ratio between the standard deviation of wood and bed elevation distributions occurs in the PI flume. At field scale, elevation was found to be connected to flood levels, while no clear link was observed in laboratory simulations. Several possible explanations for this result exist, all related to the experimental setup and/or the surveying protocol. The vertical distribution of wood essentially depends on water surface elevation, but the latter changes across the network, implying that for a given value of discharge, wood accumulations on the margins of different anabranches can be found at different elevations. In the case of field observations, surveyed wood deposits were concentrated on individual bars and therefore between-channel differences were probably limited. On the contrary, laboratory data refer to multiple network realisations and wood deposits dispersed along the entire flume length and so water surface elevation is expected to be significantly different from site to site.

Unfortunately, model setup and monitoring protocols did not allow for the survey of water surface during wood dispersal simulation; this limits the possibility to correctly interpret the vertical distribution of wood and probably obscures the expected discharge-elevation relationship. It is also important to observe that, in the Trento model, at-a-station changes in water surface elevation with discharge are extremely small (3 mm between the lowest and highest flow conditions) and comparable with between-channels variability. This result is not unexpected, as in braided rivers channel depth has been shown to change slowly with discharge, while wetted width exhibits fast increase rates. Therefore, the effect of discharge is too small to be reliably recorded at flume scale.

5.1.3 The role of log properties

Element size

In the present work, wood mobility, accumulation style and persistence have been linked to element size (log length and diameter) and shape, represented by the presence or absence of a root bole. Size distributions of driftwood elements surveyed on the Tagliamento River were used as reference values to define the ranges of dowel diameter and length used to reproduce typical 'large river' conditions at flume scale.

On the Tagliamento River, median log diameter ranges between 3.5 and 4.5 times the median bed particle size, while for trees eroded from established islands the upper quartile of log diameter is approximately seven times the D_{50}. Dowels employed in the Trento experiments (run set T1, diameter to particle size ratio between 2 and 6) provide a good characterisation of the range of diameters that can be observed in a gravel-bed braided river flanked by temperate riparian forest. Elements used for the Hull experiments have a

diameter to particle size ratio of 4.1 which closely matches median relative element size observed in the field.

In the Trento runs, wood mobility shows a threshold behaviour with element diameter, as dowels thicker than 3 mm exhibit significantly smaller travel distance values. Cumulative distributions of channel depth show that this size threshold corresponds to approximately one-half median channel depth. This result is in good agreement with both field and flume-scale observations. In particular, Abbe and Montgomery (2003) report that immobile *key members* of log jams in a meandering river usually have diameters exceeding half channel depth. Analogously, laboratory simulations performed by Braudrick et al. (1997) show that dowel flotation drops for relative element diameter exceeding 0.5. Various authors have pointed out that diameter is the crucial parameter governing element flotation (Braudrick and Grant, 2000; Gurnell and Petts, 2002). This effect is likely to be of primary importance to determine wood storage patterns in braided systems, where a large number of shallow depth areas occur across the network. Submerged bars, gently sloping banks and secondary channels act as distributed retention hotspots governing wood dispersal patterns at local and reach scale.

Dowels used for T1 flume simulations comprise 4, 6, 8 and 12 cm long elements. A negligible proportion of network channels is narrower than 8 cm, while the highest length value corresponds to the 15th percentile of channel width computed for upstream connected anabranches. This suggests that 'large river' conditions as defined by Gurnell et al. (2002) – all pieces shorter than channel width – are met in the vast majority of the network and as expected for a 'large' system, wood travel distance is not influenced by log length. However, longer elements are associated with a higher relative relevance of wood stored in jams and overall larger jam size, confirming the link between element length and jam formation suggested by Gurnell and Petts (2002).

Element shape: root boles

Two approaches have been used to investigate the effect of the presence of root wads on wood deposition patterns, namely: a) the comparison between cohorts comprising different proportions of elements with roots (short-term simulations in run set T1 and T2); and b) the comparison of the fate of elements with and without roots belonging to the same cohort (short-term simulations in run set T3 and long-term Hull runs). In the first case, extreme values of root prevalence (0% and 100% of elements with roots) were tested with the aim of defining general trends and individuating potential threshold behaviours, even if neither case realistically occurs in natural riverine systems. No information on this parameter is available in literature and estimations based on wood deposits formed after flood events may lead to an overestimation of the proportion of elements with roots, as simpler shapes are likely to be more easily dispersed.

Contrary to expectations, the analysis of wood dispersal patterns generated by individual wood inputs (run set T1 and T2) show that root prevalence has little effect on travel distance computed over the whole cohort and influences only the tail of the downstream distribution of wood. Cohorts with a high proportion of complex-shaped elements tend to form very large accumulations, especially when wood is dispersed by small to moderate flood events. However, as already observed in Chapter 4.2.6, between-run variability is especially high in the case of mixed cohorts and this effect may obscure the links between root prevalence and travel distance.

Within-cohort analyses were performed on dispersal maps from run set T3. Multivariate analysis was used to assess the effect of discharge and element shape on travel distance, relative elevation and jam size distribution. The analysis confirms the positive contribution of piece shape complexity to the formation of log jams and also shows that wood with roots tends to accumulate closer to the input point and at lower relative elevations. This result can be relevant for the prediction of the fate of deposited wood; as observed by Francis (2007) and Moggridge and Gurnell (2009), relative elevation is a key factor for wood survival and therefore for evolution of pioneer islands from deposited wood.

5.2 Wood pattern reworking and long-term storage

5.2.1 Inundation-driven wood remobilisation

In the present work, two distinct mechanisms determining wood remobilisation were investigated, namely a) network inundation (T3 runs); and b) channel pattern reworking (Hull runs). The first process induces local changes in water velocity and depth over a short time scale (the hydrodynamic scale), while the second is associated to the erosion of retention sites and occurs over a longer time scale (the morphodynamic scale). Both processes occur in riverine systems during floods and a separate characterisation of their effects is difficult to obtain from real-scale data. In contrast, the contribution of each of the two processes to wood pattern reworking can be isolated in laboratory experiments by controlling discharge and run duration.

The simulation of inundation-driven wood removal shows that the difference between *input discharge* (flow conditions associated to initial wood deposition) and peak discharge of a subsequent flood exerts a strong control on the probability of wood remobilisation. Logs originally dispersed by moderate flows are associated to a higher probability of removal, and in particular more than 50% of wood deposited at flow stage corresponding to one half of bankfull flow are removed. Remobilisation ranges between 20% and 25% for higher

values of input discharge, indicating a non-linear relationship between remobilisation rate and discharge difference. Moreover, logistic regression modelling shows that high relative elevation and large jam size positively contribute to wood persistence, while logs with root boles do not appear to be more stable than elements without roots. The absence of a noticeable influence of piece shape is discussed in detail in Chapter 5.3.3.

Finally, the magnitude of discharge variations influences the fate of remobilised wood and in particular the proportion of logs depositing on pre-existing sites. This parameter is remarkably low (10%) for wood originally deposited by moderate flows but increases to 30% for high input discharge (see Table 5.2). In the first case, wood patterns are less dispersed and sites are more likely to be eroded by a subsequent, larger flood and therefore fewer sites can trap floating wood. Interestingly, these values are comparable or even higher than those observed in long-term, steady-flow dispersal simulations. In this case, retention on pre-existing sites accounts for 10÷15% of wood deposition in networks with moderate spatial wood density (about 40 logs/m²) and also in the case of high wood storage (about 80 logs/m²), if deposition on a few very large jams is excluded. This is a remarkable result, because the small number of sites available in unsteady flow simulations appear to be much more important for retention than the large amount of deposits in steady flow runs.

Therefore, it can be hypothesized that wood removed due to a rapid increase in water level (especially if originally deposited under similar flow conditions) is more likely to be trapped on pre-existing sites than wood remobilised by channel change. Intense wood transport during the rising limb of a flood was observed by MacVicar and Piégay (2012). In this case, higher deposition on existing sites over a short time scale may be expected. However, network reorganisation during the flood implies that storage in empty areas becomes more and more relevant throughout time. In real-scale braided networks these processes are also influenced by the presence of standing vegetation, which contributes to wood trapping especially at high flow (Gurnell et al., 2000a; Gurnell et al., 2001). Pre-existing deposits on island margins are preferential sites for wood accumulation and at the same time are characterised by higher resistance to erosion, suggesting that they can exert a log-lasting influence on wood deposition patterns.

5.2.2 Channel pattern reworking and long-term wood dynamics

Flume simulations show that long-term wood dynamics are determined by the joint effect of wood supply and channel change rate, with element shape playing a minor role. Wood storage and jam size distribution exhibit distinctive trends in time and a strong dependence on wood input rate. Three values of the latter were tested, with a 1:2:3 ratio. The system characterised by the highest supply rate shows a markedly different behaviour

Table 5.1: Proportion of wood deposited on existing sites.

Discharge [l/s]	Wood deposited on existing sites
0.9	10%
1.2	17%
1.5	29%
1.8	31%

with very high wood storage and the formation of large accumulations, while wood volume and jam size distribution in the other two flumes exhibit remarkably similar values especially towards the end of the simulation. This result may suggest the existence of a threshold in wood supply that discriminates between high wood density and low wood density systems.

Large jams of driftwood elements appear to be the distinctive feature of braided networks subject to high wood supply, where these accumulations store a substantial amount of wood. For the highest value of wood supply tested in the present study, 40% and 20% of logs are stored in jams larger than 10 and 20 elements, respectively. In comparison, in the two flumes subject to lower wood input rate the first value ranges between 0 and 10%, while only one site briefly stores more than 20 logs. As already observed, large jams tend to attract floating pieces and especially logs without roots, enhancing deposition on pre-existing sites. Moreover, large accumulations are significantly less likely to be eroded and show a greater persistence over time.

However, while large log jams can act as preferential deposition sites and local hotspots of stability for wood deposits, network reorganisation remains a dominant factor for long-term wood remobilisation. Intense turnover of deposited wood – associated to the erosion of retention sites – is observed regardless of wood input rate and storage volumes. The low percentage of logs deposited on pre-existing sites is an indirect measure of the rapid reworking of dispersal patterns. If the contribution of large jams is excluded, wood found on existing sites fluctuates around 10% of all deposited logs. Higher percentages were observed for inundation-driven remobilisation, even if wood deposits occupy a much lower portion of the braidplain. This comparison demonstrates that even in braided systems with a high density of stored wood, deposition of new logs primarily occurs on empty network areas, and this is possible because channel change rate is high and the vast majority of deposits are short-lived.

The stabilising effect of jam size observed in short term simulations is confirmed, but it becomes significant only for large jams (comprising more than 10 elements), while small accumulations are unable to contrast erosive processes.

5.2.3 The role of root wads

A small positive effect of the presence of roots on element stability is observed, even if differences between logs with and without roots are small in comparison with the time and space fluctuations of remobilisation rates. Moreover, in long-term simulations, stored wood shows a higher proportion of elements with roots with respect to input flux and this effect also indicates a positive contribution of roots to long-term wood retention.

However, a stronger control of root wads on element stability may be expected on the basis of field observations of driftwood persistence in both single-thread and braided systems (Abbe and Montgomery, 1996; Gurnell et al., 2002; Manners and Doyle, 2008) and laboratory-scale data proposed by Braudrick and Grant (2000). In all cases, the authors report a marked increase in stability for pieces with root wads. A possible explanation for this discrepancy is the tendency of elements with roots to deposit at low relative elevation within the network, which makes them more susceptible to remobilisation under rising discharge. The negative effect of low elevation on element stability may override the positive contribution of piece shape complexity. In addition, the analytical model and experimental data proposed by Braudrick and Grant (2000) refer to the incipient motion of logs lying over a flat, immobile bed and therefore neglect any effect of different log positioning within a natural channel. This shows the relevance of modelling wood dispersal over a fully mobile bed where complex, self-organised channel patterns can be reproduced and the effect of bed morphology on the spatial distribution of driftwood can be investigated.

A second explanation of the absence of a significant stabilising effect of roots is related to the simplifications introduced in the physical models. Two key processes are not simulated, namely the accumulation of fines around deposited wood – because well-sorted sand was used in both cases – and vegetative regeneration of uprooted trees. On one side, these two mutually related processes play a pivotal role in wood stability because they contribute to the development of pioneer islands from deposited driftwood (Kollmann et al., 1999; Gurnell et al., 2001; Gurnell et al., 2005). On the other side, they are expected to be particularly relevant in the case of whole uprooted trees that preserve their root wads, because their complex shape induces more intense modifications of the local flow field with respect to simple cylindrical logs. Therefore, the absence of these two mechanisms may contribute to the underestimation of the stabilising effect of root wads. However, these mechanisms are neglected also in the experiments of Braudrick and Grant (2000), suggesting that different channel geometry (flat bed *versus* braided channel pattern) can have a significant effect on the evaluation of the stabilising role of element shape.

Finally, other, possibly minor effects can be associated to the choice of root wad shape and density (root boles often contain a relevant amount of sediment which increases

element weight and hinders flotation; B. Wyżga, personal communication). Abbe and Montgomery (1996) also observed that large trees are more likely to retain their rootwad, implying that the limited mobility of pieces with roots can also arise from their larger size.

5.2.4 Geomorphological and ecological implications

In the present work, field and flume-scale observations of driftwood in braided networks provided detailed information on spatial and temporal wood storage patterns. In these systems, wood is widely dispersed and forms a large number of relatively small accumulations, especially in comparison with the huge jams found in single-thread systems. Moreover, intense channel reworking determines high turnover of deposits, while a moderate stabilising influence is determined by large jam size and complex element shape. The dominant effect of channel change implies that driftwood has a limited influence on reach-scale channel morphology and dynamics. The most significant contribution to the persistence of river features is associated to large jams, whose behaviour approaches the 'hard point' effect described by Montgomery and Abbe (2006).

However, dispersed wood in braided rivers has significant effects on local hydraulics and morphology, which in turn have relevant ecological implications. Wood contributes to pool formation, accumulation of fine sediment, organic matter and seeds, moisture availability and exchanges with groundwater and therefore sustains physical habitat diversity. In addition wood has a direct, strong influence on plant colonisation through vegetative regeneration. As a consequence, wood dispersal pattern and its persistence over time has a strong influence on riverine ecosystem dynamics.

This work has showed that wood storage at sub-reach scale is strongly linked with local supply determined by the erosion of vegetated banks. Log size and shape and discharge also contribute to determine wood volumes, its planform and vertical distribution and typical accumulation sites and styles. Moreover, flume simulations allowed to identify favourable conditions for wood persistence in terms of element and jam properties, location of deposits and flow conditions. These results can contribute to the prediction of wood persistence and therefore to the nature and extent of its geomorphic and ecological influence. This applies not only to naturally-occurring in-channel wood, but information on wood stability ad its governing factors could be useful also to design wood reintroduction interventions.

However, laboratory simulations show that the fate of driftwood depends on many, mutually interacting factors and that even moderate variations (for example in element diameter or relative elevation) can yield radically different results in term of piece stability. Therefore, as already suggested in early studies, for example by Gurnell et al. (1995), river

management policies aimed at the restoration of wood supply and dispersal mechanisms can be a more effective than localised interventions and guarantee long-term benefits.

It is important to underline that physical modelling conducted for the present study does not include vegetation dynamics and in particular the formation of pioneer and established islands from deposited wood. Flume simulations show that driftwood alone has little or no direct effect on reach-scale braided river morphodynamics due to the low volume per unit area, small relative piece size and widespread dispersal, all of which limit its ability to counteract channel change. However, wood has a relevant, indirect effect on braided river morphodynamics because it favours the establishment of vegetation. Field-scale observations demonstrate that islands can reduce network complexity and limit channel pattern reworking (and therefore the variability of inundation pattern over time). At the same time, islands can promote the persistence of water bodies over time.

5.3   Suggestions for further research

The present study demonstrates that wood dynamics in large braided system can be investigated in detail by combining field-scale direct observations, remote sensing of channel and wood dynamics and physical modelling. On one side, field-scale surveys provide the invaluable opportunity to observe and describe the full complexity of the relationships and mutual feedbacks between flow, sediment wood and vegetation dynamics occurring in complex riverine systems. On the other side, laboratory-scale simulations allow the investigation of wood dispersal under controlled conditions and in particular when safety and logistical constraints limit the possibility of real-scale monitoring of the processes of interest.

Data analysis highlighted the strengths and weaknesses of the two approaches. In particular, automated ground-based imagery provides valuable, high-frequency information on inundation dynamics and wood dispersal during floods and therefore represent a significant improvement from traditional pre/post event comparisons. This method represent a cost-effective solution for a detailed characterisation of planform dynamics. However, fully three-dimensional information (obtained through LiDAR surveys, photogrammetry, terrestrial laser scanning or traditional surveys, depending on the spatial scale and nature of phenomena) is needed for a more complete understanding of braided river morphodynamics. Images also provide information on wood dispersal during floods and, if resolution is sufficiently high, are well suited to monitor changes in channel pattern over large spatial scales. However, the combination with other wood tracking techniques would be beneficial for the verification of remotely sensed data (Moulin and Piégay, 2004; MacVicar et al., 2009). In particular, radio transmitters on standing and

deposited trees could be used to evaluate supply and remobilisation rate and to estimate travel distances.

A flume scale model is a versatile tool to simulate channel and wood dynamics as it provides the opportunity to test the individual or joint effect of a wide variety of geomorphic factors (such as discharge, grain size, slope) and wood-related parameters (log properties, supply process and rate). Control on run duration also allows to isolate processes that take place at the hydrodynamic or morphodynamic scale. The present work demonstrates the importance of simulating wood dynamics over a fully mobile bed, for a comprehensive characterisation of the interactions between flow, sediment and wood dispersal. The analysis of laboratory-scale wood dispersal patterns performed in this study would greatly benefit from the availability of detailed, reliable maps of surface elevation and/or water depth, such as those computed by Tal and Paola (2010). Numerical modelling can also be employed to reconstruct the flow field. These data are of particular importance for the analysis of the vertical distribution of wood, which is known to play a relevant role in the persistence and survival of deposited trees.

A common trait of wood dispersal simulations carried out in the present study is the remarkable variability of dispersal patterns and processes between runs conducted under identical experimental conditions. Log travel distance, relative elevation of deposits, jam prevalence and size and remobilisation rate exhibit clear trends and statistically significant differences as a consequence of changes in wood properties and flow conditions. However, fluctuations observed for all parameters indicate that wood transport, accumulation and remobilisation are intrinsically highly variable phenomena, most likely due to the concurrent effect of a large number of governing factors. For instance, analytical models of log entrainment (Braudrick and Grant, 2000; Bocchiola et al., 2006b) explain the relatively simple case of incipient motion of an individual log lying in a uniform flow field on an immobile sloping bed using an extensive set of parameters (log length, diameter, shape, density and orientation; channel slope and bed roughness; flow depth and velocity). In real rivers, as well as in the laboratory-scale model built for the present work, additional factors contribute to space and time fluctuations of wood dispersal processes, the most relevant being the non-uniform flow field and the evolution of bedforms. The contribution of these factors to the variability of wood dispersal patterns can be particularly strong in complex braided networks.

Therefore, an experimental protocol based on a significant number of repetitions of model runs is of crucial importance to draw general conclusions on driftwood behaviour in complex systems. Moreover, care should be taken in defining laboratory procedures and measurement techniques in order to minimise the sources of uncertainty in model results. Finally, special attention should be devoted to the selection of relevant processes and model simplifications have to be carefully considered for the interpretation of the outcomes

of flume simulations. For example, in the present study, sediment sorting, standing vegetation and driftwood regeneration were not reproduced at laboratory scale, but these factors are known to play a major role in wood dynamics. While various strategies to simulate standing vegetation have been tested at flume scale (Coulthard, 2005; Bocchiola et al., 2006a; Tal and Paola, 2010), other processes may not be reproducible, such as vegetative regeneration and fine sediment dynamics. In the latter case, scaling issues become critical as cohesion occurs for fractions finer than sand.

Therefore, an integrated approach comprising real-scale monitoring, laboratory simulations and numerical modelling is required to fully characterise channel and driftwood dynamics and their mutual interactions and feedbacks, and this is especially true in large, complex braided systems.

6 Conclusions

In the present work, driftwood dispersal in braided systems was investigated using a combination of direct field surveys, remote sensing techniques and physical modelling, with the aim of providing a detailed, quantitative characterisation of wood dispersal patterns and processes. Multi-thread systems represent a particularly interesting, yet challenging context for the study of wood dynamics because of the spatial complexity and rapid, intense turnover of bed morphology. In braided rivers, floods are the primary driver of driftwood dynamics, governing wood supply, transport, storage and persistence over time. Major events are responsible for wood recruitment through the erosion of vegetated banks and islands; however, substantial changes in inundation patterns and significant channel reworking occur also for moderate floods, implying that in braided rivers the spatial organisation of deposits and their persistence over time is influenced by a wide range of flow conditions.

In the present study, wood recruitment and changes in channel pattern configuration have been investigated at field scale on the Tagliamento River (Italy) using high resolution, high frequency ground-based imagery. Localised wood input has been shown to exert a strong control on wood storage at sub-reach scale, as a large proportion of eroded trees are retained on the first braid bar downstream of the input location. Wood forms sparse, patchy deposition patterns and small jams.

Wood dispersal has been explored in detail through flume simulations conducted at the Hydraulics Laboratory of the University of Trento (Italy) and at the Total Environmental Simulator of the University of Hull (UK), obtaining remarkably similar spatial patterns. The physical models were employed to investigate wood mobility, accumulation and persistence and to test the influence of relevant driving factors, including flow regime, network evolution, log properties (size and shape) and wood supply rate. Deposition patterns were characterised in terms of a) longitudinal distribution; b) vertical distribution; and c) typical accumulation size. Complex relationships between flow stage and the longitudinal and vertical distribution of wood were highlighted. In particular, high flows tend to produce a more dispersed wood deposition pattern, but higher discharge is not necessarily associated with greater travel distance. This effect is most likely determined by the fact that higher flows induce an increase in the ability of the network to transfer wood (high wetted area) but also to retain wood (high braiding index, indicating a large

number of retention sites). No clear link between flow stage and the vertical distribution of wood was observed at flume scale. This effect may derive from the low rate of change of water surface elevation with discharge in flat braided river cross-sections; in general, the complex flow field, which governs wood dispersal, is not easily derived from bed elevation data. However, field scale data confirm that wood accumulates within a narrow band of relative elevation values.

The physical properties of logs (length, diameter and shape) and wood input rate also influence the spatial organisation of deposits (longitudinal distribution and tendency to jam formation). In particular, log diameter exerts a strong control on distance as it governs flotation and therefore the likeliness of deposition, while element length has little or no direct effect on mobility. This result confirms that morphological features are the main driver of deposition in large rivers, as opposed to relative log length, which is dominant in smaller systems. High log length and complex shape (presence of a root wad) both help the formation of large jams; the presence of roots is also associated to short travel distance and low relative elevation.

Two processes governing remobilisation were investigated at flume scale, namely: a) rapid changes in local water depth and velocity due to network inundation; and b) channel reworking processes, acting over a longer time scale. In the first case, the magnitude of discharge fluctuations is the dominant factor and wood dispersed by small floods is easily removed by larger events. Deposition pattern also influences wood persistence, as high relative elevation and large jam size enhance wood stability. Piece shape shows no clear link with log persistence, probably due to the fact that the presence of roots favours jam formation (a stabilising factor), but also deposition at low relative elevation.

Over a long time scale, the spatial density and size of wood deposits exhibit a threshold behaviour with wood supply, and in particular high input rates determine very high storage and the formation of large, stable jams more similar to those found in single thread systems. However, save for these large accumulations, channel pattern reworking determines intense turnover of deposits regardless of supply rate, piece properties and jam size. Due to the rapid wood pattern reorganisation, deposition occurs mostly in empty braidplain areas as opposed to pre-existing driftwood accumulation sites. This suggests that channel morphodynamics is the dominant factor and wood (alone) has little direct effect on braided pattern.

However, it is important to underline that these observations derive from a simplified physical model that neglects the effect of three key factors, namely: a) fine sediment accumulation; b) vegetative regeneration of driftwood; and c) standing vegetation. These three mutually linked factors are known to exert a strong influence on wood retention in real-scale rivers. The deposition of fines around driftwood elements can determine piece burial and, more importantly, sustains vegetative regeneration and the transformation of

instable pieces into pioneer islands. Patches of standing vegetation represent preferential deposition sites especially at high flows.

Therefore, the integration of different approaches is needed for a complete characterisation of driftwood dynamics in braided systems. On one side, field-scale surveys allow to observe and describe the full complexity of the relationships and feedbacks between flow, sediment transport, driftwood dispersal and vegetation dynamics. In particular, remote sensing (including ground-based imagery) provides valuable quantitative information on wood and channel dynamics during flood events, when direct surveys are not feasible. On the other side, physical modelling allows the investigation of wood transport, deposition and remobilisation under controlled conditions and the analysis of the role of governing factors.

The present work shows that these approaches can be combined to obtain relevant information on in-channel wood dynamics. An improved understanding of the geomorphic and ecological role of driftwood can help defining sustainable wood management practices and designing effective river restoration projects that combine safety and environmental benefits.

References

Abbe, T.B., Montgomery, D.R., 1996. Large woody debris jams, channel hydraulics and habitat formation in large rivers. Regulated Rivers-Research & Management, 12(2-3), 201-221.

Abbe, T.B., Montgomery, D.R., 2003. Patterns and processes of wood debris accumulation in the Queets river basin, Washington. Geomorphology, 51(1-3), 81-107.

Andreoli, A., Comiti, F., Lenzi, M.A., 2007. Characteristics, distribution and geomorphic role of large woody debris in a mountain stream of the Chilean Andes. Earth Surface Processes and Landforms, 32(11), 1675-1692.

Angradi, T.R., Schweiger, E.W., Bolgrien, D.W., Ismert, P., Selle, T., 2004. Bank stabilization, riparian land use and the distribution of large woody debris in a regulated reach of the upper Missouri River, North Dakota, USA. River Research and Applications, 20(7), 829-846.

Antonarakis, A.S., Richards, K.S., Brasington, J., 2008. Object-based land cover classification using airborne LiDAR. Remote Sensing of Environment, 112(6), 2988-2998.

Arscott, D.B., Tockner, K., van der Nat, D., Ward, J.V., 2002. Aquatic habitat dynamics along a braided alpine river ecosystem (Tagliamento River, Northeast Italy). Ecosystems, 5(8), 802-814.

Ashmore, P.E., 1991. How do gravel-bed rivers braid? Canadian Journal of Earth Sciences, 28(3), 326-341.

Ashmore, P.E., 2001. Braiding Phenomena: Statics and Kinetics. In: M. Mosley (Ed.), Gravel-bed Rivers V. New Zealand Hydrological Society, Wellington, pp. 95-121.

Ashmore, P.E., Sauks, E., 2006. Prediction of discharge from water surface width in a braided river with implications for at-a-station hydraulic geometry. Water Resources Research, 42(3).

Ashmore, P.E., 2009. Intensity and characteristic length of braided channel patterns. Can. J. Civ. Eng., 36(10), 1656-1666.

Baillie, B.R., Cummins, T.L., Kimberley, M.O., 1999. Measuring woody debris in the small streams of New Zealand's pine plantations. New Zealand Journal of Marine and Freshwater Research, 33(1), 87-97.

Beechie, T.J., Liermann, M., Pollock, M.M., Baker, S., Davies, J., 2006. Channel pattern and river-floodplain dynamics in forested mountain river systems. Geomorphology, 78(1-2), 124-141.

Bertoldi, W., Ashmore, P.E., Tubino, M., 2009a. A method for estimating the mean bed load flux in braided rivers. Geomorphology, 103(3), 330-340.

Bertoldi, W., Gurnell, A.M., Surian, N., Tockner, K., Zanoni, L., Ziliani, L., Zolezzi, G., 2009b. Understanding reference processes: linkages between river flows, sediment dynamics and vegetated landforms along the Tagliamento River, Italy. River Research and Applications, 25(5), 501-516.

Bertoldi, W., Zanoni, L., Tubino, M., 2009c. Planform dynamics of braided streams. Earth Surface Processes and Landforms, 34(4), 547-557.

Bertoldi, W., Zanoni, L., Tubino, M., 2010. Assessment of morphological changes induced by flow and flood pulses in a gravel bed braided river: The Tagliamento River (Italy). Geomorphology, 114(3), 348-360.

References

Bertoldi, W., Drake, N.A., Gurnell, A.M., 2011a. Interactions between river flows and colonizing vegetation on a braided river: exploring spatial and temporal dynamics in riparian vegetation cover using satellite data. Earth Surface Processes and Landforms, 36(11), 1474-1486.

Bertoldi, W., Gurnell, A.M., Drake, N.A., 2011b. The topographic signature of vegetation development along a braided river: Results of a combined analysis of airborne lidar, color air photographs, and ground measurements. Water Resources Research, 47.

Bertoldi, W., Gurnell, A.M., Welber, M., 2013. Wood recruitment and retention: The fate of eroded trees on a braided river explored using a combination of field and remotely-sensed data sources. Geomorphology, 180–181(0), 146-155.

Bilby, R.E., Ward, J.W., 1989. Changes in characteristics and function of woody debris with increasing size of streams in Western Washington. Transactions of the American Fisheries Society, 118(4), 368-378.

Bocchiola, D., Rulli, M.C., Rosso, R., 2006a. Flume experiments on wood entrainment in rivers. Advances in Water Resources, 29(8), 1182-1195.

Bocchiola, D., Rulli, M.C., Rosso, R., 2006b. Transport of large woody debris in the presence of obstacles. Geomorphology, 76(1-2), 166-178.

Bocchiola, D., Rulli, M.C., Rosso, R., 2008. A flume experiment on the formation of wood jams in rivers. Water Resources Research, 44(2).

Bocchiola, D., 2011. Hydraulic characteristics and habitat suitability in presence of woody debris: A flume experiment. Advances in Water Resources, 34(10), 1304-1319.

Booker, D.J., 2010. Predicting wetted width in any river at any discharge. Earth Surface Processes and Landforms, 35(7), 828-841.

Boruah, S., Gilvear, D., Hunter, P., Sharma, N., 2008. Quantifying channel planform and physical habitat dynamics on a large braided river using satellite data - The Brahmaputra, India. River Research and Applications, 24(5), 650-660.

Braudrick, C.A., Grant, G.E., Ishikawa, Y., Ikeda, H., 1997. Dynamics of wood transport in streams: A flume experiment. Earth Surface Processes and Landforms, 22(7), 669-683.

Braudrick, C.A., Grant, G.E., 2000. When do logs move in rivers? Water Resources Research, 36, 571–583.

Braudrick, C.A., Grant, G.E., 2001. Transport and deposition of large woody debris in streams: a flume experiment. Geomorphology, 41(4), 263-283.

Braudrick, C.A., Dietrich, W.E., Leverich, G.T., Sklar, L.S., 2009. Experimental evidence for the conditions necessary to sustain meandering in coarse-bedded rivers. Proceedings of the National Academy of Sciences of the United States of America, 106(40), 16936-16941.

Bray, J.H., Maxwell, S.E., 1982. Analyzing and interpreting significant MANOVAs. Review of Educational Research, 52(3), 340-367.

Brooks, A.P., Brierley, G.J., 2002. Mediated equilibrium: The influence of riparian vegetation and wood on the long-term evolution and behaviour of a near-pristine river. Earth Surface Processes and Landforms, 27(4), 343-367.

Brooks, A.P., Howell, T., Abbe, T.B., Arthington, A.H., 2006. Confronting hysteresis: Wood based river rehabilitation in highly altered riverine landscapes of south-eastern Australia. Geomorphology, 79(3-4), 395-422.

Chandler, J., Ashmore, P.E., Paola, C., Gooch, M., Varkaris, F., 2002. Monitoring river-channel change using terrestrial oblique digital imagery and automated digital photogrammetry. Annals of the Association of American Geographers, 92(4), 631-644.

160

Cherry, J., Beschta, R.L., 1989. Coarse woody debris and channel morphology - a flume study. Water Resour. Bull., 25(5), 1031-1036.

Chew, L.C., Ashmore, P.E., 2001. Channel adjustment and a test of rational regime theory in a proglacial braided stream. Geomorphology, 37(1-2), 43-63.

Church, M., 1992. Channel morphology and typology. In: P. Calow, G.E. Petts (Eds.), The Rivers Handbook. Blackwell, London, pp. 126-143.

Coe, H.J., Kiffney, P.M., Pess, G.R., Kloehn, K.K., McHenry, M.L., 2009. Periphyton and invertebrate response to wood placement in large Pacific coastal rivers. River Research and Applications, 25(8), 1025-1035.

Cohen, J., 1988. Statistical power analysis for the behavioral sciences. L. Erlbaum Associates, Hillsdale, N.J.

Colombini, M., Seminara, G., Tubino, M., 1987. Finite-amplitude alternate bars. Journal of Fluid Mechanics, 181, 213-232.

Comiti, F., Andreoli, A., Lenzi, M.A., Mao, L., 2006. Spatial density and characteristics of woody debris in five mountain rivers of the Dolomites (Italian Alps). Geomorphology, 78(1-2), 44-63.

Corenblit, D., Tabacchi, E., Steiger, J., Gurnell, A.M., 2007. Reciprocal interactions and adjustments between fluvial landforms and vegetation dynamics in river corridors: A review of complementary approaches. Earth-Science Reviews, 84(1-2), 56-86.

Coulthard, T.J., 2005. Effects of vegetation on braided stream pattern and dynamics. Water Resources Research, 41(4).

Crosato, A., Saleh, M.S., 2011. Numerical study on the effects of floodplain vegetation on river planform style. Earth Surface Processes and Landforms, 36(6), 711-720.

Curran, J.C., 2010. Mobility of large woody debris (LWD) jams in a low gradient channel. Geomorphology, 116(3-4), 320-329.

Díez, J.R., Larranaga, S., Elosegi, A., Pozo, J., 2000. Effect of removal of wood on streambed stability and retention of organic matter. Journal of the North American Benthological Society, 19(4), 621-632.

Díez, J.R., Elosegi, A., Pozo, J., 2001. Woody debris in north Iberian streams: Influence of geomorphology, vegetation, and management. Environmental Management, 28(5), 687-698.

Doering, M., Uehlinger, U., Rotach, A., Schlaepfer, D.R., Tockner, K., 2007. Ecosystem expansion and contraction dynamics along a large Alpine alluvial corridor (Tagliamento River, Northeast Italy). Earth Surface Processes and Landforms, 32(11), 1693-1704.

Downs, P.W., Simon, A., 2001. Fluvial geomorphological analysis of the recruitment of large woody debris in the Yalobusha river network, Central Mississippi, USA. Geomorphology, 37(1-2), 65-91.

Dufour, S., Barsoum, N., Muller, E., Piégay, H., 2007. Effects of channel confinement on pioneer woody vegetation structure, composition and diversity along the River Drome (SE France). Earth Surface Processes and Landforms, 32(8), 1244-1256.

Eaton, B.C., Millar, R.G., Davidson, S., 2010. Channel patterns: Braided, anabranching, and single-thread. Geomorphology, 120(3-4), 353-364.

Eaton, B.C., Hassan, M.A., Davidson, S.L., 2012. Modeling wood dynamics, jam formation, and sediment storage in a gravel-bed stream. J. Geophys. Res.-Earth Surf., 117.

Egozi, R., Ashmore, P.E., 2008. Defining and measuring braiding intensity. Earth Surface Processes and Landforms, 33(14), 2121-2138.

Enders, C.K., 2003. Performing multivariate group comparisons following a statistically significant MANOVA. Measurement and Evaluation in Counseling and Development, 36(1), 40-56.

Ferguson, R.I., 1986. Hydraulics and hydraulic geometry. Progress in Physical Geography, 10(1), 1-31.

References

Feurer, D., Bailly, J.S., Puech, C., Le Coarer, Y., A, V., 2008. Very high resolution mapping of river immersed topography by remote sensing. Progress in Physical Geography, 32(4), 1-17.

Filzmoser, P., Maronna, R., Werner, M., 2008. Outlier identification in high dimensions. Computational Statistics & Data Analysis, 52(3), 1694-1711.

Filzmoser, P., Gschwandtner, M., 2012. Mvoutlier: Multivariate outlier detection based on robust methods. V. 1.9.8. http://CRAN.R-project.org/package=mvoutlier.

Foufoula-Georgiou, E., Sapozhnikov, V., 2001. Scale invariances in the morphology and evolution of braided rivers. Mathematical Geology, 33(3), 273-291.

Francis, R.A., Gurnell, A.M., Petts, G.E., Edwards, P.J., 2005. Survival and growth responses of Populus nigra, Salix elaeagnos and Alnus incana cuttings to varying levels of hydric stress. Forest Ecology and Management, 210(1-3), 291-301.

Francis, R.A., 2007. Size and position matter: riparian plant establishment from fluvially deposited trees. Earth Surface Processes and Landforms, 32(8), 1239-1243.

Francis, R.A., Petts, G.E., Gurnell, A.M., 2008. Wood as a driver of past landscape change along river corridors. Earth Surface Processes and Landforms, 33(10), 1622-1626.

Gippel, C.J., Finlayson, B.L., Oneill, I.C., 1996a. Distribution and hydraulic significance of large woody debris in a lowland Australian river. Hydrobiologia, 318(3), 179-194.

Gippel, C.J., O'Neill, I.C., Finlayson, B.L., Schnatz, I., 1996b. Hydraulic guidelines for the re-introduction and management of large woody debris in lowland rivers. Regulated Rivers-Research & Management, 12(2-3), 223-236.

Gran, K., Paola, C., 2001. Riparian vegetation controls on braided stream dynamics. Water Resources Research, 37(12), 3275-3283.

GRASS Development Team, 2012. Geographic Resources Analysis Support System (GRASS) Software. V. 6.4.2. Open Source Geospatial Foundation. http://grass.osgeo.org

Gray, D., Scarsbrook, M.R., Harding, J.S., 2006. Spatial biodiversity patterns in a large New Zealand braided river. New Zealand Journal of Marine and Freshwater Research, 40(4), 631-642.

Gurnell, A.M., Gregory, K.J., Petts, G.E., 1995. The role of coarse woody debris in forest aquatic habitats: implications for management. Aquatic Conservation-Marine and Freshwater Ecosystems, 5(2), 143-166.

Gurnell, A.M., Sweet, R., 1998. The distribution of large woody debris accumulations and pools in relation to woodland stream management in a small, low-gradient stream. Earth Surface Processes and Landforms, 23(12), 1101-1121.

Gurnell, A.M., Petts, G.E., Hannah, D.M., Smith, B.P.G., Edwards, P.J., Kollmann, J., Ward, J.V., Tockner, K., 2000a. Wood storage within the active zone of a large European gravel-bed river. Geomorphology, 34(1-2), 55-72.

Gurnell, A.M., Petts, G.E., Harris, N., Ward, J.V., Tockner, K., Edwards, P.J., Kollmann, J., 2000b. Large wood retention in river channels: The case of the Fiume Tagliamento, Italy. Earth Surface Processes and Landforms, 25(3), 255-275.

Gurnell, A.M., Petts, G.E., Hannah, D.M., Smith, B.P.G., Edwards, P.J., Kollmann, J., Ward, J.V., Tockner, K., 2001. Riparian vegetation and island formation along the gravel-bed Fiume Tagliamento, Italy. Earth Surface Processes and Landforms, 26(1), 31-62.

Gurnell, A.M., Petts, G.E., 2002. Island-dominated landscapes of large floodplain rivers, a European perspective. Freshwater Biology, 47(4), 581-600.

Gurnell, A.M., Piégay, H., Swanson, F.J., Gregory, S.V., 2002. Large wood and fluvial processes. Freshwater Biology, 47(4), 601-619.

Gurnell, A.M., Tockner, K., Edwards, P.J., Petts, G.E., 2005. Effects of deposited wood on biocomplexity of river corridors. Frontiers in Ecology and the Environment, 3(7), 377-382.

Gurnell, A.M., Petts, G.E., 2006. Trees as riparian engineers: The Tagliamento River, Italy. Earth Surface Processes and Landforms, 31(12), 1558-1574.

Gurnell, A.M., Thompson, K., Goodson, J., Moggridge, H.L., 2008. Propagule deposition along river margins: linking hydrology and ecology. Journal of Ecology, 96, 553-565.

Gurnell, A.M., Surian, N., Zanoni, L., 2009. Multi-thread river channels: A perspective on changing European alpine river systems. Aquatic Sciences, 71(3), 253-265.

Gurnell, A.M., in press. Wood in fluvial systems. In: J. Shroder, E. Wohl (Eds.), Treatise on Geomorphology. Academic Press, San Diego, CA.

Haase, R.F., Ellis, M.V., 1987. Multivariate Analysis of Variance. Journal of Counseling Psychology, 34(4), 404-413.

He, Z.G., Wu, W.M., Shields, F.D., 2009. Numerical analysis of effects of large wood structures on channel morphology and fish habitat suitability in a Southern US sandy creek. Ecohydrology, 2(3), 370-380.

Hering, D., Kail, J., Eckert, S., Gerhard, M., Meyer, E.I., Mutz, M., Weiss, I., 2000. Coarse woody debris quantity and distribution in Central European streams. Int. Rev. Hydrobiol., 85(1), 5-23.

Hervoue, A., Dunford, R., Piégay, H., Belletti, B., Tremelo, M.-L., 2011. Analysis of Post-flood Recruitment Patterns in Braided-Channel Rivers at Multiple Scales Based on an Image Series Collected by Unmanned Aerial Vehicles, Ultra-light Aerial Vehicles, and Satellites. Giscience & Remote Sensing, 48(1), 50-73.

Hickin, E.J., 1984. Vegetation and river channel dynamics. Canadian Geographer-Geographe Canadien, 28(2), 111-126.

Hoey, T.B., Sutherland, A.J., 1991. Channel morphology and bedload pulses in braided rivers: a laboratory study. Earth Surface Processes and Landforms, 16(5), 447-462.

Hygelund, B., Manga, M., 2003. Field measurement of drag coefficients for model large woody debris. Geomorphology, 51, 175-185.

Iroume, A., Andreoli, A., Comiti, F., Ulloa, H., Huber, A., 2010. Large wood abundance, distribution and mobilization in a third order Coastal mountain range river system, southern Chile. Forest Ecology and Management, 260(4), 480-490.

Kail, J., Hering, D., Muhar, S., Gerhard, M., Preis, S., 2007. The use of large wood in stream restoration: experiences from 50 projects in Germany and Austria. J. Appl. Ecol., 44(6), 1145-1155.

Karrenberg, S., Kollmann, J., Edwards, P.J., Gurnell, A.M., Petts, G.E., 2003. Patterns in woody vegetation along the active zone of a near-natural Alpine river. Basic and Applied Ecology, 4(2), 157-166.

Keller, E.A., Swanson, F.J., 1979. Effects of large organic material on channel form and fluvial processes. Earth Surface Processes 4(4), 361-380.

Kollmann, J., Vieli, M., Edwards, P.J., Tockner, K., Ward, J.V., 1999. Interactions between vegetation development and island formation in the Alpine river Tagliamento. Applied Vegetation Science, 2, 25-36.

Lane, S.N., Richards, K.S., Chandler, J.H., 1993. Developments in photogrammetry - The geomorphological potential. Progress in Physical Geography, 17(3), 306-328.

Lane, S.N., 2000. The measurement of river channel morphology using digital photogrammetry. Photogramm. Rec., 16(96), 937-957.

Lane, S.N., 2006. Approaching the system-scale understanding of braided river behaviour. In: G. Sambrook-Smith, J. Best, C. Bristow, G. Petts (Eds.), Braided Rivers: Process, Deposits, Ecology and Management. Blackwell, Oxford, pp. 107-135.

Lane, S.N., Widdison, P.E., Thomas, R.E., Ashworth, P.J., Best, J.L., Lunt, I.A., Smith, G.H.S., Simpson, C.J., 2010. Quantification of braided river channel change using archival digital image analysis. Earth Surface Processes and Landforms, 35(8), 971-985.

Lassettre, N.S., Piégay, H., Dufour, S., Rollet, A.-J., 2008. Decadal changes in distribution and frequency of wood in a free meandering river, the Ain River, France. Earth Surface Processes and Landforms, 33(7), 1098-1112.

Le Lay, Y.-F., Piégay, H., Gregory, K.J., Chin, A., Doledec, S., Elosegi, A., Mutz, M., Wyżga, B., Zawiejska, J., 2008. Variations in cross-cultural perception of riverscapes in relation to in-channel wood. Transactions of the Institute of British Geographers, 33(2), 268-287.

Legleiter, C.J., Roberts, D.A., Lawrence, R.L., 2009. Spectrally based remote sensing of river bathymetry. Earth Surface Processes and Landforms, 34(8), 1039-1059.

Lepori, F., Palm, D., Malmqvist, B., 2005. Effects of stream restoration on ecosystem functioning: detritus retentiveness and decomposition. J. Appl. Ecol., 42(2), 228-238.

Lienkaemper, G.W., Swanson, F.J., 1987. Dynamics of large woody debris in streams in old-growth douglas-fir forests. Canadian Journal of Forest Research-Revue Canadienne De Recherche Forestiere, 17(2), 150-156.

Lorang, M.S., Whited, D.C., Hauer, F.R., Kimball, J.S., Stanford, J.A., 2005. Using airborne multispectral imagery to evaluate geomorphic work across floodplains of gravel-bed rivers. Ecological Applications, 15(4), 1209-1222.

Lowry, R., 2012. Concepts and Applications of Inferential Statistics. http://vassarstats.net/textbook.

Luchi, R., Bertoldi, W., Zolezzi, G., Tubino, M., 2007. Monitoring and predicting channel change in a free-evolving, small Alpine river: Ridanna Creek (North East Italy). Earth Surface Processes and Landforms, 32(14), 2104-2119.

MacVicar, B.J., Piégay, H., Henderson, A., Comiti, F., Oberlin, C., Pecorari, E., 2009. Quantifying the temporal dynamics of wood in large rivers: field trials of wood surveying, dating, tracking, and monitoring techniques. Earth Surface Processes and Landforms, 34(15), 2031-2046.

MacVicar, B.J., Piégay, H., 2012. Implementation and validation of video monitoring for wood budgeting in a wandering piedmont river, the Ain River (France). Earth Surface Processes and Landforms, 37(12), 1272-1289.

Malard, F., Uehlinger, U., Zah, R., Tockner, K., 2006. Flood-pulse and riverscape dynamics in a braided glacial river. Ecology, 87(3), 704-716.

Manners, R.B., Doyle, M.W., 2008. A mechanistic model of woody debris jam evolution and its application to wood-based restoration and management. River Research and Applications, 24(8), 1104-1123.

Marcus, W.A., Marston, R.A., Colvard, C.R., Gray, R.D., 2002. Mapping the spatial and temporal distributions of woody debris in streams of the Greater Yellowstone Ecosystem, USA. Geomorphology, 44(3-4), 323-335.

Marcus, W.A., Fonstad, M.A., 2010. Remote sensing of rivers: the emergence of a subdiscipline in the river sciences. Earth Surface Processes and Landforms, 35(15), 1867-1872.

Mazzorana, B., Hubl, J., Zischg, A., Largiader, A., 2011. Modelling woody material transport and deposition in alpine rivers. Nat. Hazards, 56(2), 425-449.

Mazzorana, B., Comiti, F., Scherer, C., Fuchs, S., 2012. Developing consistent scenarios to assess flood hazards in mountain streams. J. Environ. Manage., 94(1), 112-124.

McGill, R., Tukey, J.W., Larsen, W.A., 1978. Variations of box plots. The American Statistician 32(1), 12–16.

Millington, C.E., Sear, D.A., 2007. Impacts of river restoration on small-wood dynamics in a low-gradient headwater stream. Earth Surface Processes and Landforms, 32(8), 1204-1218.

Moggridge, H.L., Gurnell, A.M., 2009. Controls on the sexual and asexual regeneration of Salicaceae along a highly dynamic, braided river system. Aquatic Sciences, 71, 305-317.

Montgomery, D.R., Piégay, H., 2003. Wood in rivers: interactions with channel morphology and processes. Geomorphology, 51(1-3), 1-5.

Montgomery, D.R., Abbe, T.B., 2006. Influence of logjam-formed hard points on the formation of valley-bottom landforms in an old-growth forest valley, Queets River, Washington, USA. Quaternary Research, 65(1), 147-155.

Mosley, M.P., 1981. The influence of organic debris on channel morphology and bedload transport in a New Zealand forest stream. Earth Surface Processes and Landforms, 6(571-579).

Mosley, M.P., 1982. Analysis of the effect of changing discharge on channel morphology and instream uses in a braided river, Ohau River, New Zealand. Water Resources Research, 18(4), 800-812.

Mosley, M.P., 1983. Response of braided rivers to changing discharge. Journal of Hydrology New Zealand, 22(18-67).

Moulin, B., Piégay, H., 2004. Characteristics and temporal variability of large woody debris trapped in a reservoir on the River Rhone: Implications for river basin management. River Research and Applications, 20(1), 79-97.

Mutz, M., Kalbus, E., Meinecke, S., 2007. Effect of instream wood on vertical water flux in low-energy sand bed flume experiments. Water Resources Research, 43(10).

Næsset, E., 2002. Predicting forest stand characteristics with airborne scanning laser using a practical two-stage procedure and field data. Remote Sensing of Environment, 80(1), 88-99.

Nakamura, F., Swanson, F.J., 1993. Effects of coarse woody debris on morphology and sediment storage of a mountain stream system in western Oregon. Earth Surface Processes and Landforms, 18(1), 43-61.

Nimon, K.F., 2012. Statistical assumptions of substantive analyses across the general linear model: a mini-review. Frontiers in psychology, 3, 322-322.

Pettit, N.E., Naiman, R.J., Rogers, K.H., Little, J.E., 2005. Post-flooding distribution and characteristics of large woody debris piles along the semi-arid Sabie River, South Africa. River Research and Applications, 21(1), 27-38.

Piégay, H., Gurnell, A.M., 1997. Large woody debris and river geomorphological pattern: Examples from SE France and S England. Geomorphology, 19(1-2), 99-116.

Piégay, H., Thevenet, A., Citterio, A., 1999. Input, storage and distribution of large woody debris along a mountain river continuum, the Drome River, France. Catena, 35(1), 19-39.

Piegay, H., Mutz, M., Gregory, K.J., Rinaldi, M., Bondarev, V., Chin, A., Wyzga, B., Dahlstrom, N., Zawiejska, J., Elosegi, A., Gregory, S.V., Joshi, V., 2005. Public perception as a barrier to introducing wood in rivers for restoration purposes. Environmental Management, 36(5), 665-674.

Pyrce, R.S., Ashmore, P.E., 2003. Particle path length distributions in meandering gravel-bed streams: Results from physical models. Earth Surface Processes and Landforms, 28(9), 951-966.

R Development Core Team, 2008. R: A language and environment for statistical computing. V. R Foundation for Statistical Computing. http://www.R-project.org.

Ranga Raju, K.G., Rana, O.P.S., Asawa, G.L., Pillai, A.S.N., 1983. Rational assessment of blockage effect in channel flow past smooth circular cylinders. Journal of Hydraulic Research, 21, 289-302.

Richmond, A.D., Fausch, K.D., 1995. Characteristics and function of large woody debris in sub-alpine Rocky-Mountain streams in Northern Colorado. Can. J. Fish. Aquat. Sci., 52(8), 1789-1802.

Rigon, E., Comiti, F., Lenzi, M.A., 2012. Large wood storage in streams of the Eastern Italian Alps and the relevance of hillslope processes. Water Resources Research, 48.

Robertson-Rintoul, M.S.E., Richards, K.S., 1993. Braided-channel pattern and paleohydrology using an index of total sinuosity. . In: J. Best, C. Bristow (Eds.), Braided Rivers. Geological Society London, pp. 113-118.

Robison, E.G., Beschta, R.L., 1990. Coarse woody debris and channel morphology interactions for undisturbed streams in southeast Alaska, USA. Earth Surface Processes and Landforms, 15, 149-156.

Sawyer, A.H., Cardenas, M.B., 2012. Effect of experimental wood addition on hyporheic exchange and thermal dynamics in a losing meadow stream. Water Resources Research, 48.

Sear, D.A., Millington, C.E., Kitts, D.R., Jeffries, R., 2010. Logjam controls on channel:floodplain interactions in wooded catchments and their role in the formation of multi-channel patterns. Geomorphology, 116(3-4), 305-319.

Shields, F.D., Gippel, C.J., 1995. Prediction of effects of woody debris removal on flow resistance. Journal of Hydraulic Engineering-Asce, 121(4), 341-354.

Shields, F.D., Knight, S.S., Stofleth, J.M., 2006. Large wood addition for aquatic habitat rehabilitation in an incised, sand-bed stream, Little Topashaw Creek, Mississippi. River Research and Applications, 22(7), 803-817.

Smith, L.C., Isacks, B.L., Bloom, A.L., Murray, A.B., 1996. Estimation of discharge from three braided rivers using synthetic aperture radar satellite imagery: Potential application to ungaged basins. Water Resources Research, 32(7), 2021-2034.

Smith, R.D., Sidle, R.C., Porter, P.E., 1993. Effects on bedload transport of experimental removal of woody debris from a forest gravel-bed stream. Earth Surface Processes and Landforms, 18(5), 455-468.

Stanford, J.A., Lorang, M.S., Hauer, F.R., 2005. The shifting habitat mosaic of river ecosystems. Verhandlungen der Internationalen Vereinigung für Limnologie, 29, 123-136.

Sukhodolov, A., Bertoldi, W., Wolter, C., Surian, N., Tubino, M., 2009. Implications of channel processes for juvenile fish habitats in Alpine rivers. Aquatic Sciences, 71(3), 338-349.

Surian, N., Mao, L., Giacomin, M., Ziliani, L., 2009. Morphological effects of different channel-forming discharges in a gravel-bed river. Earth Surface Processes and Landforms, 34(8), 1093-1107.

Tabachnick, B.G., Fidell, L.S., 2012. Using Multivariate Statistics. Allyn and Bacon, Boston.

Tal, M., Paola, C., 2007. Dynamic single-thread channels maintained by the interaction of flow and vegetation. Geology, 35(4), 347-350.

Tal, M., Paola, C., 2010. Effects of vegetation on channel morphodynamics: results and insights from laboratory experiments. Earth Surface Processes and Landforms, 35(9), 1014-1028.

Thévenet, A., Citterio, A., Piégay, H., 1998. A new methodology for the assessment of large woody debris accumulations on highly modified rivers (example of two French piedmont rivers). Regulated Rivers-Research & Management, 14(6), 467-483.

Tockner, K., Ward, J.V., Arscott, D.B., Edwards, P.J., Kollmann, J., Gurnell, A.M., Petts, G.E., Maiolini, B., 2003. The Tagliamento River: a model ecosystem of European importance. Aquatic Sciences, 65(3), 239-253.

van der Nat, D., Schmidt, A.P., Tockner, K., Edwards, P.J., Ward, J.V., 2002. Inundation dynamics in braided floodplains: Tagliamento River, Northeast Italy. Ecosystems, 5(7), 636-647.

van der Nat, D., Tockner, K., Edwards, P.J., Ward, J.V., 2003a. Large wood dynamics of complex Alpine river floodplains. Journal of the North American Benthological Society, 22(1), 35-50.

van der Nat, D., Tockner, K., Edwards, P.J., Ward, J.V., Gurnell, A.M., 2003b. Habitat change in braided flood plains (Tagliamento, NE-Italy). Freshwater Biology, 48(10), 1799-1812.

Wallace, J.B., Webster, J.R., Meyer, J.L., 1995. Influence of log additions on physical and biotic characteristics of a mountain stream. Can. J. Fish. Aquat. Sci., 52(10), 2120-2137.

Wallerstein, N.P., Alonso, C.V., Bennett, S.J., Thorne, C.R., 2001. Distorted Froude-scaled flume analysis of large woody debris. Earth Surface Processes and Landforms, 26(12), 1265-1283.

Wallerstein, N.P., Alonso, C.V., Bennett, S.J., Thorne, C.R., 2002. Surface wave forces acting on submerged logs. ASCE Journal of Hydraulic Engineering, 128(3), 349-353.

Wallerstein, N.P., 2003. Dynamic model for constriction scour caused by large woody debris. Earth Surface Processes and Landforms, 28(1), 49-68.

Ward, J.V., Tockner, K., Edwards, P.J., Kollmann, J., Bretschko, G., Gurnell, A.M., Petts, G.E., Rossaro, B., 1999. A reference river system for the Alps: The 'Fiume Tagliamento'. Regulated Rivers-Research & Management, 15(1-3), 63-75.

Warren, D.R., Kraft, C.E., 2008. Dynamics of large wood in an eastern U.S. mountain stream. Forest Ecology and Management, 256(4), 808-814.

Warren, D.R., Kraft, C.E., Keeton, W.S., Nunery, J.S., Likens, G.E., 2009. Dynamics of wood recruitment in streams of the northeastern US. Forest Ecology and Management, 258(5), 804-813.

Winterbottom, S.J., Gilvear, D.J., 1997. Quantification of channel bed morphology in gravel-bed rivers using airborne multispectral imagery and aerial photography. Regulated Rivers-Research & Management, 13(6), 489-499.

Wohl, E.E., Cenderelli, D.A., Dwire, K.A., Ryan-Burkett, S.E., Young, M.K., Fausch, K.D., 2010. Large in-stream wood studies: a call for common metrics. Earth Surface Processes and Landforms, 35(5), 618-625.

Wulder, M.A., White, J.C., Nelson, R.F., Næsset, E., Ørka, H.O., Coops, N.C., Hilker, T., Bater, C.W., Gobakken, T., 2012. Lidar sampling for large-area forest characterization: A review. Remote Sensing of Environment, 121, 196-209.

Wyżga, B., Zawiejska, J., 2005. Wood storage in a wide mountain river: case study of the Czarny Dunajec, Polish Carpathians. Earth Surface Processes and Landforms, 30(12), 1475-1494.

Young, W.J., 1991. Flume study of the hydraulic effects of large woody debris in lowland rivers. Regulated Rivers-Research & Management, 6, 203–211.

Zanoni, L., Gurnell, A.M., Drake, N.A., Surian, N., 2008. Island dynamics in a braided river from analysis of historical maps and air photographs. River Research and Applications, 24(8), 1141-1159.

Zolezzi, G., Bertoldi, W., Tubino, M., 2006. Morphological analysis and prediction of channel bifurcations. In: G.H. Sambrook-Smith, J.L. Best, C.S. Bristow, G.E. Petts (Eds.), Braided Rivers: Process, Deposits, Ecology and Management Special Publication 36 IAS. Blackwell, Oxford, pp. 233–256.

Acknowledgements

It is a pleasure to thank the people who made this thesis possible.

The guidance of Walter Bertoldi and Marco Tubino has made my journey from the headwaters to the lowland reaches of this PhD a thoughtful and rewarding experience. In particular, I wish to thank Walter for believing in what I was doing - especially when I felt as if I were hopelessly stranded in a dry channel - and Marco for helping me to see things more clearly from the top of the mountains.

My warm and sincere thanks goes to Hervé Piégay and Jonathan Laronne. Their insightful comments and encouragement have greatly helped me to find the main channel of this thesis, and to follow it. During my PhD I have had the honour and pleasure to work with Angela Gurnell. The time spent with her on the islands of the Tagliamento River has been an extraordinary opportunity for intellectual growth.

My journey through the bifurcations and confluences of this work has been made possible by the support and friendship of the people who joined me in laboratory and field activities. My enduring gratitude goes to Sandra Zanella for the dedication and enthusiasm she has put in our work in Trento and in Hull. I am indebted to Martino Salvaro and Marco Redolfi for devoting some of their precious time to helping me. I also wish to thank the staff of the Hydraulics Lab in Trento and in particular Lorenzo Forti, who has a solution to every problem, and it is usually the best one. "A far bene..."

Being part of the GIAMT research group made my research experience complex, and complexity is richness. I am grateful to each and every one of my colleagues for contributing to my personal and professional time, and especially to Guglielmo, who keeps on climbing the steep plains of research, and Sebastiano, who taught me that, with the exception of three things, there's nothing to be afraid of.

Along the course of my PhD, I have had the great opportunity to be a member of the DEEP Crew who conducted the experiments in Hull. I am grateful to Francesco Comiti, Luca Mao, Stuart McLelland, Brendan Murphy, Nana Osei, Diego Ravazzolo, Michal Tal, and Rob Thomas for putting together their experience and efforts for this project.

Finally, I am forever indebted to my parents for their understanding, endless patience and encouragement.

Combiniamo. Si può fare tutto.